FINAL REPORT

PART I

The Study of Space Communications Spread Spectrum Systems

REPORT 88-1

PREPARED FOR THE DEPARTMENT OF COMMUNICATIONS
UNDER DSS CONTRACT NO. 36001-6-3530/0/ST

Department of Electrical Engineering

Queen's University at Kingston

Kingston, Ontario, Canada

FINAL REPORT

PART I

The Study of Space Communications Spread Spectrum Systems

REPORT 88-1

PREPARED FOR THE DEPARTMENT OF COMMUNICATIONS
UNDER DSS CONTRACT NO. 36001-6-3530/0/ST

SECURITY CLASSIFICATION OF FORM
(highest classification of Title, Abstract, Keywords)

DOCUMENT CONTROL DATA

(Security classification of title, body of abstract and indexing annotation must be entered when the overall document is classified)

1. ORIGINATOR (the name and address of the organization preparing the document. Organizations for whom the document was prepared, e.g. Establishment sponsoring a contractor's report, or tasking agency, are entered in section B.)

Department of Electrical Engineering,
QUEEN'S UNIVERSITY,
KINGSTON, Ontario, Canada. K7L 3N6

2. SECURITY CLASSIFICATION (overall security classification of the document. including special warning terms if applicable)

Unclassified.

3. TITLE (the complete document title as indicated on the title page. Its classification should be indicated by the appropriate abbreviation (S,C,R or U) in parentheses after the title.)

"The Study of Space Communications Spread Spectrum Systems"
Part I - High Data Rate Spread Spectrum Systems with Band-efficient Modulations.

4. AUTHORS (Last name, first name, middle initial. If military, show rank, e.g. Doe, Maj. John E.)

Lam, Y.M., Wittke, P.H.

5. DATE OF PUBLICATION (month and year of publication of document)

March, 1988.

6a. NO. OF PAGES (total containing information. Include Annexes, Appendices, etc.)

180

6b. NO. OF REFS (total cited in document)

52

7. DESCRIPTIVE NOTES (the category of the document, e.g. technical report, technical note or memorandum. If appropriate, enter the type of report, e.g. interim, progress, summary, annual or final. Give the inclusive dates when a specific reporting period is covered.)

Final Report Part I.

8. SPONSORING ACTIVITY (the name of the department project office or laboratory sponsoring the research and development. Include the address.)

Communications Research Centre, Department of Communications, 3701 Carling Avenue,
P.O. Box 11490, Station 'H', OTTAWA, Ontario. K2H 8S2

9a. PROJECT OR GRANT NO. (if appropriate, the applicable research and development project or grant number under which the document was written. Please specify whether project or grant)

32A99

9b. CONTRACT NO. (if appropriate, the applicable number under which the document was written)

DSS Contract 36001-6-3530/0/ST

10a. ORIGINATOR'S DOCUMENT NUMBER (the official document number by which the document is identified by the originating activity. This number must be unique to this document.)

Report 88-1, Department of Electrical Engineering, Queen's Univ., Kingston, Ont.

10b. OTHER DOCUMENT NOS. (Any other numbers which may be assigned this document either by the originator or by the sponsor)

11. DOCUMENT AVAILABILITY (any limitations on further dissemination of the document, other than those imposed by security classification)

(x) Unlimited distribution
( ) Distribution limited to defence departments and defence contractors; further distribution only as approved
( ) Distribution limited to defence departments and Canadian defence contractors; further distribution only as approved
( ) Distribution limited to government departments and agencies; further distribution only as approved
( ) Distribution limited to defence departments; further distribution only as approved
( ) Other (please specify):

12. DOCUMENT ANNOUNCEMENT (any limitation to the bibliographic announcement of this document. This will normally correspond to the Document Availabilty (11). However, where further distribution (beyond the audience specified in 11) is possible, a wider announcement audience may be selected.)

No Limitation.

Unclassified

SECURITY CLASSIFICATION OF FORM

DCD03 9/04/87

13. ABSTRACT (a brief and factual summary of the document. It may also appear elsewhere in the body of the document itself. It is highly desirable that the abstract of classified documents be unclassified. Each paragraph of the abstract shall begin with an indication of the security classification of the information in the paragraph (unless the document itself is unclassified) represented as (S), (C), (R), or (U). It is not necessary to include here abstracts in both official languages unless the text is bilingual).

In this final report, comprehensive results on hopped spread spectrum transmission that employs band-efficient modulations that are coherent during each hop, are presented. A broad range of system considerations are presented, including: signalling spectrum, optimum receivers, system complexity, and performance in the presence of noise and jamming. The particular cases where the hopped modulation is minimum-shift keying (MSK), duobinary minimum-shift keying (DMSK), or tamed-FM (TFM) are considered in detail. As well, results are presented for various modulation indices, rectangular and raised-cosine pulse shapings, and a range of hop interval lengths.

Various maximum likelihood receivers are presented. These receivers are complicated and so simplifications to achieve more practical sequence estimation algorithms are carried out. The algorithm which carries out a sequence estimation over each hop appears most promising. Its performance has been evaluated in Gaussian noise, partial band jamming and multiple-tone jamming, using bounds and a simulation of the system. In general, the compact nature of the signal spectrum prior to hopping, appears to offer dramatically improved performance in multiple-tone jamming.

14. KEYWORDS, DESCRIPTORS or IDENTIFIERS (technically meaningful terms or short phrases that characterize a document and could be helpful in cataloguing the document. They should be selected so that no security classification is required. Identifiers, such as equipment model designation, trade name, military project code name, geographic location may also be included. If possible, keywords should be selected from a published thesaurus. e.g. Thesaurus of Engineering and Scientific Terms (TEST) and that thesaurus identified. If it is not possible to select indexing terms which are Unclassified, the classification of each should be indicated as with the title.)

Frequency hopped spread spectrum systems, high data rate, band-efficient modulation, noncoherent reception.

HIGH DATA RATE SPREAD SPECTRUM SYSTEMS WITH BAND-EFFICIENT MODULATIONS

by

Y.M. Lam,

P.H. Wittke

REPORT 88-4

FINAL REPORT PART I

(of IV Parts)

PREPARED FOR THE DEPARTMENT OF COMMUNICATIONS

UNDER DSS CONTRACT NO. 36001-6-3530/0/ST

"The Study of Space Communications Spread Spectrum Systems"

Department of Electrical Engineering,

Queen's University

Kingston, Ontario, Canada

March, 1988

ABSTRACT

In this final report, comprehensive results on hopped spread spectrum transmission that employs band-efficient modulations that are coherent during each hop, are presented. A broad range of system considerations are presented, including: signaling spectrum, optimum receivers, system complexity, and performance in the presence of noise and jamming. The particular cases where the hopped modulation is minimum-shift keying (MSK), duobinary minimum-shift keying (DMSK), or tamed-FM (TFM) are considered in detail. As well, results are presented for various modulation indices, rectangular and raised-cosine pulse shapings, and a range of hop interval lengths.

Various maximum likelihood receivers are presented. These receivers are complicated and so simplifications to achieve more practical sequence estimation algorithms are carried out. The algorithm which carries out a sequence estimation over each hop appears most promising. Its performance has been evaluated in Gaussian noise, partial band jamming and multiple-tone jamming, using bounds and a simulation of the system. In general, the compact nature of the signal spectrum prior to hopping, appears to offer dramatically improved performance in multiple-tone jamming.

TABLE OF CONTENTS

Chapter One

INTRODUCTION

There is currently a high interest in military satellite communications (MILSATCOM) that is immune to electronic countermeasures. Spread spectrum communications, with its inherent interference rejection capability, has over the years become an increasingly popular military antijamming tactical communications technique. Although the current applications for spread spectrum are primarily for military communications, there is a growing interest in the use of this technique for mobile radio networks (radio telephony, packet radio and amateur radio). Other applications include collision avoidance, range measurement and position finding [1,2].

Spread spectrum signaling is a means of transmission in which the signal occupies a bandwidth in excess of the minimum necessary to send the information. The bandwidth spreading is accomplished by means of a code which is independent of the data. At the receiver the same code is used for despreading and subsequent data recovery [2]. Two commonly used techniques for spreading the spectrum are direct sequence modulation and frequency hopping [1-5]. Direct sequence modulation causes rapid phase transitions in the information carrying signal by modulating the signal directly with a pseudorandom code sequence whose bit rate is much higher than the information signal bandwidth. The spread bandwidth is directly determined by the clock rate of the pseudorandom sequence. Frequency hopping changes the transmitter carrier frequency periodically with a pseudorandom hopping pattern controlled by a pseudorandom sequence [1-5]. This spreads the spectrum sequentially rather than instantaneously. The bandwidth occupied by the frequency-hopped signal during a hop interval depends on both the hopping rate and symbol rate. The spread spectrum system bandwidth is

equal to the frequency excursion from the lowest available frequency-hopped band to the highest available frequency-hopped band. With the spectrum of the signal spread over a wide bandwidth, a jammer with a fixed finite power is forced to spread his resources thus making jamming more difficult and less effective.

The performance improvement that is achieved through the use of spread spectrum signaling is defined as the processing gain of the spread spectrum system. Processing gain is given by the ratio of the spread spectrum system bandwidth to the information bandwidth [1-6]. The greater the spread bandwidth, the greater the processing gain. For a direct sequence system, the spread bandwidth is limited to the clock rate of the pseudorandom sequence, which is limited by the achievable speed of the digital circuitry. It also requires phase coherence over the spread bandwidth. Frequency-hopped systems have no such restrictions. Large spread bandwidths can be more easily achieved by frequency hopping than by direct sequence modulation. Thus, provided that a sufficient bandwidth can be allocated such as in the Extremely High Frequency (EHF) band which is defined as the frequency band from 30 GHz to 300 GHz, frequency hopping can achieve much higher processing gain than direct sequence modulation techniques. Since the spread bandwidth need not be contiguous in a frequency-hopped system, frequency bands which are unusually noisy, are jammed, or exhibit severe fading can be hopped around. Frequency hopping also has an inherently shorter acquisition time in a serial search acquisition system, due to the fewer code states required to be tested than in direct sequence modulation with the same processing gain [5]. Judging from the above mentioned advantages, frequency hopping is hence the preferred spread spectrum technique over direct sequence modulation technique when the information signal is to be spread over the wide bandwidths available at the EHF band in MILSATCOM.

1.1 Frequency-Hopped Spread Spectrum Systems

In a frequency-hopped spread spectrum system, the transmitter carrier frequency is usually chosen from a set of 2^k frequencies which are spaced approximately the width of the data modulation spectrum apart. The hopping pattern of the carrier frequency is commonly controlled by a pseudorandom sequence or other encrypted sequence. In the receiver, the received signal is down-converted (dehopped) by a frequency synthesizer controlled by the same pseudorandom sequence which has been synchronized with the transmitter [3]. A block diagram of a frequency-hopped spread spectrum system is shown in Fig. 1.1.

The fact that frequency hopping spreads the spectrum sequentially rather than instantaneously leads to consideration of the rate at which the hops occur. The processing gain actually realized can be significantly less, depending on the jammer's ability to negate the effect of the frequency hopping. The faster the frequency hopping, the more the vulnerability to jamming by sophisticated jammers is reduced. Some sophisticated jammers, such as the repeat-back jammer which is also called the follower jammer, measure the operating signal frequency and tune the interference to that portion of the band. The difficulty of implementing such a jammer increases as the hopping rate increases. To achieve a desired bit error rate, the minimum frequency hopping rate is determined by a number of parameters such as the information rate, the amount of redundancy used, if any, and the distance to the nearest potential interferer [1]. Clearly, a repeat-back jammer's influence will be entirely eliminated if the carrier frequency hops to another new frequency before the jamming signal arrives, that is, if the hopping rate is the inverse of the difference in arrival time between the communication and jamming signals at the receiver.

Generally, hopping the carrier frequency several times during a bit interval, so-called fast frequency hopping [4], is applied to defeat the sophisticated jammers like the repeat-back

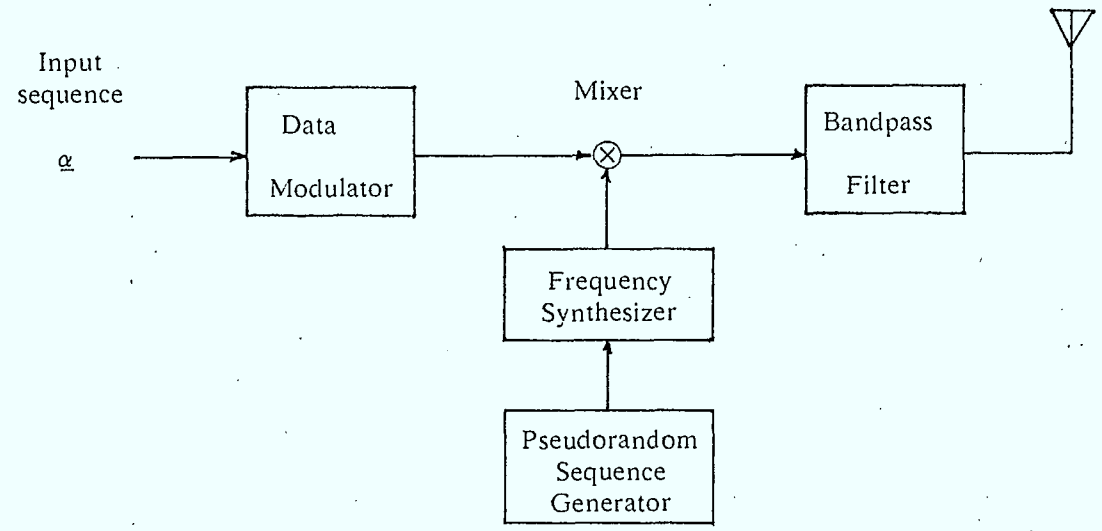

Transmitter

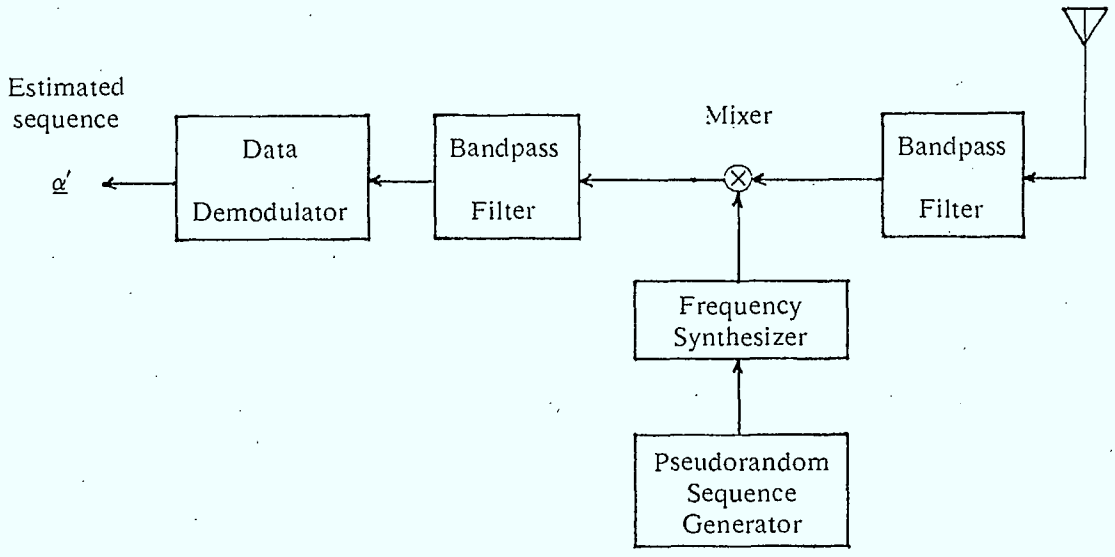

Receiver

Figure 1.1 A frequency-hopped spread spectrum system

jammer. When fast frequency hopping is used, some frequency diversity gain is seen (the same data is transmitted several times using different frequencies). This is particularly beneficial in a partial band jamming environment [3, p.354]. However, for a given spread spectrum bandwidth, the processing gain does not increase as the hopping rate increases. (How fast one hops between channels does not increase the number of available channels and, therefore, processing gain does not increase as the hopping rate increases.) The processing gain actually will decrease because of a reduction in the number of independent frequency-hopped bands within a given spread spectrum bandwidth due to the increase in the bandwidth of the frequency-hopped signal in any particular hop interval when faster hopping is employed.

For less critical antijam applications, slow frequency hopping [4], in which the carrier frequency remains constant for a time period far in excess of the propagation time may be employed. This usually allows many data bits to be transmitted at each frequency and the resulting transmitter and receiver equipment is simpler and less expensive than that for a faster frequency hopping. The point is higher data rate transmission can be achieved. Slow frequency hopping can also be used to interleave many frequency multiplexed channels within the same spread bandwidth for a multiple-user system. The multiple-access system will make it difficult for the jammer to identify a specific target signal [4].

Because of the difficulty of building truly coherent frequency synthesizers for spreading and despreading the desired information, that will hop quickly over a wide band, most frequency-hopped spread spectrum systems use noncoherent modulation schemes. Frequency-hopped noncoherent M-ary frequency shift keying (FH/NCMFSK) is the most widely used frequency hopping scheme. Its performance over channels of different characteristics and in various types of jamming environments has been studied extensively [1-13]. The degradation in the performance of FH/NCMFSK due to the effect of various imperfections in implementation such as frequency offset and phase jitter has also been studied [12,13]. The effect

of varying the processing gain of a FH/NCMFSK system using nonorthogonal tones under the constraint of fixed total spread spectrum bandwidth in the presence of partial-band noise jamming and partial-band tone jamming has also been studied [6].

Another popular frequency-hopped spread spectrum system reported in the literature is frequency-hopped differential phase shift keying (FH/DPSK) [14-16]. However, very often the system is assumed to be coherent, such that the carrier phase remains continuous when the frequency is changed. At high implementation frequency such as at the EHF band, coherent phase between hops is difficult to achieve. In fact, Lee and Miller state that frequency-hopped systems employing DPSK modulation and differentially coherent detection are not commonly employed in practice [15].

Several slow frequency-hopped spread spectrum schemes, including binary phase shift keying (BPSK), quadrature phase shift keying (QPSK) and M-ary orthogonal signaling under partial-band noise jamming and partial-band tone jamming have been considered in [8] where a slow frequency-hopped system model is adopted with coherent dehopping and demodulation. Slow frequency-hopped MFSK in simultaneous partial-band and repeat-back jamming has also been studied in [9]. Due to the vulnerability of slow frequency hopping to a repeat-back jammer, other measures such as coding, diversity and interleaving for improved antijam capability have been introduced [8,9]. A multiple-access system using slow frequency-hopped FSK has been considered and bounds and approximations are obtained for the average error probabilities over nonselective fading and wide-sense-stationary uncorrelated-scattering fading channels [11].

Consider a frequency-hopped spread spectrum system that is required to handle high speed data. Thus although on an absolute scale the frequency hopping may be fast, relative to the data rate we can have a slow frequency hopping situation, that is, many or at least several

bits of data are transmitted per chip or hop interval. Due to the wideband nature of the high speed data, a bandwidth efficient modulation scheme is highly desirable in order to enhance the electronic counter-countermeasure performance and to allow more users. When several bits are to be transmitted over a hop interval, a bandwidth efficient continuous phase modulation scheme can be used rather than simple noncoherent M-ary FSK. Recent studies have shown that continuous phase modulation (CPM) [17] schemes are band-efficient and are also power efficient when detected coherently. Correlative encoding [18], also termed partial response signaling (PRS) [19], can be used for spectral shaping and to gain spectral efficiency. Furthermore, baseband pulse shaping can be used to obtain more compact spectra as well.

The use of binary CPM schemes in a direct sequence spread spectrum system has been studied [20]. In this system, during a symbol interval the transmitter transmits one of the two different CPM waveforms generated from two different chip sequences corresponding to +1 and -1 depending on the transmitted data. The use of CPM in a direct sequence spread spectrum system is to concentrate the power in a given spread bandwidth and to control the level of energy contained in the spectral sidelobes.

The reason for proposing the use of band-efficient CPM schemes for transmitting a number of symbols per hop in a frequency-hopped system [21-24] is to obtain a more compact frequency-hopped signal bandwidth such that more frequency-hopped bands are available in a given spread bandwidth, to increase processing gain and to allow more users in a multiple-access communication system. Also, it should be noted that the slow frequency hopping situation under consideration here may arise as a result of a high data rate rather than a particularly slow absolute hopping rate. The system may have a hop time shorter than the sum of the processing time of the jammer plus the difference in arrival time between the communication and jamming signals, as in a fast frequency hopping system. Hence the usual disadvantage of slow frequency hopping such as vulnerability to a sophisticated jammer may not apply.

Even if slow frequency hopping in the usual sense is considered, the system can be useful either against simple jammers, or in conjunction with frequency division multiplexing of many signals in the wide spread spectrum system bandwidth to provide multiple-access communications. In many cases, these features, along with the lower relative cost compared with fast frequency hopping, may make this slow frequency hopping technique attractive.

1.2 Outline of the Report

The bandwidth occupied by the frequency-hopped spread spectrum signal is of prime importance as it relates directly to the processing gain, hence the degree of antijam protection achievable, and the number of possible users. Thus the power spectral density of the frequency-hopped spread spectrum signal will be evaluated in Chapter Two. The baseband autocorrelation function of the frequency-hopped spread spectrum signal is first derived. The power density spectrum is then easily obtained via a Fast Fourier Transform of the autocorrelation function. Results are presented for rectangular as well as raised cosine pulse shaping for various partial response encoding polynomials and different lengths of hop interval.

In Chapter Three, noncoherent receivers for demodulating the frequency-hopped signal will be presented. A hop-by-hop maximum likelihood noncoherent receiver is first derived. This receiver, which is optimum over each hop interval, is impractical when the hop length is long, that is when a large number of bits are transmitted during each hop interval. And so a sequential decoding algorithm aiming to achieve the performance of a maximum likelihood sequence estimation (MLSE) algorithm is presented together with the receiver structure. A ML noncoherent receiver, which detects the transmitted sequence with maximum likelihood over the entire transmission period spanning frequency hops, is also derived. A sequential decoding algorithm with metric computation spanning hops is then presented together with possible decoding algorithm simplification. A suboptimum simplified noncoherent receiver, which treats

the symbol intervals in a hop as if they were noncoherent and neglects the phase states of the frequency-hopped CPM signal during a hop, is presented. The receiver structure and decoding algorithm for this simplified receiver will also be given.

In Chapter Four, performance of the hop-by-hop sequence estimation receiver will be evaluated first in an additive white Gaussian noise (AWGN) environment. An upper bound on the bit error rate of the receiver under AWGN will be evaluated based on the union bound approach, with some approximations necessary for cases when the length of the hop interval is long. The bit error probability bounds for various correlative encoding schemes and different baseband pulse shaping will be presented for different lengths of hop interval. The receiver performance when a known symbol segment is transmitted at the beginning of each hop, for the purpose of synchronization and to improve the error performance, is also evaluated. Since ultimately the spread spectrum system is more likely to operate under intentional interference, the performance of the receiver in the presence of partial band noise jamming and multiple-tone jamming is also evaluated.

In Chapter Five, a computer simulation study of the hop-by-hop sequence estimation receiver will be presented in order to obtain a more precise error performance evaluation and to indicate the accuracy of the bounds evaluated in Chapter Four. Only frequency-hopped minimum shift keying (MSK) and differentially precoded duobinary MSK with rectangular pulse shaping are simulated for various hop lengths. Simulation results are compared with the corresponding error bounds evaluated in Chapter Four.

Finally in Chapter Six, conclusions are drawn and a summary of the report is given.

Chapter Two

SPECTRAL ANALYSIS

The spectral density function, or power spectrum, of a digitally modulated signal is an important characteristic, since it defines the distribution of average signal power as a function of frequency. Estimates of bandwidth occupancy, interference to or from adjacent channels, and relative comparisons of different modulation techniques all exemplify situations where a knowledge of the power spectrum is imperative. By calculating the power spectrum of the signal, all relevant information concerning the bandwidth efficiency can be obtained.

There are a large number of possible approaches for obtaining the power spectra of digital frequency modulated signals. In the direct approach by Anderson and Salz [25], the Fourier transform of the signal over the time interval from 0 to NT is first calculated. The power spectrum is then obtained by calculating the expected value of the square of the Fourier transform divided by the time duration NT, as N goes to infinity. Another approach is the Rowe-Prahbu method [26-28] which is a matrix method for which each possible modulator waveform is assigned to one of the dimensions of an N dimensional signal vector. The Fourier transform of this signal vector is then taken and multipled with other matrices and vectors to yield the power spectral density of the signal. An asymptotic expression for the power density spectrum at frequencies away from the center frequency can be obtained using the approach due to Baker [29]. Another approach due to Garrison [30] approximates the modulating pulses by a quantized staircase function and the resulting spectrum is computed. Note that while the power spectrum so obtained is an approximation for implementations using analog premodulation filters, it will be the power spectrum of the actual signal if the implementation uses D/A convertors to obtain the modulating pulses. An easy way to calculate the power spectra for

digital FM is the so-called autocorrelation function method [27,31,32], in which the autocorrelation function of the signal is first calculated. The power spectrum is then obtained via a Fourier transform on the autocorrelation function, usually calculated numerically. Computer simulation can also be used to estimate the power spectra.

Although the spectral properties of CPM schemes are well understood and had been calculated extensively [17,27,28,31,32], the spectral characteristics of FH/CPM have not been presented. In this Chapter the power spectral density of the slow frequency-hopped CPM spread spectrum signal will be derived using the autocorrelation function method, which is conceptually simple and straightforward to carry out. The model of the spread spectrum signal will first be presented.

2.1 Signal Model

The frequency-hopped spread spectrum signal considered in this report, is basically a continuous phase modulation signal but with a random phase jump every N transmitted symbols or every NT seconds. During any one hop interval, the modulation is assumed to be coherent frequency modulation, with correlative, or partial response encoding and shaping of the modulating pulses permissible. The information to be transmitted as denoted by $\underline{\alpha} = \{ \ldots, \alpha_{-2}, \alpha_{-1}, \alpha_0, \alpha_1, \alpha_2, \ldots \}$ is a sequence of uncorrelated input data symbols. For an M-ary scheme, each data symbol can take any of the values $\alpha_i = \pm 1, \pm 3, \ldots, \pm (M-1)$ with equal probability 1/M. The frequency-hopped correlative encoded CPM signal can be represented by

$$s(t) = \sqrt{\frac{2E}{T}} \sum_{i=-\infty}^{\infty} p(t - iNT) \cos[2\pi f_i t + \psi(t, \underline{\alpha}) + \theta_i], \qquad (2.1)$$

where E is the symbol energy, T is the symbol time, N is the number of symbols in a hop interval, p(t) is a unit amplitude rectangular pulse of length NT given by

$$p(t) = \begin{cases} 1 & 0 < t < NT \\ 0 & \text{elsewhere,} \end{cases} \tag{2.2}$$

f_i is the carrier frequency during the i^{th} hop, θ_i is the random unknown initial phase at the beginning of the i^{th} hop, and the θ_i's are assumed to be independent random variables uniformly distributed from 0 to 2π. $\psi(t, \underline{\alpha})$ is the information carrying phase function given by

$$\psi(t, \underline{\alpha}) = 2\pi h \sum_{n=-\infty}^{\infty} \alpha_n \, q(t - nT), \tag{2.3}$$

where h is the modulation index, q(t) is the phase response given by

$$q(t) = \int_{-\infty}^{t} g(\tau) \, d\tau. \tag{2.4}$$

g(t) is called the frequency pulse. Normally it is a positive smooth pulse shape over a finite time interval $0 < t < LT$ and zero elsewhere. Thus L is the length of the frequency pulse in units of the symbol time T. The shape of g(t) determines the smoothness of the transmitted information carrying phase and influences the power density spectrum of the signal. In general, the smoother the resultant phase path of the signal for a given modulation index, the more compact is the spectrum. Correlative encoding or partial response signaling is one technique for generating a smoother phase path. A correlative encoder is characterized by its partial response system (PRS) polynomial [18,19]

$$F(D) = \frac{1}{C} (k_0 + k_1 D + k_2 D^2 + \ldots + k_m D^m) \tag{2.5}$$

where D is Huffman's delay operator and the k_ℓ's are the coefficients of the polynomial. For convenience a normalization of the polynomial has been carried out with the normalization constant C given by

$$C = \sum_{\ell=0}^{m} | k_\ell |. \tag{2.6}$$

The effect of the correlative encoding is to create a new equivalent frequency pulse g(t) given by

$$g(t) = \frac{1}{C} \sum_{i=0}^{m} k_i \, b(t - iT), \tag{2.7}$$

where b(t) is the baseband pulse with a duration of one symbol interval. For a rectangular baseband pulse, b(t) is given by

$$b(t) = \begin{cases} \frac{1}{2T} & 0 < t < T \\ 0 & \text{elsewhere,} \end{cases} \tag{2.8}$$

Spectral shaping can be accomplished by the choice of system polynomial F(D) and by using various baseband pulse shapes such as the raised cosine for which b(t) is given by

$$b(t) = \begin{cases} \frac{1}{2T} (1 - \cos \frac{2\pi}{T} t) & 0 < t < T \\ 0 & \text{elsewhere.} \end{cases} \tag{2.9}$$

The length of the frequency pulse g(t) is then $L = m + 1$ symbol intervals. For the PRS polynomial F(D) and the amplitude of the baseband pulse b(t) specified above, the phase response q(t) is normalized such that

$$q(LT) = \frac{1}{2}. \tag{2.10}$$

This means that for schemes with positive frequency pulses of finite length, the maximum absolute phase change over any symbol interval is $(M - 1)h\pi$.

2.2 Spectral Analysis

Among the various methods mentioned at the beginning of this Chapter, the autocorrelation function method [27,31,32], is straightforward and easy to to use. With this method the autocorrelation function is first calculated and then the Fourier transform is numerically calculated, yielding the power spectrum.

In order to determine the power spectrum of the frequency-hopped spread spectrum signal, it is sufficient to consider the normalized complex lowpass equivalent signal $u(t, \underline{\alpha})$ as given by

$$u(t, \underline{\alpha}) = \sum_{i=-\infty}^{\infty} p(t - iNT) \exp [j\theta_i] \exp [j\psi(t, \underline{\alpha})]. \tag{2.11}$$

The complex lowpass autocorrelation function is then given by

$$R_u(t, t + \tau) = < E_\theta \{ u^*(t, \underline{\alpha}) u(t + \tau, \underline{\alpha}) \} > \tag{2.12}$$

where the superscript * denotes the complex conjugate, $< . >$ denotes the ensemble average with respect to the information symbols and $E_\theta \{.\}$ denotes the expectation with respect to the random phase. Substituting Eq.(2.11) into Eq.(2.12), we have

$$\begin{aligned} R_u(t, t+\tau) &= < E_\theta \{ \sum_{i=-\infty}^{\infty} p(t - iNT) \exp[-j\theta_i] \exp[-j\psi(t, \underline{\alpha})] \\ &\quad \sum_{\ell=-\infty}^{\infty} p(t + \tau - \ell NT) \exp[j\theta_\ell] \exp[j\psi(t+\tau, \underline{\alpha})] \} > \\ &= < E_\theta \{ \sum_{i=-\infty}^{\infty} \sum_{\ell=-\infty}^{\infty} \exp[j(\theta_\ell - \theta_i)] p(t - iNT) p(t + \tau - \ell NT) \\ &\quad \exp[j(\psi(t+\tau, \underline{\alpha}) - \psi(t, \underline{\alpha}))] \} >. \end{aligned} \tag{2.13}$$

Since the θ_i's are statistically independent and uniformly distributed in $[0, 2\pi]$

$$E_\theta \{ \exp[j(\theta_\ell - \theta_i)] \} = \delta_{i,\ell}. \tag{2.14}$$

Hence,

$$R_u(t, t+\tau) = \sum_{i=-\infty}^{\infty} p(t - iNT) p(t + \tau - iNT) R_{CPM}(t, t+\tau) \tag{2.15}$$

where $R_{CPM}(t, t+\tau)$ is used to denote the complex baseband autocorrelation function of the CPM signal without any frequency hopping and is given by

$$\begin{aligned} R_{CPM}(t, t+\tau) &= < \exp[j(\psi(t+\tau, \underline{\alpha}) - \psi(t, \underline{\alpha}))] > \\ &= < \exp[j 2\pi h \sum_{n=-\infty}^{\infty} \alpha_n [q(t+\tau - nT) - q(t - nT)]] >. \end{aligned} \tag{2.16}$$

The sum in the exponent in Eq.(2.16) can be written as a product and averaged with respect to the sequence $\underline{\alpha}$. Assuming that the M-ary data are independent and take on the values of $\pm 1, \pm 3, \ldots, \pm (M-1)$ with equal probability 1/M, we have

$$R_{CPM}(t, t+\tau) = \prod_{n=-\infty}^{\infty} \{ \frac{2}{M} \sum_{j=1}^{M/2} \cos 2\pi h(2j-1)[q(t+\tau-nT) - q(t-nT)]\}. \tag{2.17}$$

It can be easily observed from Eq.(2.17) that $R_{CPM}(t,t+\tau)$ is periodic in t with a period of T. However, $R_u(t,t+\tau)$ as given by Eq.(2.15) is periodic in t with a period of NT. Since in practice we do not have a precise time origin, we can assume that the origin is uniformly distributed over [0, NT]. The average autocorrelation is then given by

$$\begin{aligned} R_u(\tau) &= \frac{1}{NT} \int_0^{NT} R_u(t, t+\tau)\, dt \\ &= \frac{1}{NT} \int_0^{NT} \sum_{i=-\infty}^{\infty} p(t - iNT)\, p(t+\tau - iNT)\, R_{CPM}(t, t+\tau)\, dt \\ &= \frac{1}{NT} \int_{-\infty}^{\infty} p(t)\, p(t+\tau)\, R_{CPM}(t, t+\tau)\, dt. \end{aligned} \tag{2.18}$$

It can be easily seen that

$$R_u(\tau) = \begin{cases} \frac{1}{NT} \int_0^{NT-\tau} R_{CPM}(t, t+\tau)\, dt & 0 < \tau < NT \\ \frac{1}{NT} \int_{-\tau}^{NT} R_{CPM}(t, t+\tau)\, dt & -NT < \tau < 0 \\ 0 & |\tau| > NT. \end{cases} \tag{2.19}$$

Since $R_{CPM}(t, t+\tau)$ as given by Eq.(2.17) is real, $R_u(\tau)$ is then also real and therefore an even function of τ.

$$R_u(\tau) = R_u(-\tau). \tag{2.20}$$

Hence, we need to consider only positive τ. Let $\tau = aT + \tau'$, where $0 \le \tau' \le T$ and $a = 0, 1, 2, \ldots, N-1$. We have

$$
\begin{aligned}
R_u(\tau) &= R_u(aT + \tau') \\
&= \frac{1}{NT} \int_0^{(N-a)T-\tau'} R_{CPM}(t, t + aT + \tau')\, dt \\
&= \frac{1}{NT} \left\{ \int_0^{(N-a-1)T} R_{CPM}(t, t + aT + \tau')\, dt + \int_{(N-a-1)T}^{(N-a)T-\tau'} R_{CPM}(t, t + aT + \tau')\, dt \right\} \\
&= \frac{1}{NT} \left\{ \sum_{k=0}^{N-a-2} \int_{kT}^{(k+1)T} R_{CPM}(t, t + aT + \tau')\, dt + \int_{(N-a-1)T}^{(N-a)T-\tau'} R_{CPM}(t, t + aT + \tau')\, dt \right\} .
\end{aligned}
\tag{2.21}
$$

Since $R_{CPM}(t, t + \tau)$ as given by Eq.(2.16) is periodic in t with a period of T, integrating over any interval of [kT, (k+1)T] with respect to t will be the same as integrating over [0, T]. Hence we have

$$
\begin{aligned}
R_u(\tau) &= R_u(aT + \tau') \\
&= \frac{1}{NT} \left\{ \sum_{k=0}^{N-a-2} \int_0^{T} R_{CPM}(t, t + aT + \tau')\, dt + \int_0^{T-\tau'} R_{CPM}(t, t + aT + \tau')\, dt \right\} \\
&= \frac{1}{NT} \left\{ (N - a - 1) \int_0^{T} R_{CPM}(t, t + aT + \tau')\, dt + \int_0^{T-\tau'} R_{CPM}(t, t + aT + \tau')\, dt \right\} \\
&= \frac{N - a - 1}{NT} \int_0^{T} R_{CPM}(t, t + aT + \tau')\, dt + \frac{1}{NT} \int_0^{T-\tau'} R_{CPM}(t, t + aT + \tau')\, dt ;
\end{aligned}
$$

$$
\begin{aligned}
&\tau = \tau' + aT , \\
&0 \le \tau' < T , \\
&a = 0, 1, 2, \ldots, N-1,
\end{aligned}
\tag{2.22}
$$

where $R_{CPM}(t, t + aT + \tau')$ consists of an infinite product of terms as rewritten below by substituting $\tau = aT + \tau'$ into Eq.(2.17)

$$R_{CPM}(t, t + aT + \tau') = \prod_{n=-\infty}^{\infty} \{ \frac{2}{M} \sum_{j=1}^{M/2} \cos 2\pi h(2j-1)[q(t + \tau' - (n-a)T) - q(t-nT)]\}. \quad (2.23)$$

The number of terms in the infinite product in the above equation can be reduced, since the frequency pulse is of finite duration LT. From Eq.(2.4) it can be noted that

$$q(t + \tau' - (n-a)T) = q(t - nT) = 0 \qquad \text{for} \quad t + \tau' - (n - a)T < 0 \quad (2.24)$$

and

$$q(t + \tau' - (n-a)T) = q(t - nT) = q(LT) \qquad \text{for} \quad t - nT > LT. \quad (2.25)$$

Hence for $t + \tau' - (n - a)T < 0$ and $t - nT > LT$ the product terms will be equal to unity and can be omitted from Eq.(2.23). Since only $t \in [0, T]$ need be considered for calculating $R_u(\tau)$ as is evident from Eq.(2.22) and also from the fact that $R_{CPM}(t,t + \tau)$ is periodic in t with period T, the product terms in Eq.(2.23) will be unity for $n \geq a+2$ and $n \leq -L$. The infinite product in Eq.(2.23) then reduces to

$$\begin{aligned} R_{CPM}(t, t + \tau) &= R_{CPM}(t, t + aT + \tau') \\ &= \prod_{n=1-L}^{a+1} \{ \frac{2}{M} \sum_{j=1}^{M/2} \cos 2\pi h(2j-1)[q(t + \tau' - (n-a)T) - q(t-nT)] \}. \end{aligned} \quad (2.26)$$

The power spectral density of the dehopped signal is then given by

$$S_s(f) = \frac{E}{2T} \{ S_u(f + f_c) + S_u(-f - f_c) \} \quad (2.27)$$

where f_c is the intermediate carrier frequency and $S_u(f)$ is the power spectrum of the equivalent lowpass signal $u(t, \underline{\alpha})$ defined as

$$S_u(f) = \int_{-\infty}^{\infty} R_u(\tau)\, e^{-j 2\pi f \tau} d\tau. \tag{2.28}$$

Since $R_u(\tau)$ is real and even and $R_u(\tau) = 0$ for $|\tau| > NT$, from Eqs.(2.19) and (2.20), we have

$$S_u(f) = 2\int_0^{NT} R_u(\tau)\, \cos\, 2\pi f \tau\, d\tau \tag{2.29}$$

where $R_u(\tau)$ is given by Eq.(2.22). The dehopped signal spectrum can then be calculated by using Eqs.(2.29),(2.22) and (2.27). Numerical integration is performed according to Eq.(2.22) for calculating the autocorrelation function, which is then numerically Fourier transformed to obtain the spectrum.

2.3 Results

The power density spectra of the dehopped signals with various partial response encodings together with different baseband pulse shapings have been calculated. The unspread power density spectra for frequency-hopped MSK for different lengths of hop interval are shown in Fig. 2.1. As the length of the hop interval increases, the dehopped power density spectrum becomes more compact and approaches that of coherent MSK without frequency hopping. The dehopped spectrum of frequency-hopped MSK is almost identical to the spectrum of coherent MSK for hop intervals of length greater than 2048 T.

With a modulation index of 0.7 and no correlative encoding, the spectrum of hopped CPFSK is as shown in Fig. 2.2. If a comparison is made with the spectrum of MSK which has a modulation index of 0.5, we see that a change in the modulation index from 0.5 to 0.7 changes

the shape of the spectrum quite significantly especially for short hop intervals. There are large side lobes when the length of the hop interval is equal to the transmitted symbol interval T.

To see the effect of correlative encoding on the signal spectrum, the spectra for duobinary MSK are shown in Fig. 2.3. Again the bandwidth occupied by the frequency-hopped signal reduces as the length of the hop interval increases, and the spectrum approaches that of coherent duobinary MSK as the length of the hop interval becomes large. If the spectra are compared with MSK without correlative encoding, we notice that correlative encoding does not give much bandwidth reduction for short hop intervals. With long hop intervals it does. For the same duobinary polynomial $(1+D)/2$, but a higher modulation index of 0.7, the spectra for the different hop lengths are as shown in Fig. 2.4. The signal bandwidth increases with an increase in modulation index when the length of the hop interval is large. To see if a higher order encoding polynomial would give a further improvement in the spectral characteristic, spectra for the Tamed FM (TFM) polynomial, which for coherent signaling is known to be an attractive second order PRS polynomial, were calculated as shown in Fig. 2.5. A comparison of Fig. 2.5 and Fig. 2.1, shows that even for a higher order polynomial the reduction in bandwidth is insignificant at short hop intervals. However, for long hop intervals the higher order PRS polynomial yields a spectrum of even greater compactness with very low sidelobes.

To illustrate the effects of baseband pulse shaping on the spectra, the spectra for raised cosine pulse shaping with various encoding polynomials are as shown in Figs. 2.7 to 2.10. For long hop lengths the spectra of the signals with raised cosine shaping are more compact than their rectangularly shaped counterparts.

A spectral occupancy comparison of the frequency-hopped signals with different modulation indices, partial response encodings, pulse shapings and lengths of hop interval is made by calculating the 99 percent power bandwidth of the frequency-hopped signals. The 99 percent

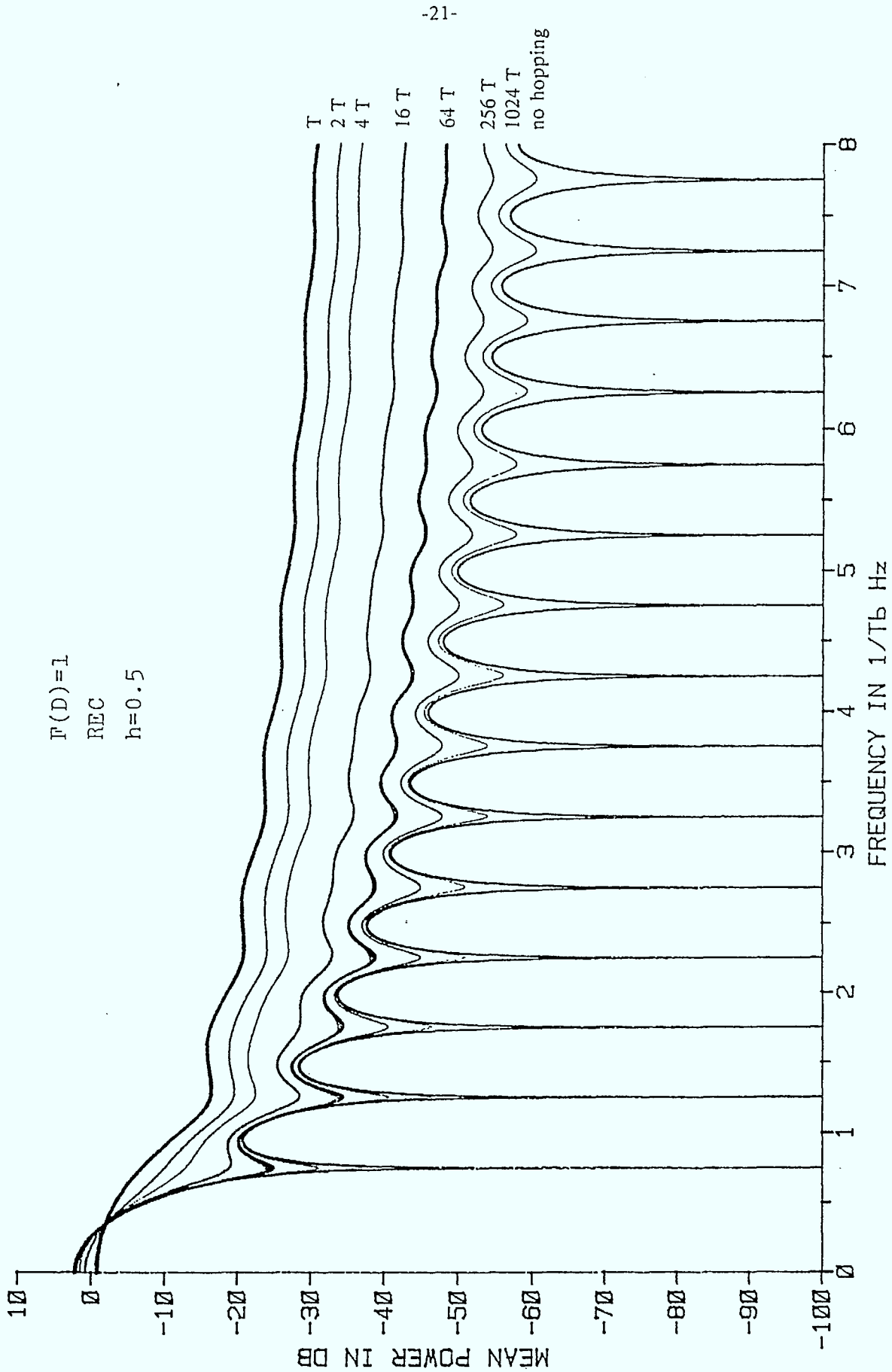

Figure 2.1 Spectra of FH/MSK with rectangular pulse shaping

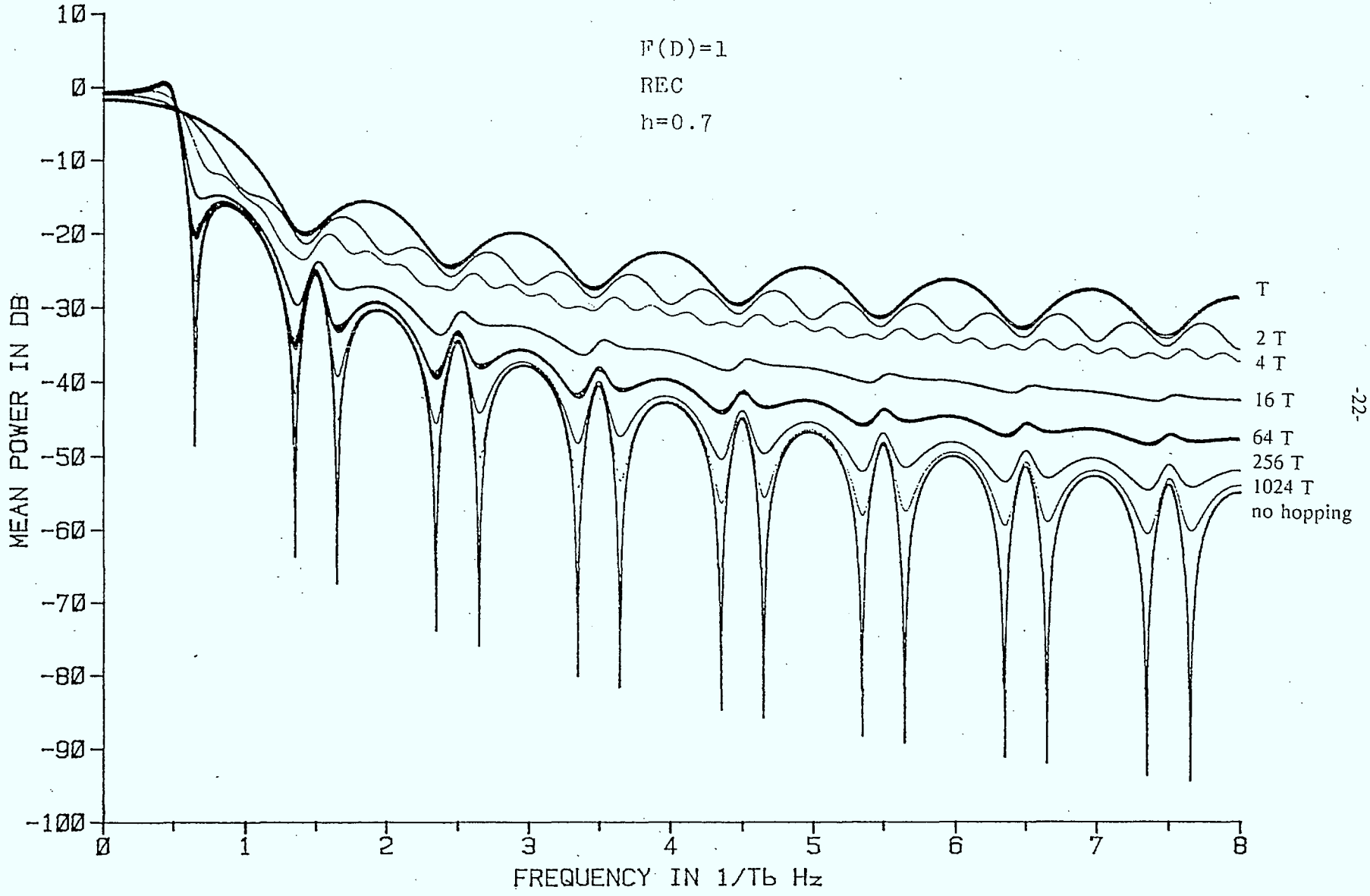

Figure 2.2 Spectra of FH/CPFSK, h = 0.7 with rectangular pulse shaping

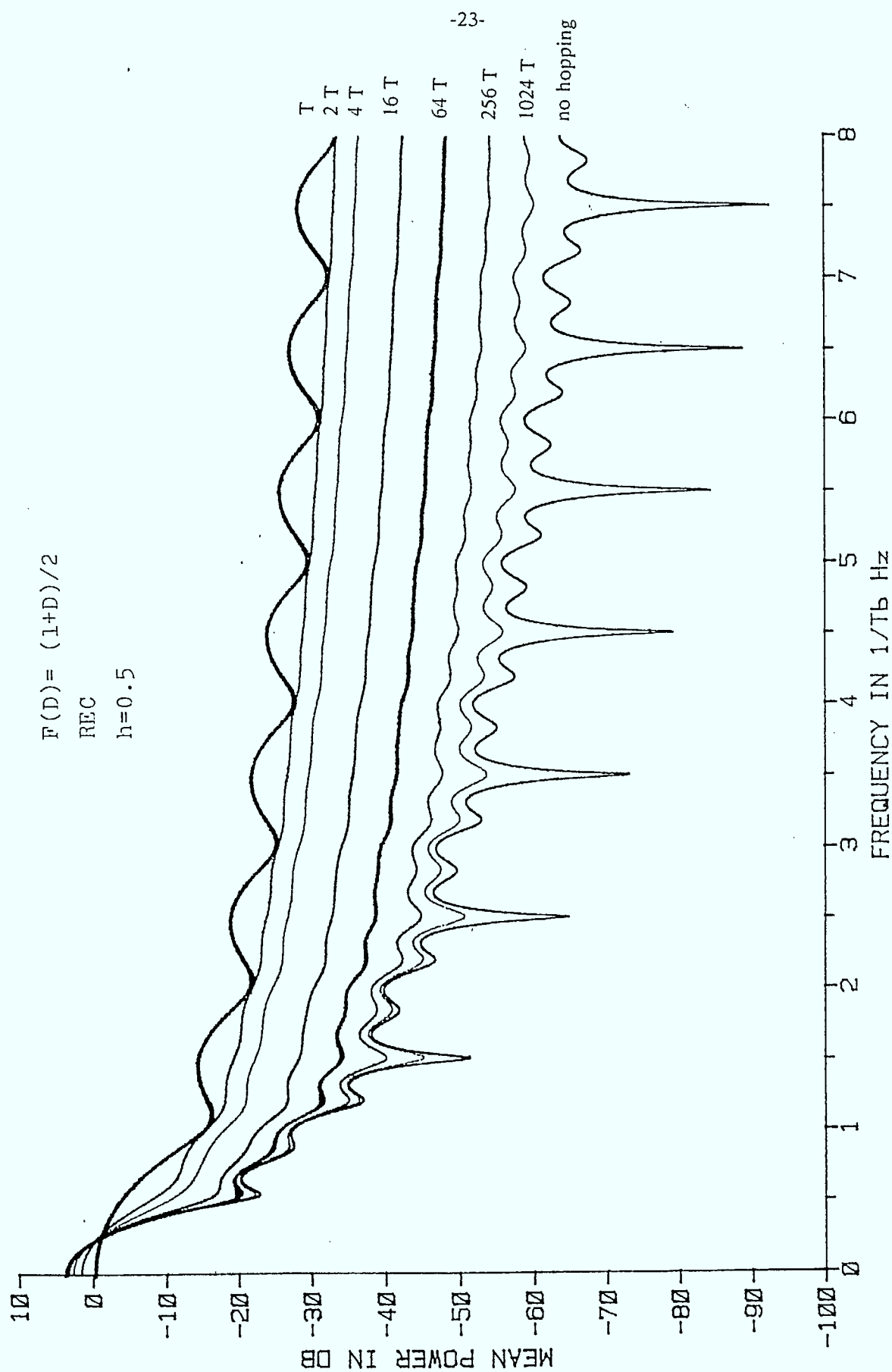

Figure 2.3 Spectra of FH/DMSK with rectangular pulse shaping

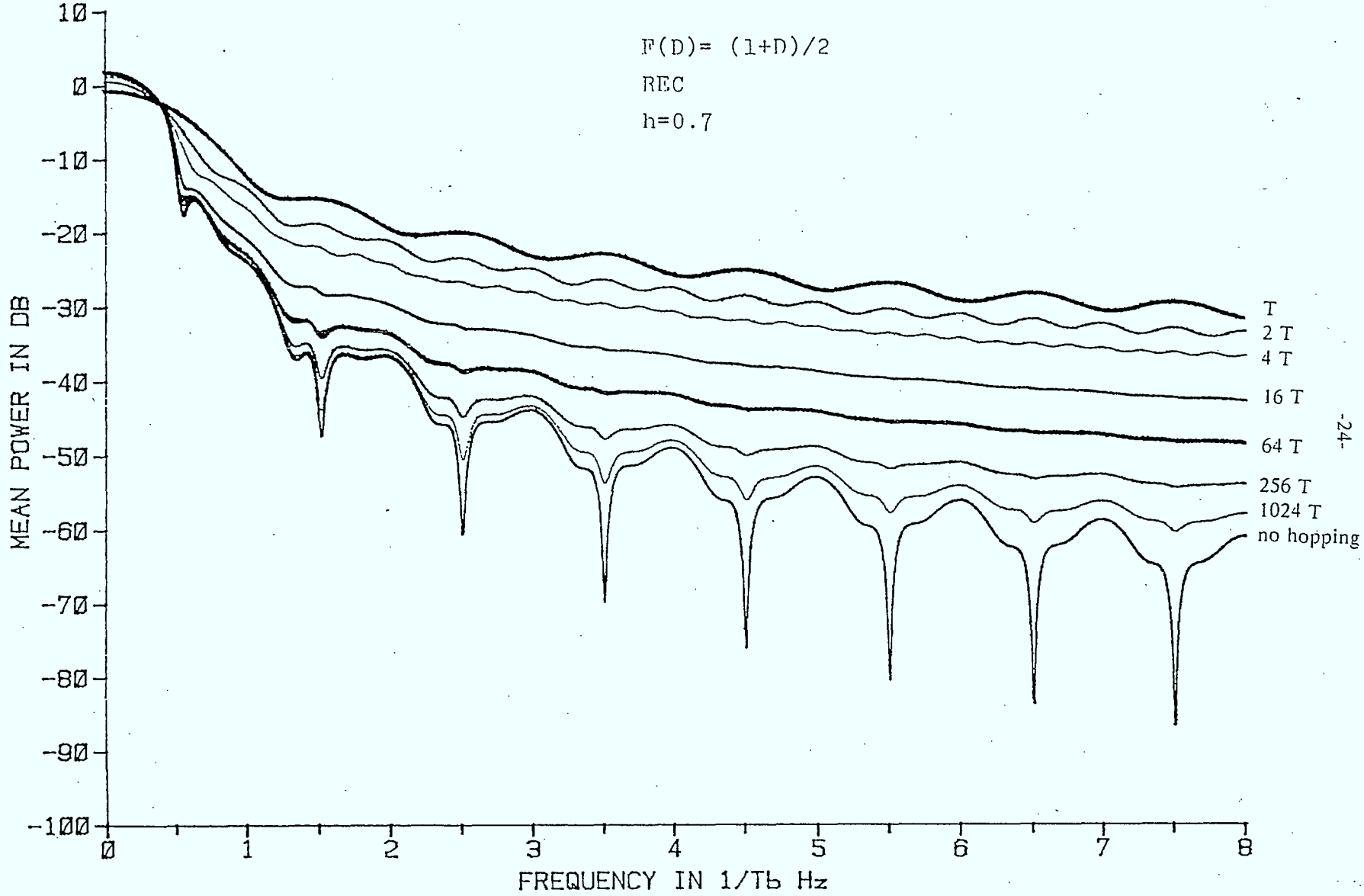

Figure 2.4 Spectra of FH/duobinary FSK, h = 0.7 with rectangular pulse shaping

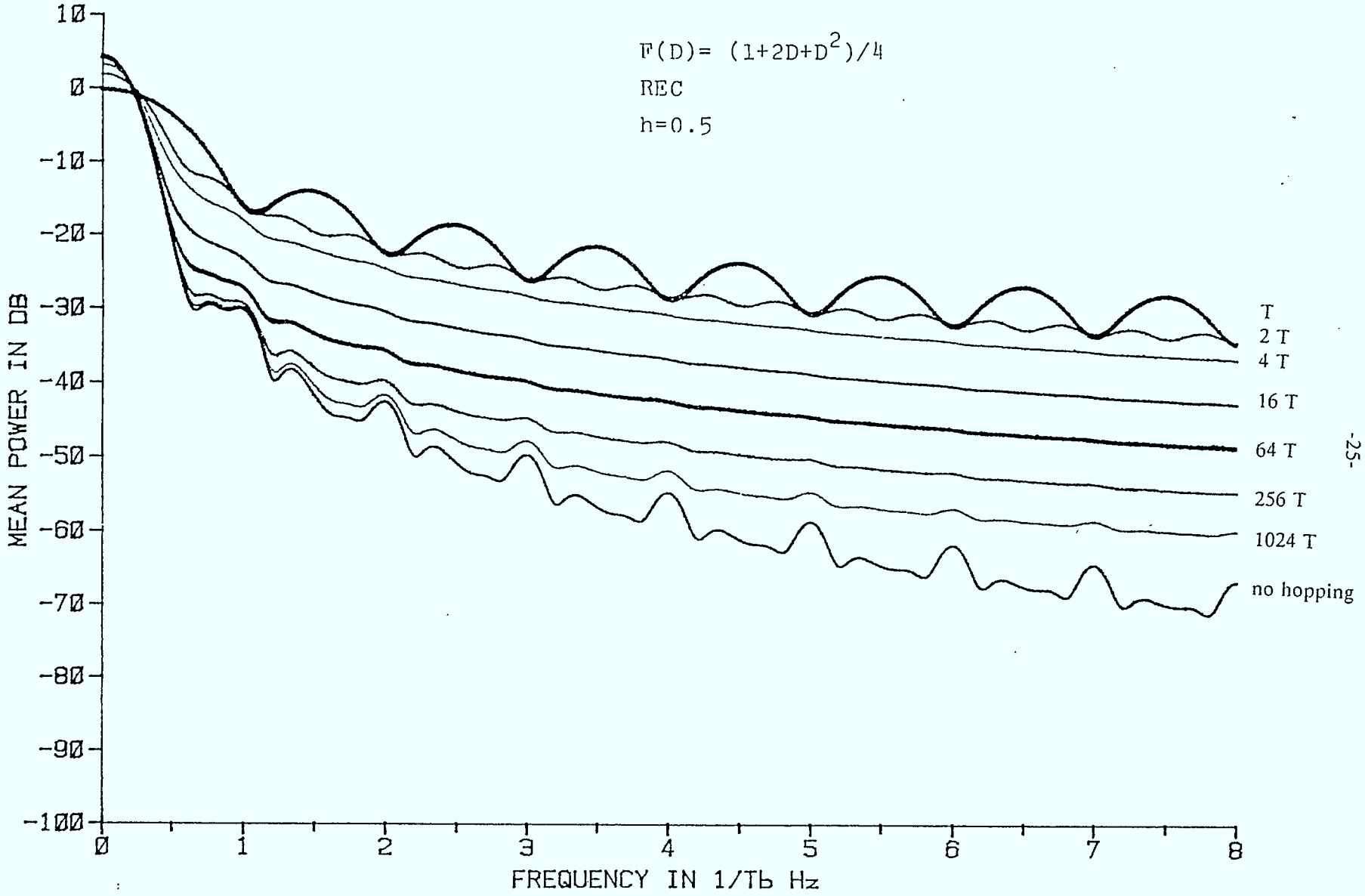

Figure 2.5 Spectra of FH/TFM, h = 0.5 with rectangular pulse shaping

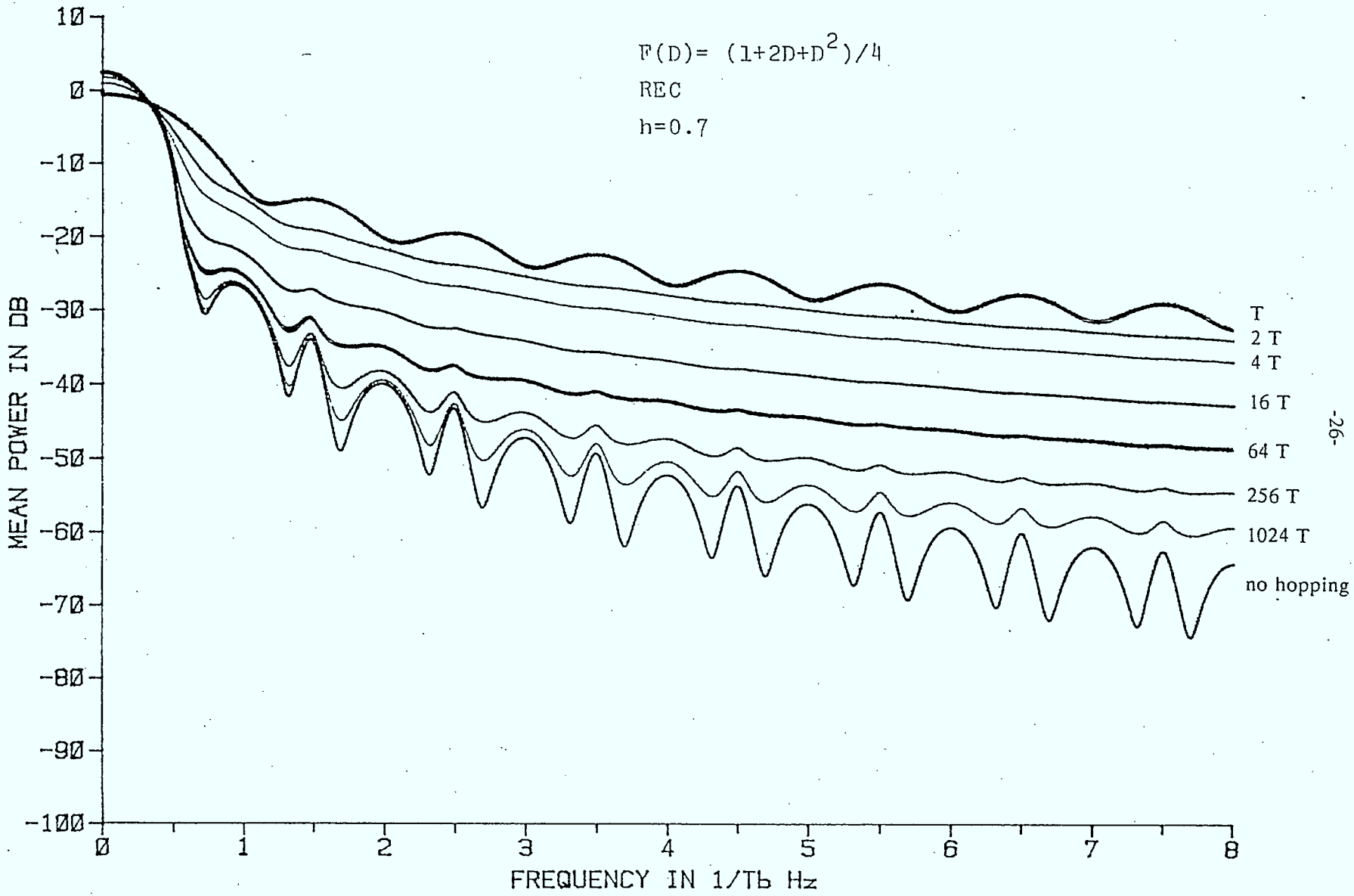

Figure 2.6 Spectra of FH/TFM, h = 0.7 with rectangular pulse shaping

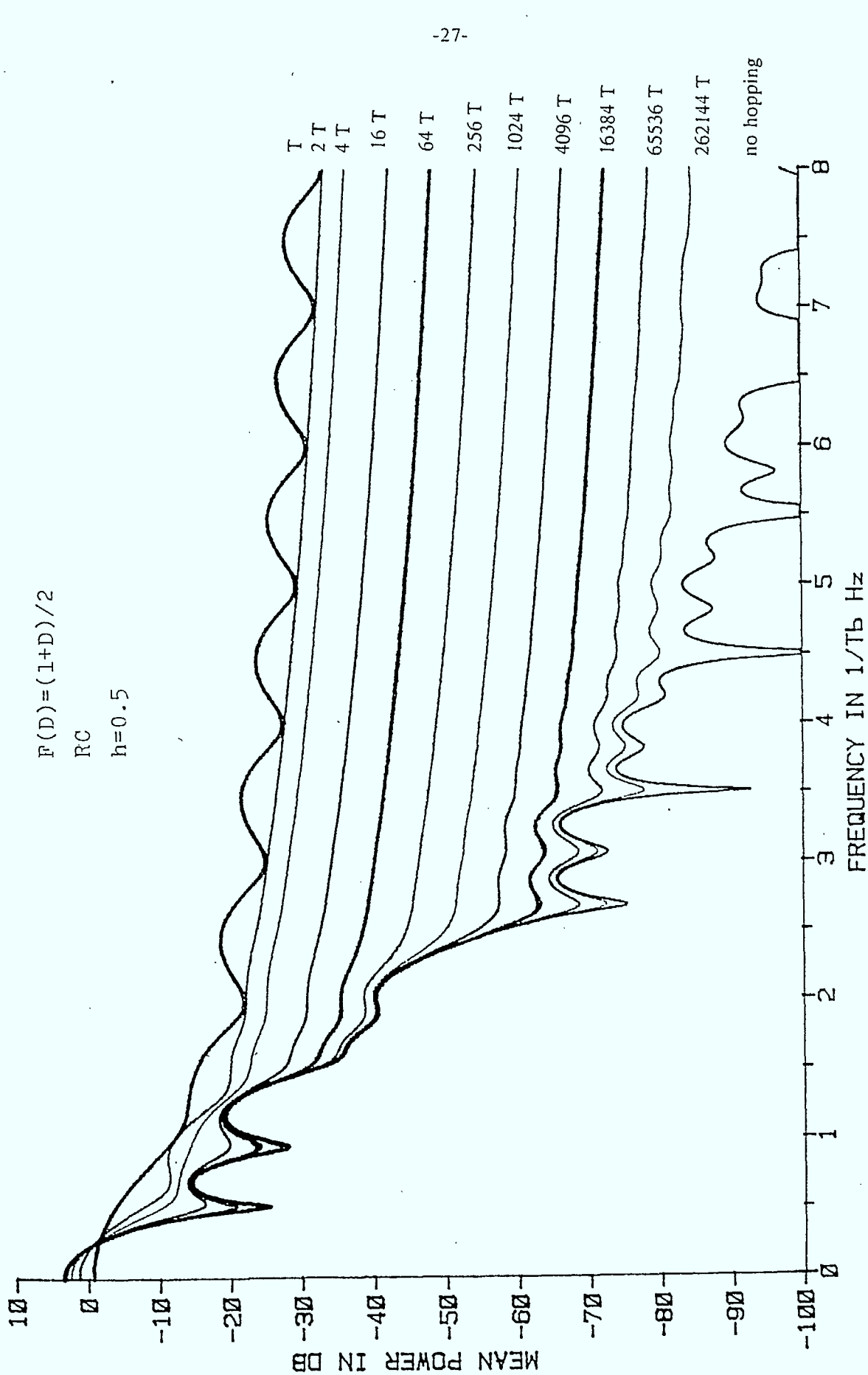

Figure 2.7 Spectra of FH/DMSK with raised cosine pulse shaping

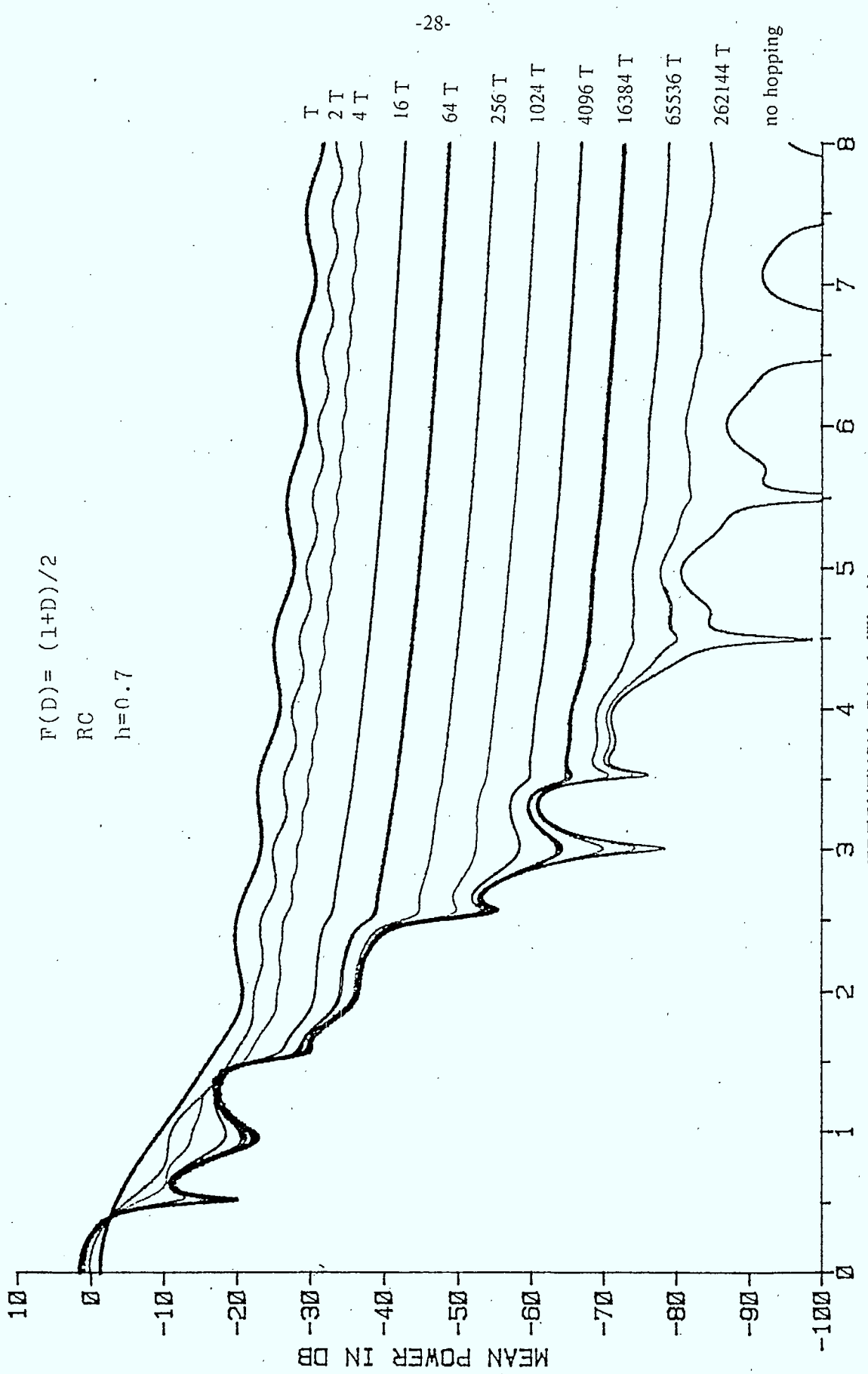

Figure 2.8 Spectra of FH/duobinary FSK, h = 0.7 with raised cosine pulse shaping

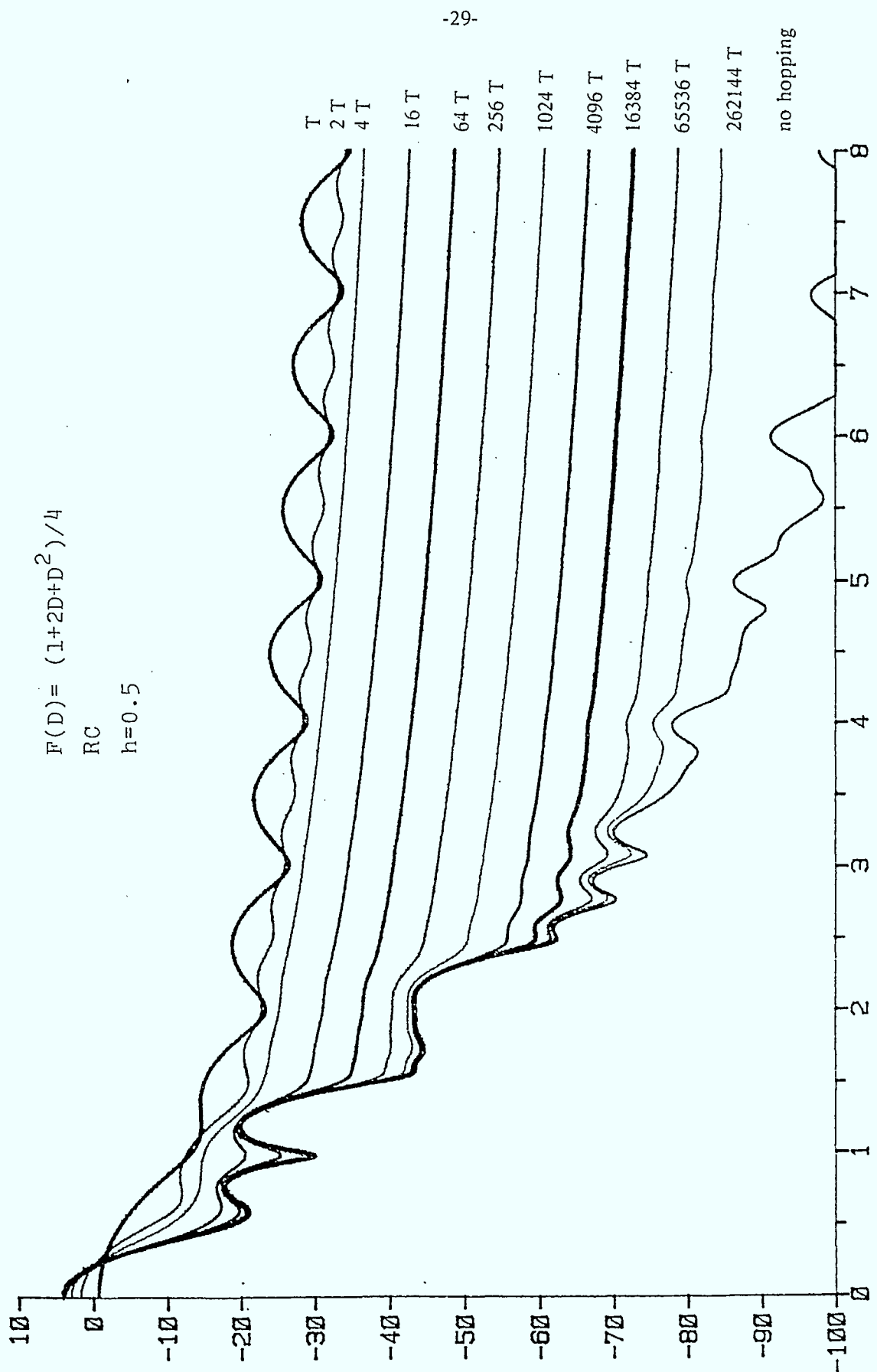

Figure 2.9 Spectra of FH/TFM, h = 0.5 with raised cosine pulse shaping

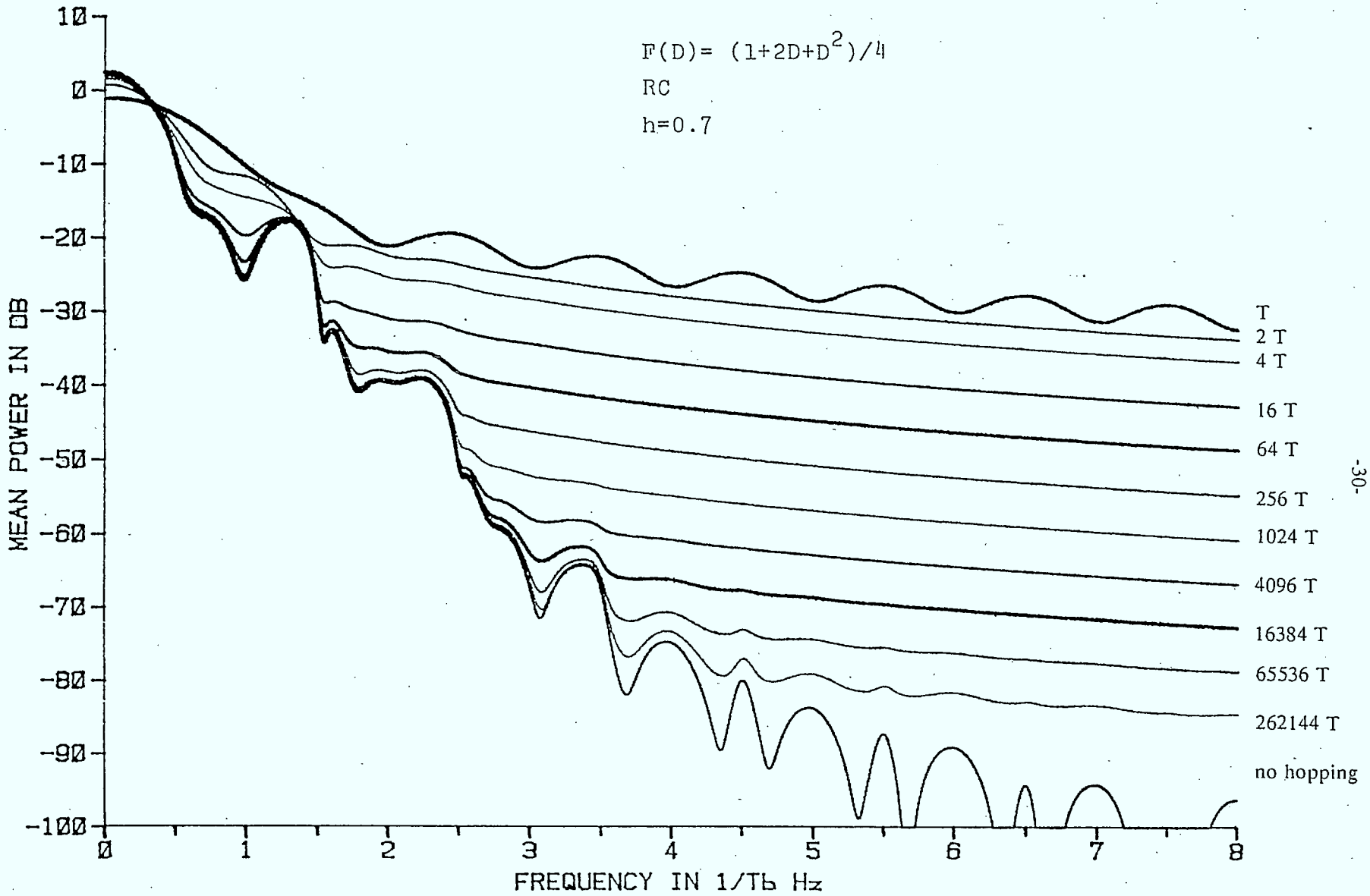

Figure 2.10 Spectra of FH/TFM, h = 0.7 with raised cosine pulse shaping

power bandwidths of the various frequency-hopped signals with rectangular pulse shaping and raised cosine pulse shaping are tabulated in Table 1 and Table 2 respectively for different lengths of hop interval. We can see that the 99 percent power bandwidth of the FH/CPM signal decreases with the increase in the length of hop interval. In general, with a hop length greater than 1024 symbol intervals, the 99 percent power bandwidth of the FH/CPM signal is the same as that for the CPM signal with no frequency hopping. Comparing entries in Table 1 with those in Table 2, it can be seen that the 99 percent power bandwidth of the FH/CPM signal with rectangular pulse shaping is smaller than the corresponding 99 percent power bandwidth of the same modulation scheme but with raised cosine pulse shaping. However, it should be noted that while the 99 percent power bandwidth is smaller for rectangular pulse shaping, the same modulation scheme but with raised cosine pulse shaping actually has a more compact spectral mainlobe and lower sidelobes as shown previously.

N	99% bandwidth in 1/T					
	F(D) = 1		F(D) = (1 + D)/2		F(D) = (1 + 2D + D²)/4	
	h = 0.5	h = 0.7	h = 0.5	h = 0.7	h = 0.5	h = 0.7
1	18.844	18.688	18.891	18.859	18.891	18.875
2	9.9375	9.9688	9.9375	9.9688	9.9375	9.9531
4	5.1875	5.2656	5.0938	5.1250	5.0781	5.1094
16	1.8906	2.1250	1.5938	1.8125	1.4688	1.6250
64	1.2813	1.8750	0.9688	1.3750	0.8438	1.0156
256	1.2031	1.8125	0.8906	1.2969	0.7813	0.9844
1024	1.1875	1.7969	0.8750	1.2813	0.7813	0.9688
No Hopping	1.1875	1.7813	0.8750	1.2813	0.7656	0.9688

Table 1 99 % power bandwidth comparison between different modulation schemes for rectangular pulse shaping

N	99% bandwidth in 1/T			
	$F(D) = (1 + D)/2$		$F(D) = (1 + 2D + D^2)/4$	
	h = 0.5	h = 0.7	h = 0.5	h = 0.7
1	18.875	18.844	18.891	18.859
2	9.9375	9.9531	9.9219	9.9375
4	5.0625	5.0781	5.0469	5.0625
16	2.2813	2.6719	2.1875	2.5313
64	1.7500	2.5156	1.6250	2.3438
256	1.6250	2.4688	1.5156	2.2656
1024	1.6094	2.4531	1.4844	2.2344
4096	1.5938	2.4531	1.4844	2.2344
16384	1.5938	2.4531	1.4844	2.2344
65536	1.5938	2.4531	1.4844	2.2344
262144	1.5938	2.4531	1.4844	2.2344
No Hopping	1.5938	2.4531	1.4844	2.2344

Table 2 99 % power bandwidth comparison between different modulation schemes for raised cosine pulse shaping

2.4 Summary

In this chapter, a model of the frequency-hopped CPM signal is presented. The baseband autocorrelation function of the FH/CPM signal is derived for arbitrary pulse shaping, modulation index, number of levels of the data and length of hop interval. Spectra of the spread spectrum signals with various correlative encoding schemes and baseband pulse shapes are evaluated and examined for various lengths of hop interval.

From these results we conclude that the spectrum becomes more compact as the hop interval lengthens and in general approaches that of the CPM signal without hopping. An increase in the modulation index will increase the bandwidth occupied by the signal for long hop lengths. For short hop lengths the increase in bandwidth due to an increase in modulation index is not significant. Although it is well known that correlative encoding and raised cosine baseband pulse shaping reduce the signal bandwidth and sidelobe level for conventional continuous phase modulation, for frequency-hopped signals with short hop interval lengths these techniques do not yield much reduction in bandwidth. Substantial spectral improvement with these methods can be achieved at the longer hop intervals.

Chapter Three

NONCOHERENT RECEIVER

As shown in the previous chapter, FH/CPM has attractive spectral mainlobe compactness and low sidelobes when a number of symbols are transmitted using CPM schemes during a hop interval. This spectral compactness is highly desirable for providing higher processing gain for possible increased antijam protection.

In this chapter, reception of the FH/CPM signal is considered. Due to the unknown random phase of the received carrier as the carrier hops from one frequency to another, a form of noncoherent demodulation has to be used. To make use of the continuous phase and the partial response memory of the signal, the optimum observation interval for deciding on a specific data symbol should be longer than one symbol interval.

The optimum symbol-by-symbol noncoherent detector for the class of constant envelope modulated signals having a continuous phase, has been derived previously [33-37]. Osborne and Luntz [33] and also Schonhoff [34] have derived the maximum likelihood noncoherent receiver for CPFSK yielding symbol-by-symbol decisions in the binary and general M-ary cases respectively. For noncoherent detection, an odd number of symbols is observed and a decision is made on the middle symbol. Aulin and Sundberg [35] have generalized the detection algorithm to allow the detected symbol to be anywhere in an observation interval of arbitrary length rather than just in the middle of the observation interval and have included partially coherent detection, where the unknown carrier phase is estimated by a tracking loop, which is assumed to have a tracking error density function. It has been shown that the optimum noncoherent detector should decide on the middle symbol lying in an observation interval consisting of an

odd number of symbols [35]. Noncoherent symbol-by-symbol detection of correlative encoded CPM is also reported in [36] and [37]. By using proper time delay and phase compensation networks, a much simpler noncoherent receiver than that in [33,34] has been devised by Pawula and Golden [38] for multiple symbol noncoherent demodulation of convolutionally coded CPFSK. The maximum likelihood demodulator is the same as that for ordinary noncoherent FSK but with additional circuitry following the integrators to remove the effects of the unknown phase of the local data tone oscillator. Additional time delay and phase weighting networks are required to form the maximum likelihood demodulator outputs of the noncoherent receiver with an observation interval of three symbols.

Due to the noncoherent frequency hopping and dehopping processes, the dehopped signal will have signal phase discontinuities every NT seconds. Symbol-by-symbol detection of the middle symbol based on multiple symbol observation, mentioned above, cannot be directly applied for optimum detection of this piecewise phase continuous signal. It has been observed that the symbol decisions ought to be based on the entire received sequence [39]. However, the transmitted signal corresponding to the information sequence can be of very long duration and there could be very long decoding delays. Also, since the source is providing a new information digit every T seconds, there will be an exponential increase with time in the number of possible signals, making decision after complete observation formidable unless a dramatic receiver simplification occurs. It is clear that some sort of sequential decision process is needed. In this chapter, a noncoherent receiver with a sequential decoding algorithm will be derived first for optimum detection on a hop-by-hop basis and then for optimum decisions based on the entire transmission spanning hops. A simplified suboptimum sequence estimation receiver is also derived by treating the signal as if every symbol interval is noncoherent, hence resulting in a simpler decoding algorithm and receiver structure. We shall first derive the maximum likelihood noncoherent receiver, which is optimum on a hop-by-hop decision basis, with the observation interval being the hop interval.

3.1 Hop-By-Hop Maximum Likelihood Receiver

We assume that the receiver mixes the received spread spectrum signal with a locally generated reference signal, which hops synchronously with the same pattern as that at the transmitter and produces a data modulated signal at some convenient intermediate carrier frequency f_c. The received dehopped waveform can be written as

$$r(t) = \sqrt{\frac{2E}{T}} \sum_{i=-\infty}^{\infty} p(t - iNT) \cos[2\pi f_c t + \psi(t, \underline{\alpha}) + \theta_i] + n(t) \tag{3.1}$$

where the symbols and notation are as defined and used previously in Chapter Two. f_c is the intermediate carrier frequency and n(t) is additive white Gaussian bandpass noise with zero mean and one-sided power spectral density of N_0 W/Hz which can be given by [3,36]

$$n(t) = \sqrt{2}\, n_c(t) \cos 2\pi f_c t - \sqrt{2}\, n_s(t) \sin 2\pi f_c t. \tag{3.2}$$

The baseband processes $n_c(t)$ and $n_s(t)$ are statistically independent, white and Gaussian with zero mean and one-sided power spectral density of N_o W/Hz.

During the i^{th} hop, the received dehopped signal can be written as

$$r(t) = \sqrt{\frac{2E}{T}} \cos[2\pi f_c t + \psi(t, \underline{\alpha}) + \theta_i] + n(t) \quad \text{for} \quad iNT < t < (i + 1)NT. \tag{3.3}$$

The random phase θ_i is constant over the hop interval and is assumed to be uniformly distributed from 0 to 2 π. We shall adopt the notation developed in [33,34] for the dehopped transmitted waveform in the i^{th} hop as $s(t, \underline{\alpha}, \theta_i)$ defined below

$$s(t, \underline{\alpha}, \theta_i) = \sqrt{\frac{2E}{T}} \cos[2\pi f_c t + \psi(t, \underline{\alpha}) + \theta_i] \quad \text{for} \quad iNT < t < (i + 1)NT. \tag{3.4}$$

Without loss of generality, we may only consider the detection over the first hop from t = 0 to NT. Subsequent hops are detected in the same manner on a hop-by-hop basis.

3.1.1 Likelihood Function

The detector must find the sequence of data symbols $\underline{\alpha}$, which maximizes the likelihood function [33,34,36]

$$\ell(\underline{\alpha}, \underline{\alpha}') = E_{\theta_0}\{ \exp[\frac{2}{N_o} \sqrt{\frac{2E}{T}} \int_0^{NT} r(t)\, s(t, \underline{\alpha}', \theta_0) dt] \} \tag{3.5}$$

where $E_{\theta_0}\{ . \}$ denotes the mathematical expectation with respect to the random variable θ_0 . Since the random phase θ_0 is assumed to be uniformly distributed from 0 to 2 π, the average over the random phase yields, as is well known [33,34,36], the zeroth-order modified Bessel function. The likelihood function is then given by

$$\ell(\underline{\alpha}, \underline{\alpha}') = I_0\{ \frac{2}{N_o} \sqrt{\frac{2E}{T}} \sqrt{\ell_c^2(\underline{\alpha}, \underline{\alpha}') + \ell_s^2(\underline{\alpha}, \underline{\alpha}')} \} \tag{3.6}$$

where $I_0\{ . \}$ denotes the zeroth-order modified Bessel function, and

$$\ell_c(\underline{\alpha}, \underline{\alpha}') = \int_0^{NT} r(t)\, \cos[2\pi f_c t + \psi(t, \underline{\alpha}')]\, dt \tag{3.7a}$$

$$\ell_s(\underline{\alpha}, \underline{\alpha}') = \int_0^{NT} r(t)\, \sin[2\pi f_c t + \psi(t, \underline{\alpha}')]\, dt. \tag{3.7b}$$

For convenience, we shall refer to $\ell_c(\underline{\alpha}, \underline{\alpha}')$ and $\ell_s(\underline{\alpha}, \underline{\alpha}')$ respectively, as the inphase and quadrature correlations over a hop interval.

Since the Bessel function $I_0\{\ .\ \}$ is a monotone increasing function, an equivalent likelihood function can simply be

$$\ell'(\underline{\alpha}, \underline{\alpha}') = \ell_c^2(\underline{\alpha}, \underline{\alpha}') + \ell_s^2(\underline{\alpha}, \underline{\alpha}'). \tag{3.8}$$

The maximum likelihood noncoherent receiver on a hop-by-hop decision basis would correlate the received signal with the inphase and quadrature components of all possible transmitted waveforms in a hop interval. The equivalent likelihood is then formed as the sum of the squares of the inphase and quadrature correlations over the hop interval and the receiver will choose the sequence $\underline{\alpha}'$, which gives the largest equivalent likelihood. Unfortunately, the number of possible transmitted signal waveforms for M-ary transmission in a hop interval of NT is M^N, which is exponentially increasing with the length of the hop interval. This brute force approach to decide on the most likely transmitted signal would be highly impractical considering the large number of correlators or matched filters required, particularly when the length of the hop interval is long.

3.1.2 Sequential Decoding Algorithm

For coherent detection, the Viterbi Algorithm, which was originally proposed for decoding convolutional codes, has been used for estimating the maximum likelihood sequence by calculating the likelihood recursively [39-43]. Since the likelihood for hop-by-hop noncoherent detection as given by Eq.(3.8) is the sum of the square of the inphase correlation and the square of the quadrature correlation, the metric calculation is not as straightforward as in the coherent case.

To derive a sequential decoding algorithm, we note that $\ell_c(\underline{\alpha}, \underline{\alpha}')$ and $\ell_s(\underline{\alpha}, \underline{\alpha}')$ given by Eq.(3.5) can be written as the sum of the partial likelihoods as

$$\ell_c(\underline{\alpha}, \underline{\alpha}') = \sum_{k=0}^{N-1} \delta_{c,k}(\underline{\alpha}, \underline{\alpha}') \tag{3.9a}$$

$$\ell_s(\underline{\alpha}, \underline{\alpha}') = \sum_{k=0}^{N-1} \delta_{s,k}(\underline{\alpha}, \underline{\alpha}'), \tag{3.9b}$$

where $\delta_{c,k}(\underline{\alpha}, \underline{\alpha}')$ and $\delta_{s,k}(\underline{\alpha}, \underline{\alpha}')$ denote the partial inphase and quadrature correlations over the k^{th} symbol interval as given by

$$\delta_{c,k}(\underline{\alpha}, \underline{\alpha}') = \int_{kT}^{(k+1)T} r(t) \cos[2\pi f_c t + \psi(t, \underline{\alpha}')] \, dt \tag{3.10a}$$

$$\delta_{s,k}(\underline{\alpha}, \underline{\alpha}') = \int_{kT}^{(k+1)T} r(t) \sin[2\pi f_c t + \psi(t, \underline{\alpha}')] \, dt. \tag{3.10b}$$

These partial correlations can be formed by correlating the received signal with the inphase and quadrature components of the transmitted signal in the k^{th} symbol interval for an estimated sequence $\underline{\alpha}'$.

The information carrying phase during the k^{th} symbol interval can be written as

$$\psi(t, \underline{\alpha}) = 2\pi h \sum_{n=k-L+1}^{k} \alpha_n \, q(t - nT) + 2\pi h \sum_{n=0}^{k-L} \alpha_n q(LT) \quad \text{for} \quad kt < t < (k+1)T. \tag{3.11}$$

The first term represents the contribution of inputs actively affecting the shape of the phase path during the k^{th} interval. The second term represents the underlying phase due to past inputs.

The output of a correlative encoder can be regarded as the output of a linear finite state machine much as in the case of a convolutional encoder. For a given correlative encoder with PRS polynomial F(D) of degree m, the encoder state can be defined by the last m, or L-1 input digits. A correlative state vector can be defined as

$$C_k = [\alpha_{k-L+1}, \ldots, \alpha_{k-2}, \alpha_{k-1}]. \tag{3.12}$$

The second term in Eq.(3.11) represents the underlying phase due to past inputs, which can be called the phase state [41]

$$\begin{aligned} \phi_k &= [\, 2\pi h \sum_{n=0}^{k-L} \alpha_n q(LT) \,]_{\text{mod } 2\pi} \\ &= [\, \pi h \sum_{n=0}^{k-L} \alpha_n \,]_{\text{mod } 2\pi}. \end{aligned} \tag{3.13}$$

For M-ary transmission, α_n can take on the values $\pm 1, \pm 3, \ldots, \pm (M-1)$, hence the sum $\sum_{n=0}^{k-L} \alpha_n$ can take on any integer values. For $h = \frac{2r}{p}$ with r and p relatively prime integers, there are at most p possible distinct phase states ($0, 2\pi/p, 4\pi/p, \ldots, 2\pi(p-1)/p$).

This does not mean that there are necessarily p phase states at any time kT. If we examine the difference between the phase states at alternate symbol intervals, we notice that

$$\phi_{k+2} - \phi_k = \pi h(\alpha_{k+2-L} + \alpha_{k+1-L}). \tag{3.14}$$

For M-ary transmission, α_k can take on the values $\{ \pm 1, \pm 3, \ldots, \pm (M-1) \}$, hence

$$(\phi_{k+2} - \phi_k) \in [\, 0, \pm 2\pi h, \pm 4\pi h, \ldots, \pm 2(M-1)\pi h \,]. \tag{3.15}$$

Hence if p is even, there will be only $\frac{p}{2}$ phase states possible at the even symbol times and the other $\frac{p}{2}$ phase states at the odd symbol times, although there are a total of p possible phase states.

The combined state $s_k \triangleq [C_k, \phi_k]$, that is, the correlative state vector and the phase state, together with the present input α_k completely specify the transmitted signal waveform during the k^{th} interval. For M-ary transmission there will then be M^m different correlative states and p phase states for a total of $\eta = pM^m$ combined states at the most. The sequence estimation receiver must operate with as few states as possible. If p is even, then there are actually $\frac{p}{2} M^m$ states per interval in the Markov state description. And so, actually only a total of $\eta = \frac{p}{2} M^m$ states are required for the sequence estimation receiver for $h = \frac{2r}{p}$ with p even. Since the mapping of the input data sequence to the state sequence is one-to-one, estimation of the state sequence will give the corresponding estimated transmitted data sequence.

A typical state trellis (the trellis for duobinary MSK [42]) showing the state transitions as a function of discrete time k is shown in Fig. 3.1. The trellis is drawn under the assumption that the initial state at time 0 is 1. All possible state transitions over 5 time units are shown. Each node corresponds to a state at a given time and the branches joining the states indicate state transitions to some new state at the next instant of time due to the input of an information bit. Dashed and solid lines correspond to state transitions for 1 and 0 input information bits, respectively.

For coherent detection, the likelihood can be broken into a sum of partial log likelihoods (branch metrics). When a path is extended by one branch, the metric of the new path is the sum of the new branch metric and the old path metric. The path with the largest accumulated log likelihood (path metric) leading to a node will always belong to the maximum likelihood path through that node, hence other paths leading to that node can be discarded from further consideration. In the case of noncoherent detection, the equivalent likelihood as given by Eq. (3.8) cannot be broken up into a sum of branch metrics, hence a branch transition metric cannot be defined. In order to determine the the maximum likelihood sequence, the decoder has to calculate and accumulate the inphase and quadrature likelihoods for all possible paths through

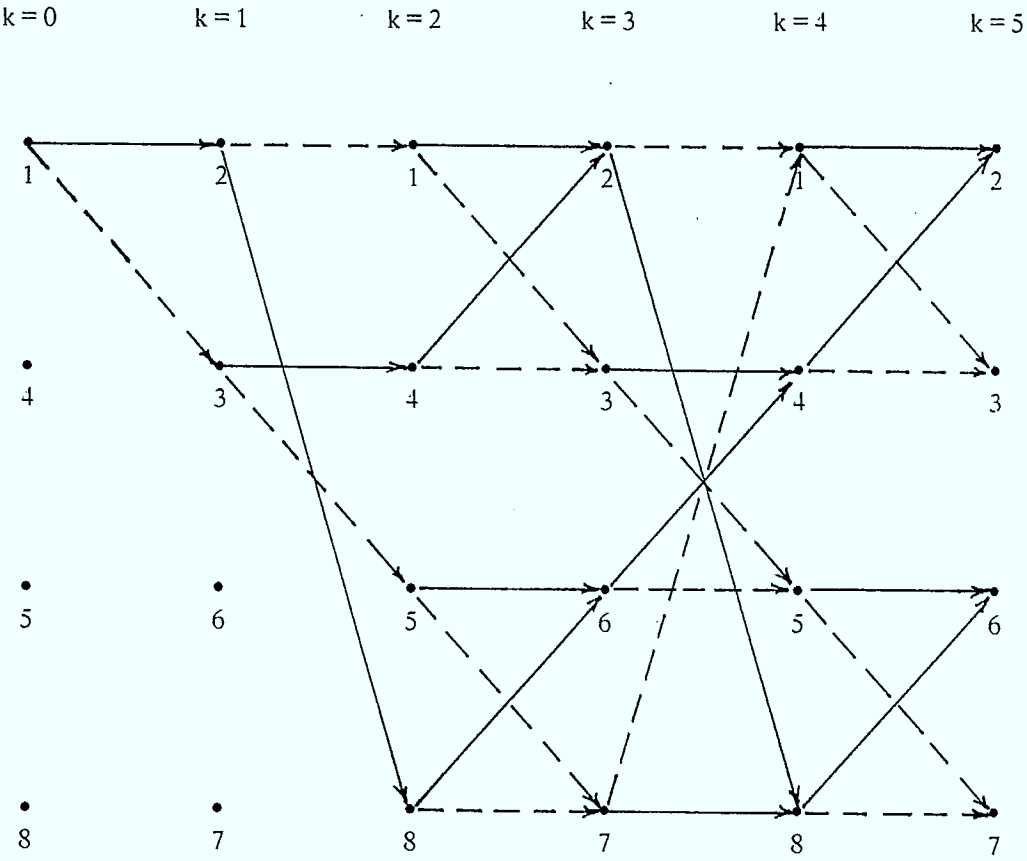

Figure 3.1 A typical state trellis

the trellis in a hop interval, besides retaining the path histories of all the possible paths. At the end of a hop interval, the equivalent likelihoods for each of the possible paths are formed by summing the squares of the inphase and quadrature likelihoods of the paths. The path history of the path with the maximum equivalent likelihood is then output as the maximum likelihood sequence over the hop interval. Only this brute force decoding approach is able to determine the maximum likelihood sequence. Unfortunately, the number of possible paths for an N symbol sequence is M^N. Thus, this brute force decoding approach quickly becomes impractical as N increases. However, the decoder may form the equivalent likelihood up to kT by summing the squares of the inphase and quadrature likelihoods of the path accumulated up to time kT. The path leading to node $s_k = j$ with the largest equivalent likelihood up to kT is the most likely path among the M paths leading to the node $s_k = j$, based on the observation interval from 0 to kT. To reduce the memory and computations from that required for maximum likelihood decoding, at any time kT the decoder may maintain only one path, which has the largest equivalent likelihood up to time kT, leading to each of the nodes $s_k = j$, $j = 1, 2, \ldots, \eta$. Some performance has been sacrificed to achieve a reduction in complexity.

The sequential decoding algorithm proceeds as follows. Starting from a known initial state $s_0 = i$, the decoder stores the inphase and quadrature likelihoods of the node $s_1 = j$ as

$$\ell^*_{c,1}(j) = \delta_c(i,j) \tag{3.16a}$$

$$\ell^*_{s,1}(j) = \delta_s(i,j) \tag{3.16b}$$

for all the M allowable transitions from state i to state j. The path history of the path leading to state j is also stored. $\delta_c(i,j)$ and $\delta_s(i,j)$ are just the inphase and quadrature correlations over a symbol interval for the allowable transition from state i to state j corresponding to an estimated sequence $\underline{\alpha}'$ as given by Eq. (3.10). They are formed from appropriate matched filter outputs with proper phase compensation weightings.

In general at time kT ($k \geq 2$), the decoder computes for each node $s_k = j$, $j = 1, 2, \ldots, \eta$, the equivalent likelihood functions of the M different paths leading to $s_k = j$, i.e.

$$\ell'_k(j) = [\ell^*_{c,k-1}(i) + \delta_c(i,j)]^2 + [\ell^*_{s,k-1}(i) + \delta_s(i,j)]^2 \tag{3.17}$$

for all allowable state transitions i to j. The sequential decoder must eliminate some paths from further consideration in order to keep the computation and memory requirement feasible. At any time kT, the only decision parameter available to the decoder is the equivalent likelihood accumulated up to kT for each of the paths leading to each state in the trellis as given by Eq. (3.17). Without prior knowledge of which one is a portion of the maximum likelihood path over the hop interval, the decoder should preserve the path with the largest equivalent likelihood accumulated up to kT leading to each node $s_k = j$, $j = 1, 2, \ldots, \eta$. Other M-1 paths ending at $s_k = j$ are discarded in order to keep the decoding process feasible for long hop lengths. We shall call the path with the largest equivalent likelihood function terminating in the node $s_k = j$ the survivor of state j, since the other paths leading to state j are discarded by the decoder. Although the survivor at node $s_k = j$ may not be a portion of the maximum likelihood path through the trellis in a hop interval, it is the most likely path leading to node $s_k = j$ based on the equivalent likelihood up to time kT among the M contending paths leading to node $s_k = j$.

Thus we define the metric of the survivor at $s_k = j$ as

$$\ell^*_k(j) = \max_{\forall(i,j)} \{ [\ell^*_{c,k-1}(i) + \delta_c(i,j)]^2 + [\ell^*_{s,k-1}(i) + \delta_s(i,j)]^2 \} \tag{3.18}$$

where $j = 1, 2, \ldots, \eta$, $k \geq 2$ and $\forall(i,j)$ denotes over all allowable transitions from state i to state j.

While $\ell_k^*(j)$ is defined as the metric of the node $s_k = j$ at time k, the pair $\{ \ell_{c,k}^*(j), \ell_{s,k}^*(j) \}$ are stored for node $s_k = j$, as given by

$$\ell_{c,k}^*(j) = \ell_{c,k-1}^*(i) + \delta_c(i,j) \tag{3.19a}$$

$$\ell_{s,k}^*(j) = \ell_{s,k-1}^*(i) + \delta_s(i,j) \tag{3.19b}$$

where i is the node index satisfying Eq.(3.18). The metric is computed sequentially from the old information $\{ \ell_{c,k-1}^*(i), \ell_{s,k-1}^*(i) \}$ and the partial correlations $\{ \delta_c(i,j), \delta_s(i,j) \}$ in the k^{th} interval according to Eq.(3.18). The sequential decoding algorithm now has to accumulate both the inphase and quadrature likelihood parameters rather than just the inphase likelihood parameter as in the coherent case. The path histories of the survivors terminating at each of the nodes $s_k = j$, $j = 1, 2, \ldots, \eta$ are also stored.

In principle the algorithm can make a final decision on the initial state sequence segment up to time (k-d)T when and only when all survivors at time kT have the same initial state sequence segment up to time (k-d)T. That is, all survivors branch out from a common node, say $s_{k-d} = j$. The initial segment of the estimated sequence is then uniquely determined independent of succeeding observation and a firm decision is available from the algorithm before the end of a hop. For this hop-by-hop sequence estimation algorithm, the survivor having the largest metric (equivalent likelihood) at time NT, that is at the end of a hop, is output as the estimated sequence. The decoding delay d for this hop-by-hop sequence estimation algorithm is at the most the length of a hop interval.

3.1.3 Receiver Structure

The noncoherent receiver must be able to provide the inphase and quadrature correlations of the received signal with every possible duration-T signal segment as indicated by Eq.(3.10). The inphase correlation over the k^{th} symbol interval required for the possible transition from state i to state j during the k^{th} symbol interval is given by

$$\begin{aligned}\delta_c(i,j) &= \int_{kT}^{(k+1)T} r(t)\cos[2\pi f_c t + \psi(t,\underline{\alpha}')]dt \\ &= \int_{kT}^{(k+1)T} r_c(t)\cos\psi(t,\underline{\alpha}')dt - \int_{kT}^{(k+1)T} r_s(t)\sin\psi(t,\underline{\alpha}')dt\end{aligned} \tag{3.20}$$

where

$$r_c(t) = r(t)\cos 2\pi f_c t \tag{3.21}$$

$$r_s(t) = r(t)\sin 2\pi f_c t \tag{3.22}$$

The information carrying phase function $\psi(t,\underline{\alpha})$ during the k^{th} symbol interval as given by Eq.(3.11) can be written as

$$\psi(t,\underline{\alpha}') = \beta_{ki}(t) + \phi_{ki}; \qquad kT < t < (k+1)T, \tag{3.23}$$

where

$$\beta_{ki}(t) = 2\pi h \sum_{n=k-L+1}^{k} \alpha_n\, q(t - nT). \tag{3.24}$$

$\beta_{ki}(t)$ is one of the M^L posible phase paths and ϕ_{ki} is one of the p possible phase states as given by Eq.(3.13). Substituting Eq.(3.23) into (3.20), we obtain

$$\begin{aligned}\delta_c(i,j) = &\cos\phi_{ki}\int_{kT}^{(k+1)T} r_c(t)\cos\beta_{ki}(t)dt \\ &- \sin\phi_{ki}\int_{kT}^{(k+1)T} r_c(t)\sin\beta_{ki}(t)dt \\ &- \cos\phi_{ki}\int_{kT}^{(k+1)T} r_s(t)\sin\beta_{ki}(t)dt \\ &- \sin\phi_{ki}\int_{kT}^{(k+1)T} r_s(t)\cos\beta_{ki}(t)dt\end{aligned} \tag{3.25}$$

Similarly, the quadrature correlation over the k th symbol interval for the transition from state i to state j is given by

$$\begin{aligned}\delta_s(i,j) = &\sin\phi_{ki}\int_{kT}^{(k+1)T} r_c(t)\cos\beta_{ki}(t)dt \\ &+ \cos\phi_{ki}\int_{kT}^{(k+1)T} r_c(t)\sin\beta_{ki}(t)dt \\ &- \sin\phi_{ki}\int_{kT}^{(k+1)T} r_s(t)\sin\beta_{ki}(t)dt \\ &+ \cos\phi_{ki}\int_{kT}^{(k+1)T} r_s(t)\cos\beta_{ki}(t)dt\end{aligned} \tag{3.26}$$

where $r_c(t)$ and $r_s(t)$ are given by Eqs.(3.21) and (3.22), which are obtained by multiplying the received signal by $\cos 2\pi f_c t$ and $\sin 2\pi f_c t$ to form quadrature channels. For some frequency dehoppers, $r_c(t)$ and $r_s(t)$ may actually be available directly from the inphase and quadrature channel outputs of the dehopper. A baseband matched filter bank is required to provide the correlations with the cosine and sine of all posible phase paths $\beta_{ki}(t)$ over each symbol interval to obtain the $\delta_c(i,j)$ and $\delta_s(i,j)$ required by the decoder. Notice that $\delta_c(i,j)$ and $\delta_s(i,j)$ given by Eqs.(3.25) and (3.26) can share the same matched filter bank, since the difference is only in the scaling multipliers, $\sin\phi_{ki}$ and $\cos\phi_{ki}$ and the sign.

The matched filter impulse response is simply

$$h_{ci}(t) = \begin{cases} \cos[\beta_{ki}(T - t)] & 0 < t < T \\ 0 & \text{elsewhere} \end{cases}$$

$$= \begin{cases} \cos 2\pi h \sum_{\ell=-L+1}^{0} \alpha_{i\ell} q[(1 - \ell)T - t] & 0 < t < T \\ 0 & \text{elsewhere} \end{cases} \tag{3.27}$$

to provide the correlation with the cosine of the i^{th} possible phase path. For the correlation with the sine of the i^{th} possible phase path, the impulse reponse of the required matched filter is given by

$$h_{si}(t) = \begin{cases} \sin[\beta_{ki}(T - t)] & 0 < t < T \\ 0 & \text{elsewhere} \end{cases}$$

$$= \begin{cases} \sin 2\pi h \sum_{\ell=-L+1}^{0} \alpha_{i\ell} q[(1 - \ell)T - t] & 0 < t < T \\ 0 & \text{elsewhere.} \end{cases} \tag{3.28}$$

For a PRS polynomial with κ nonzero coefficients and M-ary data transmission the number of distinct symbols at the output of a correlative encoder lies in the range $\kappa(M - 1) + 1 \leq \lambda \leq M^{\kappa}$, with the minimum number of distinct correlative encoded symbols being obtained when the PRS coefficients are all the same [19]. The number of distinct correlative encoded symbols corresponds to the number of different possible transmitted phase trajectories during a symbol interval. The number of matched filters required for the receiver is 4λ. For a PRS polynomial of degree m, there will be $m + 1 = L$ nonzero coefficients at the most, hence the number of matched filters required is $4M^{L}$ at most. The number of matched filters can be reduced by a factor of two by noting that for every digit sequence, there is another sequence with opposite signs. Therefore, at the most, $2M^{L}$ baseband matched filters are re-

quired in total. A block diagram of this sequence estimation noncoherent receiver is shown in Fig. 3.2.

The matched filter outputs are sampled every T seconds followed by proper phase weightings to obtain the inphase and quadrature correlations $\delta_c(i,j)$ and $\delta_s(i,j)$ for the k^{th} symbol interval. There will be $\eta = pM^m = pM^{L-1}$ combined states per interval at most. Hence the decoding algorithm requires η buffers for storing the η survivors and 2η storage locations for storing the inphase and quadrature likelihoods $\ell^*_{c,k-1}(i)$ and $\ell^*_{s,k-1}(i)$, $1 \le i \le \eta$. At each time kT, the algorithm has to perform $2M\eta$ additions to find $[\ell^*_{c,k-1}(i) + \delta_c(i,j)]$ and $[\ell^*_{s,k-1}(i) + \delta_s(i,j)]$ followed by $2M\eta$ squaring operations and $M\eta$ additions to obtain the likelihood $\ell'(\underline{\alpha}, \underline{\alpha}')$. $(M-1)\eta$ binary comparisons are then required to determine the η survivors $\underline{S}_j$, $1 \le j \le \eta$ with the largest likelihood $\ell^*_k(j)$, $1 \le j \le \eta$. Hence, at each time kT, a total of $N_{add} = 3pM^L$ additions, $N_{sq} = 2pM^L$ squaring operations and $N_{comp} = (M-1)pM^{L-1}$ binary comparisons are performed by the decoder.

The hop-by-hop sequence estimation noncoherent receivers for different modulation schemes are compared in terms of the number of possible phase states, the number of baseband matched filters, the number of decoder states and the number of mathematical operations required per symbol interval as shown in Table 3. We can see that with a modulation index of 0.5, the simplest receiver can be obtained with the minimum number of decoder states and consequently the minimum number of mathematical operations are required to be performed per symbol interval by the decoder.

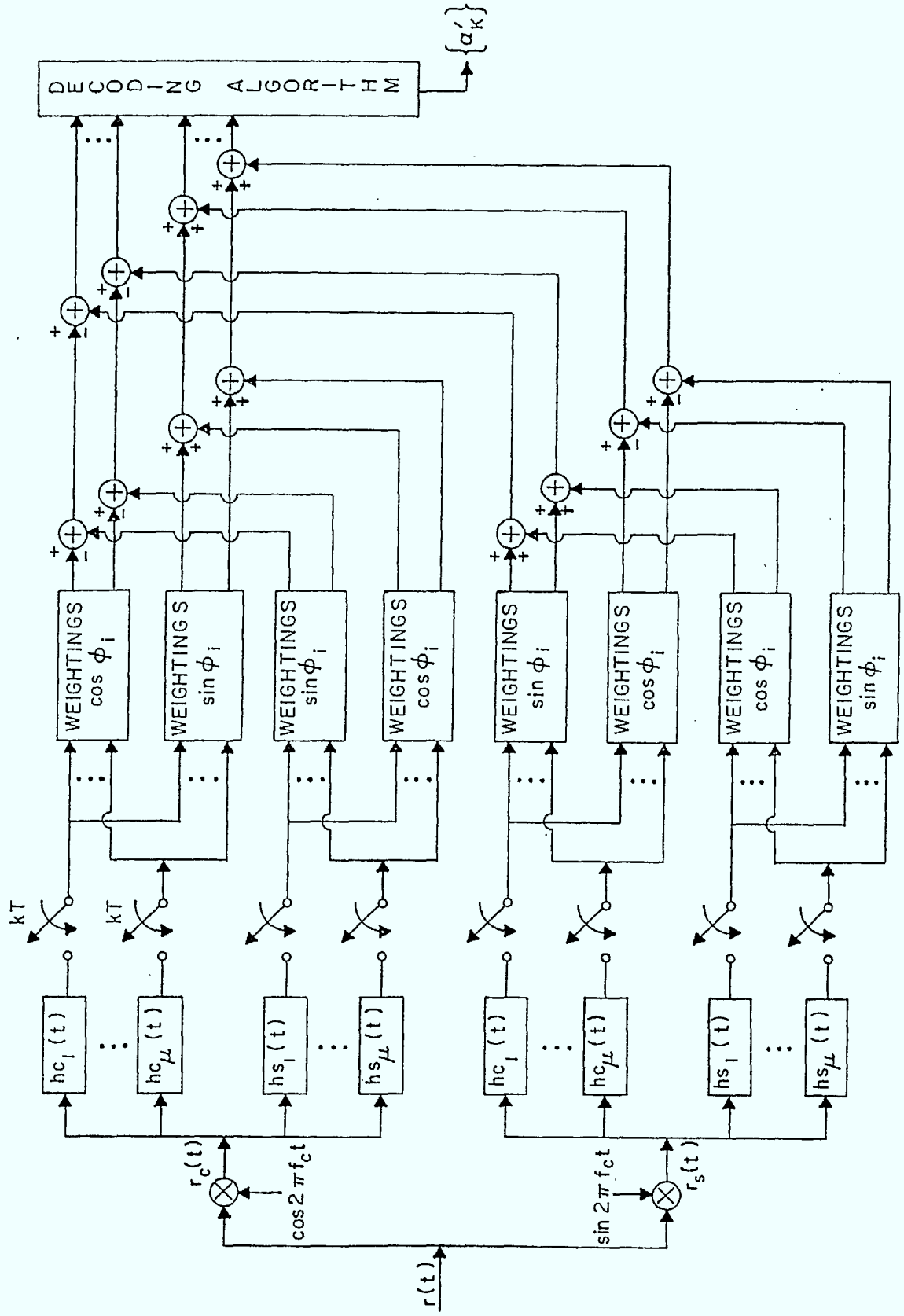

Figure 3.2 Sequence estimation noncoherent receiver structure

p	number of possible phase states
MF	number of baseband matched filters
η	number of decoder states
N_{add}	number of additions
N_{sq}	number of squaring operations
N_{comp}	number of binary comparisons

Modulation					Operations per interval		
F(D)	h	p	MF	η	N_{add}	N_{sq}	N_{comp}
1	1/3	6	4	6	36	24	6
	1/2	4	4	2	12	8	2
	2/3	3	4	3	18	12	3
(1 + D)/2	1/3	6	8	12	72	48	12
	1/2	4	8	4	24	16	4
	2/3	3	8	6	36	24	6
(1 + 2D + D²)/4	1/3	6	12	24	144	96	24
	1/2	4	12	8	48	32	8
	2/3	3	12	12	72	48	12

Table 3 Complexity comparison between different modulation schemes for the hop-by-hop sequence estimation receiver

3.2 ML Receiver Spanning Frequency Hops

In Section 3.1, the sequential decoding noncoherent receiver that decodes transmitted sequences on a hop-by-hop basis has been presented. We now extend the detection algorithm so that the receiver detects a transmitted sequence of arbitary length (greater than the hop length), based on the maximum likelihood accumulated over the entire transmission period spanning frequency hops. There will be periodic random phase jumps in the dehopped waveform every NT seconds. As one would expect, the receiver algorithm is more complex than the previous algorithm. However, a special case of the algorithm can be combined with the algorithm described in the previous section to give a simple practical algorithm for the situation where the hop interval is much longer than the length of the frequency pulse g(t).

3.2.1 Receiver Theory

The received dehopped waveform is the same as that presented previously in Eq.(3.1). Again we shall adopt a shorthand notation developed in [33,34] for the dehopped transmitted waveform as $s(t, \underline{\alpha}, \underline{\Theta})$, where $\underline{\Theta} = \{ \theta_0, \theta_1, \theta_2, \ldots \}$ is a random vector, such that $s(t, \underline{\alpha}, \underline{\Theta}) = s(t, \underline{\alpha}, \theta_i)$, for $iNT < t < (i+1)\,NT$ and $s(t, \underline{\alpha}, \theta_i)$ is defined in Eq. (3.4).

For a transmitted sequence of length n symbols, with n greater than the length of the hop interval N, the number of hop intervals for which the signal has a different value of random phase θ_i, would be the nearest integer greater than n/N denoted by q. The detector must now find the sequence of data symbols $\underline{\alpha}'$, which maximizes the likelihood function

$$\begin{aligned} \ell(\underline{\alpha}, \underline{\alpha}') &= E_{\underline{\Theta}}\{ \exp[\frac{2}{N_0} \sqrt{\frac{2E}{T}} \int_0^{nT} r(t)\, s(t, \underline{\alpha}', \Theta)\, dt] \} \\ &= E_{\underline{\Theta}}\{ \exp[\frac{2}{N_0} \sqrt{\frac{2E}{T}} \sum_{i=0}^{q-1} \int_{iNT}^{(i+1)NT} r(t)\, s(t, \underline{\alpha}', \theta_i)\, dt] \}. \end{aligned} \tag{3.29}$$

The sum in the exponent can be written as a product giving

$$\ell(\underline{\alpha}, \underline{\alpha}') = E_{\underline{\theta}}\{ \prod_{i=0}^{q-1} \exp[\frac{2}{N_0} \sqrt{\frac{2E}{T}} \int_{iNT}^{(i+1)NT} r(t)\, s(t, \underline{\alpha}', \theta_i)\, dt] \}. \tag{3.30}$$

Since the random phases θ_i are statistically independent, the expectation over the random phase can be taken as

$$\ell(\underline{\alpha}, \underline{\alpha}') = \prod_{i=0}^{q-1} E_{\theta_i}\{ \exp[\frac{2}{N_0} \sqrt{\frac{2E}{T}} \int_{iNT}^{(i+1)NT} r(t)\, s(t, \underline{\alpha}', \theta_i)\, dt] \}. \tag{3.31}$$

Assuming that the random phases θ_i are uniformly distributed between 0 and 2π, the average over the random phase yields as is well known, the zeroth-order modified Bessel function and the likelihood becomes

$$\ell(\underline{\alpha}, \underline{\alpha}') = \prod_{i=0}^{q-1} I_0\{ \frac{2}{N_0} \sqrt{\frac{2E}{T}} \sqrt{\ell_{ci}^2(\underline{\alpha}, \underline{\alpha}') + \ell_{si}^2(\underline{\alpha}, \underline{\alpha}')} \} \tag{3.32}$$

where

$$\ell_{ci}(\underline{\alpha}, \underline{\alpha}') = \int_{iNT}^{(i+1)NT} r(t)\, \cos[2\pi f_c t + \psi(t, \underline{\alpha}')]\, dt \tag{3.33a}$$

and

$$\ell_{si}(\underline{\alpha}, \underline{\alpha}') = \int_{iNT}^{(i+1)NT} r(t)\ \sin[2\pi f_c t + \psi(t, \underline{\alpha}')]\ dt. \tag{3.33b}$$

$I_0\{\ .\ \}$ denotes the zeroth-order modified Bessel function. Comparing the likelihood function in Eq.(3.32) with that for the hop-by-hop detection given in Eq.(3.8), we see that the maximum likelihood calculation is now more complicated. The likelihood calculation involves multiplications, Bessel function weighting, squaring and square root operations.

Generally in receiver implementation, addition is preferred over multiplication and the log likelihood function may be used to reduce the number of multiplications by taking the logarithm on both sides of Eq. (3.32) giving

$$\Gamma(\underline{\alpha}, \underline{\alpha}') = \sum_{i=0}^{q-1} \ell n\ I_0\{\ \frac{2}{N_0}\sqrt{\frac{2E}{T}}\sqrt{\ell_{ci}^2(\underline{\alpha}, \underline{\alpha}') + \ell_{si}^2(\underline{\alpha}, \underline{\alpha}')}\ \}. \tag{3.34}$$

To find the most likely transmitted sequence, the receiver will have to compute the log likelihood as given by Eq. (3.34) for every possible sequence $\underline{\alpha}'$ and choose the one which has the largest likelihood.

3.2.2 Sequential Decoding Algorithm

The computation for the log likelihood as given by Eq.(3.34) for an estimated sequence $\underline{\alpha}'$ can be carried out in a serial manner as follows. Again estimation of the state sequence will give the corresponding estimated data sequence, since the mapping from a data sequence to a state sequence is one to one. Initially during the first hop interval the equivalent likelihood

given by Eq.(3.8) can be used to determine the most likely transmitted sequence in the first hop. Hence, the decoding algorithm spanning frequency hops can proceed in the same manner as for the hop-by-hop sequential decoding algorithm described in Section 3.1.2. At the end of the first hop, the decoder retains η survivors having the largest equivalent likelihoods ending at each of the nodes $s_N = j, j = 1, 2, \ldots, \eta$. The decoder now has to compute the log likelihoods of the survivors terminating at each of the η nodes at time NT given by

$$\Gamma_1(j) = \ell n \left(I_0\{ \frac{2}{N_o} \sqrt{\frac{2E}{T}} \sqrt{\ell^*_{c,N}(j)^2 + \ell^*_{s,N}(j)^2} \} \right) \tag{3.35}$$

for each of the states $1 \le j \le \eta$. We shall refer to these as the partial log likelihoods accumulated over the first hop. To determine the survivors in the second hop for time $kT > NT$, the decoder must use the likelihood given by Eq.(3.34) rather than the equivalent likelihood $\ell'(\underline{\alpha}, \underline{\alpha}')$ as given by Eq.(3.8). Hence, to determine the survivor at time $(N+1)T$, the decoder computes the metric of the survivor at $s_{N+1} = j$ as

$$\ell n\, \ell^*_{N+1}(j) = \max_{\forall(i,j)} \{ \Gamma_1(i) + \ell n\, I_0[\frac{2}{N_0} \sqrt{\frac{2E}{T}} (\delta_c^2(i,j) + \delta_s^2(i,j))^{1/2}] \} \tag{3.36}$$

for $j = 1, 2, \ldots, \eta$ and all allowable state transitions i to j. $\delta_c(i,j)$ and $\delta_s(i,j)$ are the inphase and quadrature correlations for the transition from state i to state j during a symbol interval. These are obtained in the same way as for the noncoherent receiver on a hop-by-hop detection basis presented previously.

For each of the nodes $s_{N+1} = j$, $1 \le j \le \eta$, the registers for storing the inphase and quadrature correlations over the second hop, $\ell^*_{c,2,N+1}(j)$ and $\ell^*_{s,2,N+1}(j)$, are initialized as

$$\ell^*_{c,2,N+1}(j) = \delta_c(i,j) \tag{3.37a}$$

$$\ell^*_{s,2,N+1}(j) = \delta_s(i,j) \tag{3.37b}$$

where i is the node index satisfying Eq. (3.36). Note that in the notation $\ell^*_{c,m,k}$ and $\ell^*_{s,m,k}$, a second subscript m, has been introduced to indicate that the m^{th} hop is under consideration and the subscript k, as before, indicates that the states at time kT are being evaluated. The partial log likelihood accumulated over the first hop for the survivor at node $s_{N+1} = j$ is also stored as

$$\Gamma^*_1(j) = \Gamma_1(i) \tag{3.38}$$

where i is the survivor state at time N and it is the node index i that satisfies Eq. (3.36).

In general, for time k laying in the m^{th} hop other than the first hop, $(m-1)N < k < mN$, the metric of the node $s_k = j$ is defined as

$$\ell n\, \ell^*_k(j) = \max_{\forall(i,j)} \{ \Gamma^*_{m-1}(i) + \ell n\, I_0\{ \frac{2}{N_0}\sqrt{\frac{2E}{T}} [(\ell^*_{c,m,k-1}(i) + \delta_c(i,j))^2 + (\ell^*_{s,m,k-1}(i) + \delta_s(i,j))^2]^{1/2} \} \}. \tag{3.39}$$

The metric is computed sequentially from the old information $\{ \ell^*_{c,m,k-1}(i),\ \ell^*_{s,m,k-1}(i),\ \Gamma^*_{m-1}(i) \}$ and the new information $\{ \delta_c(i,j),\ \delta_s(i,j) \}$ recursively according to Eq. (3.39). $\Gamma^*_{m-1}(i)$ is the sum of the partial log likelihoods accumulated over the previous (m-1) hop intervals for the survivor ending at $s_{k-1} = i$. The likelihood parameters are updated through

$$\ell^*_{c,m,k}(j) = \ell^*_{c,m,k-1}(i) + \delta_c(i,j) \tag{3.40a}$$

$$\ell^*_{s,m,k}(j) = \ell^*_{s,m,k-1}(i) + \delta_s(i,j) \tag{3.40b}$$

$$\Gamma^*_{m-1}(j) = \Gamma^*_{m-1}(i) \tag{3.41}$$

where i is the state index that satifiies Eq. (3.39).

At the end of each hop interval say the m^{th} hop, $\Gamma^*_m(j)$ is updated through

$$\begin{aligned}\Gamma^*_m(j) &= \ell n\, \ell^*_{mN}(j) \\ &= \Gamma^*_{m-1}(j) + \ell n\, I_0\{\frac{2}{N_0}\sqrt{\frac{2E}{T}}\,[(\ell^*_{c,m,mN}(j))^2 + (\ell^*_{s,m,mN}(j))^2]^{1/2}\}\end{aligned} \tag{3.42}$$

for $j = 1, 2, \ldots, \eta$ and $\ell n\, \ell^*_{mN}(j)$ is the metric of state j as given by Eq.(3.39) when $k = mN$. The registers storing the inphase and quadrature correlations over a hop interval $\ell^*_{c,m,k}(j)$ and $\ell^*_{s,m,k}(j)$ are reset to zero at the end of each hop interval. Note that the values $\sqrt{\frac{2E}{T}}$ and N_0 are required, which was not the case in the receiver considered in Section 3.1 and the partial log likelihood sum $\Gamma^*_{m-1}(j)$ has to be stored in addition to the usual inphase and quadrature correlations $\ell^*_{c,m,k}(j)$ and $\ell^*_{s,m,k}(j)$. Natural log and Bessel function weightings have to be performed. This dictates a more complex detection algorithm than previously obtained in hop-by-hop detection.

The sequential decoder can output the initial segment of the estimated sequence when all survivors go through the same nodes up to time k-d, that is, a merge occurs at time (k-d)T and all survivors branch out from the same common node s_{k-d}. The initial segment of the estimated sequence is then determined independent of succeeding observation. The decoding delay d is unbounded. In actual implementation, the buffers for storing the path histories of the survivors will be of finite length. The path histories of the survivors are then truncated to the length of the storage buffers. The decoder will have to come to a definite decision after some fixed delay, which is the length of the storage buffers. In general, if the buffer length is chosen large enough, there is a high probability that all survivor sequences share the same initial segment and the initial segment can then be output as the decoder's firm decision. In this case, truncation of the survivor path histories does not affect the decoder's decision. In the event when all survivors at time kT do not share any common initial segment, the oldest bit of the survivor sequence with the largest metric among the η survivors is output. If the buffer length

is large enough, the effect on performance is negligible. The decoding delay for finite-length-buffer implementation is then at the most the length of the storage buffers.

3.2.3 Decoder Simplification for L << N

If the length of the frequency pulse denoted by L is much less than the hop length N, then merges in the modulation trellis will usually occur much before the end of a hop. All the η different survivors at time kT, branch out from a common node, say s_t , where (m-1)N < t < k, hence $\Gamma^*_{m-1}(i)$ will be the same for all the contending paths leading to the node $s_k = j$ and can be dropped.

$$\ell n\, \ell^*_k(j) = \max_{\forall(i,j)} \{ \Gamma^*_{m-1}(i) + \ell n\, I_0\{ [\frac{2}{N_0} \sqrt{\frac{2E}{T}} ([\ell^*_{c,m,k-1}(i) + \delta_c(i,j)]^2 + [\ell^*_{s,m,k-1}(i) + \delta_s(i,j)]^2)^{1/2} \} \}$$

$$= \max_{\forall(i,j)} \{ \ell n\, I_0\{ [\frac{2}{N_0} \sqrt{\frac{2E}{T}} ([\ell^*_{c,m,k-1}(i) + \delta_c(i,j)]^2 + [\ell^*_{s,m,k-1}(i) + \delta_s(i,j)]^2)^{1/2}] \} \}. \quad (3.43)$$

Since the log Bessel function is a monotone increasing function, the log Bessel function weighting can then be omitted without affecting the decision. Once the log Bessel function weighting is dispensed with, the multiplication with a constant and taking the square root operations can also be omitted, resulting in a simple likelihood parameter, which is the equivalent likelihood used in the hop-by-hop detection receiver. Hence once a merge has occurred within a hop the equivalent likelihood over the current hop interval can be used for determining the maximum likelihood sequence via

$$\ell^*_k(j) = \max_{\forall(i,j)} \{ [\ell^*_{c,m,k-1}(i) + \delta_c(i,j)]^2 + [\ell^*_{s,m,k-1}(i) + \delta_s(i,j)]^2 \}. \quad (3.44)$$

The decoding algorithm can then revert to the simple one as for the first hop. Note that the more complicated metric calculation in Eq.(3.39) is required only for a few symbol intervals after a frequency hop. Once a merge has occurred the comparison can then revert to the simple one as in Eq.(3.44). Although the parameters $\Gamma^*_{m-1}(j)$ for $j = 1, 2, \ldots, \eta$ can be omitted in the comparison in Eq. (3.44) after a merge has occurred, they are still needed to be stored and updated for the η survivors terminating at each of the nodes $s_k = j$, $j = 1, 2, \ldots, \eta$, as outlined in Eq.(3.41) during a hop interval. At the end of the m^{th} hop interval, the parameters $\Gamma^*_m(j)$ for all the states $j = 1, 2, \ldots, \eta$ are required to be updated through Eq. (3.42). The algorithm reverts back to the more complicated calculation as the next hop begins.

3.2.4 Receiver Structure

The only difference between the receiver obtained in this section and the one discussed in the previous section is the decoding algorithm. The receiver structure for generating $\delta_c(i,j)$ and $\delta_s(i,j)$ is the same as that presented in section 3.1.3.

3.3 Suboptimum Simplified Noncoherent Receiver

The noncoherent receiver described previously is quite complex, especially if the metric calculations are to be carried on across the hop intervals. A simplified sub-optimum receiver structure with reduced complexity may be obtained, although error performance will be sacrificed. For the correlative encoded CPM signal described, there are correlative encoder states as given by Eq.(3.12) and phase states as given by Eq.(3.13). If the phase states are ignored and only the correlative encoder states are used to estimate the transmitted sequence, we have a simplified sub-optimum decision algorithm, which automatically takes care of the metric calculation across a frequency hop. Symbol intervals are treated as if they are all noncoherent, the

continuous phase memory inherent in the signal structure is then ignored and poorer performance will result.

3.3.1 Suboptimum Receiver Algorithm

The information carrying phase function $\psi(t)$ given in Eq.(3.11) can be alternatively expressed in term of the correlated data symbols J_n as

$$\psi(t) = 2\pi h \sum_{n=0}^{\infty} J_n \, v(t - nT), \tag{3.45}$$

where the J_n are correlated data symbols given by

$$J_n = \frac{1}{C} \sum_{\ell=0}^{m} k_\ell \, \alpha_{n-\ell} \tag{3.46}$$

and

$$v(t) = \int_{-\infty}^{t} b(\tau) d\tau, \tag{3.47}$$

where b(t) is the baseband pulse of length T. v(t) is normalized such that

$$v(T) = \frac{1}{2}. \tag{3.48}$$

During the k^{th} symbol interval the information carrying phase function can be given by

$$\psi(t) = 2\pi h J_k v(t - kT) + \pi h \sum_{n=0}^{k-1} J_n; \qquad kT < t < (k + 1)T. \tag{3.49}$$

The underlying phase which stays constant during the k^{th} symbol interval is then

$$\xi_k = \pi h \sum_{n=0}^{k-1} J_n + \theta_i; \qquad iN < k < (i+1)N. \tag{3.50}$$

Rather than having a random phase angle once per hop interval, we can assume for noncoherent bit detection that we have a noncoherent phase angle in each symbol interval. The suboptimum receiver must find the data sequence $\underline{\alpha}'$ that maximizes the following likelihood function.

$$\begin{aligned} \ell(\underline{\alpha}, \underline{\alpha}') &= E_\xi\{ \exp[\frac{2}{N_o} \sqrt{\frac{2E}{T}} \int_0^{nT} r(t)\, s(t, \underline{\alpha}', \xi) dt] \} \\ &= \prod_{k=0}^{n-1} I_0\{ \frac{2}{N_o} \sqrt{\frac{2E}{T}}\, z_k(\underline{\alpha}_k, \underline{\alpha}'_k) \} \end{aligned} \tag{3.51}$$

where

$$\begin{aligned} z_k(\underline{\alpha}, \underline{\alpha}') = [&(\int_{kT}^{(k+1)T} r(t)\, \cos[2\pi f_c t + \beta_k(t, \underline{\alpha}')]\, dt)^2 \\ &+ (\int_{kT}^{(k+1)T} r(t)\, \sin[2\pi f_c t + \beta_k(t, \underline{\alpha}')]\, dt)^2]^{1/2} \end{aligned} \tag{3.52}$$

and $\beta_k(t, \underline{\alpha}')$ is the shape of the phase path during the k^{th} symbol interval due to the k^{th} correlated symbol J'_k given by

$$\beta_k(t, \underline{\alpha}') = 2\pi h J'_k v(t - kT) \tag{3.53}$$

and

$$J'_k = \frac{1}{C} \sum_{\ell=0}^{m} k_\ell\, \alpha'_{k-\ell}. \tag{3.54}$$

For M-ary transmission and a PRS polynomial of degree m, there would be at most M^m states rather than pM^m states for the MLSE receivers presented in Sections 3.1 and 3.2. The memory and computational requirement is then reduced.

Instead of having the likelihood function as a product of Bessel function weighted Rician variables $z_k(\underline{\alpha}, \underline{\alpha}')$ in Eq. (3.51), the log likelihood function can be used as given by

$$\Gamma(\underline{\alpha}, \underline{\alpha}') = \sum_{k=0}^{n-1} \ell n\, I_0\{ \frac{2}{N_0} \sqrt{\frac{2E}{T}}\, z_k(\underline{\alpha}, \underline{\alpha}') \}. \tag{3.55}$$

By treating signal symbol intervals as if they were noncoherent with random phase, a suboptimum log likelihood parameter, which can be broken into sum of branch metrics, has resulted. The path metric is now additive as in the coherent case, although the metric is suboptimum. A sequential decoding algorithm similar to the Viterbi algorithm can now be used for calculating the path metric recursively through

$$\Gamma_k^*(j) = \max_{\forall(i,j)} \{ \Gamma_{k-1}^*(i) + \ell n\, I_0[\frac{2}{N_0} \sqrt{\frac{2E}{T}}\, z_k(i,j)] \}. \tag{3.56}$$

where $\Gamma_{k-1}^*(i)$ is the old path metric of the survivor terminated at node $s_{k-1} = i$ and $\ell n\, I_0[\frac{2}{N_0} \sqrt{\frac{2E}{T}}\, z_k(i,j)]$ is the branch metric for the transition from state i to state j with $z_k(i,j)$ corresponding to that given by Eq. (3.52).

3.3.2 Suboptimum Receiver Structure

Since the phase path $\beta_k(\underline{\alpha}, \underline{\alpha}')$ during a symbol interval depends on the correlated symbol J_k only, the number of possible distinct phase paths is the number of possible distinct correlated symbols. The receiver structure must be able to provide the partial log likelihood

$\ell n[\, I_0\{ \frac{2}{N_0}\sqrt{\frac{2E}{T}}\, z_k(\underline{\alpha}, \underline{\alpha}') \}\,]$ for every possible phase path during a symbol interval. Following the approach used in section 3.1.3, we have

$$\int_{kT}^{(k+1)T} r(t)\cos[2\pi f_c t + \beta_{ki}(t)]\,dt = \int_{kT}^{(k+1)T} r_c(t)\cos\beta_{ki}(t)dt - \int_{kT}^{(k+1)T} r_s(t)\sin\beta_{ki}(t)dt \tag{3.57}$$

and

$$\int_{kT}^{(k+1)T} r(t)\sin[2\pi f_c t + \beta_{ki}(t)]\,dt = \int_{kT}^{(k+1)T} r_c(t)\sin\beta_{ki}(t)dt + \int_{kT}^{(k+1)T} r_s(t)\cos\beta_{ki}(t)dt \tag{3.58}$$

where $r_c(t)$ and $r_s(t)$ are as given by Eqs.(3.21) and (3.22) respectively. A baseband matched filter bank is then required to provide the correlations with the cosine and sine of all possible phase paths $\beta_{ki}(t)$ over each symbol interval. For the correlation with the cosine of the i^{th} possible phase path, the matched filter impulse response is given by

$$h_{ci}(t) = \begin{cases} \cos[\beta_{ki}(T-t)] & 0 < t < T \\ 0 & \text{elsewhere} \end{cases}$$

$$= \begin{cases} \cos[\,2\pi h\, J_i v(T-t)\,] & 0 < t < T \\ 0 & \text{elsewhere,} \end{cases} \tag{3.59}$$

and the matched filter impulse response for the correlation with the sine of the i^{th} possible phase path is given by

$$h_{si}(t) = \begin{cases} \sin[\beta_{ki}(T-t)] & 0 < t < T \\ 0 & \text{elsewhere} \end{cases}$$

$$= \begin{cases} \sin[\,2\pi h\, J_i v(T-t)\,] & 0 < t < T \\ 0 & \text{elsewhere.} \end{cases} \tag{3.60}$$

Comparing Eqs.(3.57) and (3.58) with Eqs.(3.25) and (3.26), we see that this suboptimum receiver requires the same number of matched filters as the ML receiver. The scaling multipliers for the ML receiver are not required but squaring operations and summers are required as well as the weightings $\ell n\, I_0 \{ \frac{2}{N_0} \sqrt{\frac{2E}{T}} \sqrt{(.)} \}$. Note that although the receiver may look as complex as the ML receiver, the function weighting is now being done in hardware which can be much faster. In the case where the software can handle the required mathematical operations, the structure of the receiver is much simpler indeed. The receiver block diagram is as shown in Fig. 3.3.

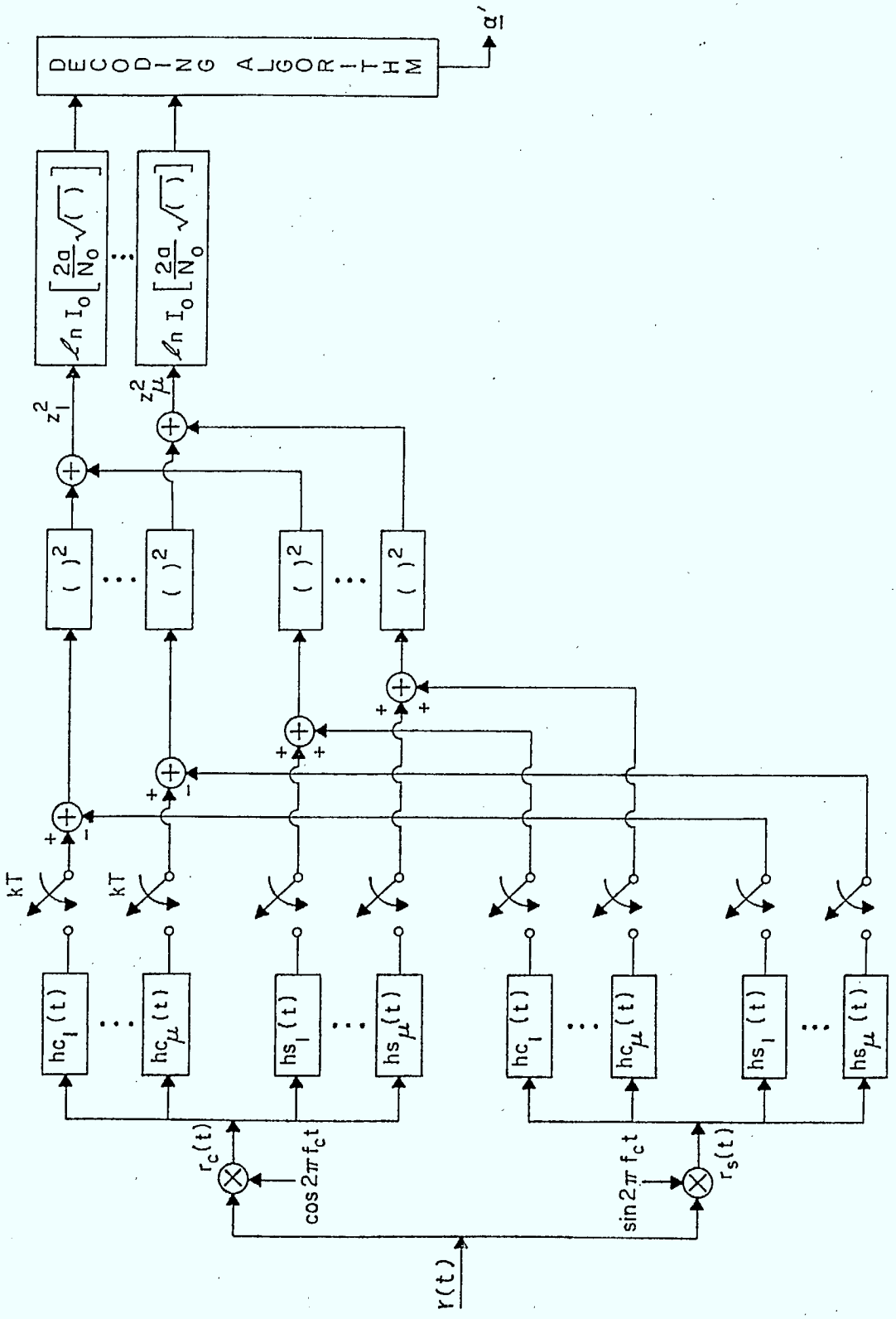

Figure 3.3 Suboptimum simplified noncoherent receiver structure

3.4 Summary

In this Chapter, three noncoherent receivers with sequential decoding algorithms have been derived. The first receiver has the simplest decoding algorithm. It is optimum over an observation interval of a single hop interval and the sequence estimation is carried out on a hop-by-hop basis. In general, a sequence estimation receiver which could decode symbols continuously rather than on a hop by hop basis is more desireable. Hence, a receiver algorithm with maximum likelihood decoding spanning hops, is derived together with the decoding algorithm. However, the resulting decoding algorithm is rather complex with a subprocedure necessary for calculating metric across hops, although simplification may be possible when the length of the frequency pulse is much shorter than the hop length. Another simplified suboptimum receiver is also derived by treating symbols as if they were all noncoherent with random phase, hence resulting in a much simpler decoding process. Only memory introduced by correlative encoding in the signal is utilized in the decoding process while the memory due to phase continuity of the signal is not put to use. The performance of this simplified receiver would be inferior to the optimum one spanning hops but the decoding algorithm is much simpler with no additional subprocedure for computing the metric across hops. However, the second and the third receivers, both of which attempt to attain a longer observation interval than the length of one hop by calculating metric across hops, require the signal to noise ratio to be known. Hence, extra circuitry for estimating the signal to noise ratio is required in order for the receivers to compute the metric across hops. This additional complexity and the already complicated decoding algorithm will drive the practical implementation to favor the noncoherent receiver on a hop-by-hop decision basis.

Chapter Four

ERROR PERFORMANCE ANALYSIS

Three algorithm-based sequence estimation receivers for decoding the dehopped CPM signal have been presented in Chapter Three. Except for the first receiver which decodes the transmitted sequence on a hop-by-hop basis, the other two receivers require the transmitted signal amplitude and the noise spectral density to be known by the receiver in order to calculate the metric across the frequency hops. Auxiliary circuitry is then required to estimate the noise spectral density and signal amplitude. This extra circuitry requirement together with the additional complexity in the decoder for spanning hops would justify a retreat to the simpler hop-by-hop sequence estimation receiver unless the difference in performance is dramatic. The hop-by-hop sequence estimation receiver thus appears to be the most promising design among the three receivers proposed in Chapter Three, for implementation.

In this chapter, the error performance of the hop-by-hop sequence estimation receiver is evaluated. The primary additive disturbance on a satellite channel can usually be reasonably modelled by white Gaussian noise. Hence the error performance of the noncoherent receiver under additive white Gaussian noise will be evaluated first. An upper bound on the bit error rate (BER) is evaluated for various partial response polynomials and with both rectangular and raised cosine baseband pulse shapings. The BER upper bounds would provide a basis for choosing the various operating parameters of the systems, such as length of the hop interval, partial response system polynomial and type of pulse shaping to be used to achieve a desired system performance. The performance improvement by transmitting an initial segment of known symbols once the carrier hops to a new frequency, either for synchronization purpose or solely for improving the error performance of the receiver, is also examined. Since many

spread spectrum communications systems are designed to operate in the presence of intentional interference, the performance of the receiver in the presence of partial band noise jamming and multiple-tone jamming will also be evaluated.

4.1 Performance In Additive White Gaussian Noise

The error probability for noncoherent detection of binary FSK has been derived by Stein [44,45]. Osborne and Luntz [33] and also Schonhoff [34] have evaluated upper bounds on the BER for symbol-by-symbol detection of CPFSK with a multiple symbol observation interval in the binary case and M-ary case respectively. Svensson and Sundberg [36,37] have analysed the error performance of the noncoherent symbol-by-symbol decision receiver for CPM, by using an equivalent distance, which asymptotically at high SNR plays the same role as the Euclidean distance in coherent reception. For the symbol-by-symbol noncoherent detection of CPM with a multiple symbol observation interval, approximate upper bounds and lower bounds on the BER have been derived in [36,37].

4.1.1 Probability of An Error Event

We shall begin our error analysis for the noncoherent hop-by-hop sequence estimation receiver presented in section 3.1 of the previous chapter. Without loss of generality, consider detection over the first hop. Let $\underline{\alpha} = \{ \alpha_0, \alpha_1, \alpha_2, \ldots, \alpha_{N-1} \}$ denote the transmitted sequence in the hop interval. For hop-by-hop sequence estimation, at time kT ($k \geq 2$) the receiver keeps η survivor paths leading to the η states in the trellis at time kT. The equivalent likelihoods for every possible path extended from the η survivors at time (k-1)T leading to each node at time kT in the modulation trellis, are compared. That is, the decoder has to decide on the maximum likelihood path leading to each state in the trellis over an observation interval of length kT. The decoder then keeps the path with the largest simplified decoder metric at time

kT as the survivor at each node. However, the path segment with the largest metric does not necessarily have to be an initial portion of the maximum likelihood path with the largest equivalent likelihood over [0 , NT]. Hence unless the decoder keeps all possible paths over the hop interval and only decides on the maximum likelihood path at the end of a hop interval (which would be impractical considering the large memory and computation requirement), the decoder may make an erroneous decision by discarding the initial segment of the true path early at the start of a hop. Once any initial segment of the true path has been discarded by the decoder, it would never be included again. However, the remaining survivor paths may still have a large portion of the sequence the same as that of the true path and also may remerge with the true path at some later time. The final estimated path will be the one with the largest simplified decoder metric at time NT. The estimated sequence is not the maximum likelihood path over the hop interval, if any initial portion of the maximum likelihood path is prematurely discarded by the decoder during the decoding process. Maximum likelihood decoding performance can be guaranteed only if the decoder keeps all the possible paths through the trellis in a hop interval and decides on the maximum likelihood sequence at the end of a hop interval.

During a hop interval the estimated path and the true path may diverge and remerge a number of times. Each distinct separation is called an error event [39,40]. The set of all possible error events starting at some time k_1T is a tree-like trellis which starts at s_{k_1} and each of whose branches ends on the correct path. Unlike the case of coherent detection in which the error events are probabilistically independent of each other [40], an error event starting at any particular time actually depends on the previous history of the estimated path due the nature of the decision parameter (which is the equivalent likelihood and the sum of the squares of the inphase and quadrature likelihoods) for noncoherent detection. However, if we consider the probability of only one error event to occur, some insight into the error mechanism can be gained.

For the hop-by-hop sequence estimation receiver, the decoder compares the η possible paths leading to each node in the trellis and keeps the one which has the largest equivalent likelihood, for each node. An error event occurs whenever the true path is rejected by the decoder at any time kT, since then the true path segment from 0 to kT will never be included in the final decision path. The probability of an erroneous decision is the probability of any error event occurring during the hop interval. For an error event ϵ starting at time k_1T and ending at time k_2T, the probability of ϵ is simply the probability that given the observation over the interval from 0 to $k_2 T$, $\underline{\alpha}'_{k_2}$, which is the estimated sequence corresponding to the error event ϵ, is more likely than the transmitted sequence $\underline{\alpha}_{k_2}$. This error probability is given by

$$\Pr[\epsilon] = \Pr[\ell'(\underline{\alpha}_{k_2}, \underline{\alpha}'_{k_2}) > \ell'(\underline{\alpha}_{k_2}, \underline{\alpha}_{k_2})], \quad \underline{\alpha}'_{k_2} \neq \underline{\alpha}_{k_2} \tag{4.1}$$

where

$$\ell'(\underline{\alpha}_{k_2}, \underline{\alpha}'_{k_2}) = \left(\int_0^{k_2T} r(t)\ \cos[2\pi f_c t + \psi(t, \underline{\alpha}')]\ dt\right)^2 + \left(\int_0^{k_2T} r(t)\ \sin[2\pi f_c t + \psi(t, \underline{\alpha}')]\ dt\right)^2 \tag{4.2}$$

and

$$\ell'(\underline{\alpha}_{k_2}, \underline{\alpha}_{k_2}) = \left(\int_0^{k_2T} r(t)\ \cos[2\pi f_c t + \psi(t, \underline{\alpha})]\ dt\right)^2 + \left(\int_0^{k_2T} r(t)\ \sin[2\pi f_c t + \psi(t, \underline{\alpha})]\ dt\right)^2, \tag{4.3}$$

where $\psi(t, \underline{\alpha})$ is the information carrying phase function given previously. Since the correlator references are the inphase and quadrature components of a constant amplitude waveform, $\ell'(\underline{\alpha}, \underline{\alpha}')$ may be regarded as the output of a complex correlator with reference $\bar{s}(t, \underline{\alpha}')$, which is given by

$$\begin{aligned} \bar{s}(t, \underline{\alpha}') &= \cos[2\pi f_c + \psi(t, \underline{\alpha}')] + j \sin[2\pi f_c + \psi(t, \underline{\alpha}')] \\ &= \exp[\, j(2\pi f_c t + \psi(t, \underline{\alpha}'))\,]. \end{aligned} \tag{4.4}$$

The likelihood parameter $\ell'(\underline{\alpha}_{k_2}, \underline{\alpha}'_{k_2})$ may be written in complex notation as

$$\ell'(\underline{\alpha}_{k_2}, \underline{\alpha}'_{k_2}) = \left| \int_0^{k_2 T} r(t) \exp j[2\pi f_c t + \psi(t, \underline{\alpha}')] dt \right|^2 = |Z_1|^2. \tag{4.5}$$

Similarly, we have

$$\ell'(\underline{\alpha}_{k_2}, \underline{\alpha}_{k_2}) = \left| \int_0^{k_2 T} r(t) \exp j[2\pi f_c t + \psi(t, \underline{\alpha})] dt \right|^2 = |Z_2|^2. \tag{4.6}$$

Thus we have

$$\Pr[\,\epsilon\,] = \Pr[\,|Z_1|^2 > |Z_2|^2\,]. \tag{4.7}$$

The probability of an error event is just the probability of one Rician variable exceeding another and the solution is known to be given by [36,44]

$$\Pr[\,\epsilon\,] = \frac{1}{2}[\,1 - Q(\sqrt{b}, \sqrt{a}) + Q(\sqrt{a}, \sqrt{b})\,], \tag{4.8}$$

where Q (x, y) is the Marcum Q function [45] defined by

$$Q(x,y) = \int_y^{\infty} \exp\left(- \frac{x^2 + u^2}{2} \right) I_0(xu)\, du \tag{4.9}$$

and $I_0(\,.\,)$ is the zeroth-order modified Bessel function. Techniques for recursive evaluation of the Marcum Q function are given in [46,47]. The parameters a and b are given by

$$\begin{Bmatrix} a \\ b \end{Bmatrix} = \frac{1}{2\sigma^2}\left\{ \frac{|M_1|^2 + |M_2|^2 - 2\mathrm{Re}\{ M_1^* M_2 \rho \}}{1 - |\rho|^2} \mp \frac{|M_2|^2 - |M_1|^2}{\sqrt{1 - |\rho|^2}} \right\}, \tag{4.10}$$

with

$$M_1 = E\{ Z_1 \}, \tag{4.11}$$

$$M_2 = E\{ Z_2 \}, \tag{4.12}$$

$$\sigma^2 = \mathrm{var}[Z_1] = \mathrm{var}[Z_2] = E\{ (Z_2 - M_2)^* (Z_1 - M_1) \}, \tag{4.13}$$

$$\rho = \frac{1}{\sigma^2} E\{ (Z_2 - M_2)^* (Z_1 - M_1) \}, \tag{4.14}$$

where the expectation is taken with respect to the complex Gaussian variables and the superscript * denotes the complex conjugate. By straightforward evaluation of Eqs.(4.11) to (4.14) and substituting the values of the parameters into Eq.(4.10), we have [33,34,35,44]

$$\begin{Bmatrix} a \\ b \end{Bmatrix} = \frac{k_2 E_b}{2N_o} \log_2 M \ [1 \mp \sqrt{1 - |\rho(\underline{\alpha}_{k_2}, \underline{\alpha}'_{k_2})|^2}], \tag{4.15}$$

where $\rho(\underline{\alpha}_{k_2}, \underline{\alpha}'_{k_2})$ is the normalized complex crosscorrelation between the two random variables Z_1 and Z_2 and the parameter $|\rho(\underline{\alpha}_{k_2}, \underline{\alpha}'_{k_2})|^2$ is given by

$$\begin{aligned} |\rho(\underline{\alpha}_{k_2}, \underline{\alpha}'_{k_2})|^2 = & \left(\frac{1}{k_2 T} \int_0^{k_2 T} \cos[\psi(t, \underline{\alpha}') - \psi(t, \underline{\alpha})] dt \right)^2 \\ & + \left(\frac{1}{k_2 T} \int_0^{k_2 T} \sin[\psi(t, \underline{\alpha}') - \psi(t, \underline{\alpha})] dt \right)^2. \end{aligned} \tag{4.16}$$

Since

$$\psi(t, \underline{\alpha}') - \psi(t, \underline{\alpha}) = \psi(t, \underline{\gamma}), \tag{4.17}$$

where

$$\underline{\gamma}_{k_2} = \underline{\alpha}'_{k_2} - \underline{\alpha}_{k_2}, \tag{4.18}$$

the evaluation of a and b in Eq. (4.8) actually depends only on the difference sequence $\underline{\gamma}_{k_2}$, rather than on both individual sequences, $\underline{\alpha}'$ and $\underline{\alpha}$. Eq. (4.16) can be rewritten as

$$\begin{aligned} |\rho(\underline{\alpha}_{k_2}, \underline{\alpha}'_{k_2})|^2 &= |\rho(\underline{\gamma}_{k_2})|^2 \\ &= \left(\frac{1}{k_2 T}\int_0^{k_2 T} \cos[\psi(t, \underline{\gamma})]\, dt\right)^2 + \left(\frac{1}{k_2 T}\int_0^{k_2 T} \sin[\psi(t, \underline{\gamma})]\, dt\right)^2. \end{aligned} \tag{4.19}$$

For an error event starting at time $k_1 T$, $\psi(t, \underline{\gamma}) = 0$ for $t < k_1 T$. Hence we have

$$\begin{aligned} |\rho(\underline{\gamma}_{k_2})|^2 &= \left[\frac{1}{k_2 T}\left(k_1 T + \int_{k_1 T}^{k_2 T} \cos\psi(t, \underline{\gamma})\, dt\right)\right]^2 \\ &\quad + \left[\frac{1}{k_2 T}\int_{k_1 T}^{k_2 T} \sin\psi(t, \underline{\gamma})\, dt\right]^2. \end{aligned} \tag{4.20}$$

The probability of any particular error event starting at time $k_1 T$ and ending at $k_2 T$, can then be calculated using Eqs.(4.8), (4.15) and (4.20). Error paths having the largest complex cross-correlations $\rho(\underline{\gamma}_{k_2})$ will have the highest probability of occurrence for all values of $\frac{E_b}{N_o}$[37,44,45]. A quantity related to the Euclidean distance in coherent detection is the equivalent Euclidean distance, introduced as an error performance measure for the noncoherent receiver in [36,37]. At high SNR, we have $b \gg 1$, $a \gg 1$ and $\sqrt{b} \gg \sqrt{b} - \sqrt{a} > 0$. Approximation of the Marcum Q function gives

$$P(\underline{\gamma}) \simeq Q(\sqrt{b} - \sqrt{a}); \qquad \text{large } \frac{E_b}{N_o}, \tag{4.21}$$

where

$$Q(x) = \frac{1}{\sqrt{2\pi}} \int_{x}^{\infty} e^{-\frac{u^2}{2}} du. \tag{4.22}$$

Substituting expressions for a and b into Eq.(4.21) and putting the probability expression in a form similar to that for coherent detection, we have

$$P(\gamma) \simeq Q\left(\sqrt{d_e^2 \frac{E_b}{N_o}}\right); \qquad \text{large } \frac{E_b}{N_o}, \tag{4.23}$$

where d_e^2 denotes the squared equivalent distance. The equivalent distance between the two signals corresponding to $\underline{\alpha}'$ and $\underline{\alpha}$ over a time interval [0, k_2T] relates to the complex correlation through the following expression.

$$d_e^2 = k_2 (1 - |\rho(\underline{\gamma}_{k_2})|) \log_2(M). \tag{4.24}$$

From Eq.(4.23), it is clear that asymptotically at high SNR the equivalent Euclidean distance plays the same role as the Euclidean distance in the coherent case.

A set of the error events which start at time 0 and have the smallest equivalent distances, is first determined. The equivalent distances of the error signal paths associated with these error events starting at various times k_1T are then calculated. The equivalent distance results for MSK, DMSK and TFM with h = 0.5 and with rectangular pulse shaping are shown in Figs. 4.1 to 4.3.

Different error events having different phase differences may have the same value of squared equivalent distance. Hence, each squared equivalent distance curve in Figs. 4.1 to 4.3 may correspond to more than one error event. In general the equivalent distance of an error event is the lowest when the error event starts at time 0. It is because the noncoherent receiver

has not acquired any information about the initial phase of the signal at time 0 and the equivalent distance between the error signal path and the transmitted signal is then the lowest. Once the noncoherent receiver has received symbols and does not make an error (the error event starts at some time $k_1T > 0$), the noncoherent receiver then gradually acquires the phase of the received signal. The equivalent distance of the signal hence increases if it starts at some time greater than 0. Also, as can be seen from these results, some error events have equivalent distances that stay constant independent of the starting time of the error event. If the error phase path $\psi(t, \underline{\gamma})$ has a particular shape over k_1T to k_2T such that

$$\int_{k_1T}^{k_2T} \sin \psi(t, \underline{\gamma})\, dt = 0, \tag{4.25}$$

then

$$|\rho(\underline{\gamma}_{k_2})|^2 = [\frac{1}{k_2T}(k_1T + \int_{k_1T}^{k_2T} \cos \psi(t, \underline{\gamma})\, dt)]^2 \tag{4.26}$$

and the squared equivalent distance for this particular error path over the time interval $[0, K_2T]$ is

$$d_e^2 = (k_2 - k_1) - \frac{1}{T}\int_{k_1T}^{k_2T} \cos \psi(t, \underline{\gamma})\, dt. \tag{4.27}$$

For any error event which satisfies Eq.(4.25), d_e^2 will be independent of the starting time k_1T of the error event. This explains why some of the d_e^2 are constant independent of starting time.

The probability of each of these error events at an SNR of 10 dB is evaluated and plotted in Figs. 4.4 to 4.6. We can see that the probability of the error events with small equivalent distances is much higher than for the other error events which have larger equivalent distance,

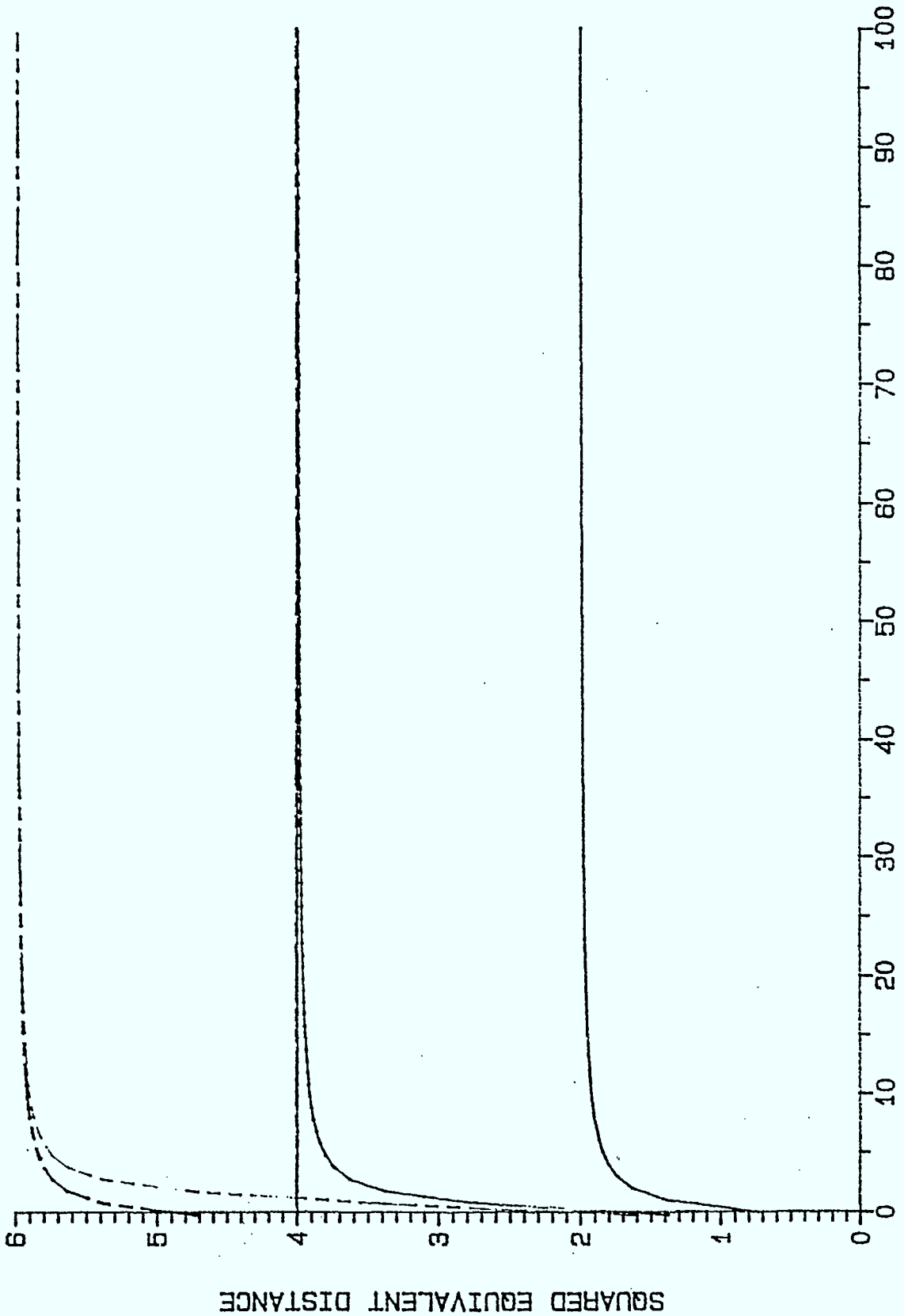

Figure 4.1 d_e^2 for FH/MSK with rectangular pulse shaping

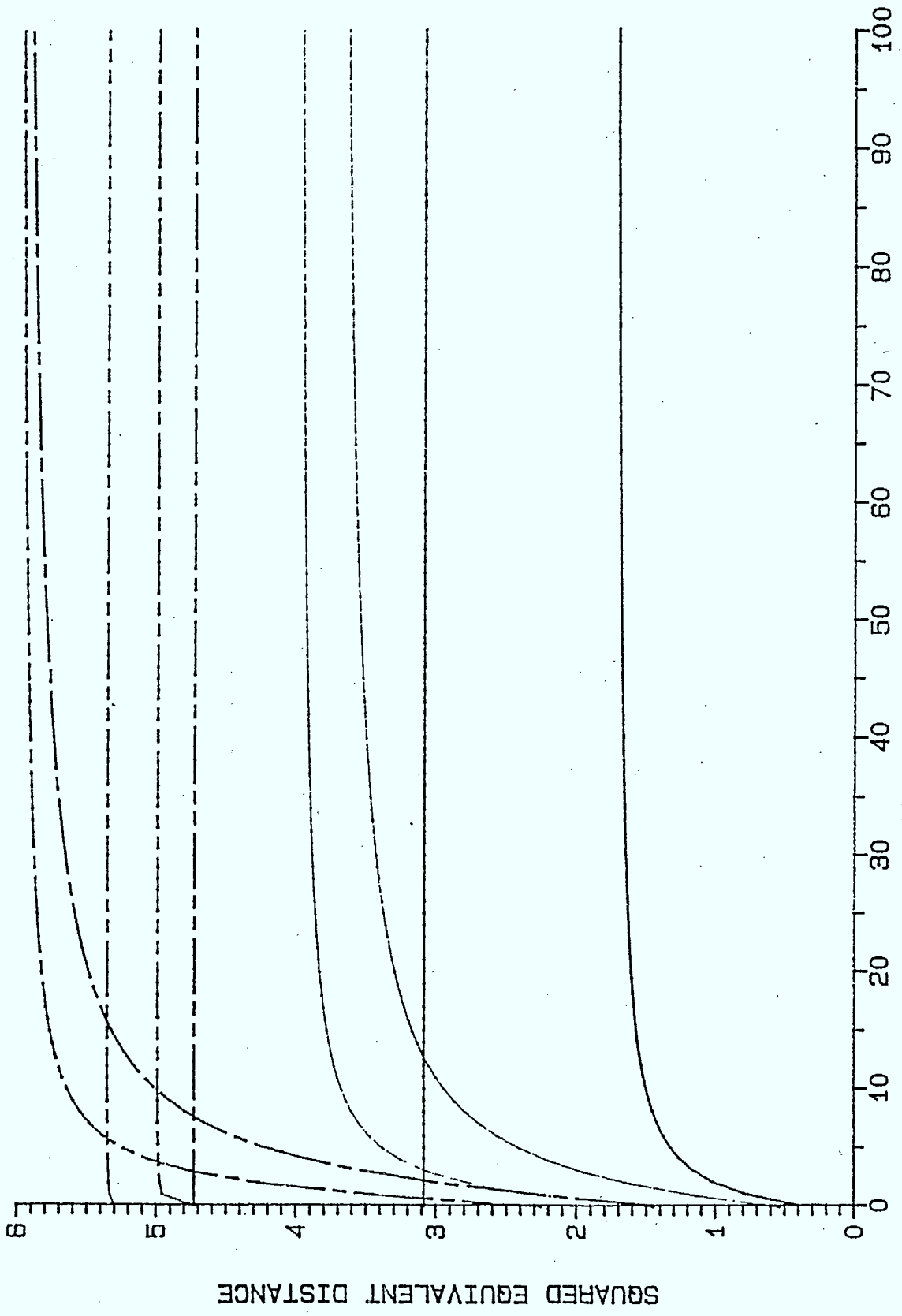

Figure 4.2 d_e^2 for FH/DMSK with rectangular pulse shaping

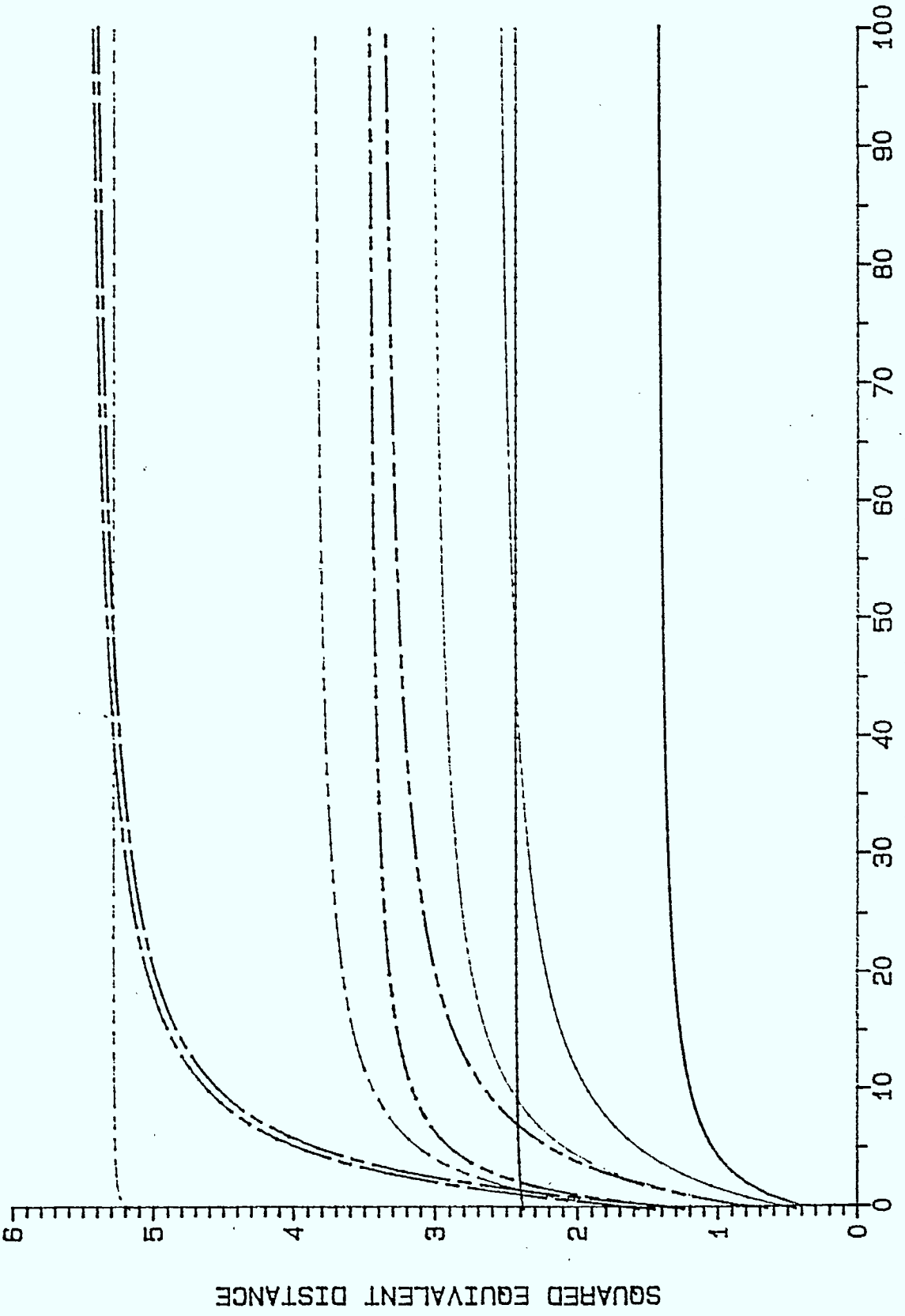

Figure 4.3 d_e^2 for FH/TFM, h = 0.5 with rectangular pulse shaping

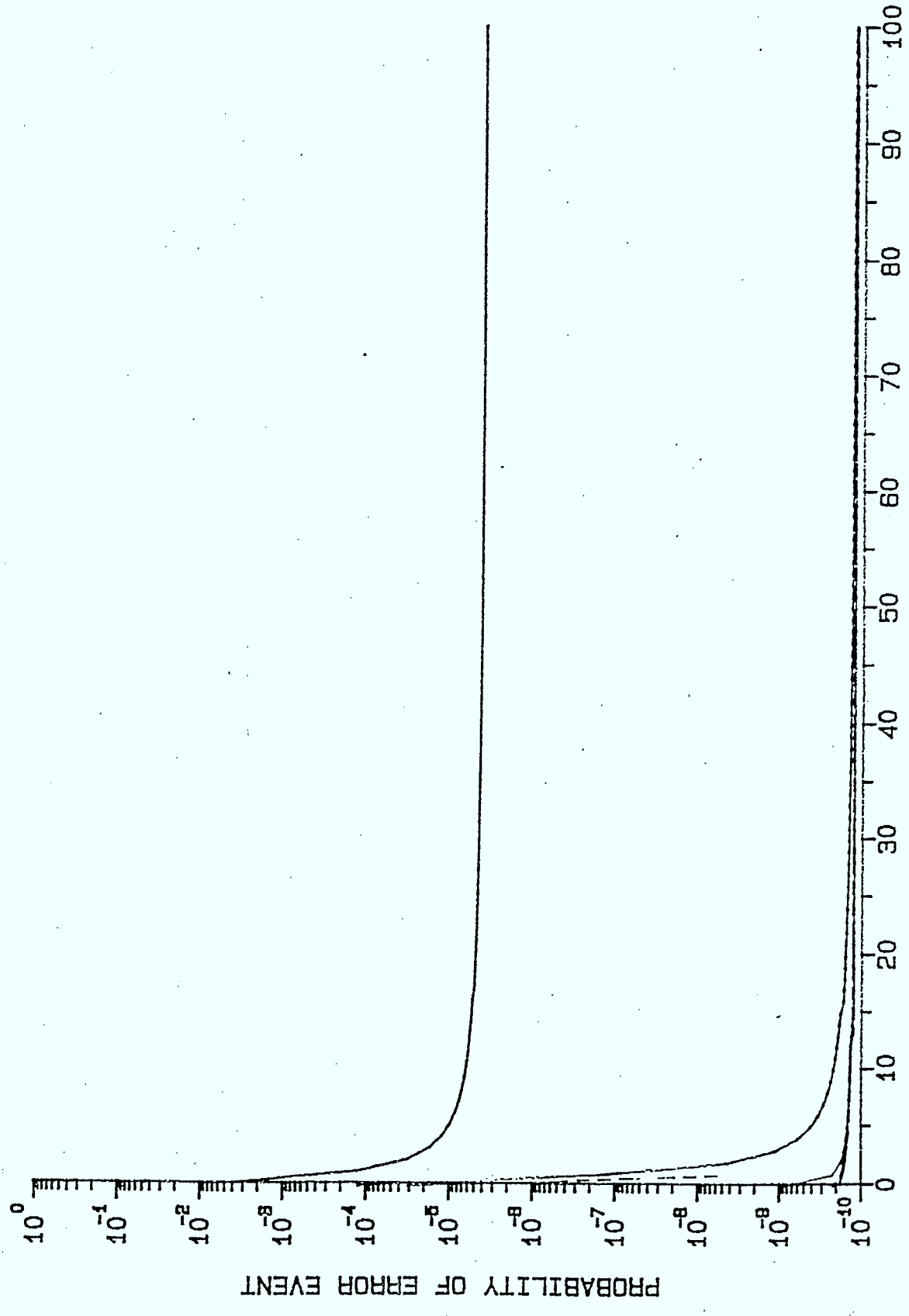

Figure 4.4 Pr[ϵ] for FH/MSK with rectangular pulse shaping at SNR = 10 dB

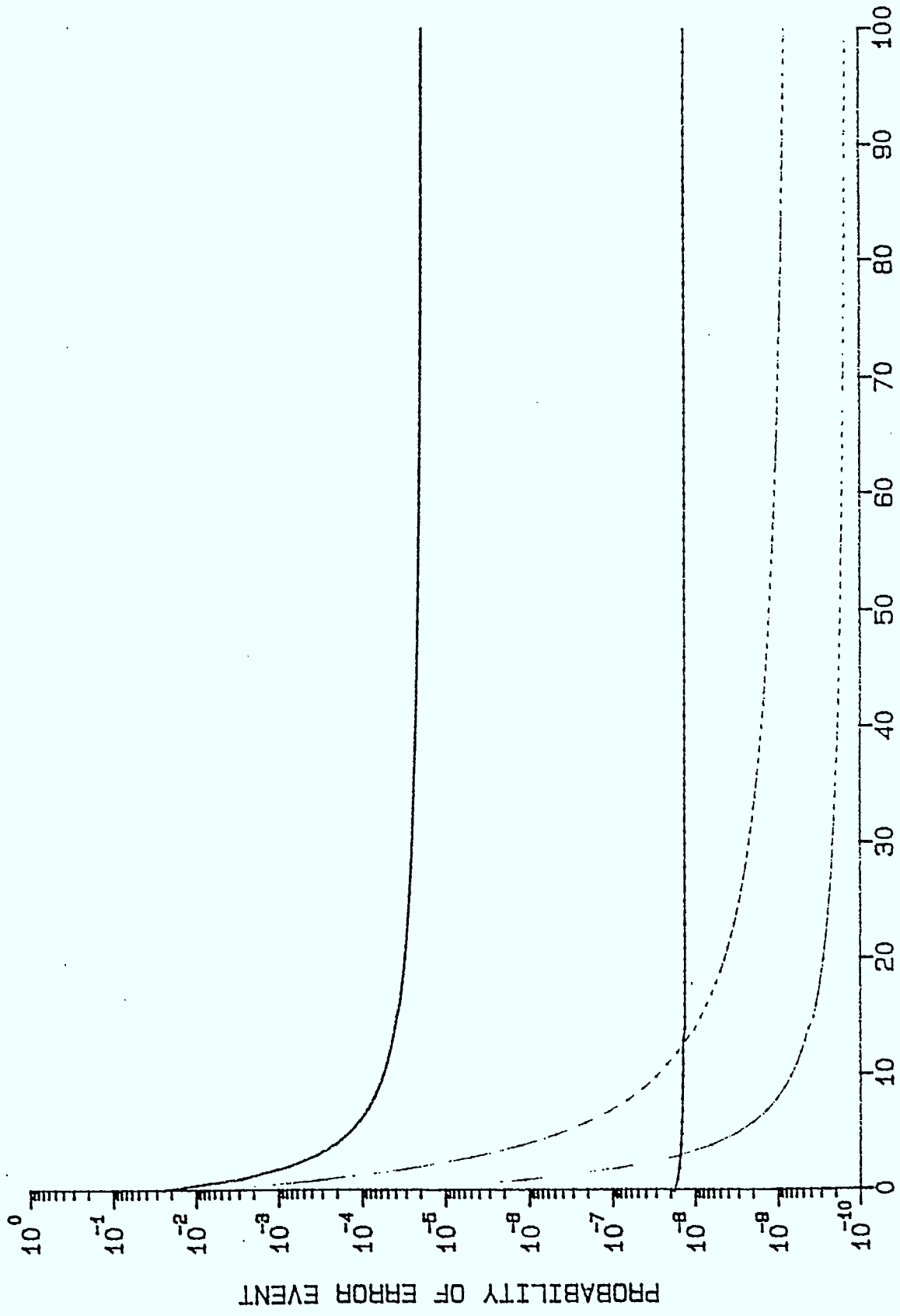

Figure 4.5 $Pr[\epsilon]$ for FH/DMSK with rectangular pulse shaping at SNR = 10 dB

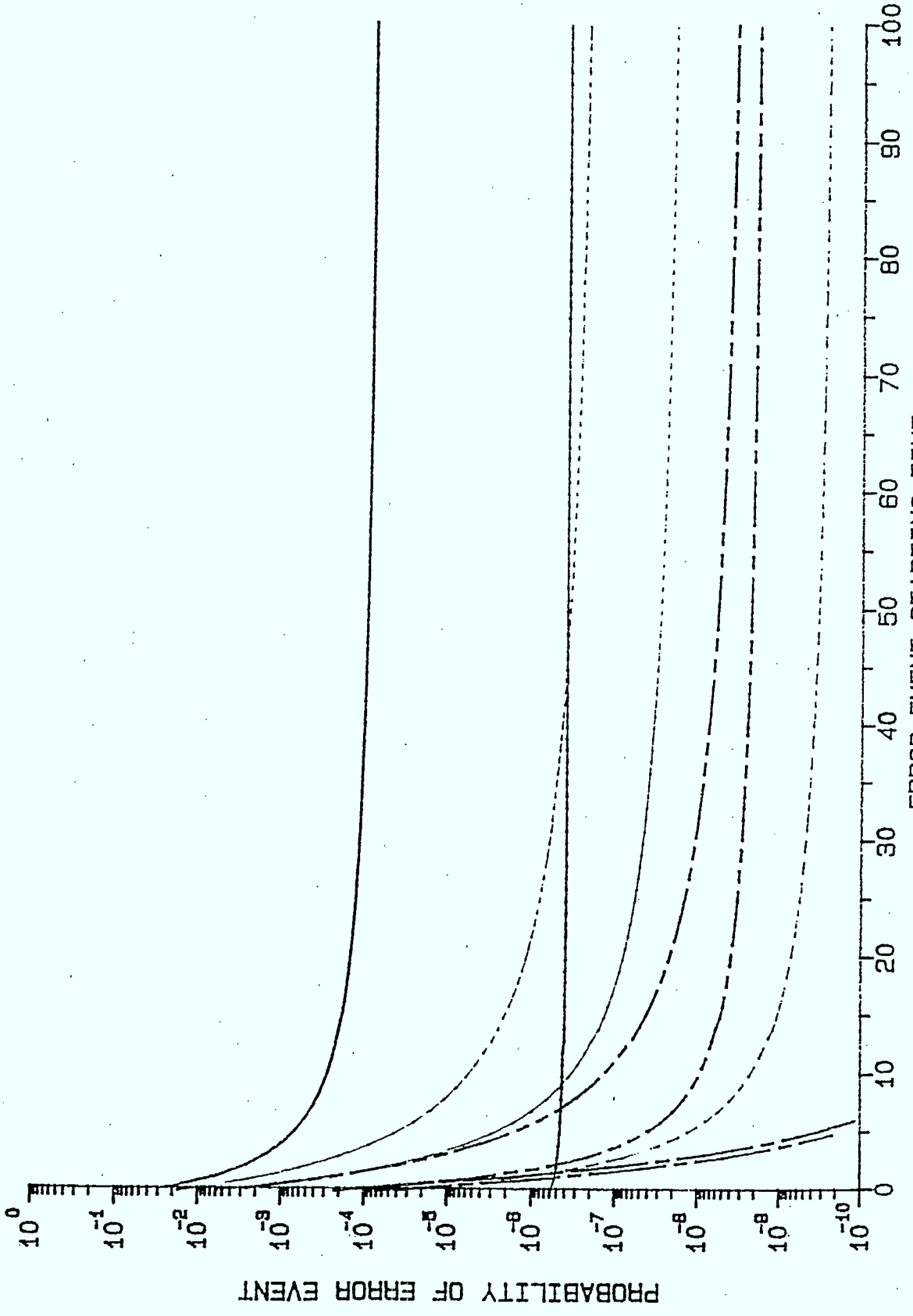

Figure 4.6 Pr[ϵ] for FH/TFM, h = 0.5 with rectangular pulse shaping at SNR = 10 dB

even at a moderately high SNR of 10 dB. At high SNR, we should expect the error performance of this sequence estimaton receiver to be dominated by those error events which have small equivalent distances. Also, error events are more likely to occur at the start of the hop interval than at some later time during the interval. This suggests the possibility of performance improvement by transmitting a known initial data segment as the carrier hops to a new frequency. Transmitting a known initial symbol segment will be investigated in section 4.1.4.

4.1.2 Upper Bound on Bit Error Probability

So far we have examined the probability of only one error event occurring during the decoding process. A number of error events may occur in the detection of the transmitted sequence in a hop interval. Since the error events are not independent but depend on the previous portion of the estimated path, the error performance of the hop-by-hop sequence estimation receiver cannot be based on the probability of only one error event to occur during a hop interval but has to be based on the probability of erroneous decisions over the entire hop interval. At the end of a hop interval, the receiver will choose the sequence $\underline{\alpha}' = \{ \alpha'_0, \alpha'_1, \alpha'_2, \ldots, \alpha'_{N-1} \}$, which has the largest simplified decoder metric at time NT. Any number of error events may have occurred during the decoding period of a hop interval. A sequence error occurs whenever the estimated sequence $\underline{\alpha}'$ is different from $\underline{\alpha}$ in one or more places.

Given that $\underline{\alpha}$ is the transmitted sequence, the probability of an erroneous decision is then given by

$$P(\text{Error}\,|\underline{\alpha}) = \Pr\Big[\max_{\underline{\alpha}' \neq \underline{\alpha}} \ell'(\underline{\alpha}, \underline{\alpha}') > \ell'(\underline{\alpha}, \underline{\alpha})\Big]. \tag{4.28}$$

This error probability is difficult to calculate exactly but it can be upper bounded by

$$P(\text{Error}\,|\underline{\alpha}) \le \sum_{\substack{\underline{\alpha}' \\ \underline{\alpha}' \neq \underline{\alpha}}} \Pr[\,\ell'(\underline{\alpha}, \underline{\alpha}') > \ell'(\underline{\alpha}, \underline{\alpha})\,]. \tag{4.29}$$

The bit error probability is given by weighting each probability $\Pr[\,\ell'(\underline{\alpha}, \underline{\alpha}') > \ell'(\underline{\alpha}, \underline{\alpha})\,]$ with the number of bit errors over the number of bits decoded as

$$P(\text{bit error}\,|\underline{\alpha}) \le \sum_{\substack{\underline{\alpha}' \\ \underline{\alpha}' \neq \underline{\alpha}}} \frac{e(\underline{\alpha}, \underline{\alpha}')}{N} \Pr[\,\ell'(\underline{\alpha}, \underline{\alpha}') > \ell'(\underline{\alpha}, \underline{\alpha})\,], \tag{4.30}$$

where $e(\underline{\alpha}, \underline{\alpha}')$ is the number of bit errors for detecting $\underline{\alpha}'$ given that $\underline{\alpha}$ is transmitted. The average bit error probability is then given by averaging over all the possible transmitted sequences as

$$P_e \le \frac{1}{\mu} \sum_{\underline{\alpha}} \sum_{\substack{\underline{\alpha}' \\ \underline{\alpha}' \neq \underline{\alpha}}} \frac{e(\underline{\alpha}, \underline{\alpha}')}{N} \Pr[\ell'(\underline{\alpha}, \underline{\alpha}') > \ell'(\underline{\alpha}, \underline{\alpha})\,], \tag{4.31}$$

where $\mu = 2^N$ is the total number of possible transmitted sequences in a hop interval of length NT. Since the error probability depends on only the difference between $\underline{\alpha}'$ and $\underline{\alpha}$ rather than on the individual $\underline{\alpha}$ and $\underline{\alpha}'$, the upper bound on the bit error probability can be rewritten in terms of $\underline{\gamma}$ as

$$P_e \le \frac{1}{\mu} \sum_{\substack{\underline{\gamma} \\ \underline{\gamma} \neq 0}} \omega(\underline{\gamma}) \frac{e(\underline{\gamma})}{N} P(\underline{\gamma}), \tag{4.32}$$

where $e(\underline{\gamma})$ is the number of nonzero sequence elements of $\underline{\gamma}$, which corresponds to the number of bit errors when $\underline{\alpha}'$ is detected given that $\underline{\alpha}$ is the transmitted sequence. $\omega(\underline{\gamma})$ is the total number of pairs of $\underline{\alpha}'$ and $\underline{\alpha}$ corresponding to a difference sequence $\underline{\gamma}$. Since a difference sequence $\underline{\gamma}$ having $e(\underline{\gamma})$ nonzero elements would result from $2^{N-e(\underline{\gamma})}$ different pairs of $\underline{\alpha}$ and $\underline{\alpha}'$, $\omega(\underline{\gamma})$ is then given by

$$\omega(\underline{\gamma}) = 2^{N-e(\underline{\gamma})}. \tag{4.33}$$

$P(\underline{\gamma})$ is the probability of error by detecting $\underline{\alpha}'$ rather than $\underline{\alpha}$ as the transmitted sequence. Similar to the expression for the probability of an error event given in the previous section, this probability is given by

$$P(\underline{\gamma}) = \frac{1}{2}[\,1 - Q(\sqrt{b}, \sqrt{a}) + Q(\sqrt{a}, \sqrt{b})\,], \tag{4.34}$$

where $Q(\ ,\ )$ is the Marcum Q function. The parameters a and b are given by Eq. (4.15) with $k_2 = N$ and rewritten in terms of $\underline{\gamma}$ as

$$\left\{ \begin{matrix} a \\ b \end{matrix} \right\} = \frac{NE_b}{2N_o} \log_2 M \left[\,1 \mp \sqrt{1 - |\rho(\underline{\gamma})|^2}\,\right], \tag{4.35}$$

with $|\rho(\underline{\gamma})|^2$ given by

$$|\rho(\underline{\gamma})|^2 = \left[\frac{1}{NT}\int_0^{NT} \cos\psi(t, \underline{\gamma})dt\,\right]^2 + \left[\frac{1}{NT}\int_0^{NT} \sin\psi(t, \underline{\gamma})dt\,\right]^2. \tag{4.36}$$

4.1.3 Computation and Approximation

In order to compute the upper bound on the bit error rate as given by Eqs. (4.32) to (4.36) systematically and efficiently, we notice that for binary transmission, the difference sequence elements γ_n can take on three possible values namely 0, +2 and - 2. Hence there can be $3^N - 1$ difference sequences $\underline{\gamma}$, for a hop interval of length NT in Eq. (4.32). For any $\underline{\gamma}$ there is always another sequence with opposite signs in all the sequence elements. The number of terms in Eq. (4.32) can be reduced by a factor of 2, since $P(-\underline{\gamma}) = P(\underline{\gamma})$ as can be easily seen from Eqs. (4.34) to (4.36). The number of difference sequences to be considered in Eq. (4.32) is then $\frac{1}{2}(3^N - 1)$. If the three possible values of each difference sequence element γ_n, namely 2, 0 and - 2 are mapped as 0, 1 and 2 respectively, then each difference sequence element γ_n can be represented as a base-3 digit and the difference sequence can then be represented by N base-3 digits. Each $\underline{\gamma}$ to be considered in the bit error rate calculation in Eq. (4.32) can be represented by a base-3 number of values from 0 to $\frac{1}{2}(3^N - 1) - 1$. Numbers from 0 to $\frac{1}{2}(3^N - 1) - 1$ are decoded sequentially as base-3 digits, which are then converted to 0, +2 or - 2 as the difference sequence elements, to be used in evaluating the upper bound on the BER as given by Eq. (4.32).

$|\rho(\underline{\gamma})|^2$ is required to calculate $P(\underline{\gamma})$ in Eq.(4.34). Eq. (4.36) can be rewritten as

$$|\rho(\underline{\gamma})|^2 = \{\frac{1}{NT}\sum_{k=0}^{N-1}\int_{kT}^{(k+1)T}\cos\psi(t,\underline{\gamma})\,dt\}^2 + \{\frac{1}{NT}\sum_{k=0}^{N-1}\int_{kT}^{(k+1)T}\sin\psi(t,\underline{\gamma})\,dt\}^2. \tag{4.37}$$

Substituting Eq. (3.49) with $\underline{\alpha}'$ replaced by $\underline{\gamma}$ in the above equation for $\psi(t,\underline{\gamma})$ in the k^{th} symbol interval, we have

$$|\rho(\underline{\gamma})|^2 = \{\frac{1}{N}\sum_{k=0}^{N-1}[\cos\zeta_k C(d_k) - \sin\zeta_k S(d_k)]\}^2 + \{\frac{1}{N}\sum_{k=0}^{N-1}[\cos\zeta_k S(d_k) + \sin\zeta_k C(d_k)]\}^2, \tag{4.38}$$

where

$$C(d_k) = \frac{1}{T}\int_{kT}^{(k+1)T}\cos 2\pi h d_k v(t)\,dt, \tag{4.39a}$$

$$S(d_k) = \frac{1}{T}\int_{kT}^{(k+1)T}\sin 2\pi h d_k v(t)\,dt, \tag{4.39b}$$

$$\zeta_k = \pi h\sum_{0}^{k-1} d_n. \tag{4.40}$$

d_k is the correlative encoded difference sequence given by

$$d_k = \frac{1}{C}\sum_{\ell=0}^{m} k_\ell \gamma_{k-\ell}, \tag{4.41}$$

where C is the normalizing constant as defined by Eq. (2.6) and the k_ℓ are the coefficients of the correlative encoding polynomial.

To speed up the calculation of $|\rho(\underline{\gamma})|^2$, all possible integrals of the cosine and sine of the possible phase over a symbol interval, $C(d_k)$ and $S(d_k)$ are initially calculated and stored in an array. This avoids repeated numerical integration to obtain $C(d_k)$ and $S(d_k)$ when the baseband pulse is not rectangular.

When N is large, evaluation of the upper bound as given by Eq. (4.32) becomes computationally infeasible, since the number of difference sequences to be considered is $\frac{1}{2}(3^N - 1)$, which grows exponentially with N. Approximation of the upper bound is then necessary for large N. At high SNR, the probabilities of those error paths which have large equivalent distances, are small compared with those having small equivalent distances. The paths having large equivalent distances over a hop interval can then be neglected. The upper bound on the bit error rate is approximated by

$$P_e \lesssim \frac{1}{\mu} \sum_{\substack{\underline{\gamma} \in \mathbf{S} \\ \underline{\gamma} \neq 0}} \omega(\underline{\gamma}) \frac{e(\underline{\gamma})}{N} P(\underline{\gamma}), \tag{4.42}$$

where **S** denotes the set of difference sequences corresponding to the set of small equivalent distance paths over the hop interval.

To determine **S**. we notice that there will be complete error events during the hop and also incomplete error events starting near the end of a hop. For the hop-by-hop detection receiver, the difference sequences $\underline{\gamma}$ corresponding to an error event ϵ of duration ℓ starting at time k_1T, will have $\gamma_n = 0$ for $n < k_1$ and $n > k_1 + \ell$. The square of the complex correlation as given by Eq. (4.36) becomes

$$\begin{aligned} |\rho(\underline{\gamma})|^2 &= \{ \frac{1}{NT} [k_1T + \int_{k_1T}^{(k_1+\ell)T} \cos\psi(t, \underline{\gamma}) dt + (N - k_1 - \ell)T] \}^2 \\ &\quad + \{ \frac{1}{NT} \int_{k_1T}^{(k_1+\ell)T} \sin\psi(t, \underline{\gamma})\, dt \}^2 \\ &= \{ \frac{1}{NT} [(N - \ell)T + \int_{k_1T}^{(k_1+\ell)T} \cos\psi(t, \underline{\gamma})\, dt] \}^2 \\ &\quad + \{ \frac{1}{NT} \int_{k_1T}^{(k_1+\ell)T} \sin\psi(t, \underline{\gamma})\, dt \}^2, \end{aligned} \tag{4.43}$$

where $k_1 + \ell \leq N$.

Hence for error events having a particular phase difference path segment from k_1T to $(k_1 + \ell)T$, $|\rho(\underline{\gamma})|^2$ will be the same independent of k_1 as long as $0 \le k_1 \le N - \ell$, and hence the P[ϵ] will be the same. It is then sufficient to determine only the segment of $\underline{\gamma}$ from 0 to $\ell - 1$ corresponding to the error event ϵ starting from t = 0. For each segment of $\underline{\gamma}$ so determined, the number of the corresponding error events occurring at different times k_1T with $0 \le k_1 \le N - \ell$ during a hop interval of length NT is $N - \ell + 1$.

For a correlative encoded CPM with frequency pulse of length LT, the minimum length of an error event is (L+1)T. Difference sequences of various lengths $\ell \ge L + 1$ are generated to find the complete error event paths starting at time 0. Once a complete error event path, which has $\gamma_0 \neq 0$ and $\zeta_\ell = 0$ (that is the difference phase path deviates from zero at time 0 and merges back to zero at time ℓT) is determined, the square of the correlation is calculated by Eq. (4.43). Since it is computationally infeasible to include all the complete error events for large N and also since long error events generally have large equivalent distances, hence only difference sequence segments of length $L + 1 \le \ell \le \ell_{max}$ are included. For $\underline{\gamma}$ of length ℓ_{max}, the number of $\underline{\gamma}$ to be included in the computation is $\frac{1}{2}(3^{\ell_{max}} - 1)$, which is the dimension of the arrays used for storing various parameters for each $\underline{\gamma}$. The maximum allowable array dimension of the program compiler dictates the maximum value of ℓ_{max} to be 10. For all the approximated upper bounds on BER computed, $\ell_{max} = 8$ is used for computational efficiency.

If an error event starts at some time (N-L)T or later, before the end of a hop, then an incomplete error event will occur. (The estimated path will never merge with the true path.) These incomplete error events starting near the end of a hop have the estimated phase path differing from the true path in only a small portion and thus are also likely to occur. The $\frac{1}{2}(3^L - 1)$ possible difference sequences corresponding to the incomplete error events at the end of a hop are generated and their probabilities evaluated.

To summarize, the bit error rate upper bound is approximated by

$$P_e \lesssim \frac{1}{\mu}\{\sum_{\epsilon_i \in E_c}(N - \ell_i + 1)\ 2^{N-e_i+1}\ \frac{e_i}{N} P(\epsilon_i) + \sum_{\epsilon_j \in E_l} 2^{N-e_j+1}\ \frac{e_j}{N} P(\epsilon_j)\}, \tag{4.44}$$

where E_c is the set of complete error events having small equivalent distances and E_l is the set of incomplete error events occurring near the end of a hop. ϵ_i denotes the i^{th} error event in the set E_c and ϵ_j denotes the j^{th} error event in the set E_l. e_i and ℓ_i are the number of bit errors and length of ϵ_i respectively.

4.1.4 Bit Error Rate Upper Bound Results

The upper bound on the error performance of the hop-by-hop noncoherent receiver has been evaluated for a variety of correlative encoding and baseband pulse shaping schemes when the length of the frequency hopping interval is 4, 16 and 64 symbol intervals. For the hop length of 4 symbol intervals, the upper bound on the BER is evaluated exactly while for the longer hop intervals of 16 and 64, approximated upper bounds are evaluated.

Minimum shift keying (MSK), duobinary MSK (DMSK) and tamed FM (TFM) encoding schemes with h = 0.5 and rectangular pulse shaping are compared as shown in Figs. 4.7 to 4.9 for N = 4, 16 and 64 respectively. It can be seen that MSK performs much better than the other two schemes for the various hop lengths. When raised cosine pulse shaping is used, the bit error rate bounds for the three schemes are as shown in Figs. 4.10 to 4.12 for N = 4, 16 and 64 respectively. Again, the higher order correlative encoding schemes have higher probability of error.

Next, the effect of the hop length on the error performance for each modulation is illustrated in Figs. 4.13 to 4.18. As expected, the performance of the receiver improves as the hop interval lengthens. However, for the same degree of increase in hop length, the improvement in error performance is less for MSK and is more pronounced for the higher order correlative encoding schemes such as TFM.

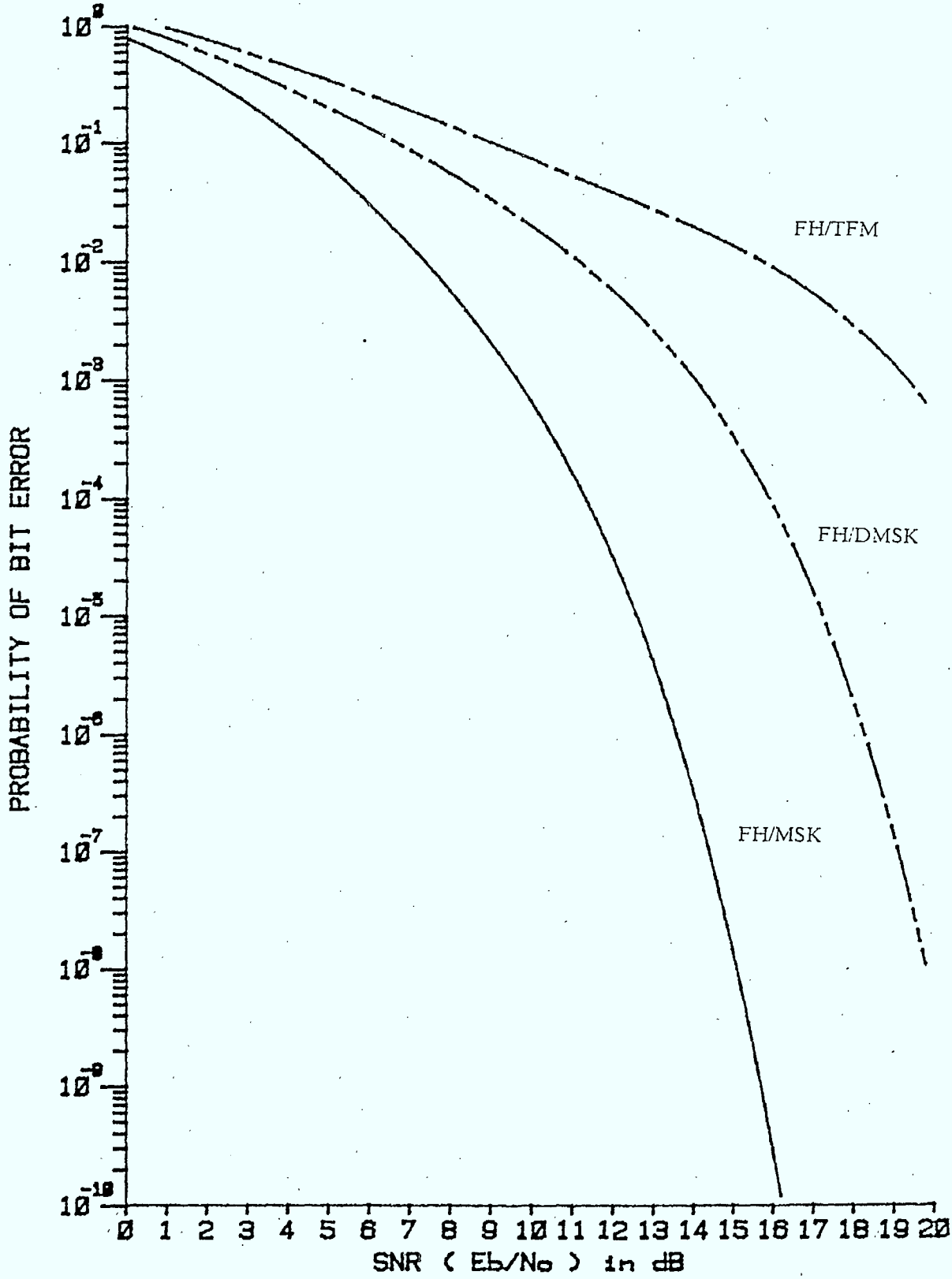

Figure 4.7 N = 4, union bounds on P_e for FH/MSK, FH/DMSK and FH/TFM with rectangular pulse shaping

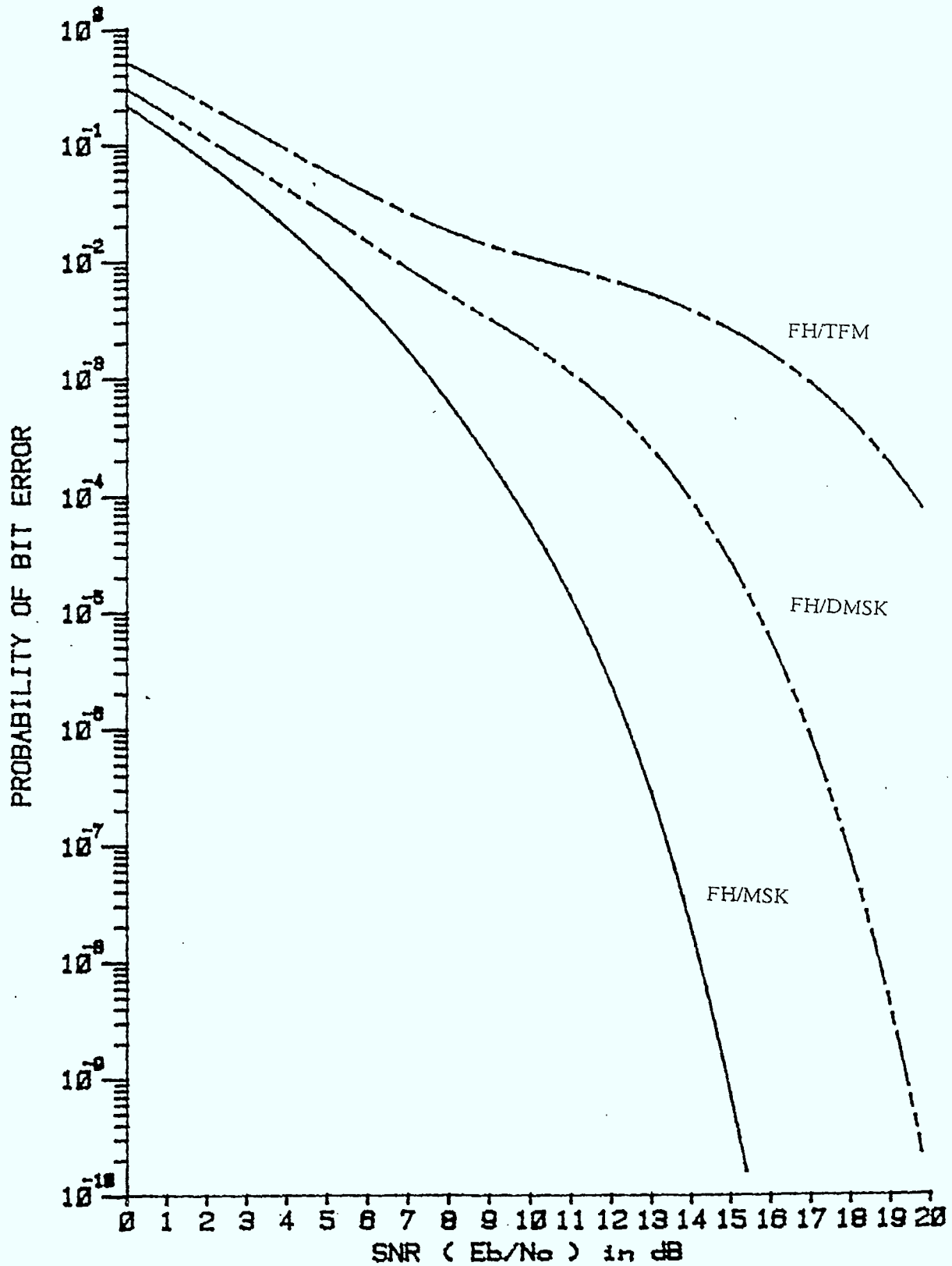

Figure 4.8 N = 16, approximated upper bounds on P_e for FH/MSK, FH/DMSK and FH/TFM with rectangular pulse shaping

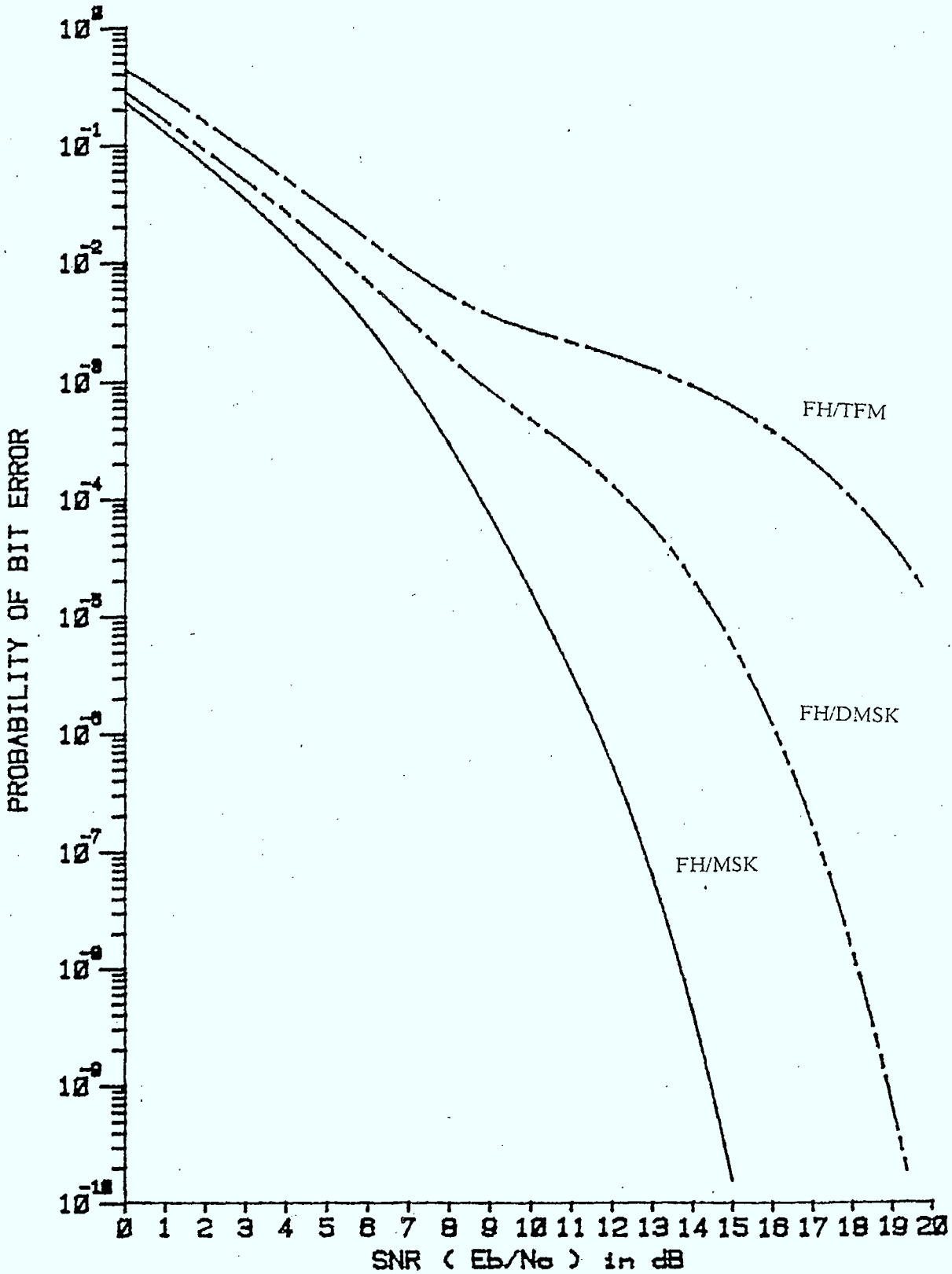

Figure 4.9 N = 64, approximated upper bounds on P_e for FH/MSK, FH/DMSK and FH/TFM with rectangular pulse shaping

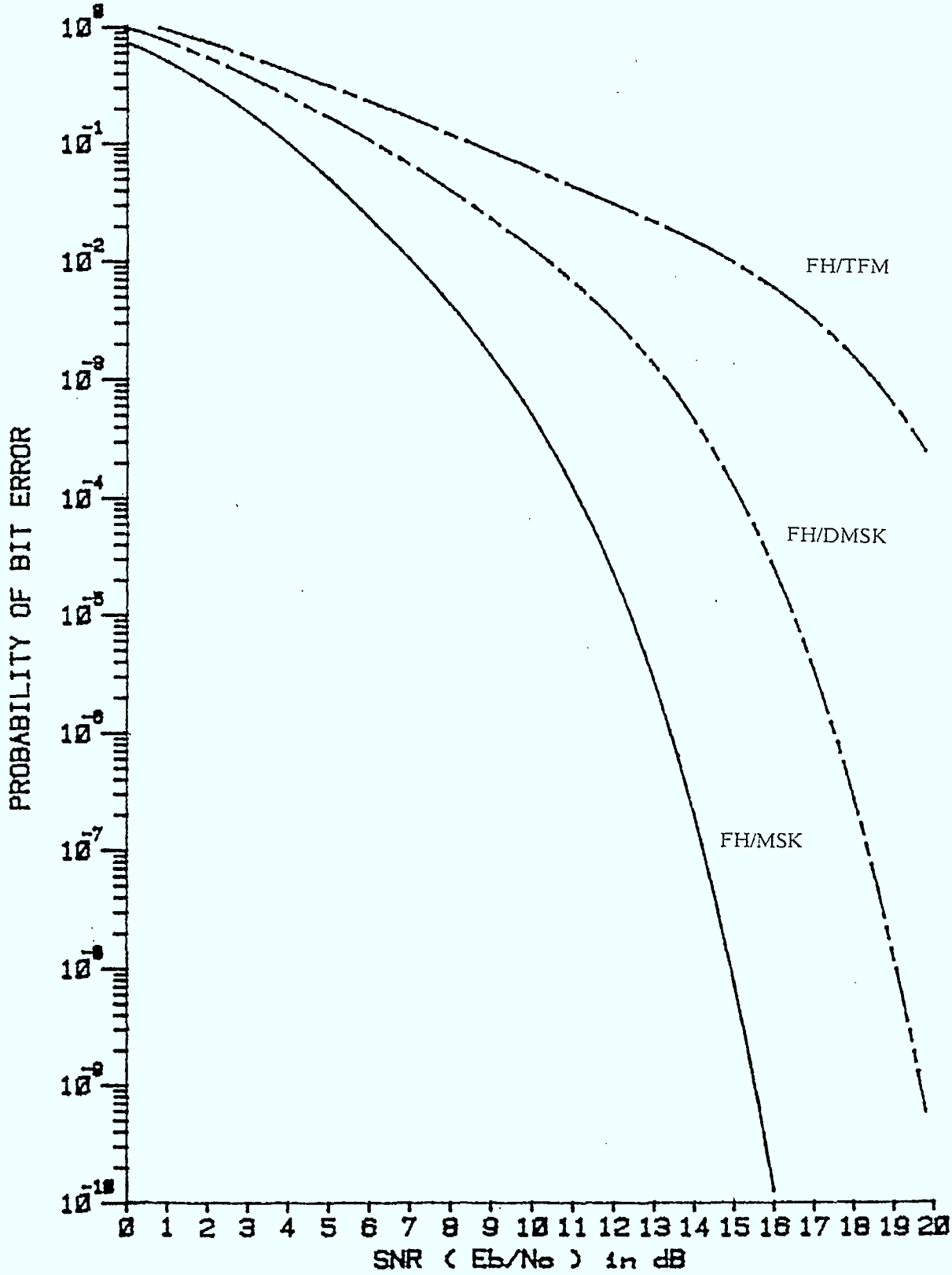

Figure 4.10 N = 4, union bounds on P_e for FH/MSK, FH/DMSK and FH/TFM with raised cosine pulse shaping

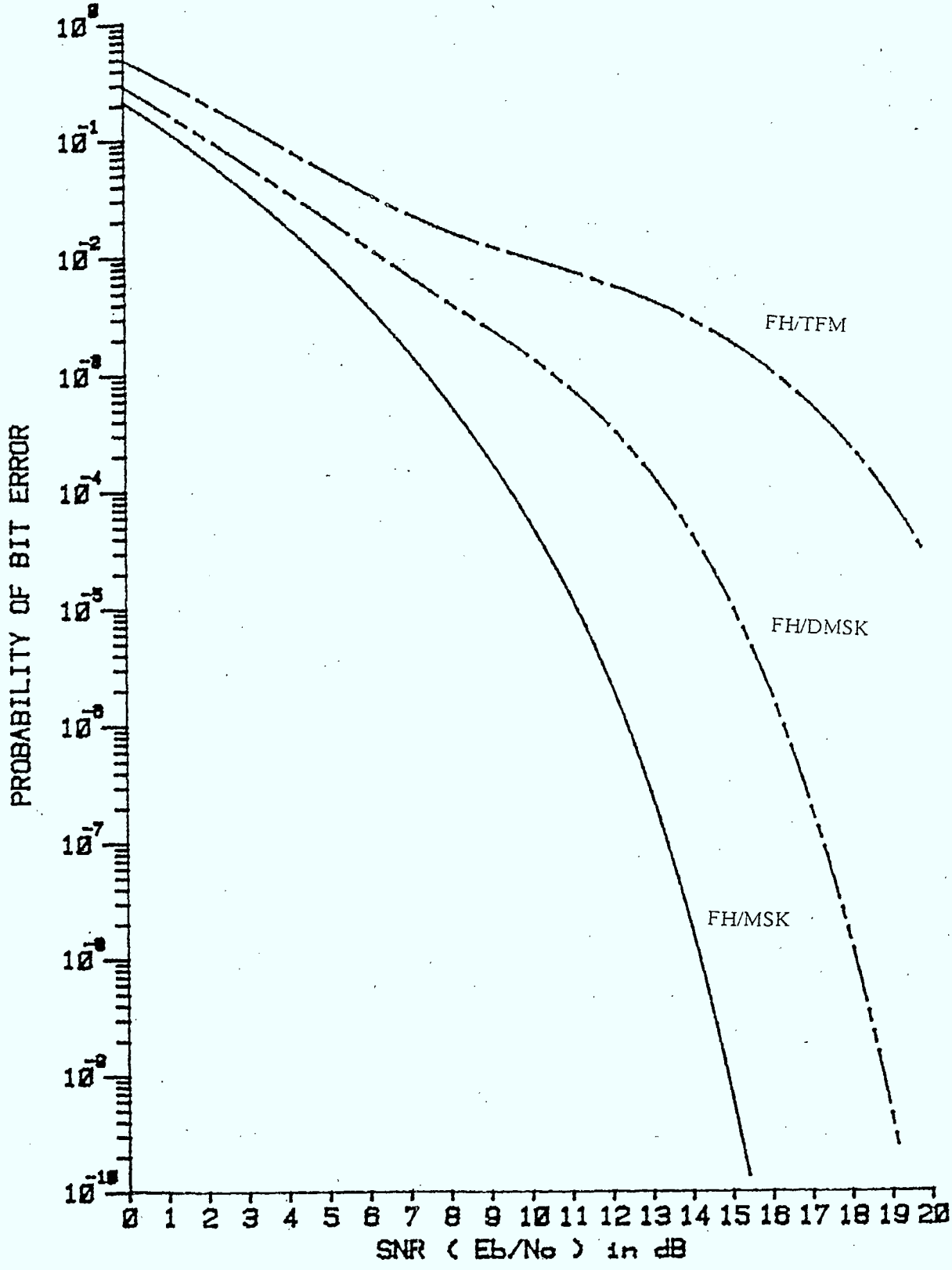

Figure 4.11 N = 16, approximated upper bounds on P_e for FH/MSK, FH/DMSK and FH/TFM with raised cosine pulse shaping

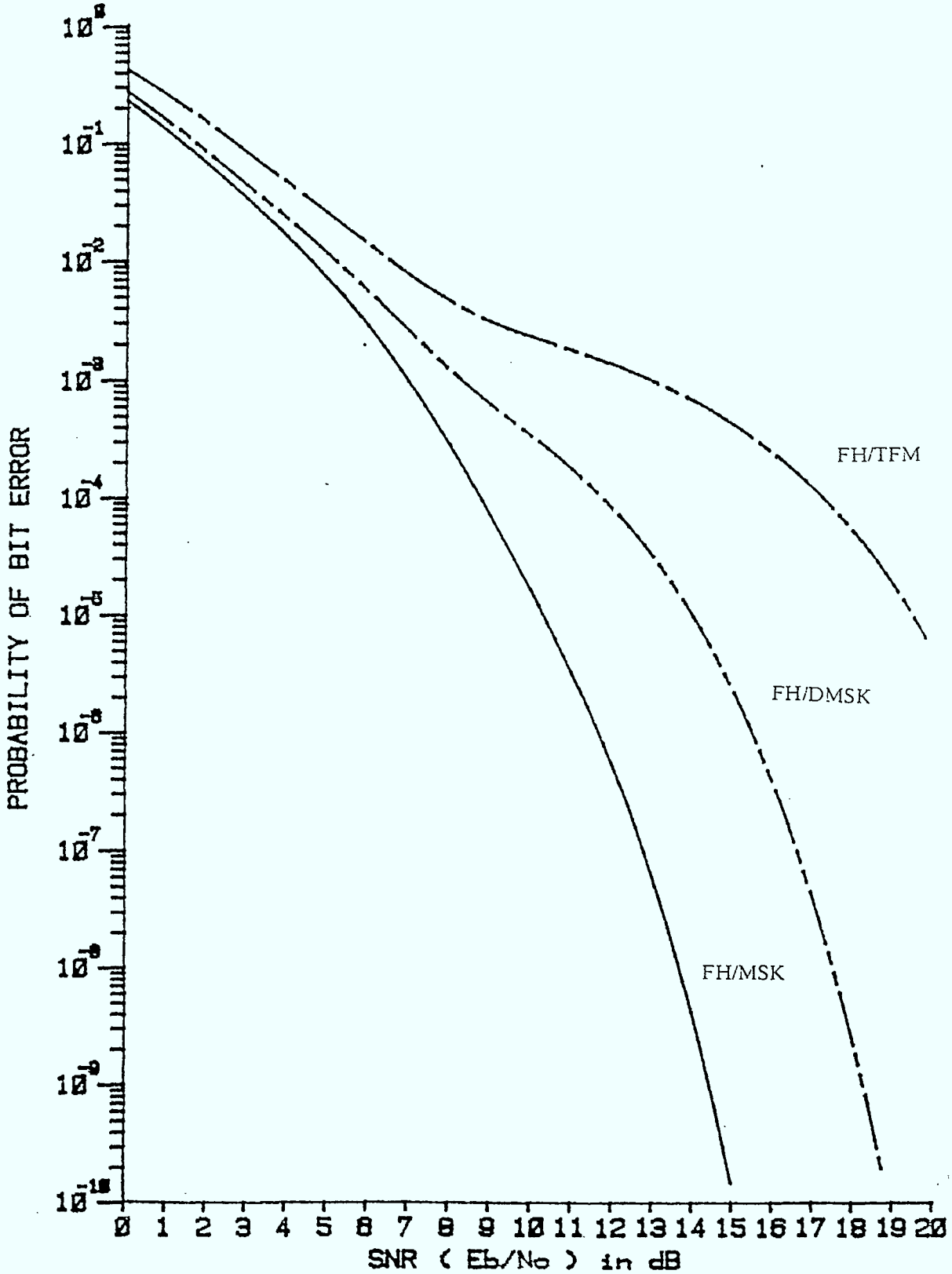

Figure 4.12 N = 64, approximated upper bounds on P_e for FH/MSK, FH/DMSK and FH/TFM with raised cosine pulse shaping

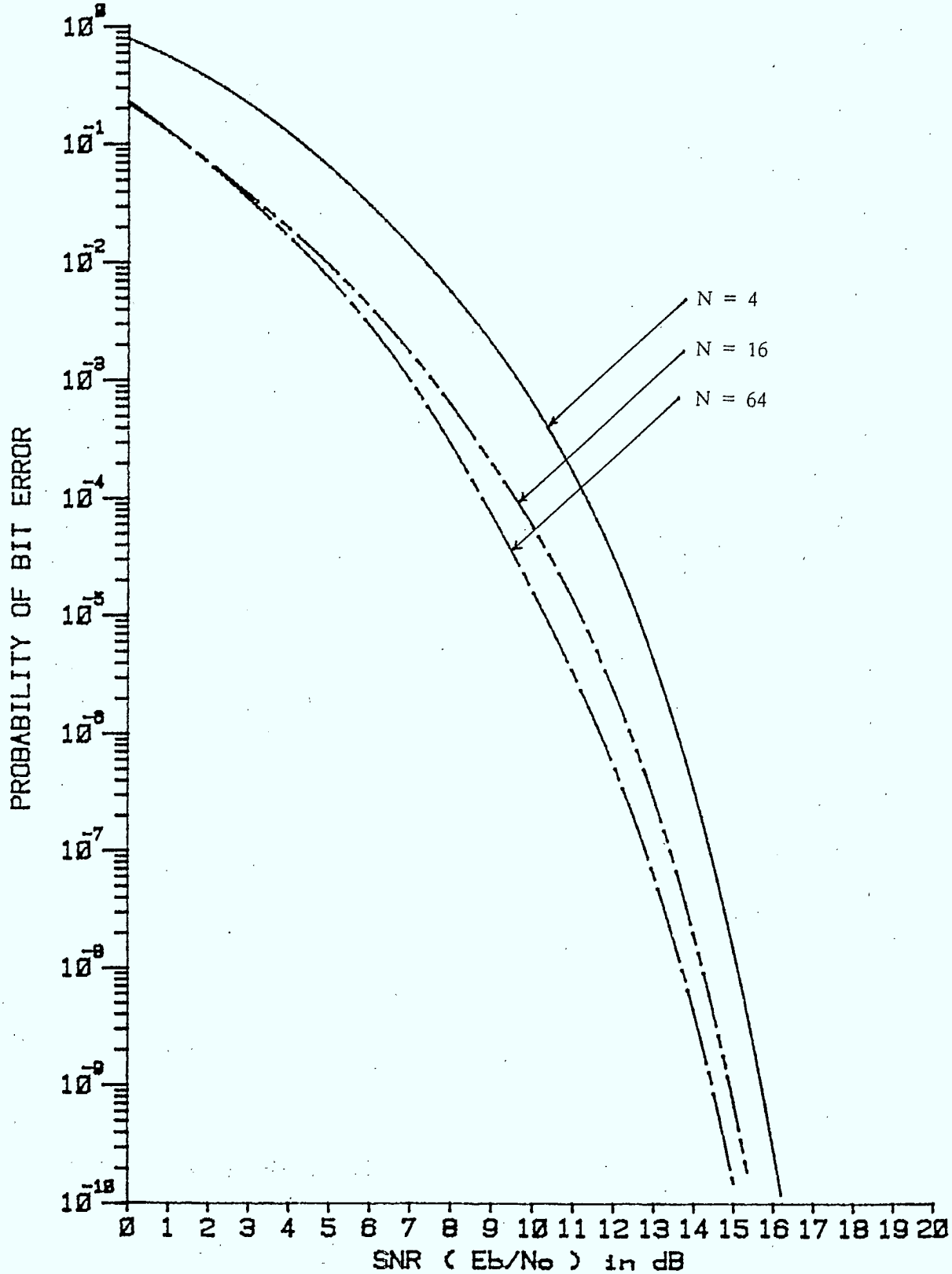

Figure 4.13 P_e bounds for FH/MSK with rectangular pulse shaping

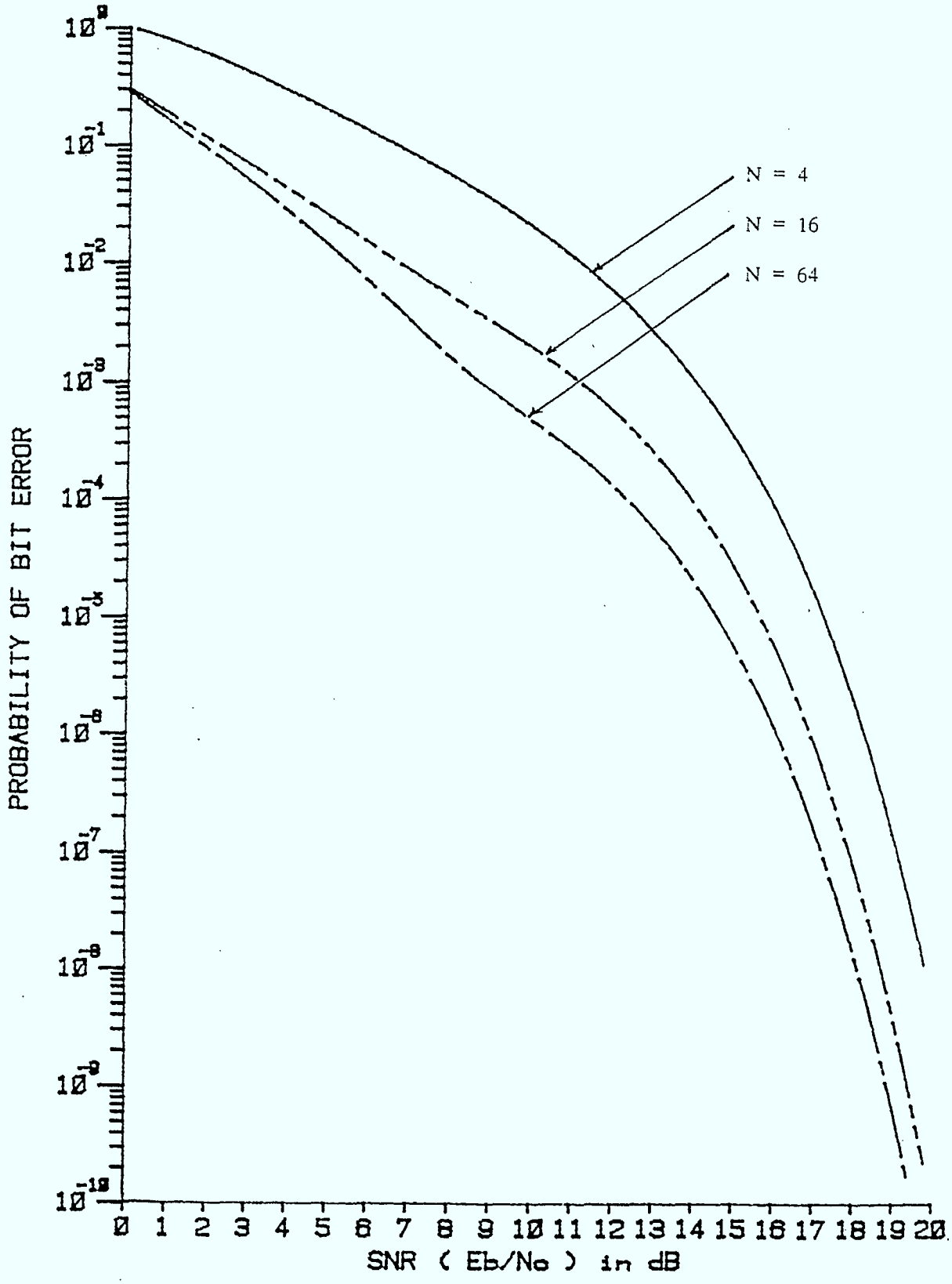

Figure 4.14 P_e bounds for FH/DMSK with rectangular pulse shaping

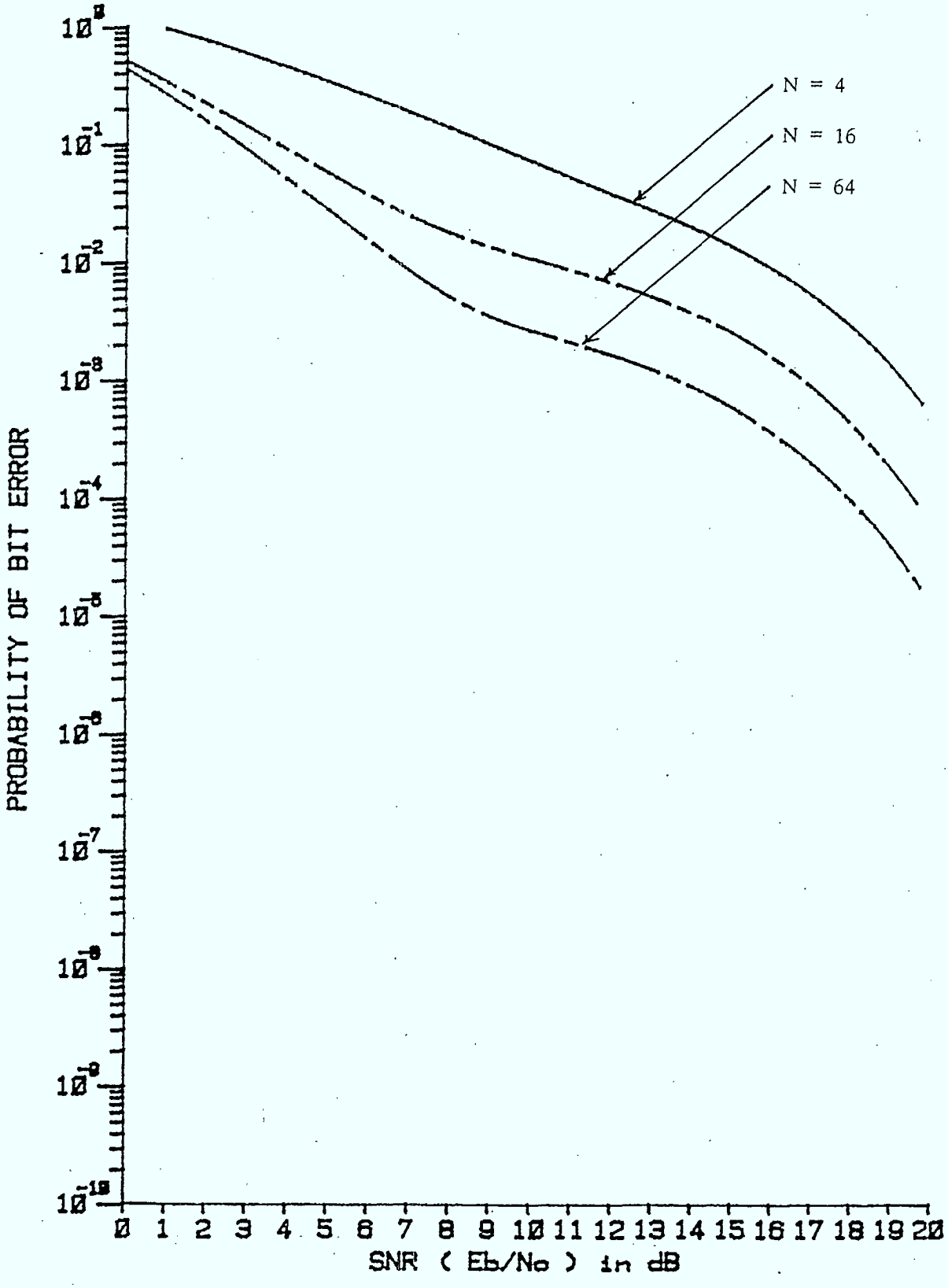

Figure 4.15 P_e bounds for FH/TFM with rectangular pulse shaping

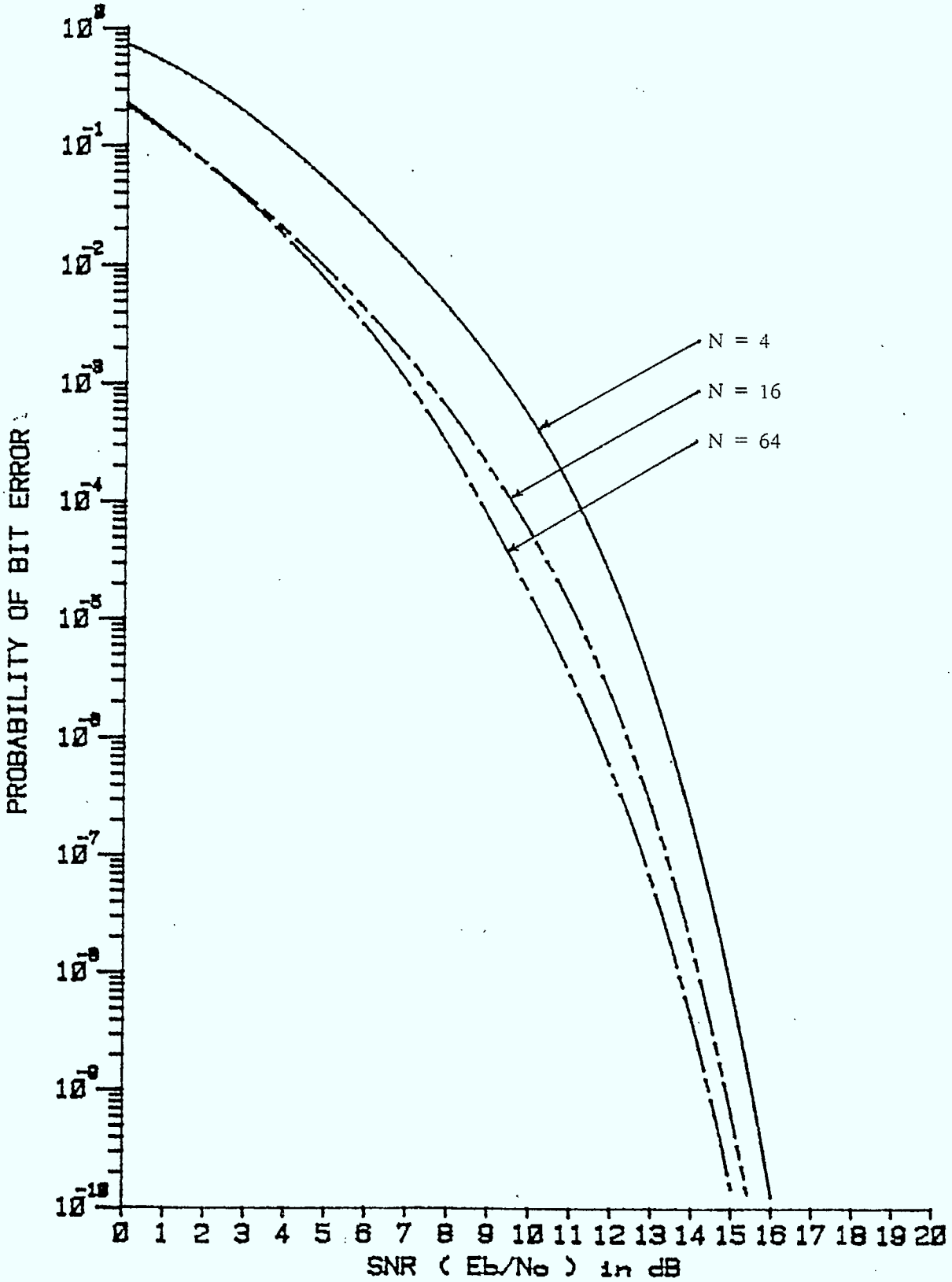

Figure 4.16 P_e bounds for FH/MSK with raised cosine pulse shaping

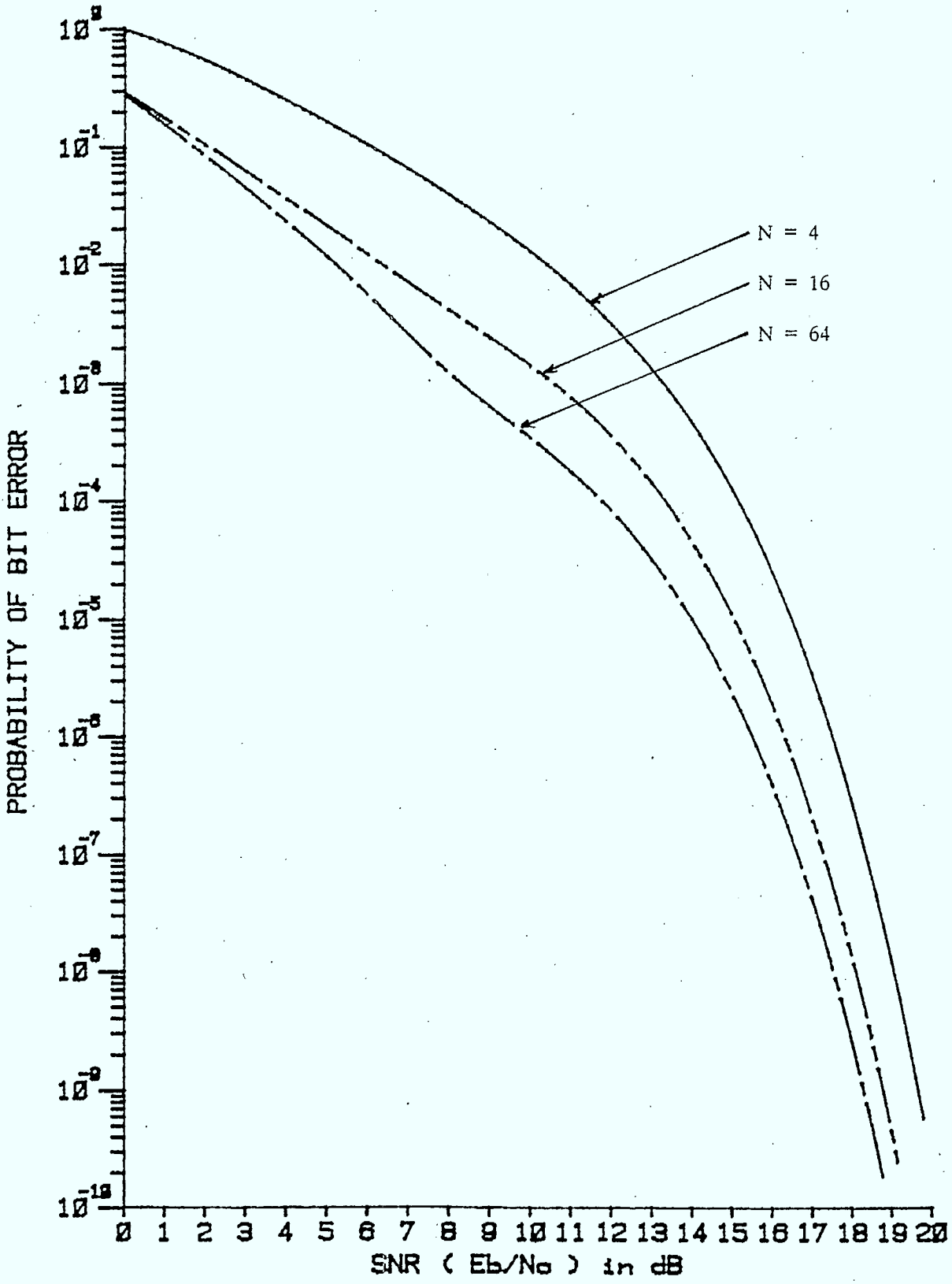

Figure 4.17 P_e bounds for FH/DMSK with raised cosine pulse shaping

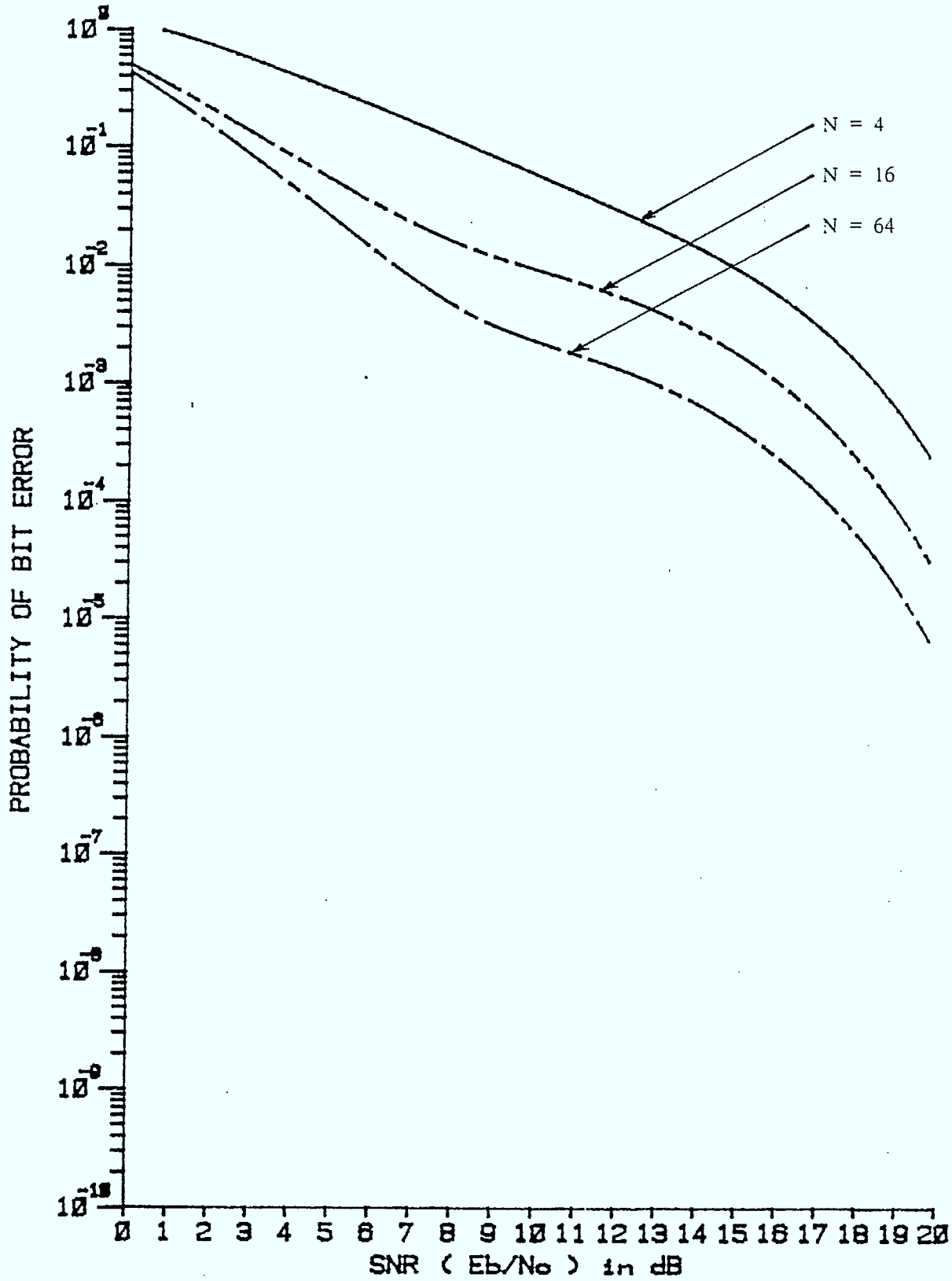

Figure 4.18 P_e bounds for FH/TFM with raised cosine pulse shaping

4.1.5 Performance Improvement By Transmitting Known Initial Symbols

As shown in section 4.1.1, the equivalent distance of the error path corresponding to an error event is smallest when the error event starts at the beginning of the hop interval. The probability of any error event occurring is then highest at the start of a hop interval. As can be seen from Figs. 4.1 to 4.3, the equivalent distance of an error event increases if the same error event starts later. Hence, if a short segment of known symbols were transmitted at the start of a hop interval, then any error event would have to start after the initial known synchronization sequence segment. The decoder is less likely to make erroneous decisions on the subsequent data symbols. The error performance of the receiver would then improve. The obvious disadvantage is that a fraction of the available transmission time is used by the initial sequence segment, which does not carry data information.

Let δ be the number of known symbols to be transmitted at the beginning of each hop. At $t = \delta T$, the decoder knowing the δ transmitted symbols, will choose the correct path through the modulation trellis corresponding to the δ symbols and reject the other $M^{\delta} - 1$ possible paths. At time $(\delta + 1)T$, this path will be extended to each of the η states in the trellis. Subsequent decoding proceeds as usual, that is, the decoder computes and compares the M possible transitions to each state in the trellis. Only the one which has the largest equivalent likelihood up to the current time, is retained as the survivor for each state. At the end of a hop, the sequence corresponding to the path with the largest equivalent likelihood is then taken as the estimated sequence.

The final decided sequence $\underline{\alpha}'$ would have $\alpha'_0, \alpha'_1, \ldots, \alpha'_{\delta-1}$ equal to $\alpha_0, \alpha_1, \ldots, \alpha_{\delta-1}$, since they are known to the decoder. For a hop interval of length N symbol intervals, the number of actual data symbols is only $N - \delta$. Hence the number of possible transmitted sequences during a hop interval is $2^{N-\delta}$. Since the first δ α'_i's are correct, we have

$$\gamma_i = 0 \qquad \text{for } i = 0, 1, \ldots, \delta - 1. \tag{4.45}$$

The upper bound of the bit error probability when a known initial sequence is transmitted is then given by

$$P_e \leq \frac{1}{\mu'} \sum_{\substack{\underline{\gamma} \\ \underline{\gamma} \neq 0 \\ \gamma_i = 0 \text{ for } i = 0, 1, \ldots, \delta - 1}} \omega'(\underline{\gamma}) \frac{e(\underline{\gamma})}{N - \delta} P(\underline{\gamma}), \tag{4.46}$$

where $\mu' = 2^{N-\delta}$ is the number of possible transmitted sequences, $\omega'(\underline{\gamma}) = 2^{N-\delta-e(\underline{\gamma})}$ is the number of pairs of $\underline{\alpha}'$ and $\underline{\alpha}$ corresponding to the difference sequence $\underline{\gamma}$, $e(\underline{\gamma})$ is the number of bit errors for the error path corresponding to $\underline{\gamma}$. $P(\underline{\gamma})$ is the probability of error by detecting $\underline{\alpha}'$ rather than $\underline{\alpha}$ and is given by Eqs. (4.34) to (4.36).

The total number of $\underline{\gamma}$'s is $3^{N-\delta} - 1$ rather than $3^N - 1$, since the first δ γ_i's are o's resulting from decoding a known sequence segment. $|\rho(\underline{\gamma})|^2$ needed for calculating $P(\underline{\gamma})$ becomes

$$|\rho(\underline{\gamma})|^2 = \{ \frac{1}{NT} [\delta T + \int_{\delta T}^{NT} \cos \psi(t, \underline{\gamma}) dt] \}^2 + \{ \frac{1}{NT} \int_{\delta T}^{NT} \sin \psi(t, \underline{\gamma}) dt \}^2. \tag{4.47}$$

The performance improvement obtained by transmitting an initial segment of 1, 2 and 3 known symbols has been evaluated for MSK, DMSK and TFM with h = 0.5 and rectangular pulse shaping. Figs. 4.19 and 4.20 show the results obtained for MSK when the number of data bits transmitted during a hop is 4 and 8 respectively. The gain in performance in transmitting the first known symbol is more significant than for the subsequent 2 or 3 symbols, as can be seen from these figures. For the shorter data length of 4 as shown in Fig. 4.19, the improvement is also greater than for the data length of 8 as shown in Fig. 4.20. When the modulation scheme is DMSK, the upper bounds on the BER for transmitting 4 and 8 data bits with different num-

bers of known symbols are shown in Figs. 4.21 and 4.22. We can see that large improvement in BER is obtained for the case when the data length is 4, by just using an initial known symbol segment of one symbol. However, the improvement is not so pronounced for the longer data length of 8 bits, as shown in Fig. 4.22. For TFM with h = 0.5 and rectangular pulse shaping, the results are shown in Figs. 4.23 and 4.24 for transmitting 4 and 8 bits respectively. The observations are similar to the cases of MSK and DMSK.

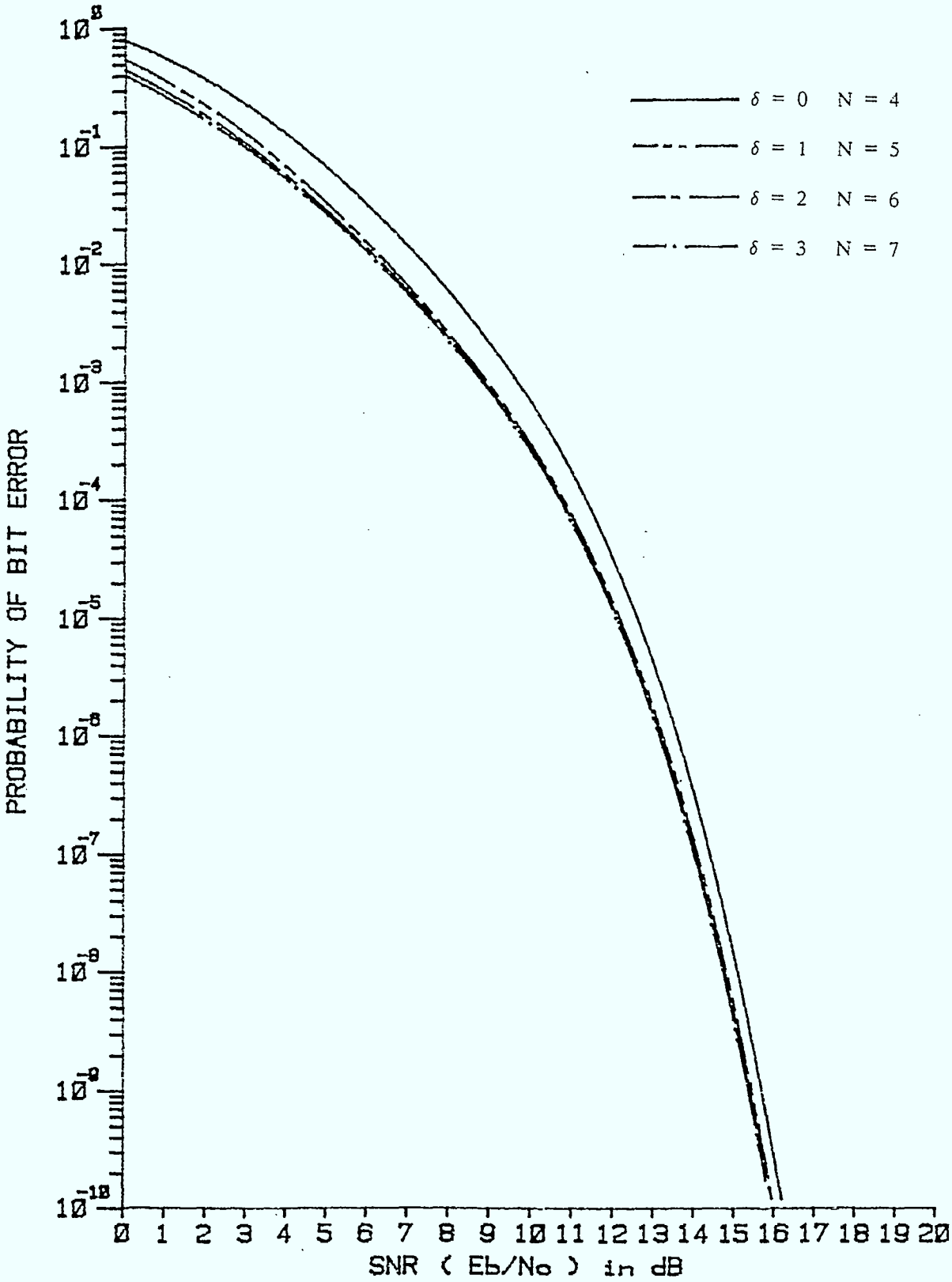

Figure 4.19 Bound on P_e of FH/MSK with rectangular pulse shaping, 4 information symbols and 0 to 3 initial known symbols

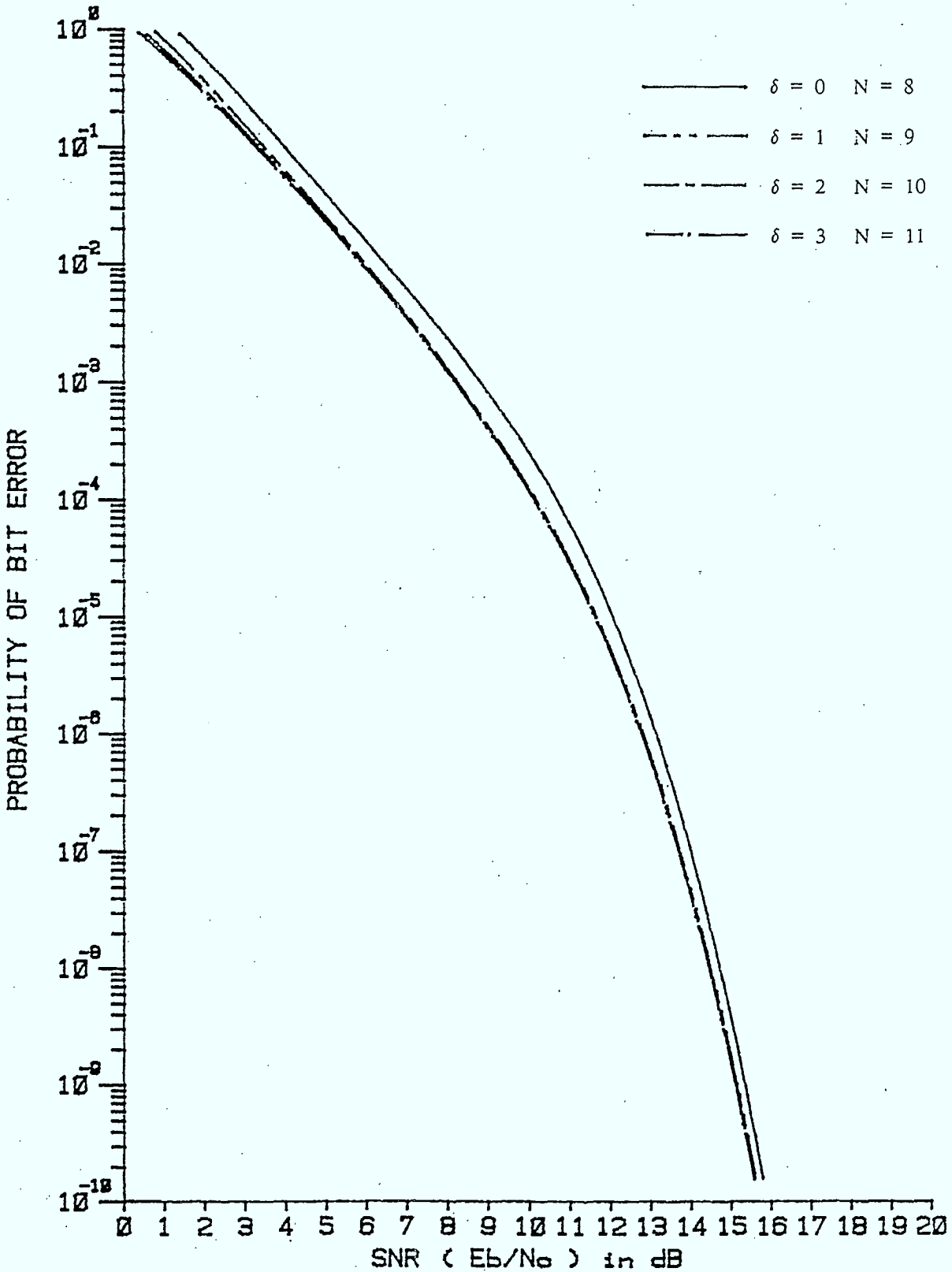

Figure 4.20 Bound on P_e of FH/MSK with rectangular pulse shaping, 8 information symbols and 0 to 3 initial known symbols

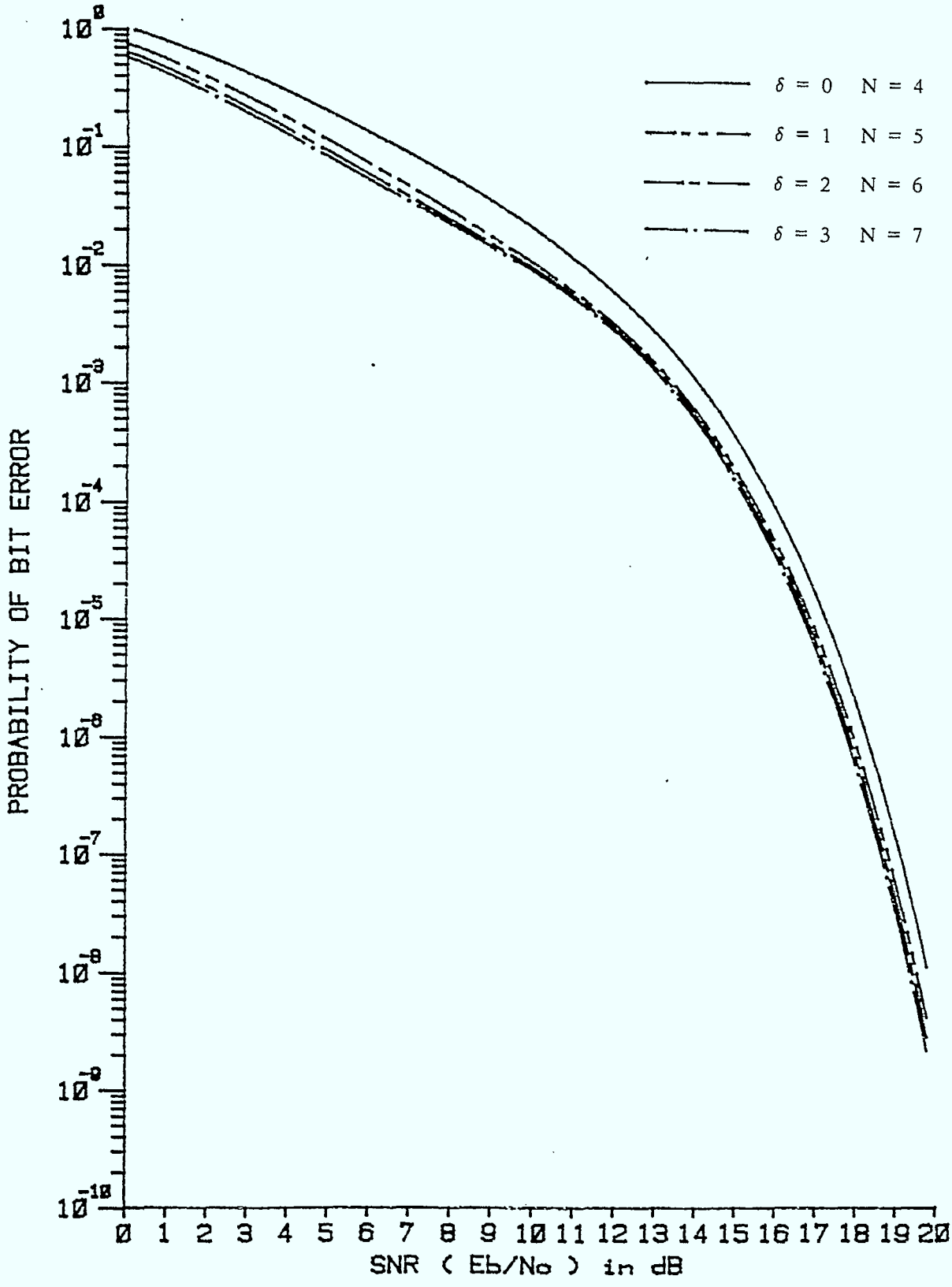

Figure 4.21 Bound on P_e of FH/DMSK with rectangular pulse shaping, 4 information symbols and 0 to 3 initial known symbols

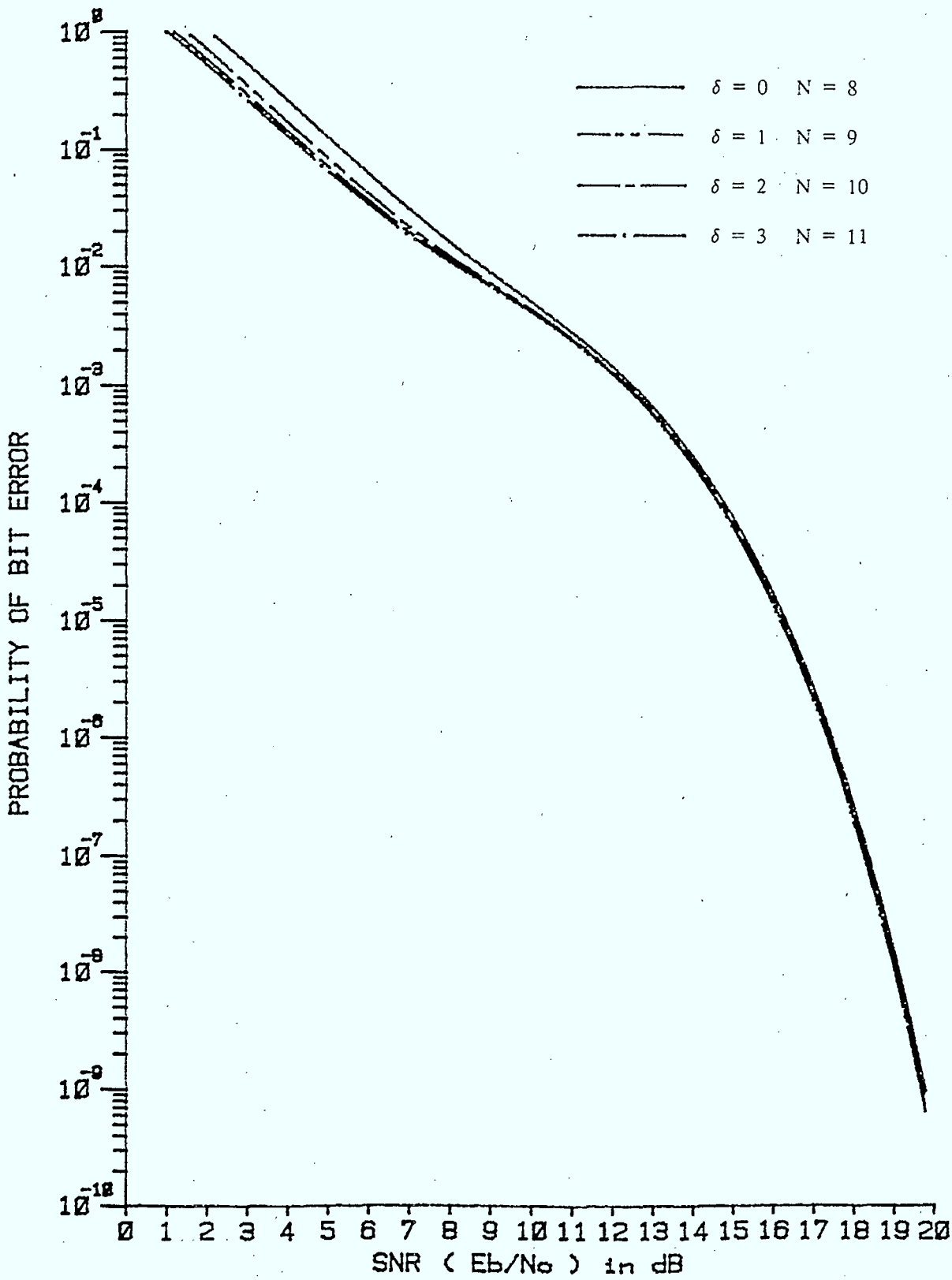

Figure 4.22 Bound on P_e of FH/DMSK with rectangular pulse shaping, 8 information symbols and 0 to 3 initial known symbols

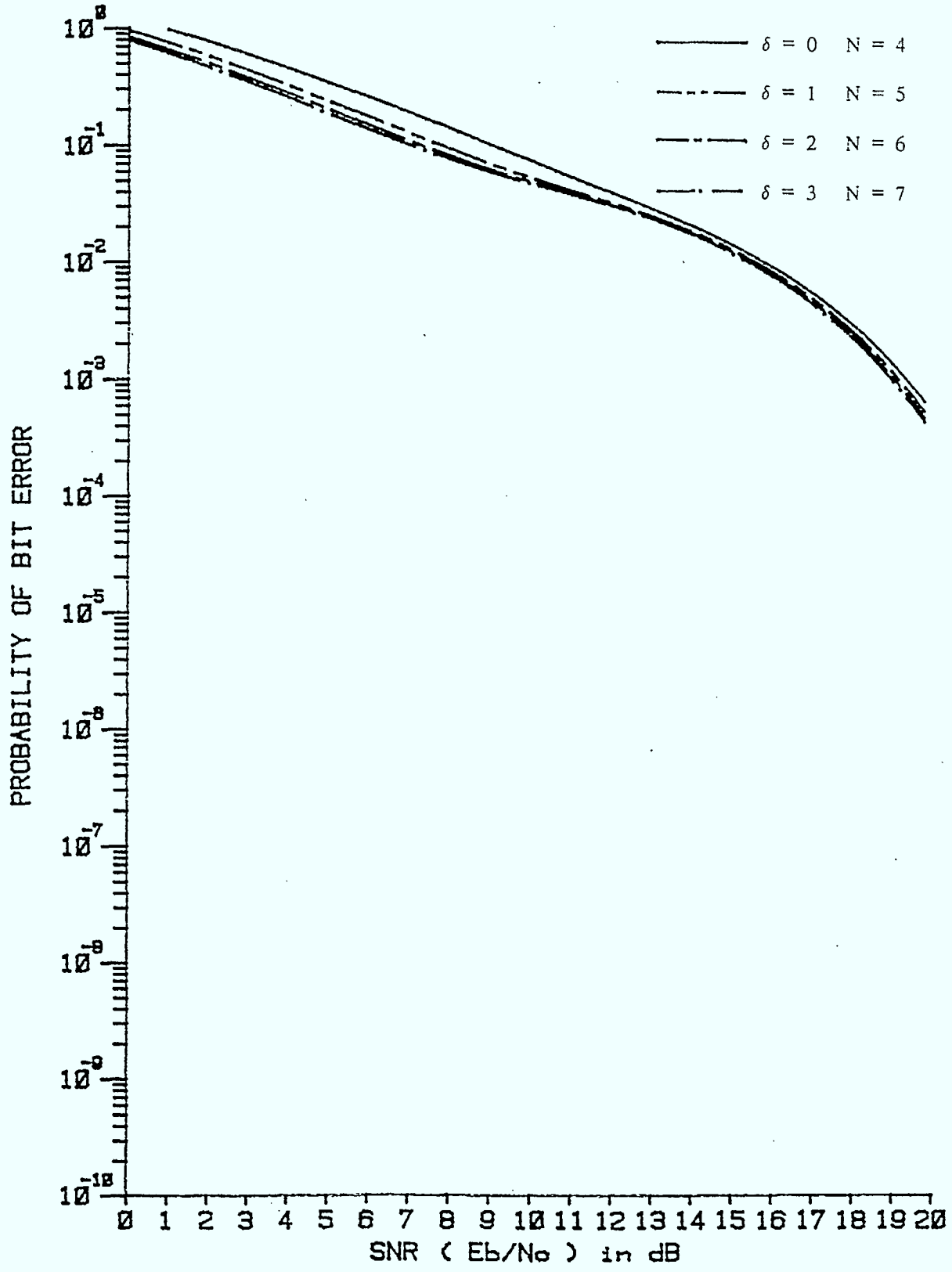

Figure 4.23 Bound on P_e of FH/TFM h = 0.5 with rectangular pulse shaping, 4 information symbols and 0 to 3 initial known symbols

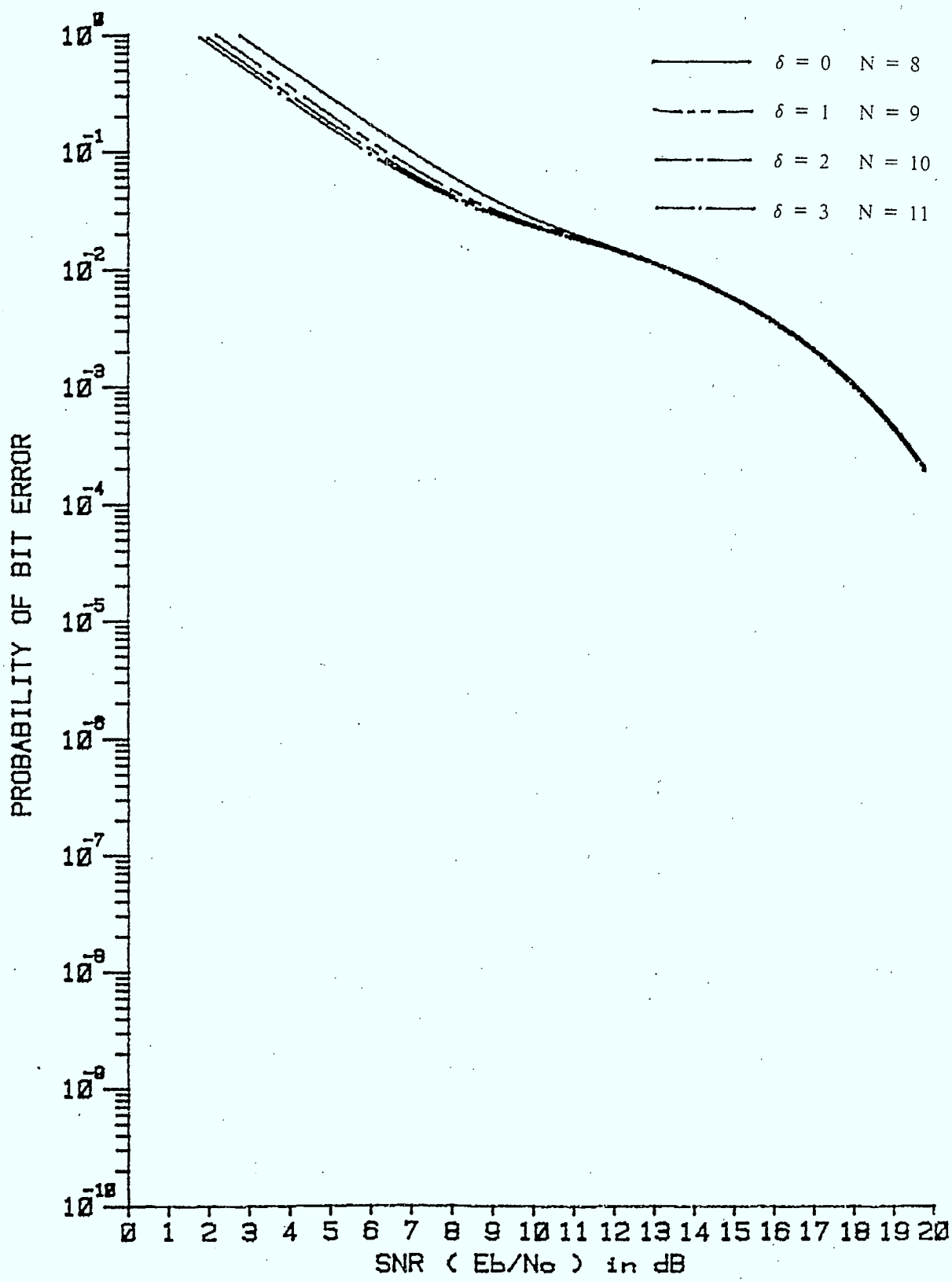

Figure 4.24 P_e for FH/TFM h = 0.5 with rectangular pulse shaping, 8 information symbols and 0 to 3 known initial symbols

4.2 Performance In The Presence Of Jamming

In the previous section the error performance of the noncoherent receiver has been evaluated under additive white Gaussian noise. In this section, the performance of the noncoherent slow FH/CPM spread spectrum system in the presence of intentional interference (jamming) will be derived. There are a large number of jamming strategies that a jammer may use for interfering with the spread spectrum communication. Depending on the jammer's available resources and sophistication, usually the familiar exponential relationship between error probability and signal to noise ratio will be degraded to an inverse linear relationship between error probability and signal to jammer power ratio [3, p.555][8,9].

There are a large number of jamming signals and jamming strategies postulated [3], such as barrage noise, partial band noise, single-tone, multiple-tone, pulsed noise and repeat back jamming. While some jamming strategies may be postulated so as to provide the worst case performance analysis of the system and may not be realistic in actual practice, some jamming strategies are practical and are real threats to the spread spectrum system. Two most effective jamming strategies for frequency-hopped systems are partial band noise jamming and multiple-tone jamming. Multiple-tone jamming is the tone equivalent of partial band noise jamming and has been shown to be more efficient than partial band noise jamming for FH/MFSK and FH/DPSK [3, p.597-601]. The performance of the noncoherent slow FH/CPM system under partial band noise jamming will first be evaluated, followed by performance analysis under multiple-tone jamming.

4.2.1 Performance In Partial Band Noise Jamming

Hopping the frequency over a wide bandwidth makes broadband noise jamming of the bandwidth difficult and much less effective. Jamming power can be more effectively used by transmitting all the available power in a limited bandwidth which is smaller than the spread spectrum system bandwidth. Because of the smaller bandwidth, the partial band jamming signal is easier to generate than the barrage noise jamming signal. The jamming model we consider is that of a partial band noise jammer [3, p.570]. In this model, the jammer uses all its power in only a fraction of the spread spectrum bandwidth while the remaining fraction of the system bandwidth has only background thermal noise present. The partial band jammer is particular effective against a frequency-hopped spread spectrum system because the signal will hop in and out of the jammed band and can be in effect useless while in the jammed band [3].

Following the approach used in [3, p.570], we assume that the frequency hopping pattern is essentially random and that the partial band noise jammer does not know or is unable to predict the hopping pattern. Interference from a jammer during a hop interval is assumed to be independent of the interference in other hop intervals. As the carrier hops to a frequency band which is jammed, the jamming noise signal is assumed to stay constant throughout the complete hop interval. The channel is then memoryless from hop to hop and the BER can be calculated using quasi-static analysis. That is, the error probability is calculated separately for hops with thermal noise interference and hops with thermal noise plus jamming interference and the two results are averaged.

Let the fraction of the spread spectrum bandwidth which is jammed be denoted by ρ. If the total jammer power is J and the spread spectrum bandwidth is W, the partial band jammer one-sided power spectral density is

$$N_J = \frac{J}{\rho W} \tag{4.48}$$

over a bandwidth ρW. When $\rho = 1$, we have the case of full band noise jamming or barrage noise jamming [3].

Let N_o be the one-sided power spectral density of the Gaussian channel thermal noise. Over the jammed portion of the transmission band we have both the jamming and Gaussian thermal noise. Assuming that the jamming noise and the Gaussian thermal noise are statistically independent, the jamming noise and thermal noise can be combined into a single Gaussian random noise process of total one-sided spectral density of $N_o + N_J$ W/Hz. The remaining portion of the band will have thermal Gaussian noise of one-sided spectral density of N_o W/Hz only.

The average bit error probability is then given by

$$\begin{aligned} \overline{P_e} &= \Pr[\text{jammed}]\,\Pr[\text{ bit error } | \text{ jammed }] + \Pr[\text{not jammed}]\,\Pr[\text{ bit error } | \text{ not jammed }] \\ &= \rho\ \Pr[\text{ bit error } | \text{ jammed }] + (1-\rho)\ \Pr[\text{ bit error } | \text{ not jammed }] \\ &= \rho\ P_e\left(\frac{E_b}{N_o + N_J}\right) + (1-\rho)\ P_e\left(\frac{E_b}{N_o}\right), \end{aligned} \tag{4.49}$$

where $P_e\left(\frac{E_b}{N_n}\right)$ denotes the bit error probability as a function of the ratio of signal bit energy to the appropriate noise power spectral density.

The evaluation of the bit error probability for our slow FH/CPM system with the hop-by-hop noncoherent receiver is difficult. Hence only an upper bound can be obtained by substituting the upper bound expression for the bit error rate presented in the previous chapter into Eq.(4.49). The BER under partial band noise jamming has an upper bound

$$\overline{P_e} \leq \frac{1}{\mu} \sum_{\substack{\underline{\gamma} \\ \underline{\gamma} \neq 0}} \omega(\underline{\gamma}) \frac{e(\underline{\gamma})}{N} \left[\rho P\left(\underline{\gamma}, \frac{E_b}{N_o + N_J}\right) + (1 - \rho) P\left(\underline{\gamma}, \frac{E_b}{N_o}\right) \right], \tag{4.50}$$

where all notation and symbols are the same as defined previously, except that the error probability $P(\underline{\gamma})$ is now denoted by $P(\underline{\gamma}, \frac{E_b}{N_n})$ with the second argument displayed to indicate the dependence on the signal bit energy to noise density ratio.

When the spread spectrum system is intended for operation in a jamming environment, the maximum possible transmitter power is generally used and thermal noise can be safely neglected. Eq. (4.50) can then be simplified to

$$\overline{P_e} \leq \frac{1}{\mu} \sum_{\substack{\underline{\gamma} \\ \underline{\gamma} \neq 0}} \omega(\underline{\gamma}) \frac{e(\underline{\gamma})}{N} \left[\rho P\left(\underline{\gamma}, \frac{E_b}{N_J}\right) \right]. \tag{4.51}$$

The bit energy to jammer noise spectral density ratio can be expressed as

$$\frac{E_b}{N_J} = \rho \frac{P}{J} \frac{W}{R}, \tag{4.52}$$

where P is the signal power, J is the jammer power, W is the spread bandwidth and $R = 1/T$ is the data rate. Substituting Eq. (4.52) into Eq. (4.51), the bit error rate upper bound is then expressed as a function of the parameter (P/J)(W/R) by

$$\overline{P_e} \leq \frac{1}{\mu} \sum_{\substack{\underline{\gamma} \\ \underline{\gamma} \neq 0}} \omega(\underline{\gamma}) \frac{e(\underline{\gamma})}{N} \left[\rho P\left(\underline{\gamma}, \rho \frac{P}{J} \frac{W}{R}\right) \right]. \tag{4.53}$$

When the system is jammed the signal power to noise density ratio is low and the usual high SNR approximation is not accurate. All $\frac{1}{2}(3^N - 1)$ difference sequences $\underline{\gamma}$'s are then required for the evaluation of the upper bound on the averge bit error probability given by Eq. (4.53). Consequently, we are able to obtain the upper bound on the average bit error rate under partial band noise jamming only for systems with small hop length N.

The performance of FH/CPM systems with MSK, DMSK and TFM modulation schemes with h = 0.5 and rectangular pulse shaping, have been evaluated in the presence of partial band noise jamming with the fraction of jammed bandwidth ρ being 1.0, 0.2, 0.04, 0.008, 0.0016 and 0.00032. For a hop interval of 4 and 8 symbols, the error performance for these three modulation schemes is illustrated in Figs. 4.25 to 4.30. For a given signal to jammer power ratio P/J, there is always an optimum value of ρ, which causes the maximum degradation in BER of the spread spectrum system. The sophisticated partial band noise jammer will always choose the optimum value of ρ, which maximizes the BER of the system, so as to cause maximum degradation to the system performance. The worst case performance of the system then becomes inversely proportional to the signal to jammer power ratio as evident from these figures. Comparing the performance of MSK, DMSK and TFM as shown in Figs. 4.25, 4.26 and 4.27 for N = 4 and Figs. 4.28, 4.29 and 4.30 for N = 8 respectively, we can see that while MSK performs much better than the other two schemes under normal additive white Gaussian noise environment or full band noise jamming, the performance of the three schemes for the same hop length is quite similar under worst case partial band noise jamming. It can be seen that the worst case performance under partial band noise jamming worsens as the hop length increases from N = 4 to N = 8.

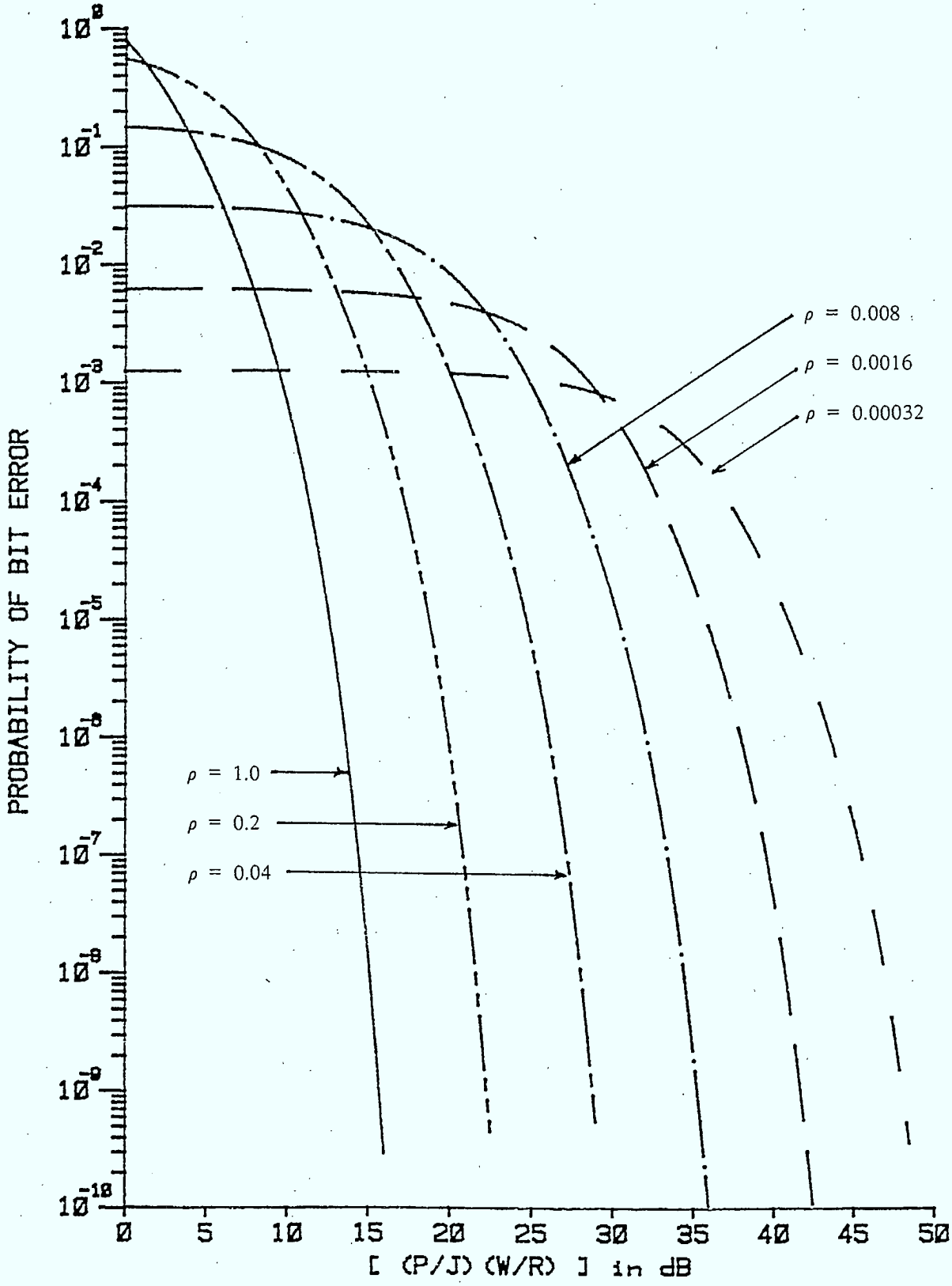

Figure 4.25 P_e of FH/MSK with rectangular pulse shaping and N = 4 under partial band noise jamming

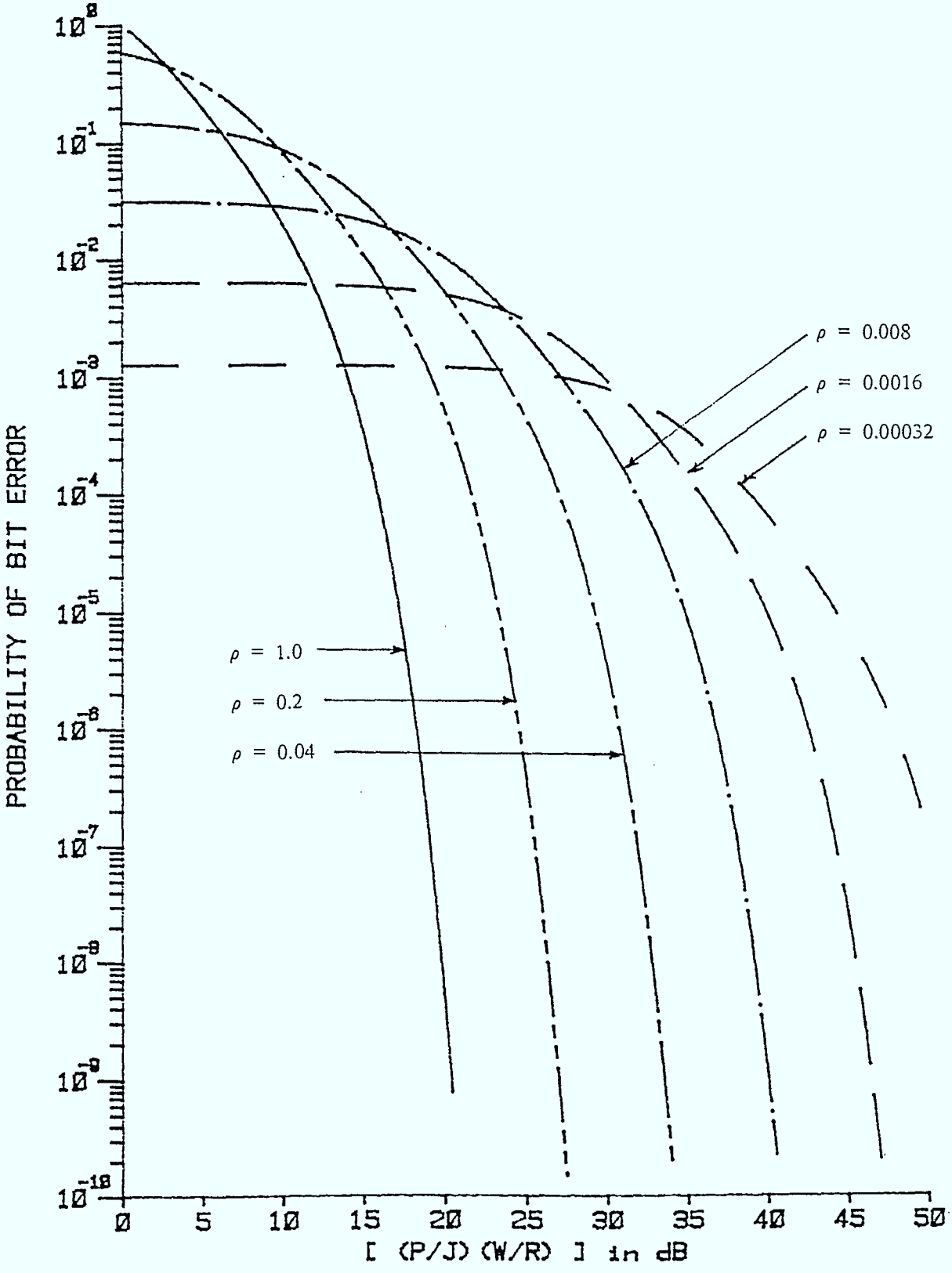

Figure 4.26 P_e of FH/DMSK with rectangular pulse shaping and N = 4 under partial band noise jamming

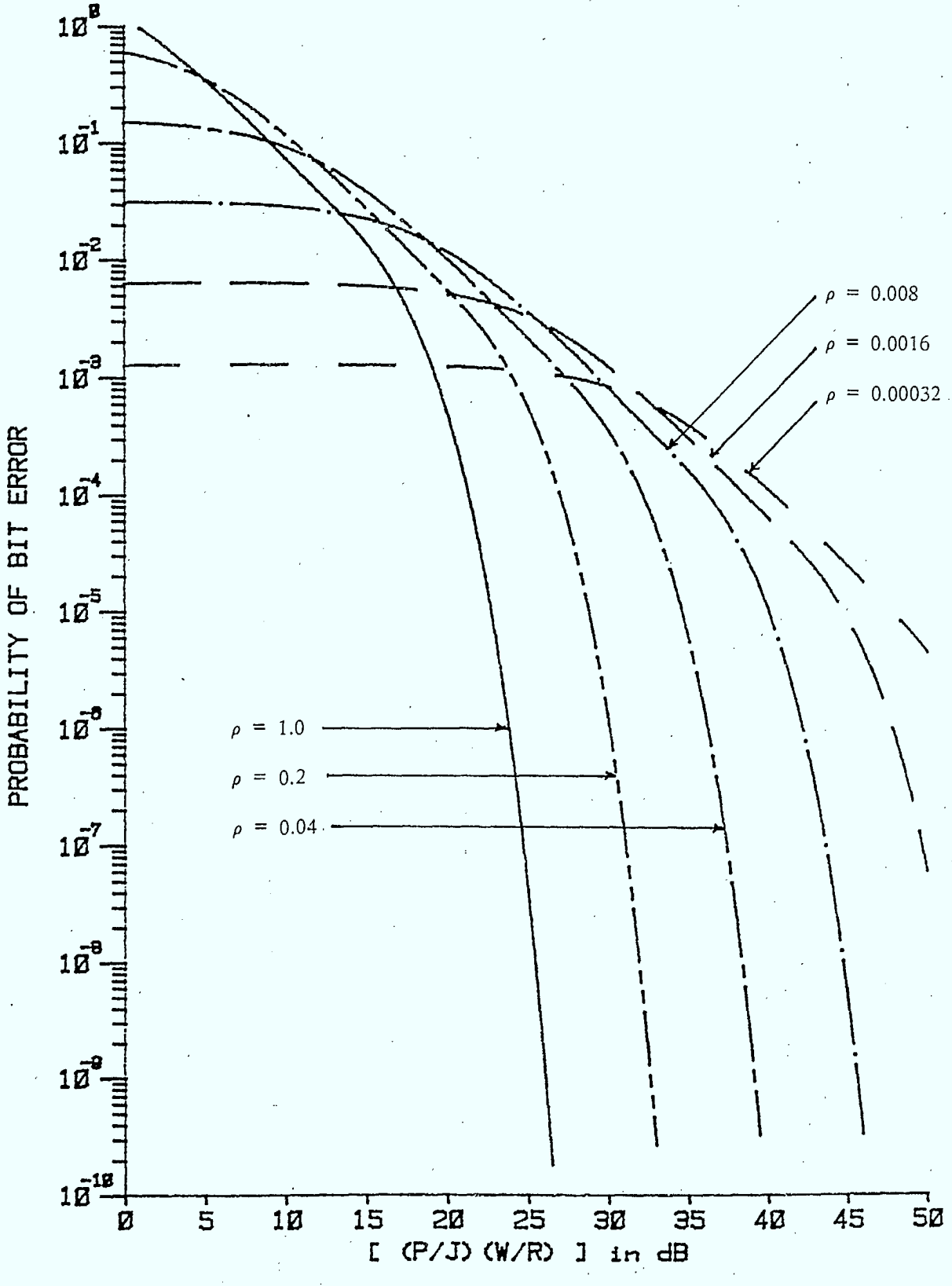

Figure 4.27 P_e of FH/TFM with rectangular pulse shaping and N = 4 under partial band noise jamming

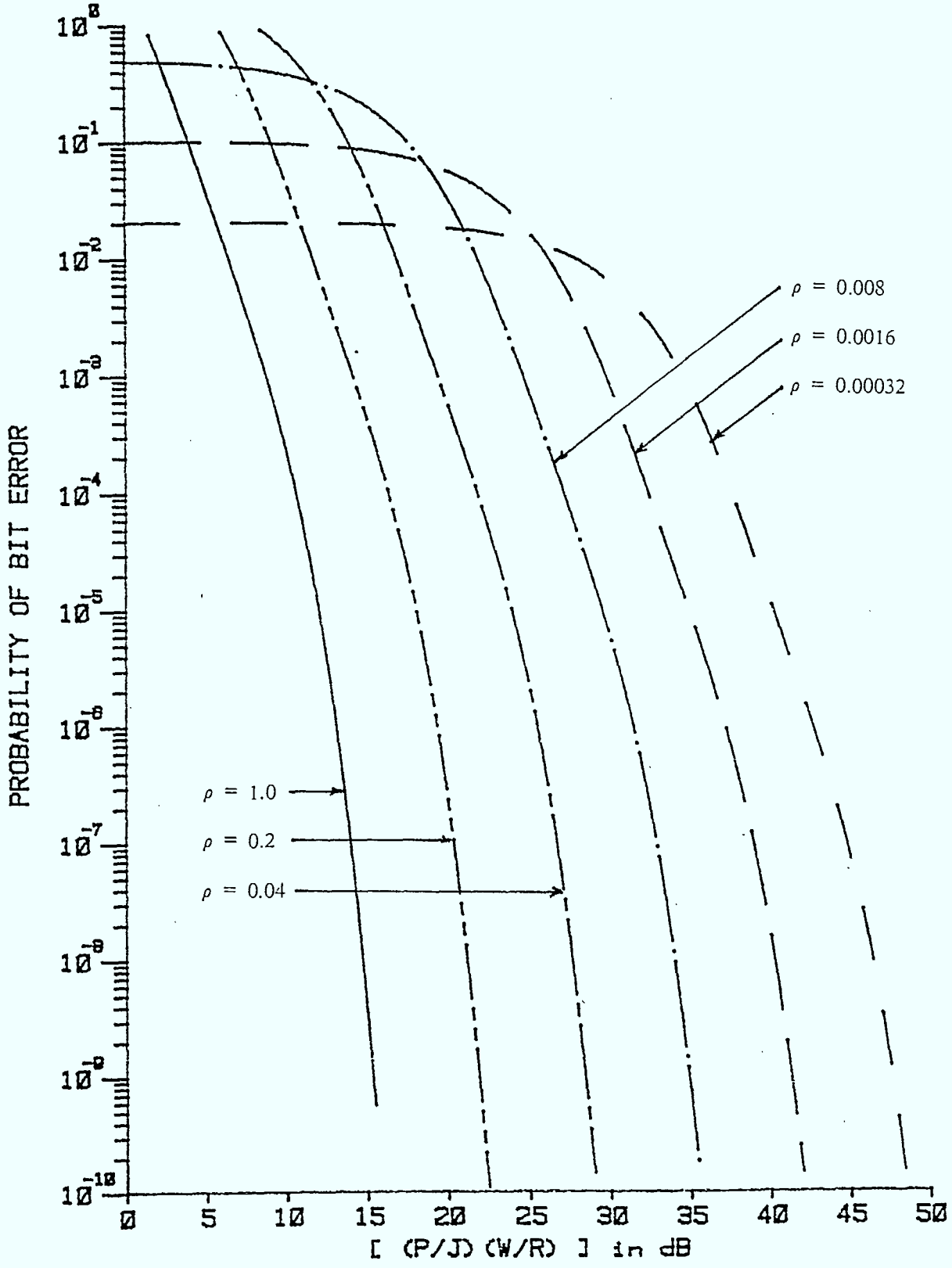

Figure 4.28 P_e of FH/MSK with rectangular pulse shaping and N = 8 under partial band noise jamming

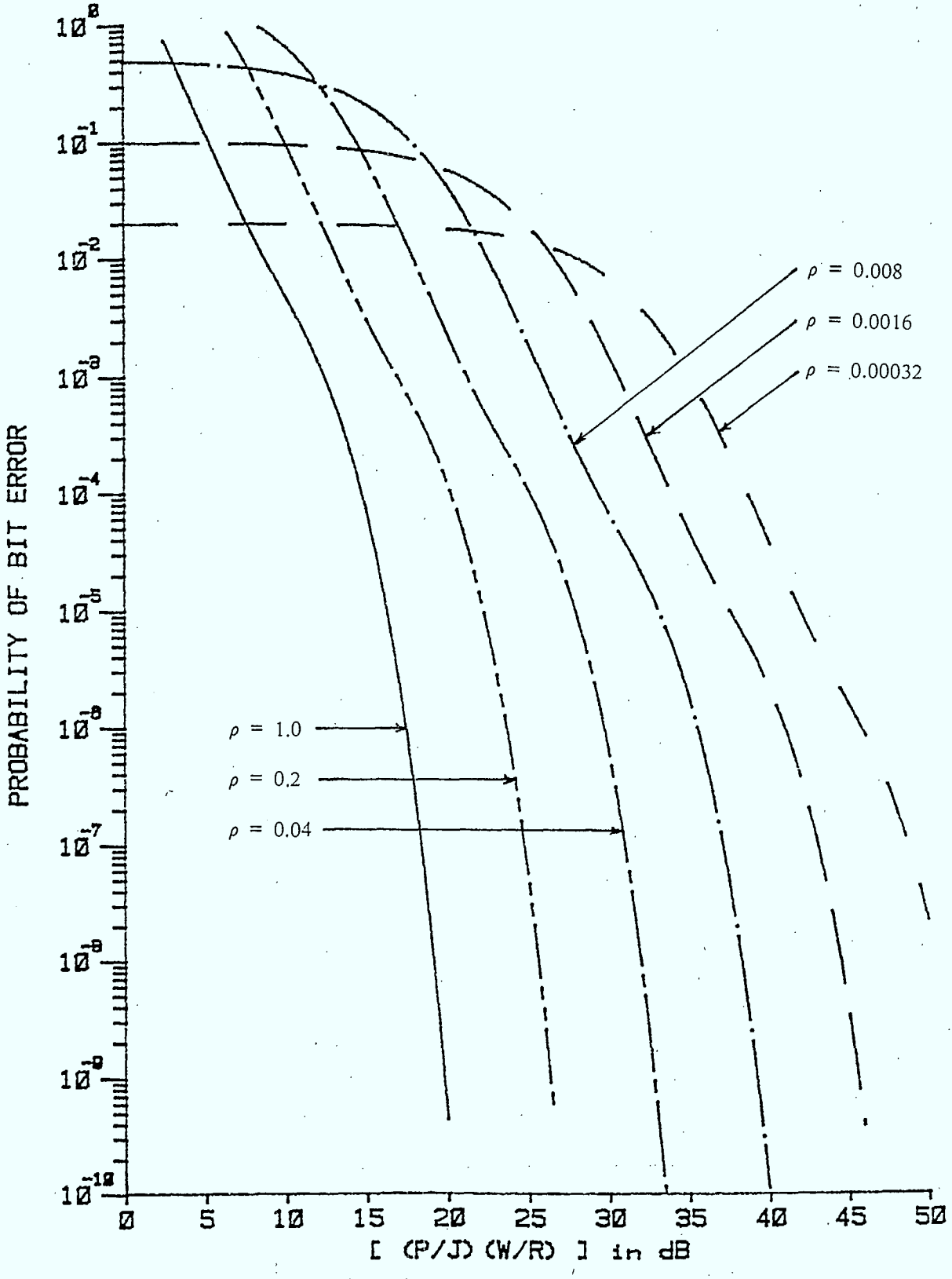

Figure 4.29 P_e of FH/DMSK with rectangular pulse shaping and N = 8 under partial band noise jamming

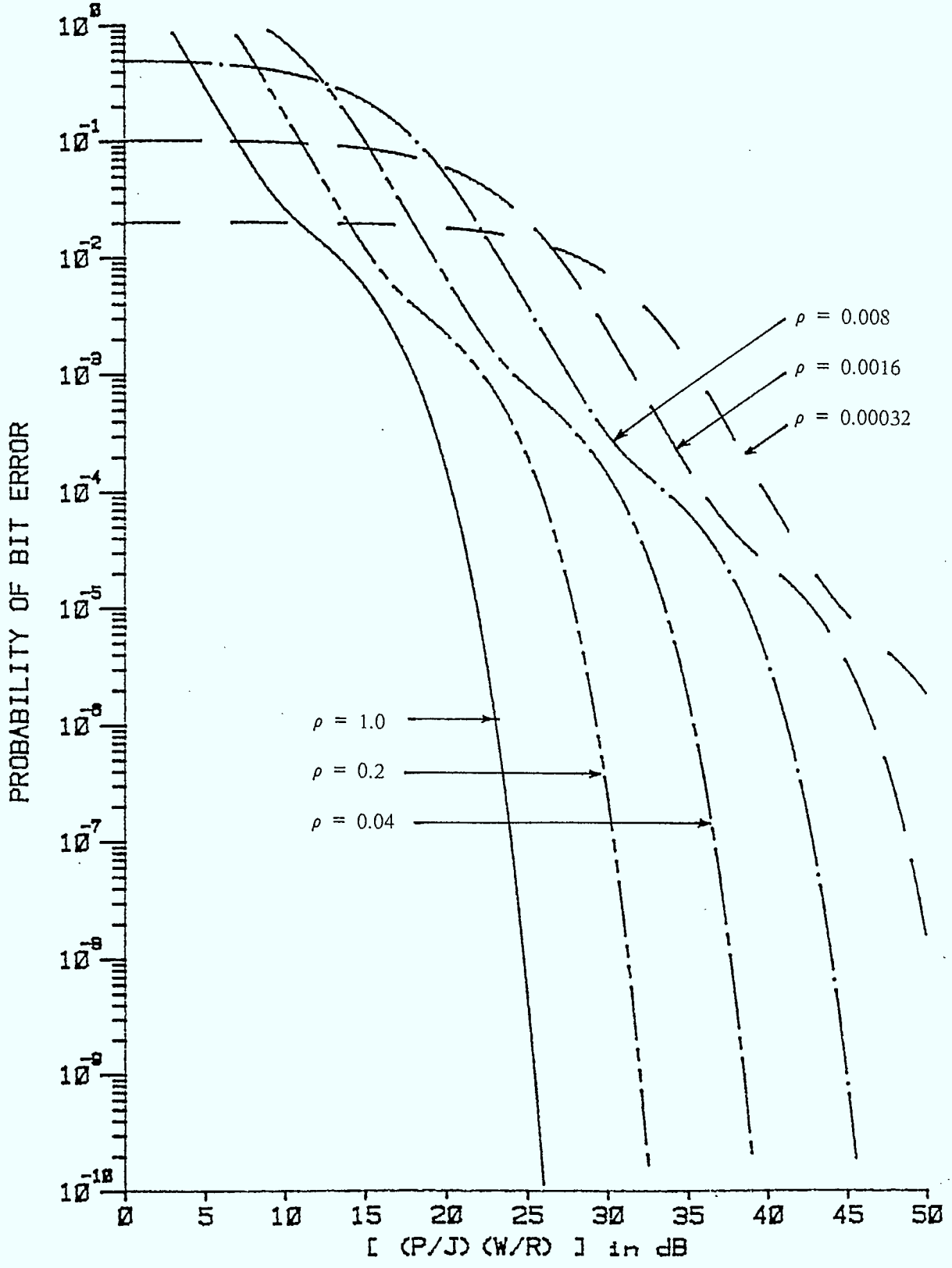

Figure 4.30 P_e of FH/TFM with rectangular pulse shaping and N = 8 under partial band noise jamming

4.2.2 Performance Under Multiple-Tone Jamming

In some cases, a more effective jamming strategy can be achieved with multiple-tone jamming [3]. The following analysis essentially follows the approach used in [3, p.597]. The jammer is assumed to have complete knowledge of the transmitted signal structure as well as the exact received signal power. However, the jammer does not know or is unable to predict the frequency hopping pattern. The jammer divides his total jamming power J into q equal power continuous-wave jamming tones distributed over the spread spectrum system bandwidth W. Each continuous-wave jamming tone signal will have power equal to

$$J_q = \frac{J}{q}. \tag{4.54}$$

The jammer will choose q and the tone spacing so that the optimum degradation occurs. Let $P = \frac{E}{T}$ be the power of the frequency-hopped CPM signal. For simplicity, suppose that thermal Gaussian noise is negligible. The dehopped received signal under multiple-tone jamming is given by

$$r(t) = s(t, \underline{\alpha}, \theta_i) + J_q(t); \qquad iNT < t < (i + 1)NT, \tag{4.55}$$

where $s(t, \underline{\alpha}, \theta_i)$ denotes the transmitted signal in the i^{th} hop interval as given by Eq.(3.4) re-written below

$$s(t, \underline{\alpha}, \theta_i) = \sqrt{2P}\ \cos[\, 2\pi f_c t + \psi(t, \underline{\alpha}) + \theta_i\,]; \qquad iNT < t < (i + 1)NT, \tag{4.56}$$

and $J_q(t)$ denotes the continuous-wave jamming tone signal given by

$$J_q(t) = \sqrt{2J_q}\ \cos[\, 2\pi f_c t + 2\pi f_J t + \phi_J\,], \tag{4.57}$$

where J_q is the power of the jamming tone, f_J is the jammer tone frequency offset from the intermediate carrier frequency f_c after being dehopped and ϕ_J is a random phase. Assuming that

the multiple-tone jammer knows the transmitted signal structure, the jammer will always select the tone frequency such that

$$2\pi f_J t = \psi(t, \tilde{\underline{\alpha}}). \tag{4.58}$$

That is, the jamming tone is one of the transmitted signals. (For example when the pulse shaping is rectangular and the tone jammer selects $f_J = \frac{h}{2T}$, then the jamming tone signal is the same as the signal, which would have been transmitted had the correlated symbols been all 1's.) The hop-by-hop receiver computes the equivalent likelihood for each of the possible sequences $\underline{\alpha}'$. When $J_q > P$, the receiver will always choose $\tilde{\underline{\alpha}}$ as the estimated transmitted sequence [Appendix A]. Hence for a given jammer power J and knowing the signal power P, the jammer will choose

$$q = \left\lfloor \frac{J}{P} \right\rfloor, \tag{4.59}$$

where $\lfloor x \rfloor$ denotes largest integer less than x. Of course, there must be at least one jamming tone and the maximum number of jamming tones is limited by the total number of frequency-hopped bands in the spread bandwidth. Let W_d be the bandwidth of the dehopped signal. The number of frequency-hopped bands will then be W/W_d. Hence, $1 \leq q \leq W/W_d$. When $\left\lfloor \frac{J}{P} \right\rfloor \leq 1.0$, no error will be made, since there is insufficient jammer power to jam even a single frequency-hopped band. The probability of any one frequency-hopped band being jammed is then

$$\rho = \frac{q}{W/W_d}. \tag{4.60}$$

For a slow FH/CPM system with a hop interval length of N symbol intervals, there are $\mu = 2^N$ possible transmitted sequences. The presence of a jamming tone with power greater than the signal power will force the hop-by-hop receiver to choose one particular sequence $\tilde{\underline{\alpha}}$.

Assuming that all sequences are equiprobable, when a jamming tone is present in the frequency-hopped band the bit error probability is given by

$$P[\text{ bit error }|\text{jammed}] = \frac{1}{2^N}\sum_{e=1}^{N}\binom{N}{e}\frac{e}{N} = \frac{1}{2}, \tag{4.61}$$

where $\binom{N}{e} = \frac{N!}{e!\,(N-e)!}$. Since thermal Gaussian noise is assumed to be negligible, probability of bit error is zero when the frequency-hopped band is not jammed. The bit error probability is then given by

$$P_e = \begin{cases} \frac{1}{2} & \frac{W}{W_d} < \left\lfloor \frac{J}{P} \right\rfloor, \\ \frac{1}{2}\, q\, \frac{W_d}{W} & 1.0 \le \left\lfloor \frac{J}{P} \right\rfloor \le \frac{W}{W_d}, \\ 0.0 & \left\lfloor \frac{J}{P} \right\rfloor < 1.0, \end{cases} \tag{4.62}$$

where the number of jamming tones is taken to be the optimum value as given by Eq.(4.59). The performance of the system will depend on the number of frequency-hop bands. For a given spread spectrum system bandwidth W, the smaller the frequency-hopped signal bandwidth W_d the greater number of tones required by the jammer to effectively jam communications. If we use the 99 percent poweer bandwidth of the frequeency-hopped signal as the bandwidth of each frequeenccy-hopped band, the bit error probability can be rewritten in terms of the parameter (P/J)(W/R) as

$$P_e = \begin{cases} 0.5 & \frac{P}{J}\frac{W}{R} < B, \\ \frac{B}{2}\ \frac{1}{(P/J)(W/R)} & B \le \frac{P}{J}\frac{W}{R} \le \frac{W}{R}, \\ 0.0 & \frac{W}{R} < \frac{P}{J}\frac{W}{R}, \end{cases} \tag{4.63}$$

where B is the 99 percent bandwidth normalized to the data rate, of the frequency-hopped signal. B has been evaluated for various modulation schemes previously in Chapter Two and listed in Tables 1 and 2. For example, B = 1.1875, 0.875 and 0.7656 for FH/MSK, FH/DMSK and FH/TFM with h = 0.5 and rectangular pulse shaping for N $\geq$ 1024 symbol intervals. Comparing with FH/DPSK which has B = 16 [3, p.127], we see that FH/MSK, FH/DMSK and FH/TFM outperform FH/DPSK by 11.29 dB, 12.62 dB and 13.2 dB in the inverse linear region. The more compact the frequency-hopped signal bandwidth, the greater the improvement in performance under multiple-tone jamming. Hence using slow FH/CPM improves immunity to multiple-tone jamming compared with conventional FH/MFSK or FH/DPSK.

4.3 Summary

In this chapter, the performance of the hop-by-hop noncoherent receiver is evaluated first under additive white Gaussian noise and then in the presence of partial band noise jamming and multiple-tone jamming. An upper bound on the bit error probability of the receiver under white Gaussian noise is derived using a union bound approach. The large number of possible error paths makes approximation necessary when the hop length is long. The upper bound is approximated by ignoring those error paths which have large equivalent distances and hence are less likely to occur. Results are presented for MSK, DMSK and TFM with h = 0.5 and both rectangular and raised cosine pulse shapings for three different lengths of hop interval: N = 4, 16 and 64. The error performance is better when the length of the hop interval is lengthened, as expected. The error performance worsens as higher order correlative encoding is employed.

Performance improvement when a segment of known symbols are transmitted initially at the start of a hop interval, is also investigated. The results show that for the three schemes namely MSK, DMSK and TFM, all with h = 0.5 and rectangular pulse shaping, transmission of one known initial symbol will improve the BER significantly for short hop sequences. Transmitting longer known initial symbol segments gives only slight additional improvement in performance. Also, for long hop lengths, the improvement in BER is not so pronounced as with the short hop interval cases.

An upper bound on the bit error probability in the presence of partial band noise jamming has been derived. Error results under partial band noise jamming are presented for MSK, DMSK and TFM with h = 0.5 and rectangular pulse shaping for various values of the fractional band jammed ρ. It can be seen that the three schemes performs quite similarly under worst case partial band noise jamming. The performance of the receiver in the presence of multiple-tone jamming is also derived. The antijam capability to multiple-tone jamming will be enhanced by using bandwidth efficient slow FH/CPM as compared to conventional schemes such as M-ary noncoherent FSK.

Chapter Five

SYSTEM SIMULATION

Theoretical upper bounds on the bit error probability of the hop-by-hop ML noncoherent receiver for various modulation schemes, baseband pulse shapings and hop lengths have been evaluated in the previous chapter under additive white Gaussian noise. The upper bounds obtained can serve as an index to the relative performance of the different modulation schemes. In this chapter, a computer simulation of the slow frequency-hopped spread spectrum systems with the hop-by-hop sequence estimation will be presented. The objective of the simulation is to evaluate the performance of the system under additive white Gaussian noise in order to indicate the tightness of the theoretical error bounds computed previously and to obtain a more precise performance evaluation of the system. Also, modification of the decoding algorithm can be easily incorporated in order to observe system performance improvement when more than one survivor is kept for each state in the modulation trellis. (A brute force maximum likelihood decoder would keep all possible paths through the trellis.)

Due to the large amount of computing time required for the simulation, only two systems employing two different modulation schemes have been simulated. The choice of the systems to be simulated is based on the findings obtained thus far. As can be seen from Chapter Two, the spectrum occupied by the frequency-hopped signal is rather insensitive to the type of correlative encoding scheme employed when the hop interval is short. Hence, for systems designed to transmit a few symbols over each frequency hop, a simple continuous phase modulation scheme will do well in regard to spectrum economy. For systems transmitting a large number of symbols during a hop interval, it would be beneficial to employ a suitable correlative encoding scheme in order to obtain a more compact spectrum for enhancing the antijam capa-

bility of the system, and for allowing more users in a multiple access system. With regard to receiver complexity, a high order correlative encoding scheme will generally require a more complex receiver due to the increased number of correlated output levels. More matched filters and more states in the decoder are usually required for correlative encoding with a higher order system polynomial. However for a long hop interval, the increased receiver complexity with a higher order correlative encoding scheme is accompanied by increased spectral efficiency.

The two systems simulated both have the modulation index h equal to 0.5, corresponding to four possible phase states. Actually only two phase states are possible at odd bit times and the other two possible at even bit times. Hence two phase states are actually required in the Markov state description of the signal. This choice of modulation index results in the lowest number of states in the state trellis regardless of the correlative polynomial employed. The first modulation scheme considered is minimum shift keying (MSK) and the other is the simplest form of correlative encoding, namely duobinary MSK. For both schemes, the baseband pulse shaping is rectangular, allowing possibly easier implementation of matched filter banks than the raised cosine examples. For each modulation scheme, systems with three different hop lengths of 4, 16 and 64 symbols have been simulated.

5.1 System Model

The system model used in the simulation is shown in Fig. 5.1. The data source provides binary data $\{\alpha_k\}$ at a rate of 1/T bits per seconds. For MSK, the binary data goes directly into the CPM modulator. For duobinary MSK, differential precoding [19,48], which is generally applied to prevent error propagation, is applied to avoid the problem of unknown initial encoder state, which would result in decoding ambiguity of some input sequences. Consider the input sequences with alternate +1 and -1. When the input sequence is $\{+1, -1, +1, -1, \ldots\}$ and the initial encoder state is -1, the duobinary encoded sequence

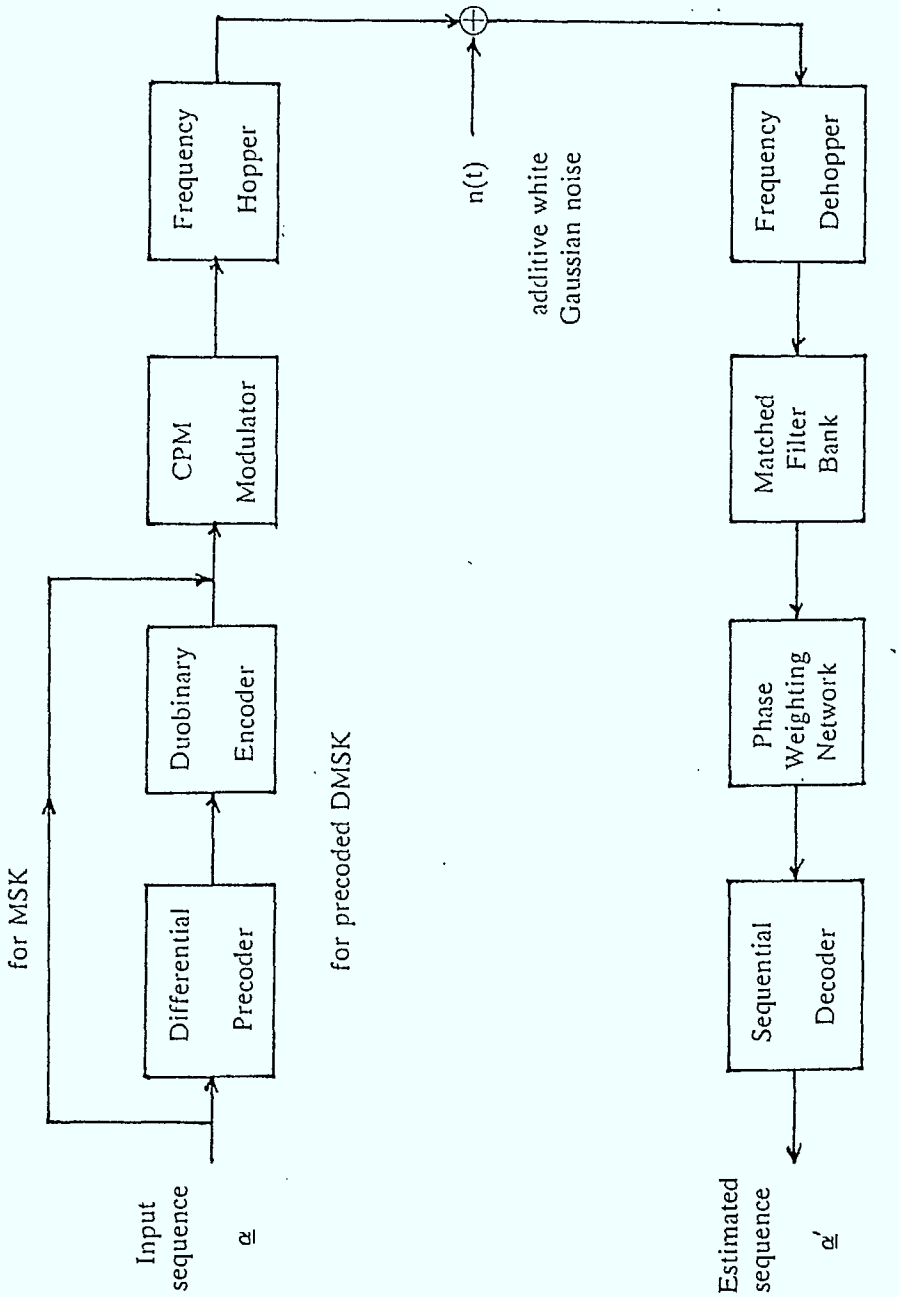

Figure 5.1 System model

will be a sequence of all zeros. When the input sequence is $\{ -1, +1, -1, +1, \ldots \}$ and the initial encoder state is $+1$, the same all zero duobinary sequence will result. Even if the receiver correctly estimated the transmitted correlated sequence as an all zero sequence, the decoder without prior knowledge of the initial encoder state cannot tell whether a $\{ +1, -1, +1, -1, \ldots \}$ or a $\{ -1, +1, -1, +1, \ldots \}$ is the input data sequence. Worst of all, picking the wrong sequence leads to all bits transmitted over the hop being in error. A trivial solution to this problem is to require the initial state of the encoder at the start of every hop interval to be known by the decoder. However, this would waste a fraction of the time interval for transmitting the initial encoder state, since the initial encoder state at the beginning of every hop would otherwise be the last input symbol in the previous hop interval. This input sequence ambiguity due to unknown initial state can be avoided by differential precoding of the input sequence. The input sequence $\{ \alpha_k \}$ is transformed into another set of independent binary random variables $\{ b_k \}$, with

$$\begin{aligned} b_k &= -b_{k-1} \quad \text{if } \alpha_k = +1 \\ b_k &= b_{k-1} \quad \text{if } \alpha_k = -1 \end{aligned} \tag{5.1}$$

This precoded symbols $\{ b_k \}$ then go to a duobinary encoder yielding duobinary symbols $\{ J_k \}$, which are given by

$$J_k = \frac{1}{2}(b_k + b_{k-1}) \tag{5.2}$$

The differentially precoded duobinary sequence will still depend on the initial encoder state but different initial encoder states will produce the same precoded duobinary sequence but with opposite signs for all the duobinary sequence elements. The estimated duobinary sequence $\{ J'_k \}$ is decoded back to the input sequence by

$$\alpha'_k = 2 |J'_k| - 1 \tag{5.3}$$

Hence, the maximum likelihood precoded duobinary sequence will always be decoded back to the same input data sequence independent of the initial encoder state. For FH/DMSK with differential precoding, the binary data first goes through a differential precoder followed by the duobinary encoder before going into the CPM modulator. The frequency hopper then transmits the signal at a carrier frequency that hops every NT seconds. We assume that the only disturbance on the channnel is the additive white Gaussian noise. The hopping and dehopping processes are assumed to be perfectly synchronized and the dehopper output is the exact replica of the transmitted signal but with random initial phase occurring at the beginning of every hop interval and the Gaussian channel noise added as given by Eq. (3.1). The dehopped received signal then goes to a bank of matched filters, which correlate the dehopped signal with every possible signal phase trajectories over a symbol interval. The matched filter outputs then go to a phase weighting network to provide the sequential decoder with the inphase and quadrature partial likelihoods for every possible signal over a symbol interval. These inphase and quadrature partial likelihoods for every possible signal phase then go to the sequential decoder, which estimates the transmitted sequence on a hop-by-hop basis, as described in section 3.1.

5.2 Simulation Method

There are basically two ways to simulate the effects of interferences in a noisy communications system. The first is to simulate only the noise-free signal path which is deterministic, and to utilize knowledge of the statistical properties of the noise or any other random interference to calculate their effects. The second approach is to use a straightforward Monte-Carlo simulation where all random effects are simulated as well [49]. The advantage of the first approach is that it is computationally efficient. However, the implementation of the technique requires extensive knowledge of the random processes. On the other hand the Monte-Carlo simulation approach does not usually require as much knowledge of the statistical properties of the random processes. The disadvantage is that it may be computationally less efficient,

especially if the events of interest occur only rarely (for example occurrence of errors in a high signal to noise ratio).

Since the sequential decoder is a nonlinear system with memory, the effect of preceding noise and signal components on the present samples are very difficult to evaluate. A Monte-Carlo simulation of the sequential decoder operation is then necessary. As mentioned in the previous section, the channel noise is modelled as additive white Gaussian noise and is assumed to be the only disturbance to the system. The received signal plus noise goes through a bank of matched filters followed by a phase weighting network to provide the decoder with the in-phase and quadrature correlations for every possible phase path over a symbol interval. Since the effect of the noise can be determined up to the decoder input, a noise-free signal path up to the decoder input can be simulated to avoid unnecessary simulation of the matched filter operation. Inphase and quadrature partial likelihoods for every possible signal phase path in a symbol interval are calculated as if there were no noise present. The filtered noise components are then added to form the likelihoods going to the decoder. Simulation of the system up to the sequential decoder simply requires generation of the inphase and quadrature partial likelihoods for a given transmitted sequence.

5.2.1 Inphase and Quadrature Partial Likelihoods

The inphase and quadrature partial likelihoods as given by Eqs. (3.9a) and (3.9b) are rewritten below.

$$\delta_{c,k}(\underline{\alpha}, \underline{\alpha}') = \int_{kT}^{(k+1)T} r(t) \cos[2\pi f_c t + \psi(t, \underline{\alpha}')] \, dt \qquad (5.4a)$$

$$\delta_{s,k}(\underline{\alpha}, \underline{\alpha}') = \int_{kT}^{(k+1)T} r(t) \sin[2\pi f_c t + \psi(t, \underline{\alpha}')] \, dt \qquad (5.4b)$$

Both partial correlations can be further decomposed by expanding the cosine and sine terms in Eqs. (5.4a) and (5.4b) as done in section 3.1.3. Without loss of information, Eqs. (5.4a) and (5.4b) can be used to express $\delta_{c,k}(\alpha, \underline{\alpha}')$ and $\delta_{s,k}(\alpha, \underline{\alpha}')$. During the k^{th} symbol interval in the i^{th} hop, the dehopped received signal is given by

$$r(t) = \sqrt{\frac{2E}{T}} \cos[2\pi f_c t + \psi(t, \underline{\alpha}) + \theta_i] + n(t) \quad \text{for} \quad iNT < t < (i+1)NT \tag{5.5}$$

where the symbols and notation are the same as those defined and used previously. n(t) is the additive Gaussian bandpass noise with zero mean and one-sided power spectral density N_o W/Hz which can be represented by

$$n(t) = \sqrt{2}\, n_c(t) \cos 2\pi f_c t - \sqrt{2}\, n_s(t) \sin 2\pi f_c t \tag{5.6}$$

The baseband processes $n_c(t)$ and $n_s(t)$ are statistically independent, white and Gaussian with zero mean and one-sided spectral density of N_o W/Hz. Substituting Eqs. (5.5) together with (5.6) into Eqs. (5.4a) and (5.4b) and assuming that $2\pi f_c t \gg 1$, we obtain the partial likelihoods corresponding to a transmitted sequence $\underline{\alpha}$ and an estimated sequence $\underline{\alpha}'$ over the k^{th} symbol interval as

$$\begin{aligned}\delta_{c,k}(\underline{\alpha}, \underline{\alpha}') = {} & \frac{1}{2}\sqrt{\frac{2E}{T}} \int_{kT}^{(k+1)T} \cos[\psi(t, \underline{\alpha}') - \psi(t, \underline{\alpha}) - \theta_i]\, dt \\ & + \frac{1}{\sqrt{2}} \int_{kT}^{(k+1)T} n_c(t) \cos\psi(t, \underline{\alpha}')\, dt + \frac{1}{\sqrt{2}} \int_{kT}^{(k+1)T} n_s(t) \sin\psi(t, \underline{\alpha}')\, dt\end{aligned} \tag{5.7a}$$

and

$$\begin{aligned}\delta_{s,k}(\underline{\alpha}, \underline{\alpha}') = {} & \frac{1}{2}\sqrt{\frac{2E}{T}} \int_{kT}^{(k+1)T} \sin[\psi(t, \underline{\alpha}') - \psi(t, \underline{\alpha}) - \theta_i]\, dt \\ & + \frac{1}{\sqrt{2}} \int_{kT}^{(k+1)T} n_c(t) \sin\psi(t, \underline{\alpha}')\, dt - \frac{1}{\sqrt{2}} \int_{kT}^{(k+1)T} n_s(t) \cos\psi(t, \underline{\alpha}')\, dt\end{aligned} \tag{5.7b}$$

Let

$$n_{c,k}(\underline{\alpha}') = \int_{kT}^{(k+1)T} n_c(t) \cos \psi(t, \underline{\alpha}') \, dt + \int_{kT}^{(k+1)T} n_s(t) \sin \psi(t, \underline{\alpha}') \, dt \tag{5.8a}$$

$$n_{s,k}(\underline{\alpha}') = \int_{kT}^{(k+1)T} n_c(t) \sin \psi(t, \underline{\alpha}') \, dt - \int_{kT}^{(k+1)T} n_s(t) \cos \psi(t, \underline{\alpha}') \, dt \tag{5.8b}$$

Eqs. (5.7a) and (5.7b) can be rewritten as

$$\delta_{c,k}(\underline{\alpha}, \underline{\alpha}') = \frac{1}{2} \sqrt{\frac{2E}{T}} \int_{kT}^{(k+1)T} \cos[\, \psi(t, \underline{\alpha}') - \psi(t, \underline{\alpha}) - \theta_i \,] \, dt + \frac{T}{\sqrt{2}} n_{c,k}(\underline{\alpha}') \tag{5.9a}$$

$$\delta_{s,k}(\underline{\alpha}, \underline{\alpha}') = \frac{1}{2} \sqrt{\frac{2E}{T}} \int_{kT}^{(k+1)T} \sin[\, \psi(t, \underline{\alpha}') - \psi(t, \underline{\alpha}) - \theta_i \,] \, dt + \frac{T}{\sqrt{2}} n_{s,k}(\underline{\alpha}') \tag{5.9b}$$

$n_{c,k}(\underline{\alpha}')$ and $n_{s,k}(\underline{\alpha}')$ are both Gaussian and zero mean, since $n_c(t)$ and $n_s(t)$ are both zero mean and white Gaussian processes. Their variances can be shown to be

$$\text{var}[\, n_{c,k}(\underline{\alpha}') \,] = \frac{N_o}{2} \frac{1}{T} \tag{5.10a}$$

$$\text{var}[\, n_{s,k}(\underline{\alpha}') \,] = \frac{N_o}{2} \frac{1}{T} \tag{5.10b}$$

Normalizing the Gaussian noise variables by their variances, we obtain

$$\delta_{c,k}(\underline{\alpha}, \underline{\alpha}') = \frac{\sqrt{N_o T}}{2} \{ \sqrt{\frac{2E}{N_o}} \frac{1}{T} \int_{kT}^{(k+1)T} \cos[\psi(t, \underline{\alpha}') - \psi(t, \underline{\alpha}) - \theta_i] dt + X_{c,k}(\underline{\alpha}') \} \tag{5.11a}$$

$$\delta_{s,k}(\underline{\alpha}, \underline{\alpha}') = \frac{\sqrt{N_o T}}{2}\{\sqrt{\frac{2E}{N_o}}\ \frac{1}{T}\int_{kT}^{(k+1)T} \sin[\psi(t, \underline{\alpha}') - \psi(t, \underline{\alpha}) - \theta_i]dt + X_{s,k}(\underline{\alpha}')\} \quad (5.11b)$$

Since the constant $\frac{1}{2}\sqrt{N_o T}$ in Eqs. (5.11a) and (5.11b) is common in the comparison for all estimated paths, hence it can be dropped, resulting in

$$\delta_{c,k}(\underline{\alpha}, \underline{\alpha}') = \sqrt{\frac{2E}{N_o}}\ \frac{1}{T}\int_{kT}^{(k+1)T} \cos[\,\psi(t, \underline{\alpha}') - \psi(t, \underline{\alpha}) - \theta_i\,]\,dt + X_{c,k}(\underline{\alpha}') \quad (5.12a)$$

$$\delta_{s,k}(\underline{\alpha}, \underline{\alpha}') = \sqrt{\frac{2E}{N_o}}\ \frac{1}{T}\int_{kT}^{(k+1)T} \sin[\,\psi(t, \underline{\alpha}') - \psi(t, \underline{\alpha}) - \theta_i\,]\,dt + X_{s,k}(\underline{\alpha}') \quad (5.12b)$$

where $\frac{E}{N_o}$ is the signal to noise ratio and $X_{c,k}(\underline{\alpha}')$ and $X_{s,k}(\underline{\alpha}')$ are the filtered noise components of unit variance.

In order to generate the likelihoods efficiently, we note that $\psi(t, \underline{\alpha}') - \psi(t, \underline{\alpha}) = \psi(t, \underline{\gamma})$ with $\underline{\gamma} = \underline{\alpha}' - \underline{\alpha}$ and that the signal phase can be expressed as an active time varying phase plus an underlying constant phase state. Hence, the inphase and quadrature likelihoods can be expressed as

$$\delta_{c,k}(\underline{\alpha}, \underline{\alpha}') = \sqrt{2\frac{E}{N_o}}\ \{\ \cos(\zeta_k - \theta_i)C(d_k) - \sin(\zeta_k - \theta_i)S(d_k)\ \} + X_{c,k}(\underline{\alpha}') \quad (5.13a)$$

and

$$\delta_{s,k}(\underline{\alpha}, \underline{\alpha}') = \sqrt{2\frac{E}{N_o}}\ \{\ \sin(\zeta_k - \theta_i)C(d_k) + \cos(\zeta_k - \theta_i)S(d_k)\ \} + X_{s,k}(\underline{\alpha}') \quad (5.13b)$$

where $C(d_k)$, $S(d_k)$, ζ_k and d_k are defined in Eqs. (4.36) to (4.38) rewritten below.

$$C(d_k) = \frac{1}{T}\int_{kT}^{(k+1)T} \cos 2\pi h d_k v(t)\, dt \tag{5.14a}$$

$$S(d_k) = \frac{1}{T}\int_{kT}^{(k+1)T} \sin 2\pi h d_k v(t)\, dt \tag{5.14b}$$

$$\zeta_k = \pi h \sum_{n=0}^{k-1} d_n \tag{5.15}$$

d_k is the correlative encoded difference sequence given by

$$d_k = \frac{1}{C}\sum_{\ell=0}^{m} k_\ell \gamma_{k-\ell} \tag{5.16}$$

where C is the normalizing constant as defined by Eq. (2.6) and the k_ℓ's are the coefficients of the correlative encoding polynomial.

All possible integrals of the cosine and sine of the possible phase over a symbol interval, $C(d_k)$ and $S(d_k)$, are initially calculated and stored in an array. To get the inphase and quadrature correlations over the k^{th} symbol interval for an estimated path, the correlated difference symbol d_k is first determined by subtracting the correlated symbol of the transmitted path from the correlated symbol of the estimated path. $C(d_k)$ and $S(d_k)$ can then be obtained through table lookup. The correlated difference phase state ζ_k as defined by Eq. (5.15) can be obtained simply as the phase state of the estimated path minus the phase state of the transmitted path. The likelihoods can then be easily determined according to Eq. (5.13a) and (5.13b).

5.2.2 Generating the Filtered Noise Components

The filtered noise components $X_{c,k}(\underline{\alpha}')$ and $X_{s,k}(\underline{\alpha}')$ in Eqs. (5.13a) and (5.13b) are the normalized $n_{c,k}(\underline{\alpha}')$ and $n_{s,k}(\underline{\alpha}')$ respectively. They are Gaussian random variables with zero mean and unit variance and are given by

$$X_{c,k}(\underline{\alpha}') = \int_{kT}^{(k+1)T} X_c(t) \cos \psi(t, \underline{\alpha}') \, dt + \int_{kT}^{(k+1)T} X_s(t) \sin \psi(t, \underline{\alpha}') \, dt, \tag{5.17a}$$

$$X_{s,k}(\underline{\alpha}') = \int_{kT}^{(k+1)T} X_c(t) \sin \psi(t, \underline{\alpha}') \, dt - \int_{kT}^{(k+1)T} X_s(t) \cos \psi(t, \underline{\alpha}') \, dt, \tag{5.17b}$$

where $X_c(t)$ and $X_s(t)$ are the normalized $n_c(t)$ and $n_s(t)$ respectively, and hence are statistically independent, white Gaussian processes with zero mean and one-sided spectral density of unity. It can be shown that

$$E\{ X_{c,k}(\underline{\alpha}') X_{s,k}(\underline{\alpha}') \} = 0. \tag{5.18}$$

That is, noise components of the inphase and quadrature partial likelihoods resulting from matched filtering of the dehopped received signal matched to a particular signal corresponding to $\underline{\alpha}'$, are themselves uncorrelated. However, it can be shown that

$$E\{ X_{c,k}(\underline{\alpha}') X_{c,k}(\underline{\alpha}) \} = \frac{1}{T} \int_{kT}^{(k+1)T} \cos[\psi(t, \underline{\alpha}') - \psi(t, \underline{\alpha})] \, dt, \tag{5.19}$$

$$E\{ X_{c,k}(\underline{\alpha}') X_{s,k}(\underline{\alpha}) \} = -\frac{1}{T} \int_{kT}^{(k+1)T} \sin[\psi(t, \underline{\alpha}') - \psi(t, \underline{\alpha})] \, dt. \tag{5.20}$$

Hence, the noise component of the output of the filter matched to the inphase signal component for $\underline{\alpha}'$ may be correlated with that from the inphase matched filter for $\underline{\alpha}$ according to Eq.(5.19).

The noise component of the output of the filter matched to the inphase component for $\underline{\alpha}'$ may also be correlated with the noise component of the output of the quadrature matched filter for $\underline{\alpha}$ as indicated by Eq. (5.20).

Depending on the modulation scheme employed for transmission, the noise components $\{X_{c,k}(\underline{\alpha}'), X_{s,k}(\underline{\alpha}')\}$ of the inphase and quadrature partial likelihoods of different signals over a symbol interval can be generated simply as independent Gaussian random variates, only if their correlations as given by Eqs. (5.19) and (5.20) are zero. In order to generate the filtered noise components having correlations given by Eqs. (5.19) and (5.20), Eq. (3.23) for the phase over the k^{th} symbol interval is substituted into Eqs. (5.17a) and (5.17b) yielding

$$\begin{aligned} X_{c,k}(\underline{\alpha}') = {} & \cos\phi_k(\underline{\alpha}')\, X_{cc}(\underline{\alpha}') - \sin\phi_k(\underline{\alpha}')\, X_{cs}(\underline{\alpha}') \\ & + \sin\phi_k(\underline{\alpha}')\, X_{sc}(\underline{\alpha}') + \cos\phi_k(\underline{\alpha}')\, X_{ss}(\underline{\alpha}') \end{aligned} \tag{5.21a}$$

and

$$\begin{aligned} X_{s,k}(\underline{\alpha}') = {} & \sin\phi_k(\underline{\alpha}')\, X_{cc}(\underline{\alpha}') + \cos\phi_k(\underline{\alpha}')\, X_{cs}(\underline{\alpha}') \\ & - \cos\phi_k(\underline{\alpha}')\, X_{sc}(\underline{\alpha}') + \sin\phi_k(\underline{\alpha}')\, X_{ss}(\underline{\alpha}'), \end{aligned} \tag{5.21b}$$

where

$$X_{cc}(\underline{\alpha}') = \int_{kT}^{(k+1)T} X_c(t)\, \cos\beta_k(t, \underline{\alpha}')\, dt, \tag{5.22a}$$

$$X_{cs}(\underline{\alpha}') = \int_{kT}^{(k+1)T} X_c(t)\, \sin\beta_k(t, \underline{\alpha}')\, dt, \tag{5.22b}$$

$$X_{sc}(\underline{\alpha}') = \int_{kT}^{(k+1)T} X_s(t)\, \cos\beta_k(t, \underline{\alpha}')\, dt, \tag{5.22c}$$

$$X_{ss}(\underline{\alpha}') = \int_{kT}^{(k+1)T} X_s(t) \sin \beta_k(t, \underline{\alpha}')\, dt. \tag{5.22d}$$

To generate the filtered noise components $X_{cc}(\underline{\alpha}')$, $X_{cs}(\underline{\alpha}')$, $X_{sc}(\underline{\alpha}')$ and $X_{ss}(\underline{\alpha}')$, an orthonormal expansion of the signals $\cos \beta_k(t, \underline{\alpha}')$ and $\sin \beta_k(t, \underline{\alpha}')$ is determined using the Gram-Schmidt orthogonalization procedure [50,51]. The random variates $X_{cc}(\underline{\alpha}')$, $X_{cs}(\underline{\alpha}')$, $X_{sc}(\underline{\alpha}')$ and $X_{ss}(\underline{\alpha}')$ can be obtained by generating independent Gaussian random variates with zero mean and unit variance and then weighting them by the corresponding orthonormal coefficients in the orthonormal expansion. These random variates are then multiplied by the appropriate sines and cosines of the phase state of the estimated path and are summed according to Eqs. (5.21a) and (5.21b) to form the filtered noise components $X_{c,k}(\underline{\alpha}')$ and $X_{s,k}(\underline{\alpha}')$.

Considering MSK for example, there are two possible signal phase trajectories over the k^{th} symbol interval, namely $\alpha_k \frac{\pi}{2T} t$ corresponding to $\alpha_k = +1$ and -1. Using the Gram-Schmidt procedure, the matched filter signal references can be expanded in terms of orthonormal functions. The orthonormal representations for the signal references corresponding to α'_k are given by

$$\begin{aligned} \cos \alpha'_k \frac{\pi}{2T} t &= \alpha'_k a_1 \phi_1(t), \\ \sin \alpha'_k \frac{\pi}{2T} t &= \alpha'_k (a_2 \phi_1(t) + a_3 \phi_2(t)) \end{aligned} \tag{5.23}$$

for $\alpha'_k = +1$ and -1. The $\phi_i(t)$ are orthonormal functions and the orthonormal coefficients a_i are given by

$$\begin{aligned} a_1 &= \sqrt{\frac{T}{2}}, \\ a_2 &= \frac{\sqrt{2T}}{\pi}, \\ a_3 &= \sqrt{\frac{\pi^2 T - 4T}{2\pi^2}}. \end{aligned} \tag{5.24}$$

The random variates $X_{cc}(\underline{\alpha}')$, $X_{cs}(\underline{\alpha}')$, $X_{sc}(\underline{\alpha}')$ and $X_{ss}(\underline{\alpha}')$ depend only on α'_k and are given by

$$\begin{aligned} X_{cc}(\alpha'_k) &= \alpha'_k\, a_1\, x_1, \\ X_{cs}(\alpha'_k) &= \alpha'_k\, (\, a_2\, x_1 \;+\; a_3\, x_2\,), \\ X_{sc}(\alpha'_k) &= \alpha'_k\, a_1\, x_3, \\ X_{ss}(\alpha'_k) &= \alpha'_k\, (\, a_2\, x_3 \;+\; a_3\, x_4\,), \end{aligned} \tag{5.25}$$

where the x_i are independent zero-mean Gaussian random variates of unit variance. The inphase and quadrature filtered noise components for an estimated sequence can then be formed using Eqs. (5.21a) and (5.21b).

5.2.3 Decoder Simulation

Due to incomplete knowledge of the effect of noise on the decoder operation, a Monte-Carlo technique is used to simulate the operation of the sequential decoder. The decoder estimates the transmitted sequence by calculating the inphase and quadrature likelihoods recursively and chooses the one with the largest equivalent likelihood as described in section 3.1. For MSK, there are only four possible phase states in the state description. For DMSK, there are four possible phase states and two correlative encoder states corresponding to +1 and -1 being the previous symbol. Thus there are a total of 8 combined states. Decoders with all possible states at each time kT are simulated for simplicity, although the number of states can be reduced by a factor of two considering that only half of the states are possible at odd bit times and the other half at even bit times. The method used to simulate the decoder is given in the next section together with details of the simulation program.

5.3 Program Description

A brief description of the simulation program will be given in this section with emphasis on the methodology, rather than describing the program in detail. For simplicity only binary data transmission is considered. Separate programs were written to simulate the FH/MSK and FH/DMSK systems with the hop-by-hop sequence estimation receiver.

There is input of parameters and initialization of various variables and tables at the start of the program execution as is usual in computer simulation programs. The input parameters are the length of the hop interval in number of symbols, length of decoder buffer for storing path histories of the survivors, the number of survivors to be kept for each state in the trellis, the maximum simulation time and maximum number of bit errors before the simulation terminated, the range of SNR values to be simulated and lastly, three large odd integers as seeds for the random number generators. Various constants, variables and tables are then initialized. These include the coefficients of the orthonormal vector representation of all possible inphase and quadrature signal components in a symbol interval, a table of the integrals of the cosine and sine of all possible difference signal phase trajectories in a symbol interval, the value of the underlying constant phase corresponding to each state and the state transition table which provides the index of the next state given the index of the present state and the present input symbol. The system is then simulated for the number of SNR values as specified by the input parameters.

For each SNR value, the simulation runs for a specified length of time or until a given number of bit errors has occurred. A flowchart showing the logic flow of the program execution is shown in Fig. 5.2. A number of counters, flags and tables are first initialized. These include the counters for simulation time, the number of bits in the current hop, the number of bits transmitted, the number of bits decoded and the number of bit errors. The random initial phase

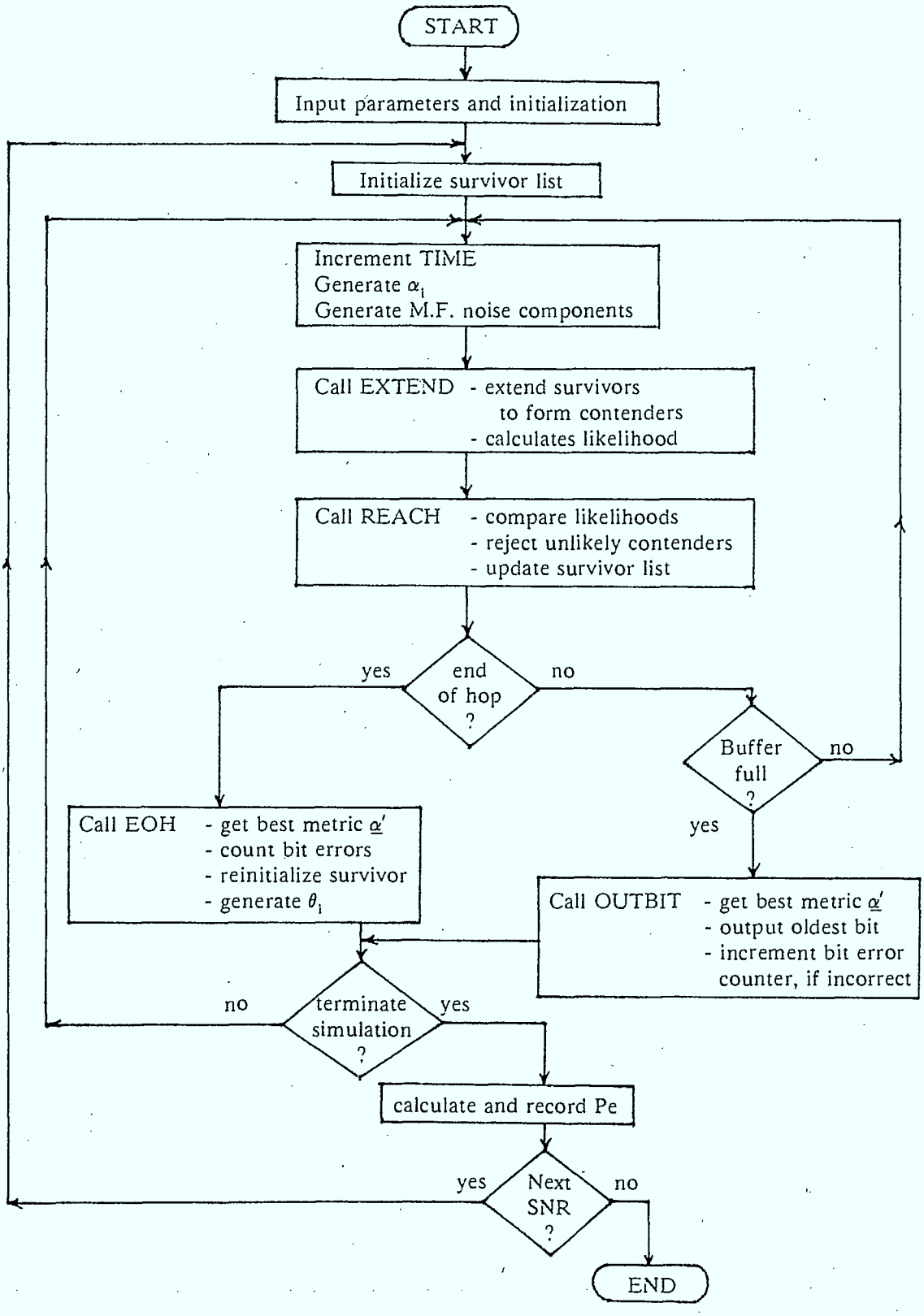

Figure 5.2 Simulation program flowchart

due to the hopping and dehopping processes is generated uniformly distributed from 0 to 2π. The initial state of the transmitter is initialized arbitrarily to state one in the state trellis.

Pertinent information associated with each survivor is the state at which the survivor path ends, the inphase and quadrature likelihoods from which the metric for the path can be formed by summing the squares, and the history of the survivor path. For the MSK simulation, the history of the survivor is the estimated data sequence, while for DMSK with precoding, the correlated sequence is stored as the history of the survivors. All these parameters of the survivors are stored in a number of variables and arrays which are collectively called the survivor list for convenience. The survivor list is initialized during the start of the simulation and every time a frequency hop occurs for the hop-by-hop sequence estimation receiver. In order for the decoder simulation program to proceed, the survivor list is initialized with a dummy survivor into the initial state. Since noncoherent detection is used, the initial state of the decoder can be arbitrarily assigned to any state for MSK modulation, which has only four phase states but no correlator state. For DMSK modulation, there are three different correlated symbols, namely +1, -1 and 0. The transmitted path can either increase or decrease by $\frac{\pi}{2}$ radians or stay at the same constant phase at the end of the symbol interval. Since there can be only two paths diverging from any one state, two initial states are then required for DMSK in order that the estimated paths will include all three possible phase trajectories. The two initial states for the DMSK decoder are chosen such that they have different correlative encoder states. The number of dummy initial survivors is initialized to one for the FH/MSK simulation and to two for the FH/DMSK simulation. All the likelihood parameters and path bit histories for these initial survivors are set to zero with the state at which they end assigned to the initial state or states accordingly.

The simulation of the system then begins by incrementing the counters for the time and number of symbols in the current hop. The input data for this symbol interval is generated

randomly with equal probability for +1 and -1 and recorded in an array. For the DMSK simulation program, differential precoding is first applied followed by duobinary encoding to form the transmit symbols. Four filtered noise components are needed for the MSK simulation, while six filtered noise components are needed for the DMSK simulation. Marsaglia's polar method [52], which generates two independent Gaussian random variates at a time, is used to generate the required number of independent Gaussian random variates with zero mean and unit variance. These random variates are then multipled by the corresponding orthonormal coefficients of the orthonormal vector representation of the filter response, to form the inphase and quadrature filtered noise components. The required filtered noise components in the partial likelihoods for each state transition are formed later when required by summing the appropriate inphase and quadrature noise components each weighted by the cosine and sine of the phase state of the estimated path segment.

The program execution then goes to subroutine EXTEND, which extends each survivor in the survivor list to form two contender paths. One contender path has a +1 as the present symbol, while the other has a -1 as the present symbol. To obtain the likelihoods of the contender, the present correlated difference symbol which is simply the present correlated symbol for this contender path minus the present correlated symbol of the transmitted path, is first calculated. The inphase and quadrature matched filter outputs are then obtained through table lookup. The signal component of the inphase partial likelihood is then obtained by summing the matched filter outputs weighted by the appropriate cosines or sines of the difference phase state. The filtered noise components from the matched filters for the present symbol of this contender path are obtained by table lookup. The noise component of the inphase partial likelihood of this contender path during the present symbol interval is then calculated by summing these noise samples weighted by the cosine and sine of the phase state of this contender path. The inphase likelihood of this contender is obtained by adding the signal component and noise component of the partial likelihood to the inphase likelihood of the survivor from which

this contender is formed. Similarly, the quadrature likelihood of this contender path is calculated also. The equivalent likelihood for each contender path which is the sum of the squares of the inphase and quadrature likelihoods are also calculated to facilitate comparisons. A flag associated with each contender path to indicate whether this contender has been rejected or not is then clear. The variables, pointers and flags for all the contenders are collectively referred to as the contender list. When the program execution returns to the main program from the subroutine EXTEND, the contender list will contain all possible contender paths, corresponding to all possible state transitions during a symbol interval, with all pertinent information about each contender paths calculated.

Subroutine REACH is then called to sort out the most likely survivor paths from the contender list. There are a counter and table for each state to record the number of contender paths with largest likelihoods and their indices in the contender list. These counters and tables are first initialized. Starting from the first contender in the contender list, the state which this contender leads into is noted. The counter for that state is first checked to see how many contenders have been recorded for that state. If the number of most likely contender paths to that state is less than the number of survivors to be kept for each state, then the index of the contender path currently visiting that state is entered in a table associated with that state. Otherwise if the number of most likely contenders is equal to the number of survivors to be kept for each state, then the equivalent likelihood for the present visiting contender is compared against the equivalent likelihoods of all those contenders recorded for that state. If the equivalent likelihood of the present contender is less than all those recorded, it is rejected by setting the reject flag in the contender list. Otherwise it replaces the one with the smallest likelihood recorded for that state, and the reject flag for that less likely contender is set. After all the contenders in the contender list have been checked, the most likely contenders would have been sorted out. The new survivors are those contender paths which do not have the reject flag set.

The survivor list is then updated by copying the pertinent information of all those contenders, which have not been rejected, to the new survivor list.

There are actually two survivor lists in the program for storing pertinent information on the survivors such as the state at which the survivor ends, the likelihood parameters of the survivor: namely the inphase and quadrature correlations up to the present time and also the path history of the survivor. A flag is used to indicate which survivor list contains the valid data. By using two survivor lists only pointers are required for pointing to the survivor, from which the contender is extended rather than copying all the information to the contender list. After the proper contenders which will be the survivors are sorted out, the pertinent data of the survivors are recorded to the new list by updating the old list. In this way copying long bit history from the survivor list to the contender list and then copying the updated information of those new survivors from the contender list back to the survivor list is not required. Hence execution time is reduced significantly especially when the hop length is long.

Execution then returns to the main program which then checks if this is the end of a hop. At the end of each hop, subroutine EOH is called to simulate the procedure of the decoder. Equivalent likelihoods of all survivors in the survivor list are compared and the index of the survivor with the largest equivalent likelihood is obtained. For the MSK simulation, the bit history corresponding to this maximum likelihood survivor is fed out as the decoded sequence for this hop. For the DMSK simulation, the corresponding correlated sequence of the most likely survivor is decoded back to the estimated input data sequence by operating on each estimated correlated symbol through Eq. (5.3). The decoded sequence is checked against the transmitted sequence to determined the number of bit errors. The counters for the number of symbols decoded and the number of bit errors are incremented accordingly. The random initial phase for the start of the next hop is then generated, and the new survivor list is initialized.

Provision has been made in the program for simulating systems with long hop intervals, in which case practical implementation would have the decoder buffers shorter than the hop length. The buffer pointer is checked to see if the buffers are full. If the buffers are full, then subroutine OUTBIT is called to release the oldest bit of the survivor which has the largest equivalent likelihood, and hence is the decoded symbol. The counter for decoded bits is incremented and the bit error counter is incremented if the decoded bit is different from the corresponding transmitted bit. To avoid shifting bit history through the buffers, all buffers are implemented as circular queues.

The simulation time and number of bit errors are then checked to see if the simulation is needed to be terminated. If not, program control loops back to simulate the next symbol interval as described above.

If the simulation for this SNR is complete, the bit error probability calculated as the number of bit errors divided by the total number of symbols decoded is then recorded in a data file together with the value of this SNR. If this is the last SNR value to be simulated the program comes to an end, otherwise the simulation begins for the next SNR value.

5.4 Simulation Results

Both the FH/MSK and FH/DMSK systems have been simulated for three different hop interval lengths of 4, 16 and 64 symbol intervals. All simulations are run for at least 100,000 symbol intervals at low signal to noise ratios and until at least 30 bit errors have occurred at high signal to noise ratios, in order to get statistically significant simulation results. Also the buffer length of each decoder buffer was set to be of the same length as the hop interval, although provision was made in the program for simulating systems with very long hop interval and circular buffers of reasonable length.

Performance improvement of the decoder by keeping more than one survivor for each state in the modulation trellis was also investigated through computer simulation. It was found that the error performance of the receiver improves if the decoder keeps more than one survivor for each state in the modulation trellis. The FH/MSK system was simulated also for a hop interval of a single symbol interval, in which case the system performance should be the same as noncoherent FSK with $h = 0.5$. The simulated bit error probability for $N = 1$ is plotted together with the theoretical average bit error rate in Fig. 5.3. We can see that the simulation result coincides with the theoretically computed bit error rate. For the FH/MSK scheme with a hop interval of length $N = 4$, 16 and 64, the performance of the hop-by-hop sequence estimation receiver as the number of survivors to be kept for each state is varied from 1 to 4, is shown in Figs. 5.4 to 5.6 respectively. We see that if the decoder keeps more than one survivor for each state in the modulation trellis, the bit error rate improves. However, keeping more than two survivors improves the bit error rate insignificantly. It can be seen that by increasing the number of survivors to two, essentially optimum error performance for hop-by-hop noncoherent detection is obtained. The error rate improves by about 1 dB at moderate SNR for all hop lengths simulated. In Figs. 5.4 to 5.6, the corresponding theoretical upper bound evaluated for FH/MSK with rectangular pulse shaping for $N = 4$, 16 and 64, is plotted together with the simulation results in order to indicate the tightnesss of the upper bounds evaluated in Chapter Four. At moderate to high signal to noise ratio, the upper bound for $N = 4$ is tight, while for longer hop intervals such as 16 and 64, the bounds are not as accurate. It can be seen that for most of the range where simulations were carried out, the upper bounds are within 0.5 dB of the simulation results for the decoder keeping 2 survivors per state. The simulation results for the hop-by-hop sequence estimation receiver for various lengths of hop interval are shown in Figs. 5.7 and 5.8 for the decoder keeping one and two survivors for each state respectively. The upper bound on the bit error probability of a coherent Viterbi receiver for MSK [42] is plotted also for comparison purposes. It can be seen that the error rate decreases

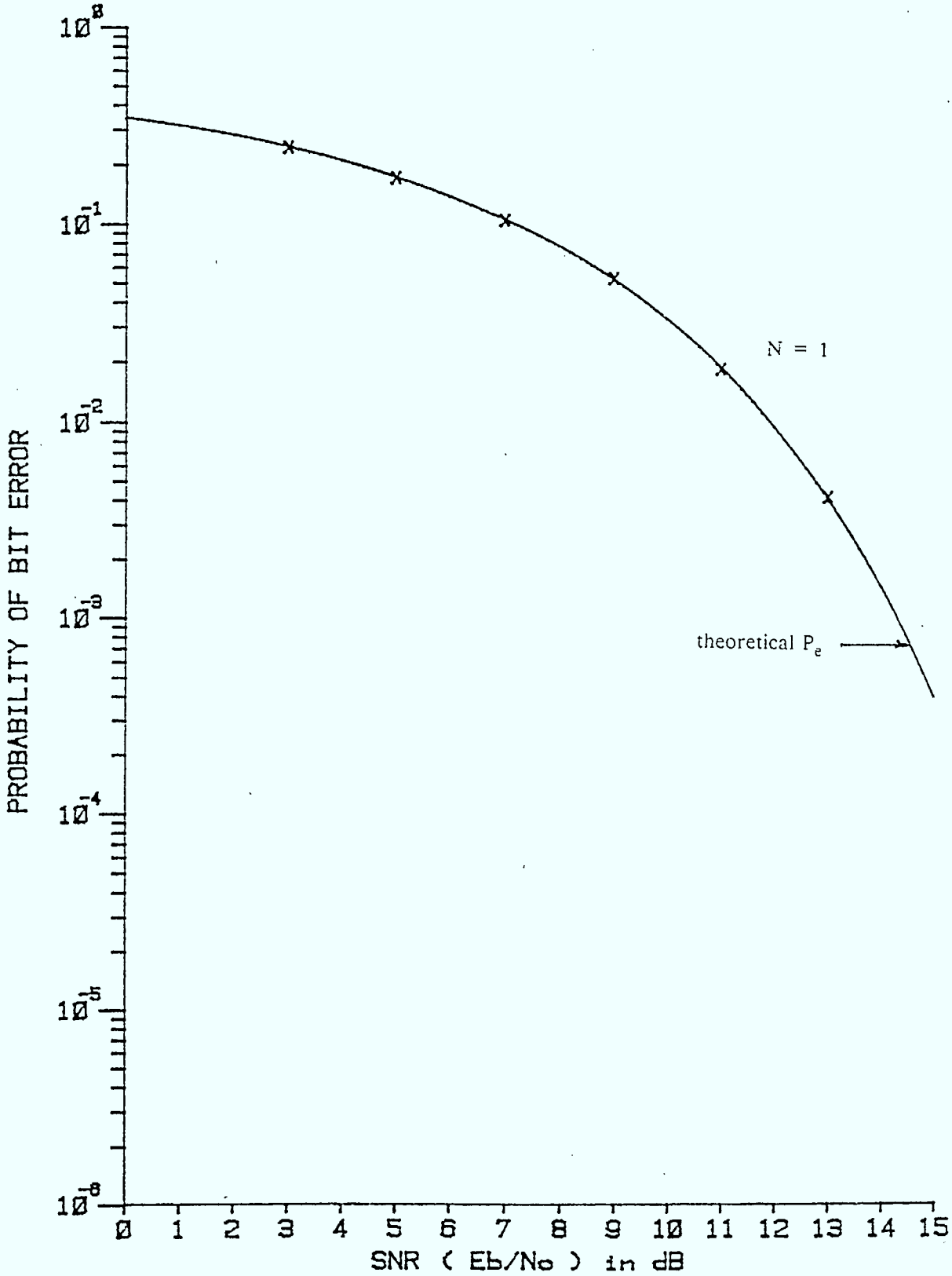

Figure 5.3 N = 1, FH/MSK simulation results and theoretical P_e

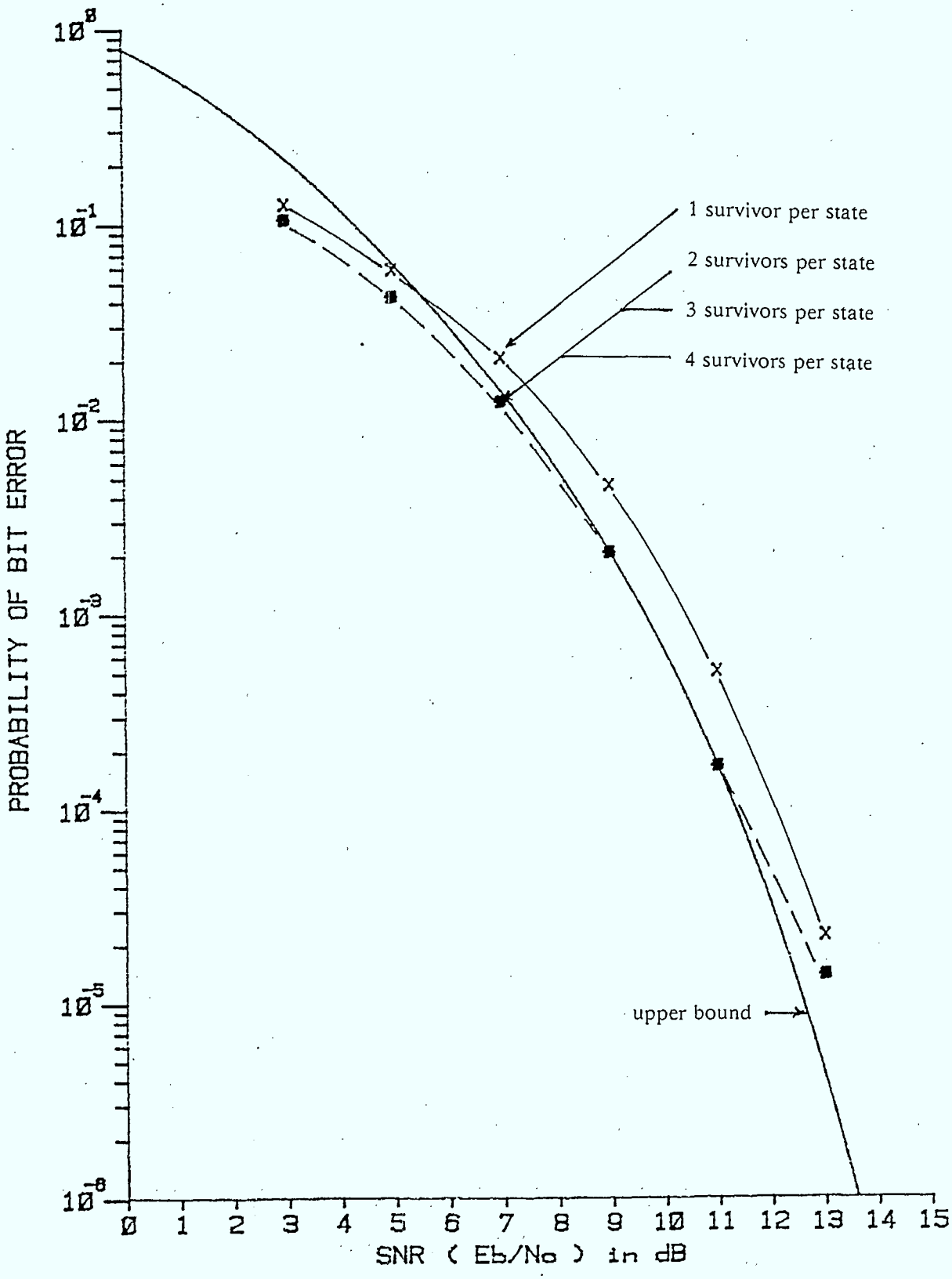

Figure 5.4 N = 4, FH/MSK simulation results and upper bound

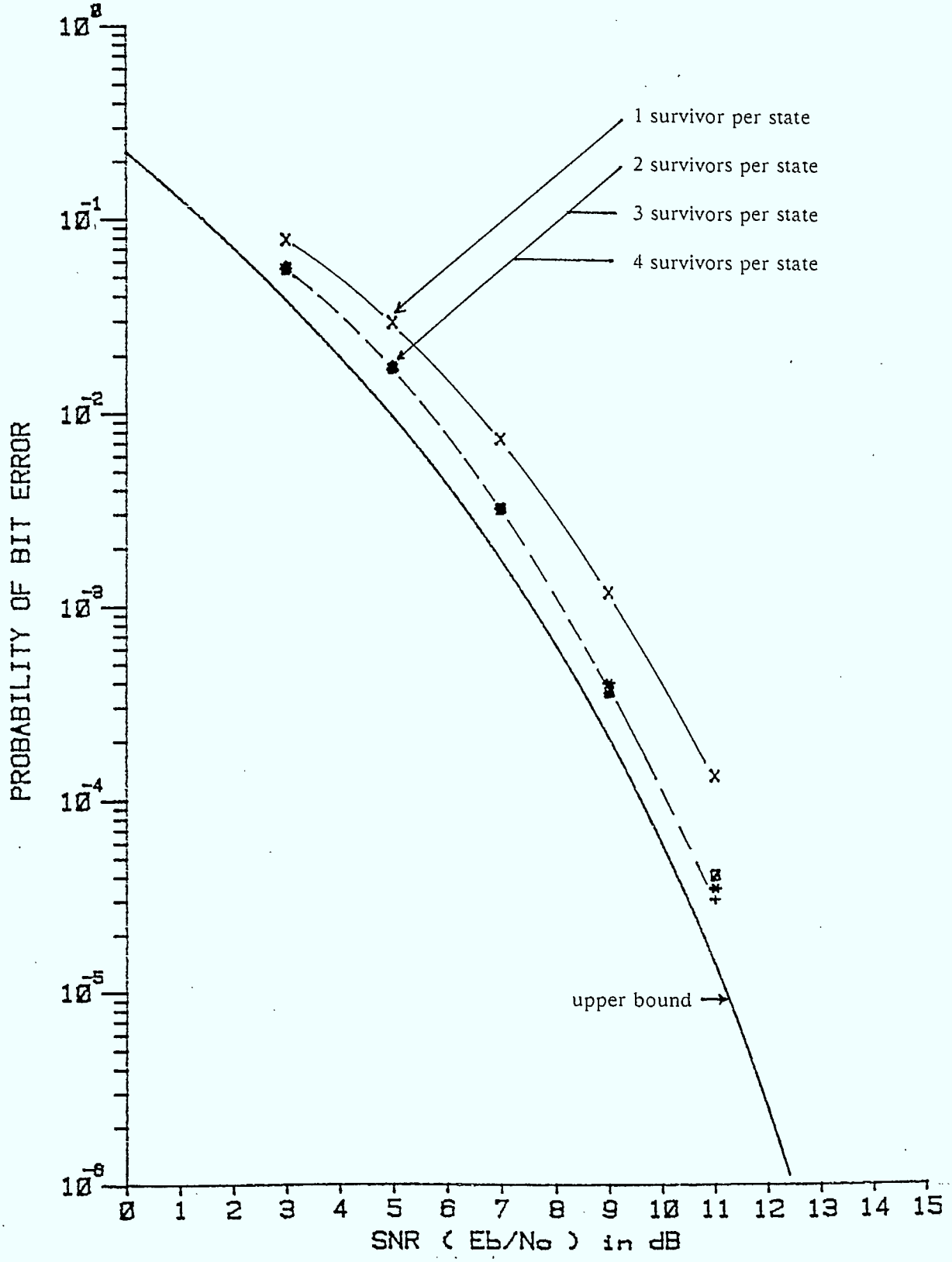

Figure 5.5 N = 16, FH/MSK simulation results and upper bound

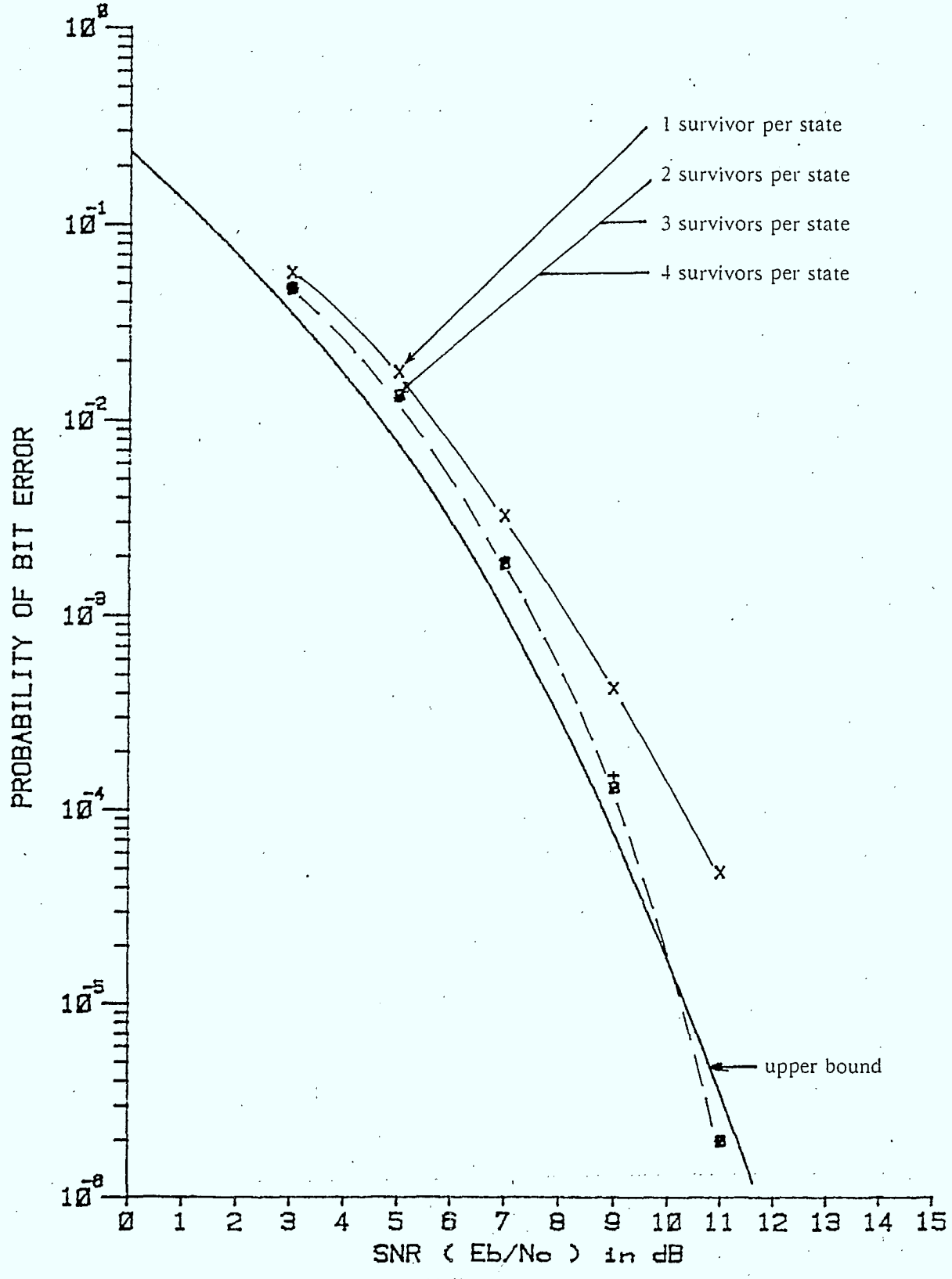

Figure 5.6 N = 64, FH/MSK simulation results and upper bound

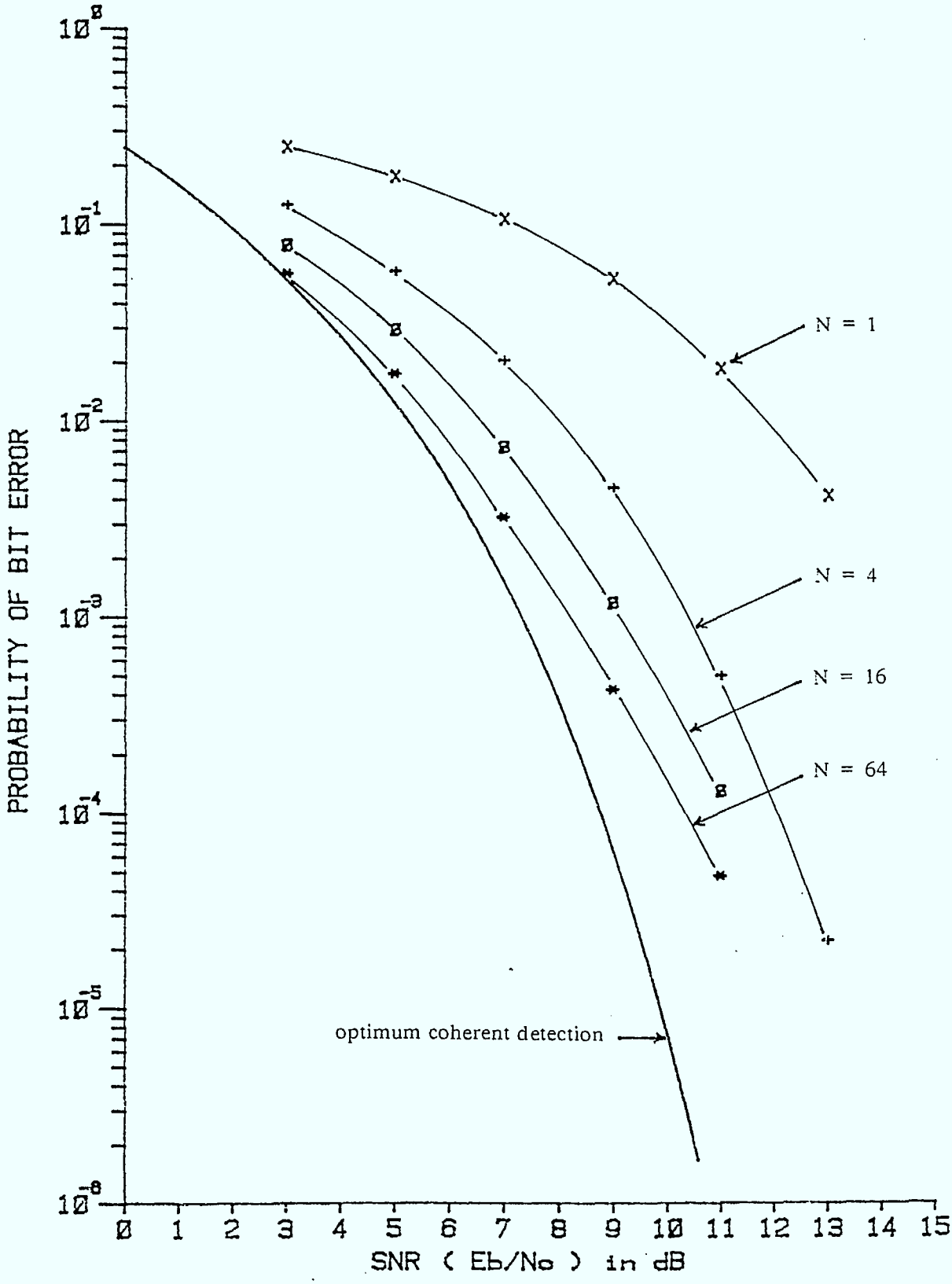

Figure 5.7 Simulation results for FH/MSK, 1 survivor per state

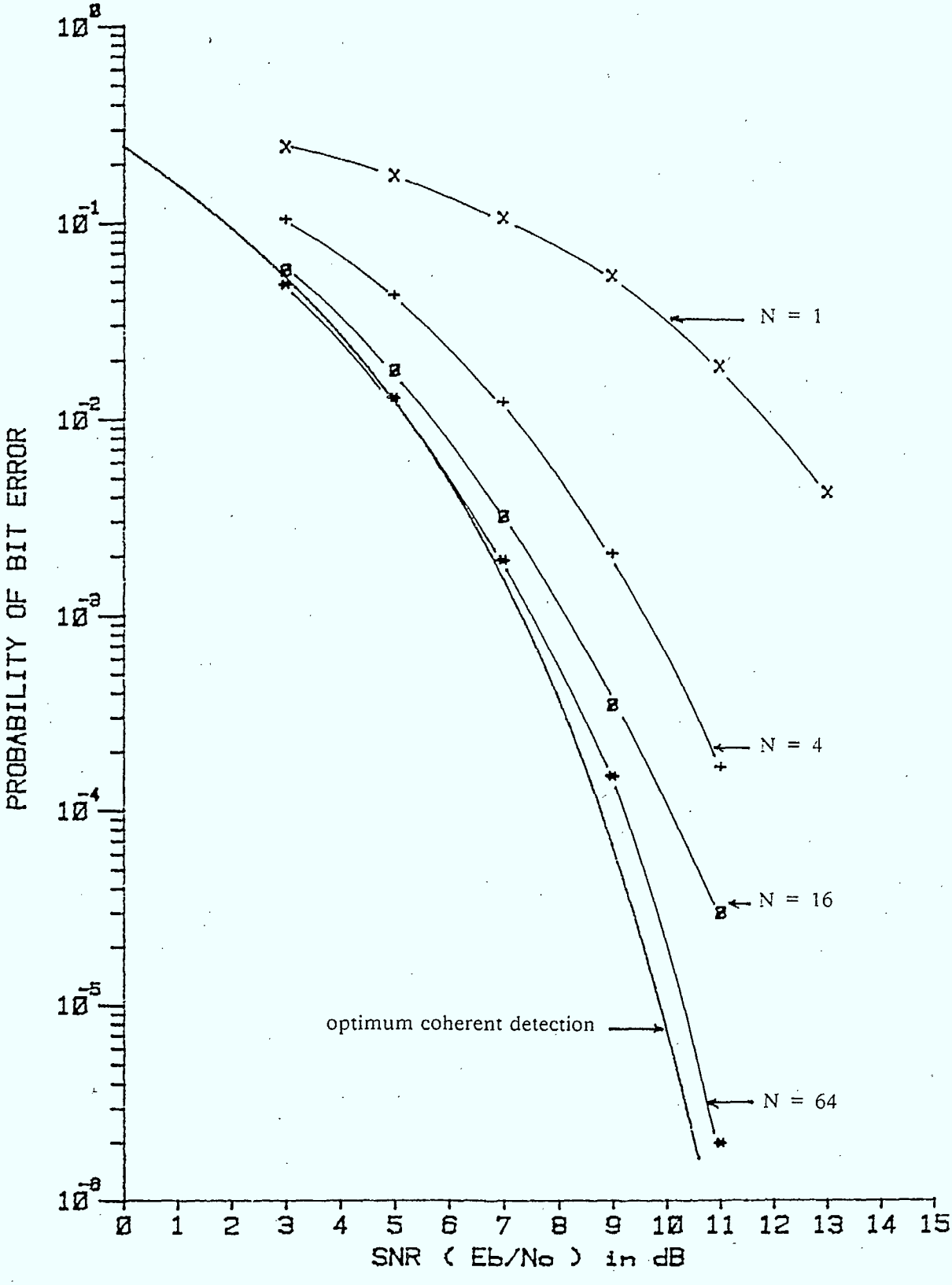

Figure 5.8 Simulation results for FH/MSK, 2 survivors per state

as the length of the hop interval increases and approaches the error performance of the optimum coherent MSK receiver.

For DMSK with differential precoding, decoders that keep 1, 2, 4 and 8 survivors for each state have been simulated. The improvement in bit error rate as the survivors kept for each state increases from 1 for hop intervals of length 4, 16 and 64 symbol intervals together with the corresponding theoretical upper bounds are illustrated in Figs. 5.9 to 5.11 respectively. For a hop length of 4 symbol intervals, there is little performance improvement in keeping more than 1 survivor for each state in the modulation trellis, as can be seen from Fig. 5.9. This apparent small improvement is due to the equivalent baseband pulse length of DMSK being 2 symbol intervals. Symbols transmitted at the end of a hop will have high error probability since only half of the symbol energy is transmitted at the end of a hop. For a hop length of 4 symbol intervals, which is small compared with the equivalent baseband pulse length of DMSK, the high error rate of the symbol at the end of a hop will dominate the error rate. Hence, keeping more than one survivor for each state in an attempt to avoid premature discarding of the true path during the decoding process has little effect on the bit error rate. For $N=4$, the simulated bit error rate result is higher than the upper bound at moderate to high SNR, but is still close to the bound. For the cases where $N = 16$ and 64, we see that keeping 2 survivors for each state brings significant improvement in the bit error rate as shown in Figs. 5.10 and 5.11. Again the improvement in error performance levels off as the number of survivors kept at each state has been increased to 2. The effect of keeping more than one survivor for each state is to retain more paths during the decoding process. If a competing path which has a likelihood larger than the true path due to noise merges with the true path, the true path will be retained by the decoder with higher probability when the number of survivors to be kept is more than one for each state. Further increase in the number of survivors to be kept for each state will only retain more paths which may actually have less likelihood than the true path. Hence the performance will increase only marginally once a certain number of survivors are kept for each state. The

important thing is to make sure that the true path is not being prematurely rejected during the decoding process unless its equivalent likelihood over the hop interval is less than that for the other competing paths. However, at low signal to noise ratio there is not much improvement in BER in keeping more than one survivor for each state. That is because at low SNR there is a high probability that any competing path will have larger equivalent likelihood than that of the true path. Even if the true path is being retained until the end of a hop interval, the probability that the decoder decides on an incorrect path is still high. Hence the increase in the number of survivor paths kept by the decoder is of little consequence. At high SNR, the true path will be very likely to be kept by the decoder even if only one survivor is kept for each state. Hence the increase in the number of survivors for each state will not help. The BER is largely determined by the probability that any competing path will have a high likelihood and hence be chosen by the decoder to be the transmitted path at the end of a hop interval rather than due to premature discarding of the true path. The theoretical upper bound is lower than the simulated bit error rate except at very low SNR range for N = 16 and 64. Generally, the upper bounds are within a dB of the simulated error performance for the receiver keeping two survivors per state for most of the range of bit error rate of interest.

The simulation results for FH/DMSK with precoding when 1 and 2 survivors are kept for each state, are plotted in Figs. 5.12 and 5.13 for various lengths of hop interval together with the bit error rate upper bound provided by the performance of the coherent Viterbi receiver for DMSK [42]. We see that the error performance improves with the length of the hop interval whether 1 or 2 survivors are kept for each state during the decoding process. As the hop length gets longer, the error performance of the hop-by-hop sequence estimation receiver approaches that of the coherent DMSK Viterbi receiver. Comparing Fig. 5.11 to Fig. 5.7 for 1 survivor per state or Fig. 5.12 to Fig. 5.8 for 2 survivors per state, we see that the rate at which the error performance approaches the coherent Viterbi receiver performance as the hop length increases, is not as great for DMSK as it is for MSK.

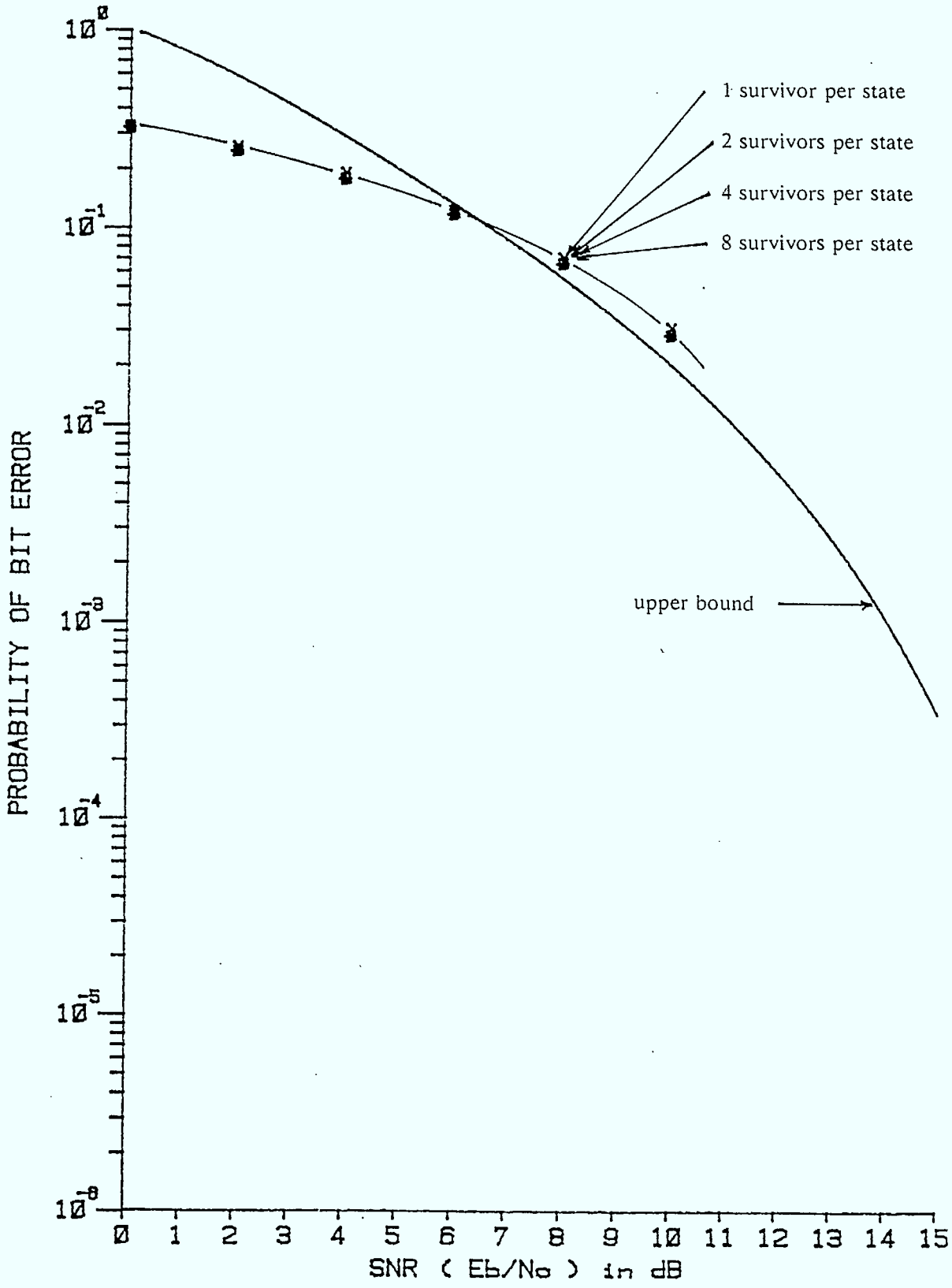

Figure 5.9 N = 4, FH/DMSK simulation results and upper bound

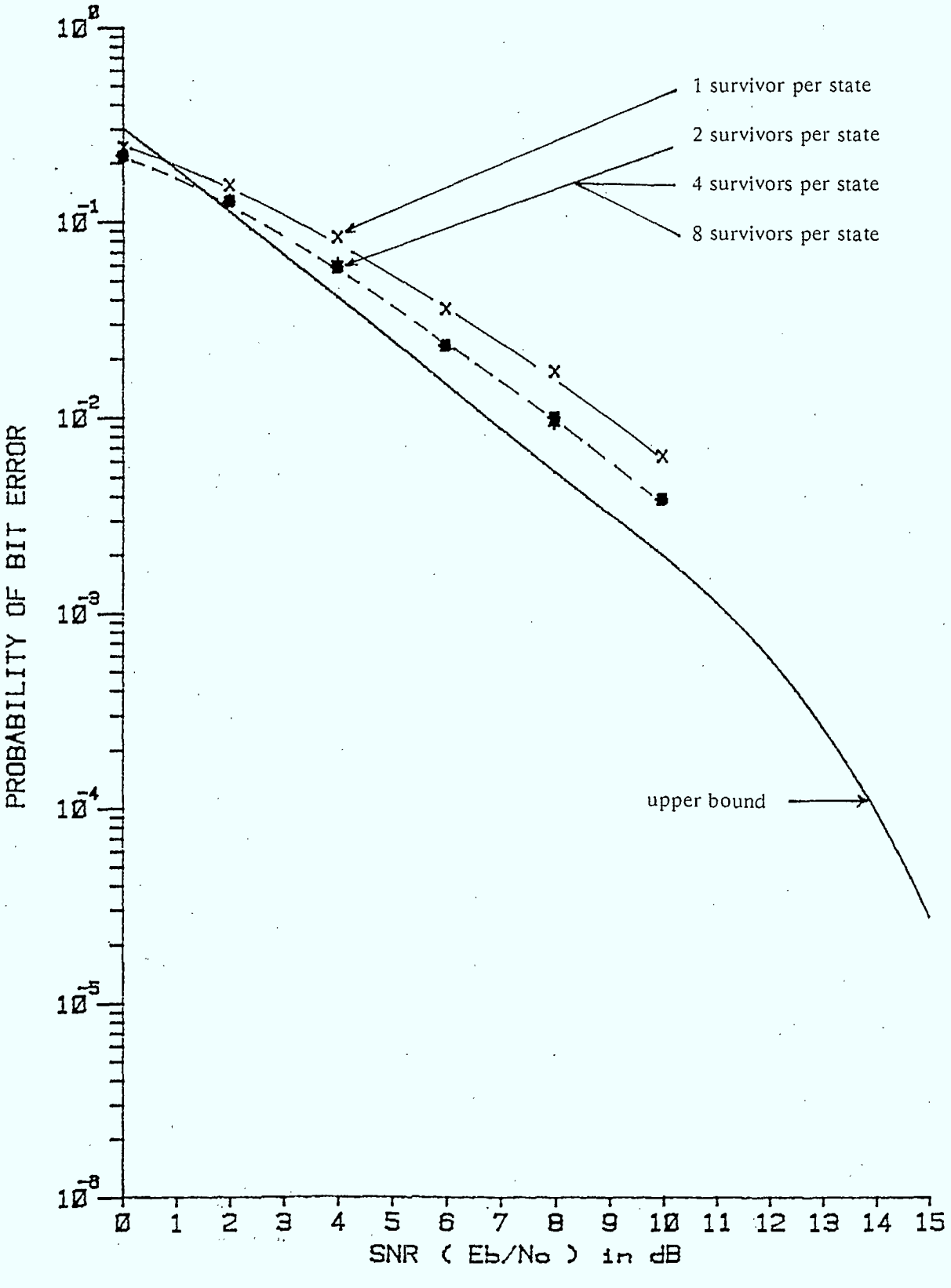

Figure 5.10 N = 16, FH/DMSK simulation results and upper bound

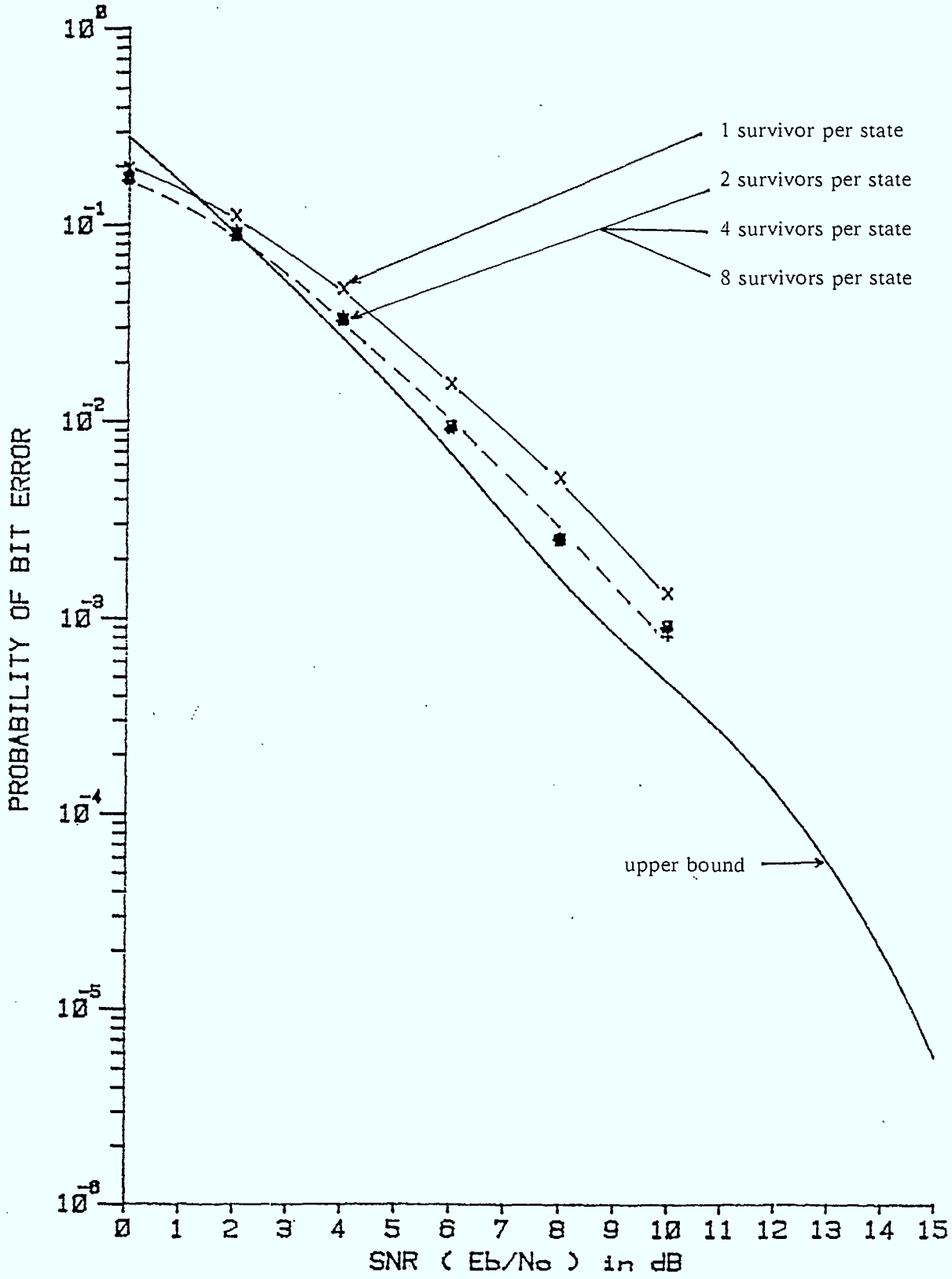

Figure 5.11 N = 64, FH/DMSK simulation results and upper bound

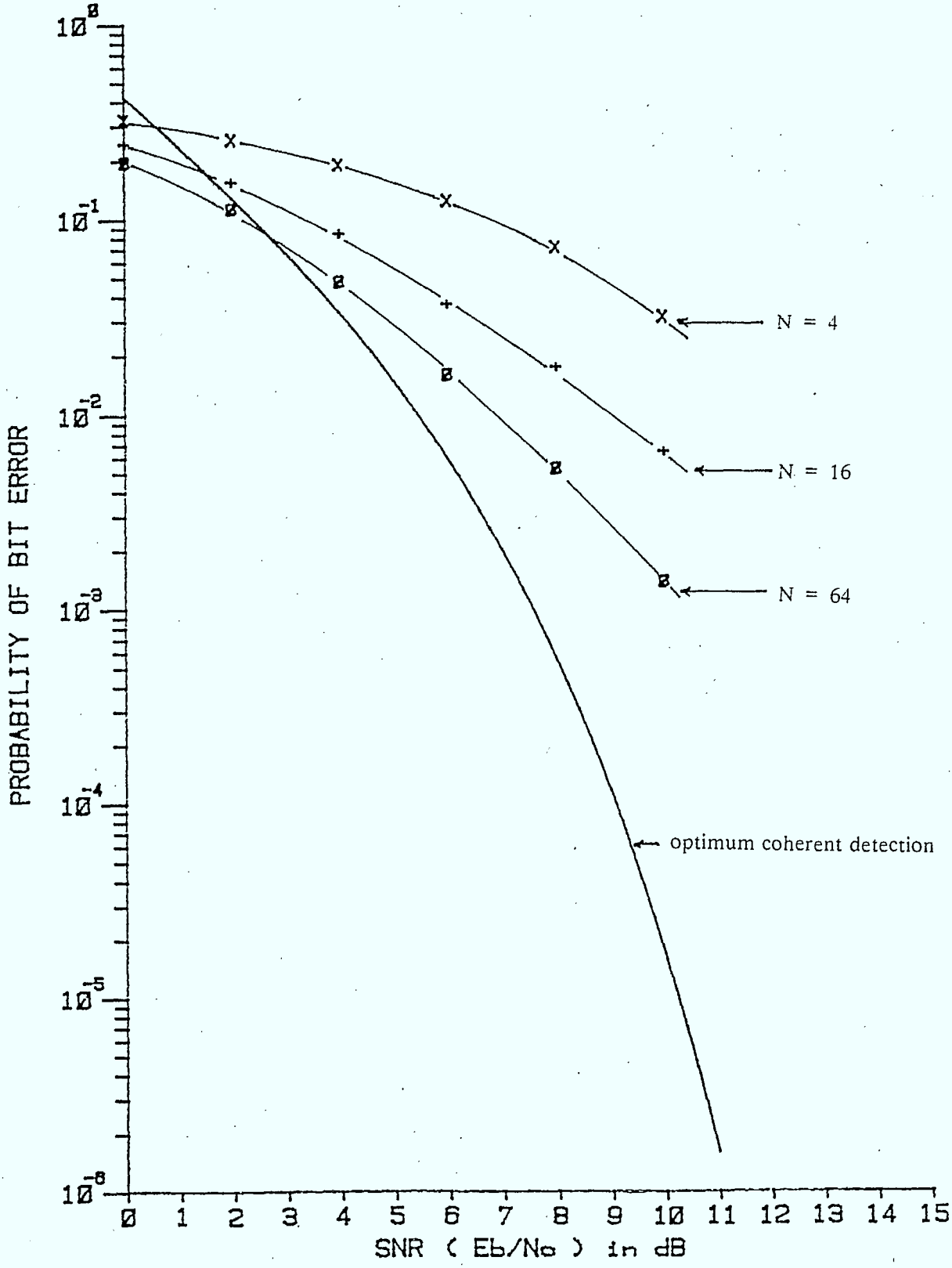

Figure 5.12 Simulation results for FH/DMSK, 1 survivor per state

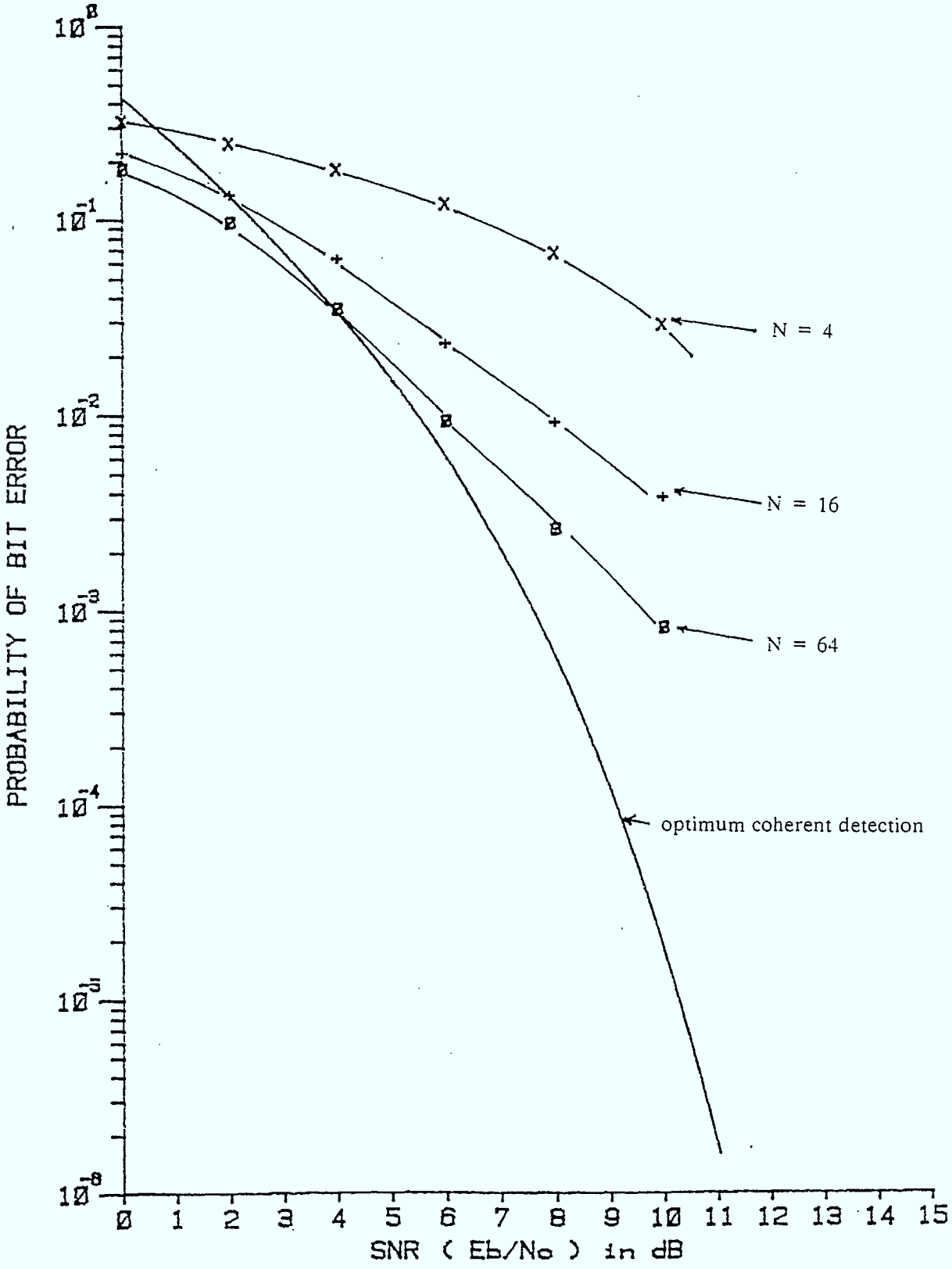

Figure 5.13 Simulation results for FH/DMSK, 2 survivors per state

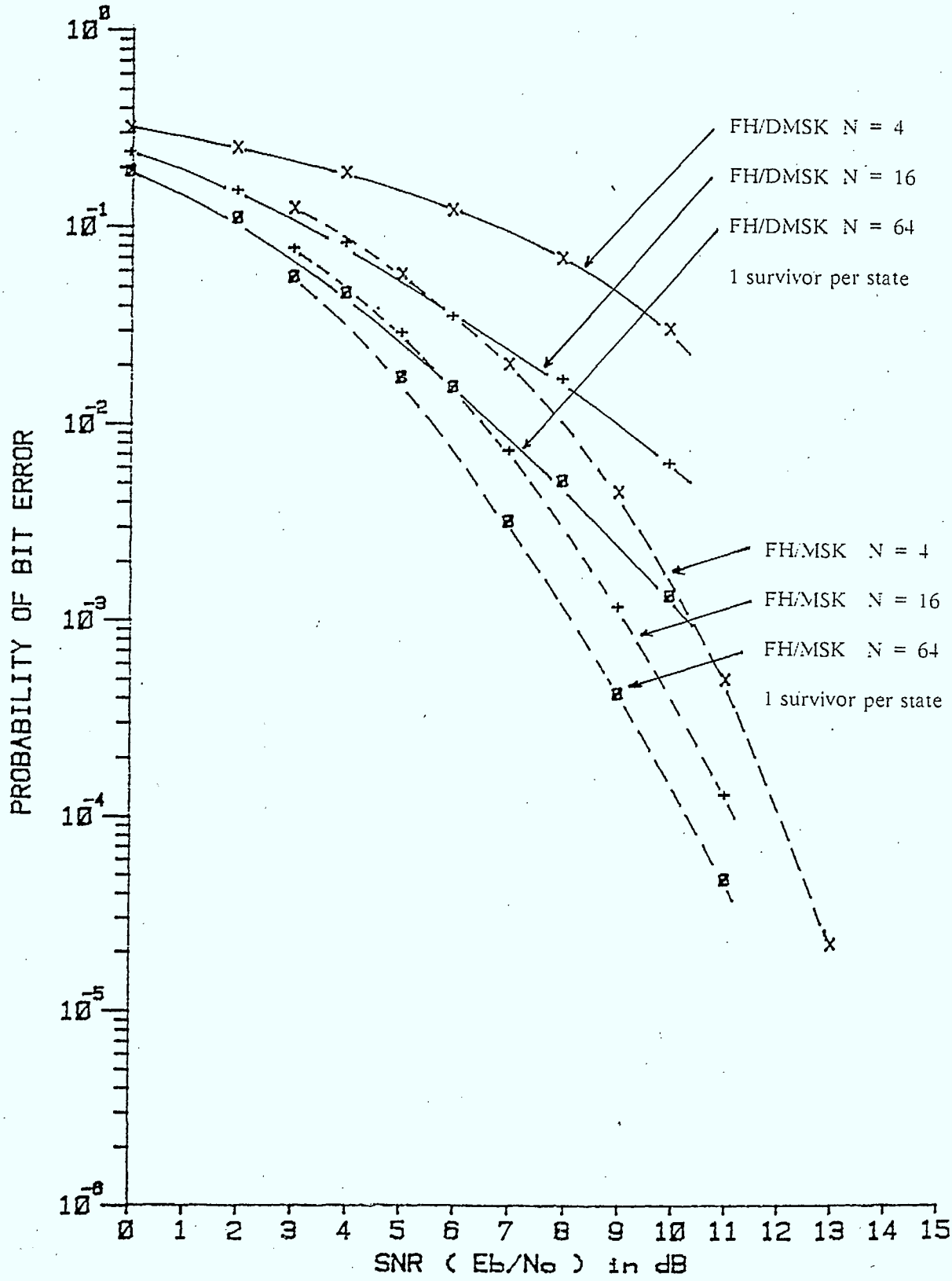

Figure 5.14 Simulation results of FH/MSK versus FH/DMSK for 1 survivor per state

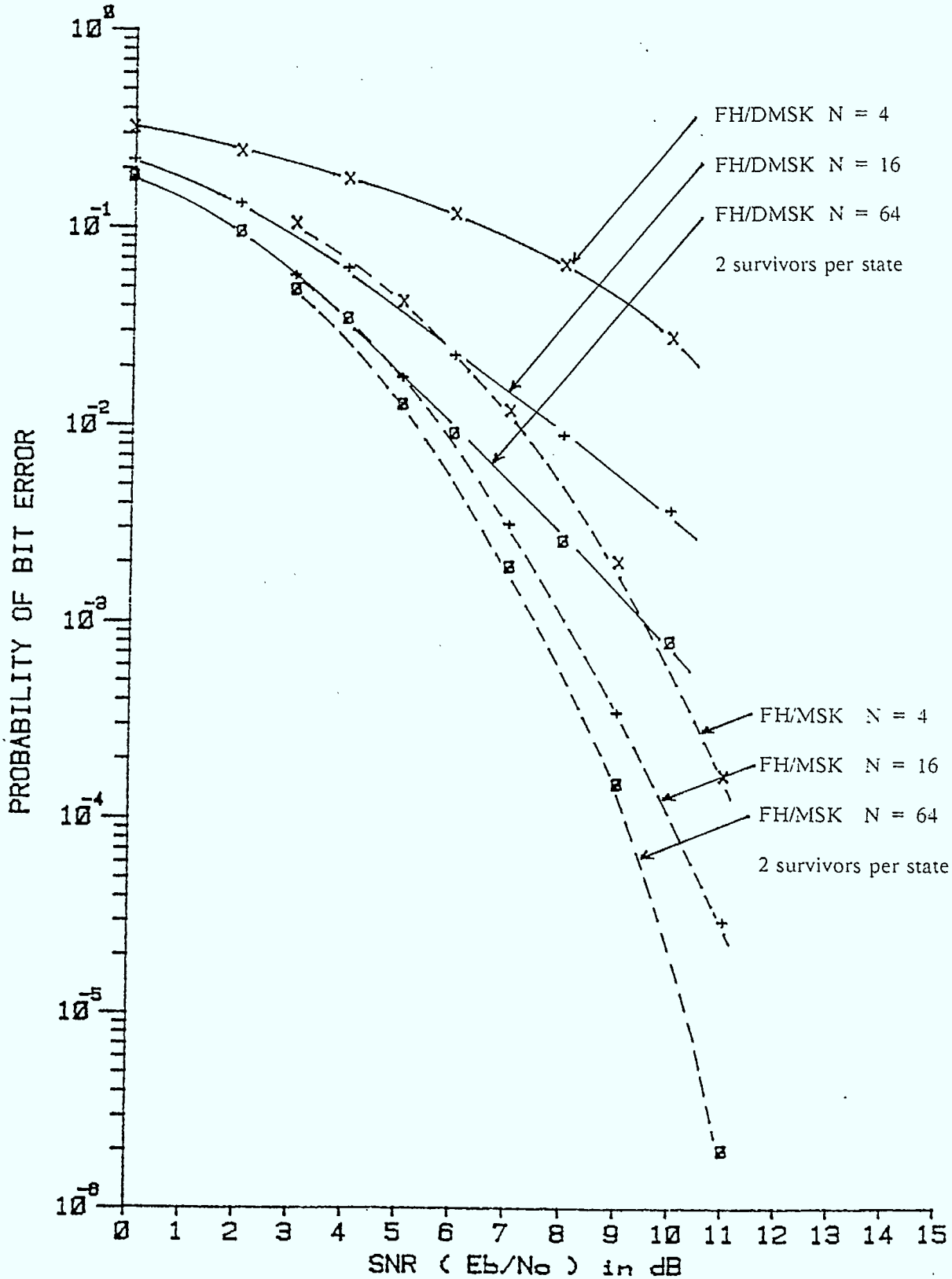

Figure 5.15 Simulation results of FH/MSK versus FH/DMSK for 2 survivors per state

The error performance of FH/MSK compared with FH/DMSK with precoding, for N = 4, 16 and 64, and for one and two survivors per state are shown in Figs. 5.14 and 5.15 respectively. We can see that for a given length of hop interval MSK has lower bit error rate than DMSK with precoding.

5.5 Summary

In this chapter, a simulation study of two frequency-hopped continuous phase modulation spread spectrum systems with a hop-by-hop sequential decoding receiver have been presented. Both the MSK and the precoded DMSK modulation schemes have been simluated for hop lengths of 4, 16 and 64. The performance improvement to the sequential decoding algorithm by keeping more than one survivor for each state in the trellis has been presented. For both MSK and DMSK, keeping two survivors for each state will bring the performance close to that of the optimum hop-by-hop ML noncoherent receiver. With the continuing decrease in price of memory devices, the increase in memory required to keep more than one survivor per state may not be of concern but the increase by more than a factor of two in computations when two survivors are kept for each state is not desirable for high speed operation. It is found from the simulation results that the maximum degradation in error performance by keeping just one survivor for each state in the trellis is only about 0.5 dB for MSK and about 1 dB for DMSK. This penalty of .5 or 1 dB in error performance degradation is small considering the number of computations and the memory saved. It has also been shown that the performance of the FH/MSK spread spectrum system with the hop-by-hop sequence estimation receiver gets very close to the performance of the coherent receiver with Viterbi decoding for long hop interval lengths such as 64 symbol intervals.

Chapter Six

CONCLUSIONS

A slow frequency-hopped spread spectrum communications system with continuous phase modulation for transmitting high speed data has been presented. The use of a bandwidth efficient modulation scheme, namely continuous phase modulation to transmit a number of symbols during a frequency hop interval results in a frequency-hopped spread spectrum signal, which has attractive mainlobe compactness and low sidelobes. Its compact hop bandwidth allows higher processing gain to be realized, hence a higher degree of antijam protection. For a multiple user system, the compact hop bandwidth allows more users to share a given spread spectrum system bandwidth.

Spectral analysis of frequency-hopped continuous phase modulations has been presented. The autocorrelation function of the dehopped spread spectrum signal has been derived for any arbitrary correlative encoding, baseband pulse shaping, modulation index, number of levels and length of frequency hop interval. The baseband power density spectrum of the dehopped signal can then be obtained via a Fourier transform of the autocorrelation function. Results on the baseband power density spectra of frequency-hopped signals with various partial response encodings and pulse shapings, and different hop lengths have been presented. In general, the spectrum becomes more compact with lower sidelobes and approaches that of the CPM signal without hopping, as the length of the hop interval increases.

It is found that the use of higher order PRS polynomials and pulse shaping, which are known to reduce the bandwidth significantly for usual continuous phase modulation, do not result in more compact spectra if the hop length is short. The use of higher order PRS

polynomials and pulse shaping is effective in bandwidth and sidelobe reduction for long hop intervals only.

Due to the unknown random phase of the carrier as it hops from one frequency to another, noncoherent detection has to be used. Three noncoherent receivers with sequential decoding have been presented. The first one is derived based on a hop-by-hop maximum likelihood decoding approach and is optimum over a hop interval. It has the simplest receiver structure and decoding algorithm.

The second receiver is derived based on the maximum likelihood spanning frequency hops and has a more complex decoding algorithm than the first one, although it has the same general receiver structure. However, simplification of the decoding algorithm is possible when the length of the hop interval is much greater than the length of the frequency pulse. The receiver operates generally in the same manner as the hop-by-hop receiver, but it has a subprocedure for metric calculation across each frequency hop and relies on the assumption that a merge in the trellis will occur well before the end of a hop.

With the aim to obtain a simpler decoding algorithm, the third receiver neglects the continuous phase structure of the signal within a frequency hop. Every symbol interval is treated as if it were noncoherent but with memory introduced by the partial response signaling. The performance is expected to be worst than the optimum receivers but a path transition metric can then be defined. Consequently, a decoding algorithm such as the Viterbi algorithm can easily be incorporated. However, the last two receivers both need the signal amplitude and the noise spectral density to be known for computing the metric. This will necessitate the use of some extra circuitry for estimating the signal to noise ratio before the metric computation can be carried out. The performance of the receiver will then depend also on the accuracy of the estimated signal to noise ratio. Due to this extra requirement of estimating the signal to

noise ratio and the complexity involved in the decoding algorithm, the receiver spanning frequency hops and the suboptimum receiver that neglects the signal phase structure are not suggested approaches for demodulating the spread spectrum signal. The noncoherent receiver, which estimate the transmitted sequence on a hop by hop basis, appears to be the most promising design.

Error performance of the sequence estimation hop-by-hop noncoherent receiver under additive white Gaussian noise has been analysed. Upper bounds on the bit error probability have been derived and evaluated for different partial response polynomials and pulse shapings using a union bound approach. As expected, the bit error rate decreases as the hop interval lengthens. The performance of the system using higher order correlative encoding is generally inferior to the one with no correlative encoding like minimum shift keying because of the increased number of output levels due to correlative encoding. The performance improvement by transmitting known symbols at the beginning of every hop interval is also investigated. An error bound on the bit error rate is derived also based on an union bound approach. Results for MSK, DMSK and TFM all with $h = 0.5$ and rectangular pulse shaping are presented. It is found that the gain in performance by transmitting known initial symbols is small when the hop interval is long.

The performance of the hop-by-hop noncoherent receiver under the presence of intentional interference (jamming) has been evaluated in Chapter Four. The performance of the receiver under partial band noise jamming is calculated based on the union bound approach. It has been shown that under partial band noise jamming, there is always an optimum value of the fraction of jammed band to the total system bandwidth to bring maximum degradation to the system. The partial band jammer can bring the usual exponential relationship between the bit error rate and the signal to noise ratio to an inverse linear relationship.

In a multiple-tone jamming envirnoment, it is found that the bandwidth efficient property of FH/CPM spread spectrum signal increases the system performance under multiple-tone jamming due to the increased number of frequency-hopped bands possible.

A simulation study of two systems, namely frequency-hopped MSK and frequency-hopped differentially precoded duobinary MSK was presented. It is found that the error performance of the hop-by-hop sequence estimating noncoherent receiver can be improved if the decoder keeps more than one survivor for each state in the trellis. Keeping two survivors for each state is sufficient to achieve close to the optimum error performance for both MSK and DMSK with differential precoding. Keeping more than two survivors for each state will improve the bit error rate insignificantly. The degradation in performance if the decoder keeps just one survivor for each state is only about 0.5 dB for MSK and 1 dB for DMSK, which is possibly small enough to justify the reduced decoder complexity and simpler decoder operation.

REFERENCES

1. R.C. Dixon, Spread Spectrum Systems, second edition, John Wiley and Sons, Inc., 1984.
2. R.L. Pickholtz, D.L. Schilling and L.B. Milstein, "Theory of Spread-Spectrum Communications - A Tutorial", IEEE Trans. on Comm., Vol. COM-30, No. 5, pp. 855-884, May 1982.
3. R.E. Ziemer and R.L. Peterson, Digital Communications and Spread Spectrum Systems, Macmillan Publishing Company, Inc., 1985.
4. C.E. Cook and H.S. Marsh, "An Introduction to Spread Spectrum", IEEE Communications Magazine, Vol. 21, No.2, pp. 8-16, March 1983.
5. M. Spellman, "A Comparison Between Frequency Hopping and Direct Spread PN as Antijam Techniques", IEEE Communications Magazine, Vol. 21, No.2, pp.37-51, March 1983.
6. L.B. Milstein, R.L. Pickholtz annd D.L. Schilling, "Optimization of the Processing Gain of an FSK-FH System", IEEE Tranns on Comm, Vol. COM-28, No. 7, pp.1062-1079, July 1980.
7. T.C. Huang and L. Yen, "Error Probability of a Noncoherent MFSK/FH Receiver in the Presence of Interference and Gaussian Noise", MILCOM'82 Proceedings, Boston, Mass., Oct. 17-20, 1982, pp. 14.3.1-14.3.7.
8. W.E. Stark, "Coding for Coherent Frequency-Hopped Spread-Spectrum Communication in the Presence of Jamming", MILCOM'82 Proceedings, Boston, Mass., Oct. 17-20, 1982, pp.14.2.1-14.2.5.
9. R.S. Orr, "Performance of MFSK in Simultaneous Partial-Band and Repeat-Back Jamming", MILCOM'82 Proceedings, Boston, Mass., Oct. 17-20, 1982, pp. 28.5.1-28.5.4.

10. L.B. Milstein and D.L. Schilling, "The Effect of Frequency-Selective Fading on a Non-coherent FH-FSK System Operating with Partial-Band Tone Interference", IEEE Trans. on Comm., Vol. COM-30, No. 5, pp. 904-912, May 1982.

11. E.A. Geraniotis and M.B. Pursley, "Error Probability of Slow-Frequency-Hopped Spread-Spectrum Multiple-Access Communications Over Fading Channels", IEEE Trans. on Comm., Vol. COM-30, No. 5, pp. 996-1009, May 1982.

12. P.H. Wittke, P.J. McLane and P. Ma, "Study of the Reception of Frequency Dehopped M-ary FSK", Dept. of Elect. Eng., Queen's University, Research Report No. 83-1, March 1983.

13. P.H. Wittke and J. Yau, "Performance of Frequency-Hopped M-ary FSK in the Presence of Phase Jitter", Dept. of Elect. Eng., Queen's University, Research Report No. 84-2, March 1984.

14. M. Matsumoto and G.R. Cooper, "Performance of a Nonlinear FH-DPSK Spread-Spectrum Receiver with Multiple Narrow-Band Interfering Signals", IEEE Trans. on Comm., Vol. COM-30, No. 5, pp. 937-942, May 1982.

15. J.S. Lee and L.E. Miller, "Error Performance Analyses of Differential Phase-Shift-Keyed/Frequency-Hopping Spread-Spectrum Communication System in the Partial Band Jamming Environments", IEEE Trans. on Comm., Vol. COM-30, No. 5, pp. 943-952, May 1982.

16. M.K. Simon, "The Performance of M-ary FH-DPSK in the Presence of Partial-Band Multitone Jamming", IEEE Trans. on Comm., Vol. COM-30, No. 5, pp. 953-958, May 1982.

17. C-E. Sundberg, "Continuous Phase Modulation", IEEE Communications Magazine, Vol. 24, No. 4, pp. 25-38, April 1986.

18. G.S. Deshpande and P.H. Wittke, "Correlative Encoded Digital FM", IEEE Trans. on Comm., Vol. COM-29, pp. 156-162, Feb. 1981.

19. P. Kabal and S. Pasupathy, "Partial-Response Signaling", IEEE Trans. on Comm., Vol. COM-23, pp. 921-934, Sept. 1975.

20. A. Svensson, C-E. Sundberg and G. Lindell, "On Direct Sequence Spread Spectrum Systems with Continuous Phase Modulation", Technical Report TR-184, Sept. 1984, Telecommunication Theory, University of Lund, Lund.

21. P.H. Wittke, P.J. McLane, S.J. Simmons and Y.M. Lam, "A Bandwidth Efficient Frequency-Hopped Spread Sprectrum Modulation Study", Dept. of Elect. Eng., Queen's University, Resarch Report No. 85-03, March 1985.

22. P.H. Wittke, P.J. McLane, Y.M. Lam and S.J. Simmons, "A Bandwidth Efficient Frequency-Hopped Spread Sprectrum Modulation Study", Dept. of Elect. Eng., Queen's University, Resarch Report No. 86-02, March 1986.

23. Y.M. Lam and P.H. Wittke, "A Bandwidth Efficient Frequency-Hopped Spread Sprectrum Modulation Study", Proceedings of the 13 th Biennial Symposium on Communications at Queen's University, Kingston, Ontario, Canada, pp.C.5.11-C.5.13, June 1986.

24. P.H. Wittke, P.J. McLane, S.J. Simmons, M.G. Wearring, Y.M. Lam and W. Hopkins, "The Study of Space Communications Spread Spectrum Systems (Phase IV)", Dept. of Elect. Eng., Queen's University, Resarch Report No. 87-1, June 1987.

25. R.R. Anderson and J. Salz, "Spectra of Digital FM", Bell System Tech. J., Vol. 44, pp. 1165-1189, July-August 1965.

26. H.E. Rowe and V.K. Prabhu, "Power Spectrum of a Digital Frequency-Modulation Signal", Bell System Tech. J., Vol. 54, pp. 1095-1125, Aug. 1975.

27. T. Aulin and C-E. Sundberg, "Numerical Calculation of Spectra for Digital FM Signals", National Telecommunications Conference, NTC'81, New Orleans, Louisianna, November 29 - December 3, 1981, Conference Record, pp. D8.3.1-D8.3.7.

28. P. Ho and P.J. McLane, "The Power Spectral Density of Digital Continuous Phase Modulation with Correlated Data Symbols: Part Two - The Rowe-Prabhu Method", IEE Proc., Vol. 133, Part F, pp. 106-114, Feb. 1986.

29. T.J. Baker, "Asymptotic Behaviour of Digital FM Spectra", IEEE Trans. on Comm., Vol. COM-22, pp. 1585-1594, Nov. 1975.

30. G.J. Garrison, "A Power Spectral Density Analysis for Digital FM ", IEEE Trans. on Comm., Vol. COM-23, pp. 1228-1243, Nov. 1975.

31. T. Aulin and C-E. Sundberg, "An easy way to calculate power spectra for digital FM", IEE Proceedings, Vol. 130, Part f, No. 6, pp. 519-526, Oct. 1983.

32. P. Ho and P.J. McLane, "The Power Spectral Density of Digital Continuous Phase Modulation with Correlated Data Symbols: Part One - The Correlation Function Method", IEE Proc., Vol. 133, Part F, pp. 95-105, Feb. 1986.

33. W.P. Osborne and M.B. Luntz, "Coherent and Non-coherent Detection of CPFSK", IEEE Trans. on Comm., Vol. COM-22, pp. 1023-1036, August 1974.

34. T.A. Schonhoff, "Symbol Error Probabilities for M-ary CPFSK: Coherent and Non-coherent Detection", IEEE Trans. on Comm., Vol. COM-24, pp. 644-652, July 1976.

35. T. Aulin and C-E. Sundberg, "On Partially Coherent Detection of Digital Continuous Phase Modulation Signals", Technical Report TR-127, May 1979, Telecommunication Theory, University of Lund, Lund.

36. A. Svensson and C-E. Sundberg, "Error Probability Bounds for Noncoherently Detected CPM", Technical Report TR-183, August 1984, Telecommunication Theory, University of Lund, Lund.

37. A. Svensson and C-E. Sundberg, "On Error Probability for Several Types of Noncoherent Detection of CPM", IEEE GLOBECOM'84, Conference Record, pp. 22.5.1-22.5.7.

38. R.F. Pawula and R. Golden, "Simulations of Convolutional Coding/Viterbi Decoding with Noncoherent CPFSK", IEEE Trans. on Comm., Vol. COM-29, No. 10, pp. 1522-1526, Oct. 1981.

39. G.D. Forney, "Maximum-Likelihood Sequence Estimation of Digital Sequences in the Presence of Intersymbol Interference", IEEE Trans. on Information Theory, Vol. IT-18, pp. 363-378, May 1972.

40. G.D. Forney, "The Viterbi Algorithm", Proc. of the IEEE, Vol. 61, No. 3, pp. 268-278, March 1973.

41. S.J. Simmons and P.H. Wittke, "Low Complexity Decoder for Constant Envelope Digital Modulations", IEEE Trans. on Comm., Vol. COM-31, No. 12, pp. 1273-1280, Dec. 1983.

42. P.J. McLane, "The Viterbi Receiver for Correlative Encoded MSK Signals", IEEE Trans. on Comm., Vol. COM-31, No. 2, pp. 290-295, Feb. 1983.

43. H. Kobayashi, "Correlative Level Coding and Maximum-Likelihood Decoding", IEEE Trans. on Information Theory, Vol. IT-17, No. 5, pp. 586-594, Sept. 1971.

44. S. Stein, "Unified Analysis of Certain Coherent and Noncoherent Binary Communication Systems", IEEE Trans. on Information Theory, Vol. IT-10, pp. 43-51, Jan. 1964.

45. M. Schwartz, W.R. Bennett and S. Stein, Communication Systems and Techiques, McGraw-Hill, 1966.

46. W.F. McGee, "Another Recursive Method of Computing the Q Function", IEEE Trans. on Information Theory, Vol. IT-16, pp. 500-501, July 1970.

47. S. Parl, "A New Method of Calculating the Generalized Q Function", IEEE Trans. on Information Theory, Vol. IT-26, pp. 121-124, Jan. 1980.

48. T.T. Tjhung, C.S. Ng, K.K. Yeo and P.H. Wittke, "Error Performance Analysis for Narrow-Band Duobinary FM with Discriminator Detection", IEEE Trans. on Comm., Vol. COM-33, No. 5, pp.399-408, May 1985.

49. D.P. Taylor and H.C. Chan, "A Simulation Study of Two Bandwidth-Efficient Modulation Techniques", IEEE Trans. on Comm., Vol. COM-29, No. 3, pp.267-275, March 1981.

50. J.M. Wozencraft and I.M. Jacobs, Principles of Communication Engineering, John Wiley and Sons, 1967.

51. V.K. Bhargava, D. Haccoun, R. Matyas and P.P. Nuspl, Digital Communications by Satellite, John Wiley and Sons, Inc., 1981.

52. G. Marsaglia and T.A. Bray, "A convenient method for generating normal variables", SIAM Review, Vol. 6, pp. 260-264, 1964.

APPENDIX A

Multiple-Tone Jammer Power

For simplicity, suppose that thermal Gaussian noise is negligible. The dehopped received signal when a jamming tone is present is given by

$$r(t) = s(t, \underline{\alpha}, \theta_i) + J_q(t); \qquad iNT < t < (i + 1)NT, \tag{A.1}$$

where $s(t, \underline{\alpha}, \theta_i)$ denotes the transmitted signal in the i^{th} hop interval as given by Eq.(3.4) re-written below

$$s(t, \underline{\alpha}, \theta_i) = \sqrt{2P}\ \cos[\, 2\pi f_c t + \psi(t, \underline{\alpha}) + \theta_i\,]; \qquad iNT < t < (i + 1)NT \tag{A.2}$$

and $J_q(t)$ denotes the continuous-wave jamming tone signal given by

$$J_q(t) = \sqrt{2J_q}\ \cos[\, 2\pi f_c t + 2\pi f_J t + \phi_J\,], \tag{A.3}$$

where J_q is the power of the jamming tone, f_J is the jammer tone frequency offset from the intermediate carrier frequency f_c after being dehopped and ϕ_J is a random phase. The hop-by-hop receiver computes the equivalent likelihood for each of the possible sequences $\underline{\alpha}'$ given by

$$\begin{aligned} \ell'(\underline{\alpha}, \underline{\alpha}') &= \left| \int_0^{NT} r(t)\ \exp[\, j\,(\, 2\pi f_c t + \psi(t, \underline{\alpha}')\,)\,]\, dt \right|^2 \\ &= \Big| \int_0^{NT} s(t, \underline{\alpha}, \theta_i)\ \exp[\, j\,(\, 2\pi f_c t + \psi(t, \underline{\alpha}')\,)\,]\, dt \\ &\quad + \int_0^{NT} J_q(t)\ \exp[\, j\,(\, 2\pi f_c t + \psi(t, \underline{\alpha}')\,)\,]\, dt \Big|^2 \end{aligned} \tag{A.4}$$

Substituting Eqs.(A.2) and (A.3) into Eq. (A.4) and assuming that $f_c \gg 1$, we obtain

$$\ell'(\underline{\alpha}, \underline{\alpha}') = \left| \sqrt{\frac{P}{2}} \int_0^{NT} \exp[\, j\,(\psi(t, \underline{\alpha}') - \psi(t, \underline{\alpha}) - \theta_i\,)]\, dt + \sqrt{\frac{J_q}{2}} \int_0^{NT} \exp[\, j\,(\psi(t, \underline{\alpha}') - 2\pi f_J t - \phi_J\,)]\, dt \right|^2. \tag{A.5}$$

Assuming that the multiple-tone jammer knows the transmitted signal structure, the jammer will always select the tone frequency such that

$$2\pi f_J t = \psi(t, \tilde{\underline{\alpha}}). \tag{A.6}$$

That is, the jamming tone is one of the transmitted signals. (For example when the pulse shaping is rectangular and the tone jammer selects $f_J = \frac{h}{2T}$, then the jamming tone signal will be the same as the signal, which would have been transmitted had the correlated symbols been all 1's.) The equivalent likelihood for that particular sequence $\tilde{\underline{\alpha}}$ corresponding to the jamming tone is then

$$\begin{aligned} \ell'(\underline{\alpha}, \tilde{\underline{\alpha}}) &= \left| \sqrt{\frac{P}{2}} \int_0^{NT} \exp[\, j\,(\psi(t, \tilde{\underline{\alpha}}) - \psi(t, \underline{\alpha}) - \theta_i\,)]\, dt + \sqrt{\frac{J_q}{2}} \int_0^{NT} \exp[\, -j\phi_J\,]\, dt \right|^2 \\ &= \left| \sqrt{\frac{P}{2}} \int_0^{NT} \exp[\, j(\psi(t, \tilde{\underline{\alpha}}) - \psi(t, \underline{\alpha}) - \theta_i)]\, dt + \sqrt{\frac{J_q}{2}}\, (NT) \exp[\, -j\phi_J] \right|^2. \end{aligned} \tag{A.7}$$

The equivalent likelihood for the transmitted sequence $\underline{\alpha}$ is given by

$$\begin{aligned} \ell'(\underline{\alpha}, \underline{\alpha}) &= \left| \sqrt{\frac{P}{2}} \int_0^{NT} \exp[\, -j\theta_i\,]\, dt + \sqrt{\frac{J_q}{2}} \int_0^{NT} \exp[\, j\,(\psi(t, \underline{\alpha}) - \psi(t, \tilde{\underline{\alpha}}) - \phi_J\,)]\, dt \right|^2 \\ &= \left| \sqrt{\frac{P}{2}}\, (NT) \exp[\, -j\theta_i\,] + \sqrt{\frac{J_q}{2}} \int_0^{NT} \exp[\, j\,(\psi(t, \underline{\alpha}) - \psi(t, \tilde{\underline{\alpha}}) - \phi_J\,)]\, dt \right|^2. \end{aligned}$$

(A.8)

The hop-by-hop ML receiver will always choose $\tilde{\underline{\alpha}}$ as the estimated sequence, if $\ell'(\underline{\alpha}, \tilde{\underline{\alpha}}) > \ell'(\underline{\alpha}, \underline{\alpha})$.

$$
\begin{aligned}
&\ell'(\underline{\alpha}, \tilde{\underline{\alpha}}) - \ell'(\underline{\alpha}, \underline{\alpha}) \\
&= \Big\{\sqrt{\frac{P}{2}}\int_0^{NT} \cos[\psi(t, \tilde{\underline{\alpha}}) - \psi(t, \underline{\alpha}) - \theta_i]dt + \sqrt{\frac{J_q}{2}}(NT)\cos\phi_J\Big\}^2 \\
&\quad + \Big\{\sqrt{\frac{P}{2}}\int_0^{NT} \sin[\psi(t, \tilde{\underline{\alpha}}) - \psi(t, \underline{\alpha}) - \theta_i]dt + \sqrt{\frac{J_q}{2}}(NT)\sin\phi_J\Big\}^2 \\
&\quad - \Big\{\sqrt{\frac{P}{2}}(NT)\cos\theta_i + \sqrt{\frac{J_q}{2}}\int_0^{NT} \cos[\psi(t, \underline{\alpha}) - \psi(t, \tilde{\underline{\alpha}}) - \phi_J]dt\Big\}^2 \\
&\quad - \Big\{-\sqrt{\frac{P}{2}}(NT)\sin\theta_i + \sqrt{\frac{J_q}{2}}\int_0^{NT} \sin[\psi(t, \underline{\alpha}) - \psi(t, \tilde{\underline{\alpha}}) - \phi_J]dt\Big\}^2
\end{aligned}
$$

$$
\begin{aligned}
&= \frac{P}{2}\Big\{\int_0^{NT} \cos[\psi(t, \tilde{\underline{\alpha}}) - \psi(t, \underline{\alpha}) - \theta_i]\,dt\Big\}^2 + \frac{J_q}{2}(NT)^2\cos^2\phi_J \\
&\quad + \sqrt{PJ_q}(NT)\cos\phi_J\int_0^{NT} \cos[\psi(t, \tilde{\underline{\alpha}}) - \psi(t, \underline{\alpha}) - \theta_i]\,dt \\
&\quad + \frac{P}{2}\Big\{\int_0^{NT} \sin[\psi(t, \tilde{\underline{\alpha}}) - \psi(t, \underline{\alpha}) - \theta_i]\,dt\Big\}^2 + \frac{J_q}{2}(NT)^2\sin^2\phi_J \\
&\quad - \sqrt{PJ_q}(NT)\sin\phi_J\int_0^{NT} \sin[\psi(t, \tilde{\underline{\alpha}}) - \psi(t, \underline{\alpha}) - \theta_i]\,dt \\
&\quad - \frac{P}{2}(NT)^2\cos^2\theta_i - \frac{J_q}{2}\Big\{\int_0^{NT} \cos[\psi(t, \underline{\alpha}) - \psi(t, \tilde{\underline{\alpha}}) - \phi_J]\,dt\Big\}^2 \\
&\quad - \sqrt{PJ_q}(NT)\cos\theta_i\int_0^{NT} \cos[\psi(t, \underline{\alpha}) - \psi(t, \tilde{\underline{\alpha}}) - \phi_J]\,dt \\
&\quad - \frac{P}{2}(NT)^2\sin^2\theta_i - \frac{J_q}{2}\Big\{\int_0^{NT} \sin[\psi(t, \underline{\alpha}) - \psi(t, \tilde{\underline{\alpha}}) - \phi_J]\,dt\Big\}^2 \\
&\quad + \sqrt{PJ_q}(NT)\sin\theta_i\int_0^{NT} \sin[\psi(t, \underline{\alpha}) - \psi(t, \tilde{\underline{\alpha}}) - \phi_J]\,dt
\end{aligned}
$$

$$= \frac{P}{2}\left|\int_0^{NT} \exp[\,j\,(\psi(t,\tilde{\underline{\alpha}}) - \psi(t,\underline{\alpha}) - \theta_i)]\,dt\,\right|^2$$
$$+ \frac{J_q}{2}(NT)^2 + \sqrt{PJ_q}\,(NT)\int_0^{NT}\cos[\psi(t,\tilde{\underline{\alpha}}) - \psi(t,\underline{\alpha}) - \theta_i + \phi_J]\,dt$$
$$- \frac{J_q}{2}\left|\int_0^{NT} \exp[\,j\,(\psi(t,\underline{\alpha}) - \psi(t,\tilde{\underline{\alpha}}) - \phi_J)]\,dt\,\right|^2$$
$$- \frac{P}{2}(NT)^2 - \sqrt{PJ_q}\,(NT)\int_0^{NT}\cos[\psi(t,\underline{\alpha}) - \psi(t,\tilde{\underline{\alpha}}) - \phi_J + \theta_i]\,dt$$

$$= \frac{(NT)^2}{2}(J_q - P) + \frac{P}{2}\left|\int_0^{NT} \exp[\,j\,(\psi(t,\tilde{\underline{\alpha}}) - \psi(t,\underline{\alpha}))]\,dt\,\right|^2$$
$$- \frac{J_q}{2}\left|\int_0^{NT} \exp[\,j\,(\psi(t,\underline{\alpha}) - \psi(t,\tilde{\underline{\alpha}}))]\,dt\,\right|^2$$

$$= \frac{(NT)^2}{2}(J_q - P) + \frac{(J_q - P)}{2}\left\{\left|\int_0^{NT} \exp[\,j\,(\psi(t,\tilde{\underline{\alpha}}) - \psi(t,\underline{\alpha}))]\,dt\,\right|^2\right\}$$

$$= \frac{(J_q - P)}{2}\left\{(NT)^2 - \left|\int_0^{NT} \exp[\,j\,(\psi(t,\tilde{\underline{\alpha}}) - \psi(t,\underline{\alpha}))]\,dt\,\right|^2\right\}$$

$$= \frac{(J_q - P)}{2}\left\{NT + \left|\int_0^{NT} \exp[j(\psi(t,\tilde{\underline{\alpha}}) - \psi(t,\underline{\alpha}))]dt\right|\right\}$$
$$\left\{NT - \left|\int_0^{NT} \exp[j(\psi(t,\tilde{\underline{\alpha}}) - \psi(t,\underline{\alpha}))]dt\right|\right\}. \qquad (A.9)$$

Since

$$NT + \left|\int_0^{NT}\exp[j(\psi(t,\tilde{\underline{\alpha}}) - \psi(t,\underline{\alpha}))]dt\right| > 0$$

and

$$NT - \left|\int_0^{NT}\exp[j(\psi(t,\tilde{\underline{\alpha}}) - \psi(t,\underline{\alpha}))]dt\right| > 0\ ,$$

$\ell'(\underline{\alpha}, \tilde{\underline{\alpha}}) > \ell'(\underline{\alpha}, \underline{\alpha})$ when $J_q > P$. If $J_q > P$, the receiver will always decode the transmitted sequence to be $\tilde{\underline{\alpha}}$, which corresponds to the jamming tone frequency given by Eq.(A.6) no matter what the transmitted sequence is.